1993

Earthquake Source Spectra And Attenuation In Southeastern Canada

Gail Marie Atkinson

EARTHQUAKE SOURCE SPECTRA AND ATTENUATION IN SOUTHEASTERN CANADA

by

Gail Marie Atkinson

Geophysics Department

Submitted in partial fulfilment
of the requirements for the degree of
Doctor of Philosophy

Faculty of Graduate Studies
The University of Western Ontario
London, Ontario
March 1993

ISBN 0-315-81278-8

Canada

ABSTRACT

Definition of the spectrum of ground motion as a function of earthquake magnitude and distance is a crucial component of seismic hazard evaluations of engineered structures. This study uses an empirical approach to investigate the Fourier spectra of earthquake ground motions in southeastern Canada. The primary dataset is comprised of 1500 digital seismograms, from 100 earthquakes of magnitude 3.0 to 6.5 recorded on 30 stations of the Eastern Canada Telemetered Network (ECTN). The distance range of the observations is 10 to 1700 km; focal depths are from 5 to 30 km.

Regression analyses of the ECTN data are used to determine the source spectrum for each event and describe its attenuation with distance. Simulations demonstrate that observed ground motions can be accurately modeled using the regression results, in conjunction with a simple stochastic model.

The attenuation curve has three distinct sections. At distances (R) less than 70 km, corresponding to attenuation of direct S-waves, Fourier spectral amplitudes decay as $R^{-1.1}$. Between 70 and 130 km, where the direct-wave is joined by S_mS, spectral amplitudes are approximately constant. Beyond 130 km, corresponding to the Lg-phase, amplitudes decay at a rate that is consistent with $R^{-0.5}$ and $Q = 670\ f^{0.33}$. The findings indicate that postcritical

reflections from the Moho discontinuity play a significant role in determining the shape of the attenuation curve. However the influence of S_mS is subtle, allowing the shape to be approximated by simple functional forms. There is little evidence for any dependence of attenuation on focal depth or tectonic province.

A database for source spectral amplitudes in eastern North America (ENA) is compiled for earthquakes of $3 < M < 7$. The database is developed from the ECTN data, strong-motion data, teleseismic data, and Modified Mercalli Intensity (MMI) data. The inclusion of MMI data is made possible by the finding that the felt area of an earthquake is an accurate measure of its high-frequency spectral level at the source.

The source-spectral data suggest that ENA source spectra may differ significantly from those in western North America (WNA). Numerous studies have shown that WNA source spectra are adequately predicted by the Brune source model, with an average stress parameter of approximately 100 bars. For ENA sources, by contrast, observed high-frequency (5 to 10 Hz) spectral amplitudes correspond to a Brune stress parameter of 200 bars, while intermediate-frequency (1 Hz) amplitudes are matched by a stress parameter of 50 bars. A new empirical source model is proposed for events of $M > 4$. The proposed source model has significant implications for ENA ground motion relations and seismic hazard assessment.

ACKNOWLEDGMENTS

I thank Bob Mereu, Dave Boore, Tom Hanks, Jack Boatwright, Paul Somerville, Bill Joyner, John Adams, Alan Beck, Alan Davenport, Rick Secco and Dieter Weichert for helpful discussions and suggestions. Data were provided by the Geophysics Division of the Geological Survey of Canada; the generous technical support in obtaining and formatting data, provided by Bill Shannon, Bob North, Janet Drysdale and Wayne McNeil is much appreciated. The financial support of Ontario Hydro and the Province of Ontario is gratefully acknowledged. The support I value most of all is that provided by my family: Glenn, Peri and Wesley.

EARTHQUAKE SOURCE SPECTRA AND ATTENUATION IN SOUTHEASTERN CANADA

TABLE OF CONTENTS

LIST OF TABLES

LIST OF FIGURES

LIST OF FREQUENTLY-USED SYMBOLS AND ACRONYMS

A(f) - Fourier amplitude spectrum of ground acceleration (ie. the absolute value of the Fourier transform of an acceleration time series). Also referred to as 'Fourier spectrum', 'spectrum', 'earthquake spectrum', or 'spectral amplitudes'. Note that the units of the acceleration spectrum are those of velocity (ie. mm/s); this is due to the multiplication of the discete Fourier transform by the time increment of the sample data, which converts the discrete transform to the equivalent continuous representation (see Press et al., 1986, p. 389).

A_{HF} - the amplitude of the Fourier acceleration spectrum of the earthquake source (R=1km), for high-frequencies (ie. for $f>>f_o$).

A_{1Hz} - the amplitude of the Fourier acceleration spectrum of the earthquake source (R=1km), for f=1 Hz.

a_f - the felt area of an earthquake (ie. area experiencing MMI levels I to III).

b - attenuation coefficient expressing the apparent rate of geometric attenuation, R^{-b}. See Equation 1.6.

c - attenuation coefficient expressing the apparent rate of anelastic attenuation, 10^{-cR}. See Equation 1.6.

ECTN - Eastern Canada Telemetred Network. See Figure 2.1.

ENA - Eastern North America.

EPRI - Electric Power Research Institute.

f - frequency in Hertz (Hz).

f_o - corner frequency of the Brune source spectrum (which is characterized by a single corner frequency). See Equation 1.2 and Figure 1.1. Note that $A(f) = A_{HF}/2$ at $f=f_o$.

f_A - lowest observed corner frequency in the source spectrum, for spectra exhibiting two corner frequencies.

f_B - highest observed corner frequency in the source spectrum, for spectra exhibiting two corner frequencies.

FFT - Fast Fourier Transform.

h - focal depth of an earthquake (km).

H/V ratio - the ratio of the horizontal to the vertical component of ground motion.

Lg-phase - the most prominent seismic phase in ENA at distances greater than about 200 km. The Lg-phase is comprised of multiply-reflected and refracted shear waves, trapped within the crustal waveguide.

M - moment magnitude, which is defined by the seismic moment of an earthquake. See Equation 1.5.

M_N - Nuttli magnitude, which is defined from the maximum ground displacement, as measured on regional seismograph recordings. Also referred to as Lg magnitude.

MMI - Modified Mercalli Intensity, which is a qualitative measure of an earthquake's effects on people and objects.

M_o - seismic moment, which is a physically-based measure of the size of an earthquake.

NBCC - National Building Code of Canada.

PGA - peak ground acceleration (ie. maximum value of the ground acceleration, in the time domain).

PGV - peak ground velocity (ie. maximum value of the ground velocity, in the time domain).

PSA(f) - pseudo-acceleration, defined as the maximum displacement of a single-degree-of-freedom oscillator of specified frequency and damping, times $(2\pi f)^2$ (Chopra, 1981). Also referred to as 'response spectrum'.

Q - the quality factor, which is inversely proportional to anelastic attenuation. See Equation 3.2.

R - hypocentral distance (km).

R_o - distance at which a transition in the nature of the attenuation curve occurs. See Equation 3.1.

residual - the misfit between an observed data point and the corresponding theoretical prediction for the point. See Equation 3.3 for an example.

S(f) - site response terms, describing the spectral amplification of incoming ground motions according to the local site conditions. See Equation 1.6.

S-waves - shear waves generated by an earthquake and propagated through the earth.

S_mS - the seismic phase consisting of the first post-critical reflection of S-waves from the Moho discontinuity at the base of the crust.

S_n - the seismic phase consisting of waves refracted from the base of the crust.

WNA - Western North America.

$\Delta\sigma$ - Brune stress parameter, describing the required shear stress across the fault surface to produce the high-frequency source spectral amplitude, A_{HF} (see Equation 1.2). Also referred to as the stress drop.

ρ - crustal density (assumed = 2.8 g/cm^3 at the average ENA focal depth of 10 km).

β - shear wave velocity (assumed = 3.8 km/s at the average ENA focal depth of 10 km).

1 - INTRODUCTION

1.1 Overview

An empirical model is developed to describe the generation and propagation of earthquake ground motions in southeastern Canada. The primary data are 1500 seismograms from 100 earthquakes of magnitude 3.0 to 6.5, recorded on the Eastern Canada Telemetred Network (ECTN) in the past decade (Figure 2.1). Most of the ECTN events are of small magnitude (less than 5). To improve the distribution of the data in magnitude, the database is supplemented by available strong-motion data, teleseismic data, and Modified Mercalli Intensity data, for larger events in the same region.

Regression analyses of the Fourier spectra of the ECTN records are used to investigate the shape of the attenuation curve, and determine the Fourier spectrum of ground acceleration near the earthquake source for each event. This allows characterization of the shape and level of earthquake spectra as a function of magnitude and distance.

The importance of earthquake spectra stems from their role in the development of ground motion relations, which describe average ground motion amplitudes (in the time domain) as a function of earthquake magnitude and distance. These relations are in turn a key parameter for seismic hazard analyses of engineered structures. The ground motion parameters of interest are peak ground acceleration and velocity, and response spectra.

In the western U.S. there are sufficient strong-motion data to derive ground motion relations empirically. Eastern relations, by contrast, must be at least partly guided by theoretical models which allow extension of the existing database to larger magnitudes and closer distances. Current ground motion relations for eastern North America (ENA) (Boore and Atkinson, 1987; Toro and McGuire, 1987; EPRI, 1988; Atkinson and Boore, 1990) are based on a stochastic model (Hanks and McGuire, 1981; Boore, 1983), which uses random process theory in conjunction with a seismological model of the source mechanism and propagation processes.

The stochastic method has been validated empirically for the western U.S. (Hanks and McGuire, 1981; Boore, 1983; Boore, 1986; Boore et al., 1992) and is well-accepted in theory. However its application to ENA has been controversial due to uncertainty in the source model for ENA. The source model which is most often used in both the east and the west is the Brune 100-bar stress drop model. Its use in ENA was justified on the basis of limited studies of a half-dozen recent ENA earthquakes (Atkinson, 1984, 1989), conclusions reached from analyses of teleseismic records of historical ENA events (Somerville et al., 1987), and inferences from other regions, primarily the western U.S. The model appears to have worked well for some events, but very poorly for the 1988 Saguenay earthquake (Boore and Atkinson, 1992). In particular, the 100-bar Brune model

predicts high-frequency ground motions from the Saguenay earthquake that are too low by as much as a factor of five. This raises questions concerning the validity of the underlying source model for ENA, and how its definition could be improved. It is the aim of this study to address these questions.

A secondary aim is to investigate the shape of the ground motion attenuation curve. Previous attenuation studies for ENA (eg. Hasegawa, 1985; Gupta and McLaughlin, 1987; Chun et al., 1987; Shin and Herrmann, 1987; Woodgold, 1990) have assumed a steady decay of ground motion amplitudes with distance, with a fixed slope. However theoretical studies of wave propagation within a layered crust suggest that supercritical reflections from the Moho and internal crustal discontinuities should cause systematic elevation of amplitudes in the distance range from approximately 50 to 200 km (Burger et al., 1987; Somerville et al., 1990; Ou and Herrmann, 1990). Empirical evidence for this potential disruption of the attenuation curve is sought, and its impact on our ability to determine source spectra from regional data is assessed.

This study provides the first systematic empirical evaluation of a large suite of ENA source spectra in the frequency band of engineering interest (0.5 to 10 Hz). The spectral model developed provides an important step towards improving estimates of ground motion from future large ENA

earthquakes, and defining variability of predicted ground motions. This will help to reduce uncertainty in seismic hazard estimates for a wide range of facilities.

1.2 Background and Motivation

1.2.1 Ground Motion Relations. Ground motion relations provide the quantitative link between the occurrence of earthquakes and the resulting site ground motions which an engineered structure must be able to withstand. The ground motion may be described by a simple measure of one of its characteristics, such as the peak ground acceleration (PGA) or velocity (PGV), or a frequency-dependent measure such as response spectra - typically the pseudo-acceleration, PSA(f). (PSA(f) is defined as the maximum displacement of a single-degree-of-freedom linear oscillator, of specified frequency and damping, times $(2\pi f)^2$; see Chopra (1981). Note that PSA(f) is a time domain measure.) Response spectra are particularly useful since they are the input parameters for widely-used methods of dynamic analysis, and underlie the seismic design provisions of most North American building codes.

The ground motion parameter of interest is almost always predicted as a function of earthquake magnitude, distance, and sometimes site condition. Relations predict the horizontal component of ground motion since this is the most critical for the majority of structures. The magnitude and distance range of engineering interest is $M > 4$ at

distances less than 200 km. The frequency band of most interest is from about 0.5 Hz to 10 Hz.

Until recently (ie. about 1985), engineering ground motion relations were nearly always obtained by empirical analysis. In western North America (WNA), the analyses were based on regression of recorded strong ground motions. Until the late 1970's, such data were rather limited. Consequently ground motion predictions tended to vary significantly according to the time and method of their development (Idriss, 1979). Since then, however, the ground motion database for California has improved greatly, although there are still significant shortcomings for large ($M > 7$) earthquakes at close ($R < 30$ km) distances. As a result of the improved database, empirical ground motion relations for WNA have 'stabilized', and there is reasonable agreement among different investigators (Joyner and Boore, 1988). Empirical ground motion relations for PGA, PGV, and PSA(f) in WNA are available for rock and soil sites (eg. Joyner and Boore, 1981; 1982; Campbell, 1981a; Sadigh et al., 1986).

In eastern North America (ENA), the development of empirical ground motion relations has been hampered by the lack of a strong motion database. The first ENA ground motion relations were entirely based on indirect data sources, such as observed Modified Mercalli Intensity (MMI) distributions for historical earthquakes, or inferences from

other comparable regions for which there are more strong motion data (eg. Milne and Davenport, 1969; Nuttli and Herrmann, 1978; Hasegawa et al., 1981; Campbell, 1981b).

In the last decade there have been major improvements in the ground motion database for ENA. At the same time, there have been significant advances in understanding the physical basis for observed ground motions. These factors have led to advances in developing ENA ground motion relations.

The advances have followed the work of Hanks and McGuire (1981), who showed that observed PGA in WNA is successfully predicted (ie. within about a factor of two for any individual earthquake) by a simple stochastic model. The model treats high-frequency ground motion as band-limited finite-duration Gaussian noise, with amplitude spectra given by a simple seismological model of the source. Boore (1983) and McGuire et al. (1984) showed that the stochastic model also predicts PGV and PSA(f) in WNA.

Success of the stochastic model in predicting WNA motions led to its application to ENA. Atkinson (1984) showed that the model predicts observed ENA values of PGA and PGV from moderate (M ~ 5) earthquakes, at distances from 10 to 200 km. Boore and Atkinson (1987) and Toro and McGuire (1987) extended the model to the prediction of ENA response spectra, and to the relationship between moment and Nuttli magnitudes (M vs. M_N).

The method begins with the specification of the amplitude of the Fourier spectrum of ground motion, A(f), which can be represented by (Boore, 1983):

$$A(f) = E(f)\ D(f)\ I(f) \qquad (1.1)$$

E(f) specifies the source function. The source function generally adopted for both the east and west has been that given by the Brune (1970) model, which relates the spectrum of the shear radiation to the stress released across the fault surface. The Brune acceleration spectrum increases with the square of frequency, up to a corner frequency, above which near-source spectral amplitudes are constant (Figure 1.1). The Brune model assumes a circular rupture; its radius (or, equivalently, its duration) determines the corner frequency. The high-frequency level of the spectrum is controlled by the stress parameter (Brune, 1970; Boatwright, 1984), while the low-frequency level is, by definition, proportional to the seismic moment. Thus the model provides a simple interpretation of observed spectra in terms of moment magnitude and stress drop. The expression for the basic Brune acceleration spectrum near the source (horizontal component) is (Boore, 1983):

$$E(f) = C\ M_o\ (2\pi f)^2/[1 + (f/f_o)^2] \qquad (1.2)$$

with $C = R_p\ F\ V\ /\ (4\pi\ \beta^3\ R)$, and $f_o = 4.9 \times 10^6 \beta (\Delta\sigma/M_o)^{0.3333}$ where R_p = average radiation pattern (0.55), F = free surface amplification (2.0), V = partition onto two horizontal components (0.71), ρ = crustal density (2.8

g/cm^3), β = shear wave velocity (3.8 km/sec), M_o = seismic moment (dyne-cm), R is distance and $\Delta\sigma$ = stress parameter (bars). Note that the factor C includes the attenuation due to geometric spreading in a homogeneous whole-space. The adopted values of ρ and β are typical mid-crustal values for southeastern Canada (Mereu et al., 1986).

D(f) is a diminution function that models frequency-dependent anelastic attenuation of waves. It is given by:

$$D(f) = P(f,f_m)\ \exp[-\pi\ f\ R\ /\ (Q(f)\ \beta)] \qquad (1.3)$$

where Q is the frequency-dependent quality factor that describes the anelastic attenuation and $P(f,f_m)$ is a high-cut filter formulated in such a way as to rapidly reduce amplitudes for all frequencies above a high frequency cut-off, f_m. In ENA, f_m is typically 40 Hz or greater, and so is not important for the frequency range of this study ($1 \leq f \leq 10$ Hz).

I(f) is a filter used to shape the spectrum to correspond to the particular ground motion measure of interest. If, for example, response spectra are to be computed, I is the response of an oscillator to ground acceleration. For free-field ground motion parameters, I is simply

$$I(f) = 1/(2\ \pi\ f)^p \qquad (1.4)$$

where p = 0 for acceleration, 1 for velocity, or 2 for displacement.

The important unknown variables in the above equations are M_0, $\Delta\sigma$, and R. M_0 is directly related to moment magnitude M, since by definition (Hanks and Kanamori, 1979):

$$M = 2/3 \log M_0 - 10.7 \quad (1.5)$$

The ground motion equations can thus be reduced to functions of magnitude and distance only, by a relationship between M_0 and $\Delta\sigma$.

Figure 1.1 provides an illustration of Fourier spectra of acceleration for the Brune model, showing the dependence on M, R and $\Delta\sigma$. Note that the corner frequency is much lower for the M 6.5 event than for the M 5 event. This is because the corner frequency is inversely proportional to the radius (and duration) of rupture; a larger moment requires a larger fault surface, which takes longer to rupture.

In western North America (WNA), ground motions appear to be well-predicted on average by the Brune model with a constant stress parameter ($\Delta\sigma$) of 100 bars (Hanks and McGuire, 1981; Boore, 1983), or, equivalently, a value of 70 bars, allowing for ground-motion amplifications (beyond those of the free surface) of about a factor of two by the near-surface sedimentary layer, coupled with the appropriate attenuation of high frequencies (Boore et al., 1992).

The relationship between M and $\Delta\sigma$ in ENA has been a controversial topic. Limited studies suggested that stress drops in ENA are comparable to those in WNA, with the

average ENA stress parameter being perhaps a factor of two larger (Kanamori and Anderson, 1975; Atkinson, 1984, 1989; Boore and Atkinson, 1987; Somerville et al., 1987). However it has also been proposed that stress increases with seismic moment in ENA (Nuttli, 1983; Nuttli et al., 1987; Chael, 1987; Chun et al., 1989). ENA source spectra are discussed in more detail in the next section.

The equations given above can be used to specify the Fourier amplitude spectrum of the ground motion, knowing just moment magnitude and distance. For convenience in application, the same model can also be used to compute a relationship between moment magnitude and more commonly reported magnitudes such as Nuttli magnitude, M_N, as described by Boore and Atkinson (1987) and Toro and McGuire (1987). All that is required is appropriate definition of the filter function I(f) of Equation 1.1.

The time domain implementation of the stochastic approach to ground motion prediction (Boore, 1983) begins with the generation of a windowed time series of bandlimited random Gaussian noise with zero mean amplitude; the variance is chosen such that the spectral amplitude is unity on average. The spectrum of the windowed time series is multiplied by the desired amplitude spectrum (A(f) from Equation 1.1). The filtered spectrum is then transformed back into the time domain to yield the simulated earthquake record for the specified magnitude and distance.

By repeated applications of the computations, a predicted 'data set' of ground motions for various magnitudes and distances can be generated. Regression analysis of this simulated data set can then provide simple equations for ground motions as a function of magnitude and distance, for use in engineering analyses. (Alternatively, equations from random process theory may be used to relate the spectral parameters to time-domain ground motion measures.) Relations of this type have been developed for ENA by several investigators (Boore and Atkinson, 1987; Toro and McGuire, 1987; EPRI, 1988).

1.2.2 Source Spectra. Studies of source processes are ideally based on analysis of near-field strong motion records; path effects are minimized, and the high-frequency characteristics from which the details of fault rupture can be discerned have not been greatly attenuated. Detailed studies of WNA source processes are relatively abundant (see Aki, 1982 for a brief review). In ENA, unfortunately, there are insufficient strong motion data to make use of such approaches.

Teleseismic records are a more plentiful source of information for ENA, particularly for large historical earthquakes, and these have been used in deriving gross source properties (Somerville et al., 1987), and estimating source spectra for long periods (greater than 1 sec) (Boatwright and Choy, 1992). However the number of useful

teleseismic records is severely limited by the paucity of events large enough to be recorded at teleseismic distances. Furthermore, the recoverable bandwidth does not extend very far into the frequency range of engineering interest.

The most plentiful source of information for ENA earthquakes are seismographic recordings at regional distances (hundreds of km). The dominant ground motion signal on these records is attributed to the Lg phase, which is composed of a complex suite of supercritical reflections of S-waves, bouncing back and forth between the crust-mantle boundary and the free surface (Herrmann, 1985; Kennett, 1986), and supercritical reflections at internal interfaces (Burger et al., 1987; Ou and Herrmann, 1990). Street and Turcotte (1977) and Shin and Herrmann (1987) have established, through empirical studies and analysis of synthetic seismograms, that the Lg spectrum can be directly related to the source spectrum for S-waves, by correcting for geometric and anelastic attenuation. In fact, it has been argued (Shin and Herrmann, 1987) that the Lg phase is actually a more robust indicator of source properties than near-field data; it samples more of the focal sphere, provides a wide range of incident angles at receiver stations, and the randomness of arrivals avoids the coherence which may lead to resonance effects.

The attenuation corrections to obtain source spectra from Lg spectra can be determined either by examination of

synthetic seismograms (Shin and Herrmann, 1987; Ou and Herrmann, 1990) or by regression analysis. Studies indicate that these approaches provide similar results (Boore and Atkinson, 1992; Atkinson and Somerville, 1992). Other factors for which corrections are required are radiation pattern (usually treated as an average over the focal sphere), free surface amplification, and vectorial partitioning of energy onto horizontal components, where applicable.

The 1988 Saguenay earthquake highlights current uncertainties regarding source spectra. As shown in Figure 1.2, the observed spectrum deviates dramatically from the Brune shape. The high-frequency amplitudes are very large relative to the seismic moment, implying a stress parameter of more than 500 bars. However a 500-bar stress parameter would grossly overestimate amplitudes at intermediate frequencies. This could imply that the Brune model is an inadequate representation of ENA earthquakes in general, or that there is large variability of spectra about the model.

Other source models which have been proposed for ENA (Nuttli, 1983; Nuttli et al., 1987) feature an increase in stress drop with increasing seismic moment. This would be in distinct contrast to scaling in western North America, for which plentiful strong motion data have established a constant stress parameter (Kanamori and Anderson, 1975; Hanks and McGuire, 1981; Boore, 1983). The evidence in

support of an increasing stress drop model for ENA is indirect, based on arguments concerning relations between magnitude scales (Nuttli, 1983). It does not appear compatible with more direct evidence from teleseismic data (Somerville et al., 1987; Boatwright and Choy, 1992) which suggests a constant stress drop in ENA. However, it would provide some explanation for the large high-frequency amplitudes of the Saguenay earthquake.

Recent studies of teleseismic data from large intra-plate earthquakes (Boatwright and Choy, 1992) suggest that the issue of stress drop in ENA is obscured, and perhaps overshadowed, by departures of observed spectra from the Brune spectral shape. They find that the spectra generally exhibit two corner frequencies (the Saguenay earthquake being a good example of this phenomenon). The concept of a spectral model that involves two corner frequencies is not new. Savage (1972) showed that a two-corner spectrum results from the Haskell (1969) fault model of a rectangular (as opposed to circular) dislocation; the lower corner frequency is related to fault length and the higher corner frequency is related to fault width. Dynamic models implying two corner frequencies have been discussed by Boatwright (1982, 1988), Aki (1982) and Joyner (1984), among others. The lower corner may be related to the overall rupture duration (generally associated with fault length) while the higher corner may reflect some 'roughness'

characteristic, such as the spacing of asperities or barriers on the fault surface. Not until the Saguenay earthquake, however, has it been fully appreciated that a two-corner source spectrum may have significantly different implications for ground motions in ENA than the Brune representation.

In general, it appears that current data are insufficient to allow definitive conclusions on the shape or levels of ENA source spectra. The current empirical study is thus much needed.

1.2.3 Attenuation. The attenuation of spectral amplitudes with distance from the source has been relatively well-studied in eastern Canada. Regression analyses have been used to study attenuation along Canadian Shield travel paths (Hasegawa, 1985) and Appalachian paths (Shin and Herrmann, 1987). Alternative techniques to the regression approach have also been explored (Chun et al., 1987), and the regional variation of attenuation within eastern Canada has been investigated (Woodgold, 1990).

Attenuation studies are generally based on fitting data to an equation of the form:

$$\log A_{ij}(f) = \log A_{io}(f) - b \log R_{ij} - c(f)\, R_{ij} + \log S_j(f) \qquad (1.6)$$

where $A_{ij}(f)$ is the observed spectral amplitude of earthquake i at station j, for frequency f, $A_{io}(f)$ is the source amplitude of earthquake i, R is hypocentral distance,

b is the geometric spreading coefficient, c(f) is the coefficient of anelastic attenuation, and $S_j(f)$ is the site response term for station j (eg. Hasegawa, 1985; Shin and Herrmann, 1987; Chun et al., 1987; Atkinson, 1989; Woodgold, 1990). The anelastic coefficient, c(f), is inversely related to the quality factor, Q. Q is believed to be attributable to intrinsic absorption, plus the frequency-dependent effects of scattering (Dainty, 1981). Equation 1.6 may be applied to any ground motion phase; the shear-wave phases are of most engineering interest since their amplitudes are typically about 5 times larger than the P-wave amplitudes.

The shear-wave energy is carried by the direct-S wave at distances less than approximately 60 km. Between 60 and 150 km, the direct wave is joined by the first postcritical reflections from internal crustal interfaces and the Moho discontinuity (Burger et al., 1987). At regional distances (200 to 1000 km) the dominant phase is the Lg-phase, comprised of multiple postcritical reflections of S-waves trapped within the crustal waveguide (Kennett, 1986). Wave propagation in a layered crustal model is illustrated in Figure 1.3. The S_n phase (refracted S-wave from the base of the crust) is also significant at regional distances, particularly for frequencies above 5 Hz (Shin and Herrmann, 1987).

Past attenuation studies of the Fourier spectrum have assumed that, for distances less than 100 km from the source, the geometric spreading coefficient b = 1.0, the theoretical value for geometric spreading in a whole-space. At distances beyond approximately 100 km, b was assumed to equal 0.5, the theoretical value for surface waves in a half-space (Hasegawa, 1985; Shin and Herrmann, 1987; Chun et al., 1987). The validity of assuming a simple underlying shape for the attenuation curve, with specific geometric spreading coefficient values of 1.0 and 0.5 for near-source and regional distances, respectively, has recently been called into question. The wave propagation studies of Burger et al. (1987) and Ou and Herrmann (1990) indicate that the expected shape of amplitude decay for simple layered crustal models is complex. Layering in the crust causes direct-wave amplitudes to decay more rapidly than R^{-1}. Then, as the direct arrivals are joined by post-critical reflections off the Moho and intracrustal discontinuities, there may be distance ranges where amplitudes actually increase with distance, between approximately 50 km and 200 km. This is illustrated in Figure 1.3. Beyond 200 km, geometric attenuation may be significantly greater than $R^{-0.5}$, depending on the nature of the crust-mantle transition (Burger et al., 1987; Bowman and Kennett, 1991). A sharp velocity contrast traps energy within the crustal waveguide, while a velocity gradient

allows leakage into the mantle, increasing the apparent geometric attenuation. Further complexity may be introduced by crustal heterogeneity, which causes significant perturbations of travel paths and erratic, indeterminate amplitude variations (Ojo and Mereu, 1986).

Empirical evidence on the shape of the attenuation curve is often ambiguous. It is not easy to separate the attenuation from other factors which are equally important in determining the recorded ground motions, such as source effects, site response, radiation pattern and directivity. Interpretation of empirical data is also obscured by the large random variability (about a factor of two) that is typical for ground motion amplitudes. The large scatter of data allows a trade-off between the geometric spreading and anelastic attenuation coefficients; in essence, the data cannot distinguish between a steep slope with little curvature, and a gentle slope with significant curvature.

To my knowledge, there is no unambiguous empirical evidence regarding the 'true' value for the geometric spreading coefficient in eastern North America, at either near-source or regional distances. Neither is there compelling empirical evidence concerning the impact of the S_mS arrival on attenuation of earthquake ground motion amplitudes in the 'transition zone' from direct-wave to Lg-wave behaviour. However, reflection/refraction studies (eg. Mereu et al., 1986) clearly demonstrate that S_mS is a

significant arrival in the distance range from 90 to 150 km, as shown in Figure 1.4.

It is important to know the 'true' shape of the average attenuation curve for two reasons. First, without this knowledge we cannot reliably infer source properties from distant observations. Second, the shape of the curve may be an important consideration in seismic hazard analyses, particularly for sites 50 to 200 km from an active seismic source zone.

1.3 Organization of Thesis

The remainder of this thesis is organized as follows. In Chapter 2, I describe the ECTN dataset and the processing procedures used to obtain the Fourier spectrum of ground acceleration for all records. Chapter 2 also examines two ground motion parameters of interest in the development of predictive ground motion relations (and used in Chapters 4 and 5): the horizontal-to-vertical component ratio (H/V), and the distance-dependence of the duration of shaking. The regression analyses used to invert the observations to determine the Fourier spectrum of ground acceleration at the source, the regional attenuation, and the station amplification factors, are presented in Chapter 3; attenuation issues are discussed in some detail. In Chapter 4 simulated ground motions based on the derived source spectra and attenuation are compared to actual records for four example events; this provides a demonstration of the

veracity and utility of the regression results. The source spectra obtained from the regressions are examined in Chapter 5, and supplemented by other data sources, in order to define an empirical source spectral model as a function of magnitude. In Chapter 6 the results are summarized and their implications for ground motion relations and seismic hazard evaluation discussed.

Appendices A and B are lists of the Fourier spectra of ground acceleration for all ECTN records, and the source parameters determined from the regression analyses. Appendix C provides key computer programs used to compute the spectra, do regression analyses and Monte Carlo simulations, and simulate ground motions in the time domain.

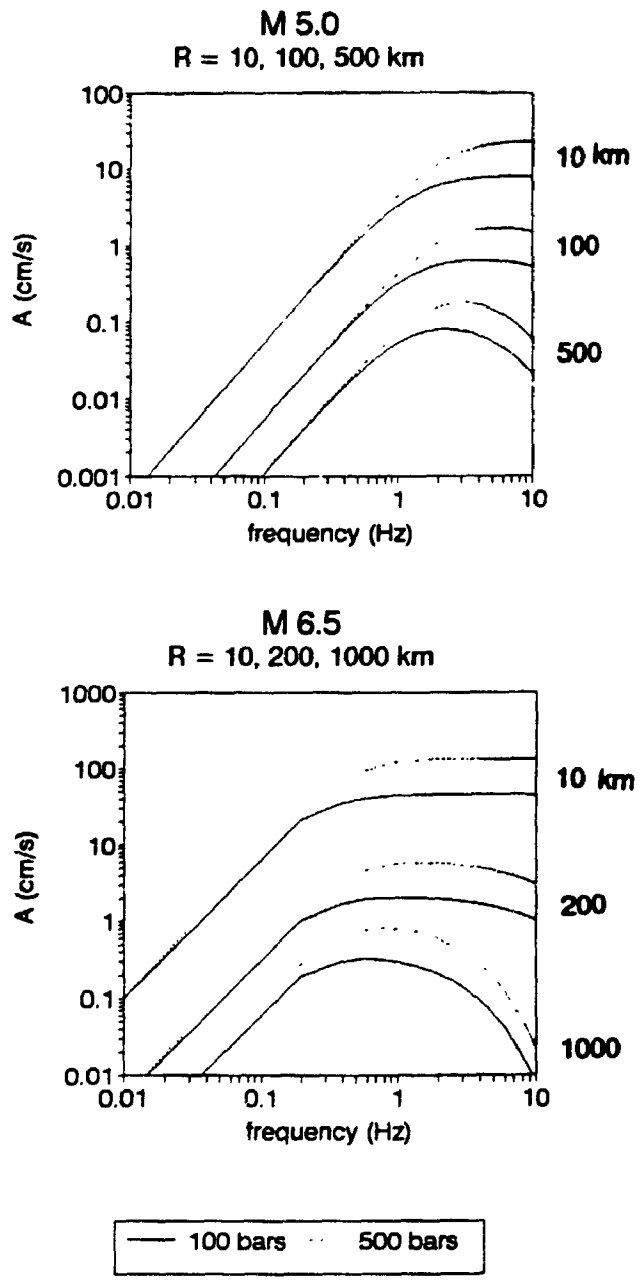

FIGURE 1.1 - Idealized Brune spectra, showing the influence of magnitude, distance and stress parameter on ground motion amplitudes. Top frame plots M 5 spectra for stress parameters of 100 and 500 bars, at distances of 10, 100 and 500 km. Lower frame plots M 6.5 spectra for stress parameters of 100 and 500 bars, at distances of 10, 200 and 1000 km. Figure assumes geometric and anelastic attenuation model of this study (Chapter 3). For a stress parameter of 100 bars, the corner frequency is 1.2 Hz for M 5 and 0.2 Hz for M 6.5.

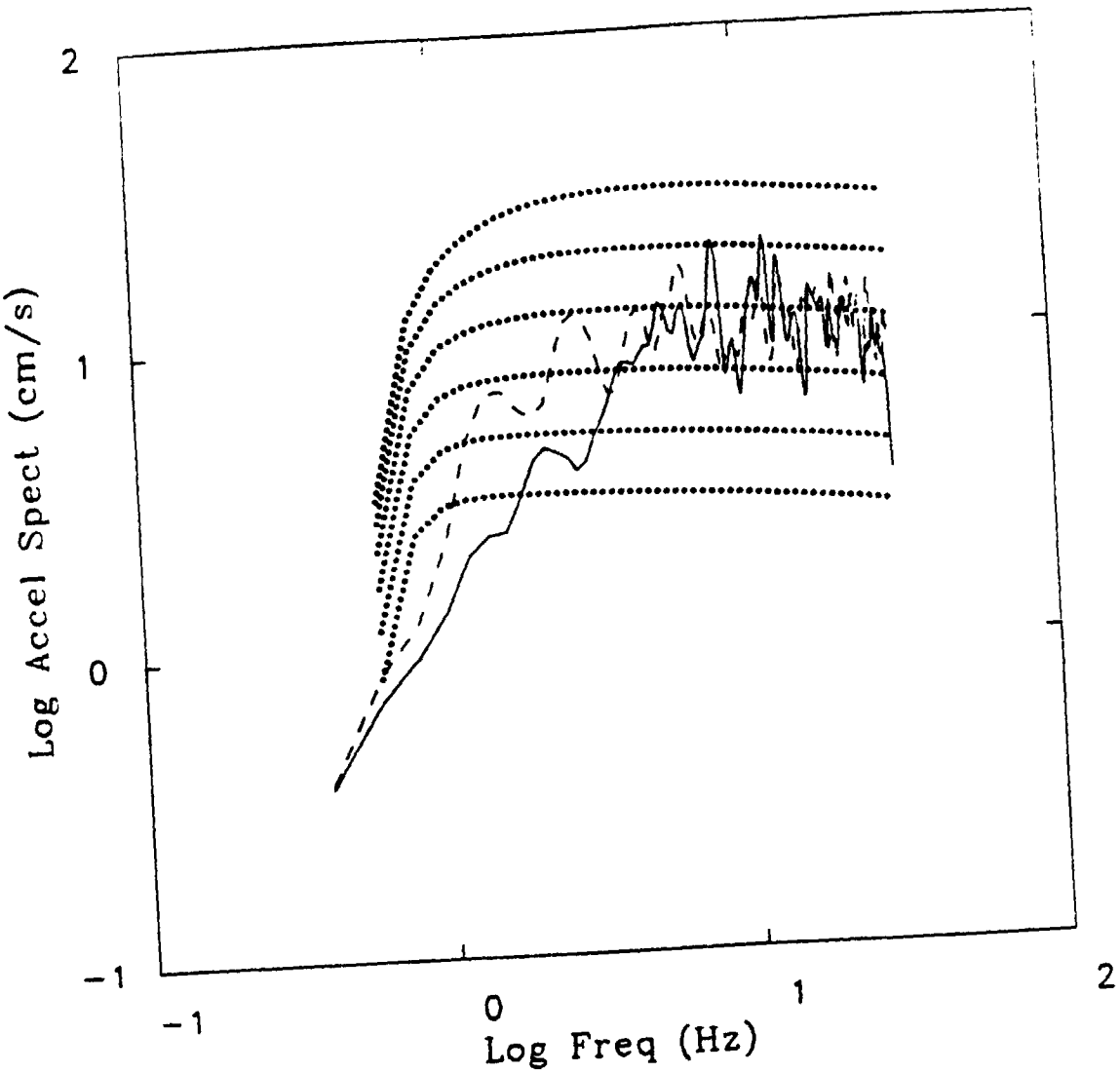

FIGURE 1.2 - Example of observed spectra (horizontal components) for the Saguenay earthquake, compared to theoretical Brune spectra for stress parameters of 50 (lowest curve), 100, 200, 400, 800 and 1600 bars (from Boore and Atkinson, 1992).

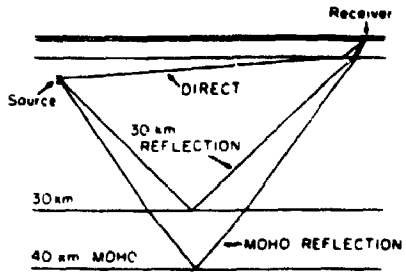

a

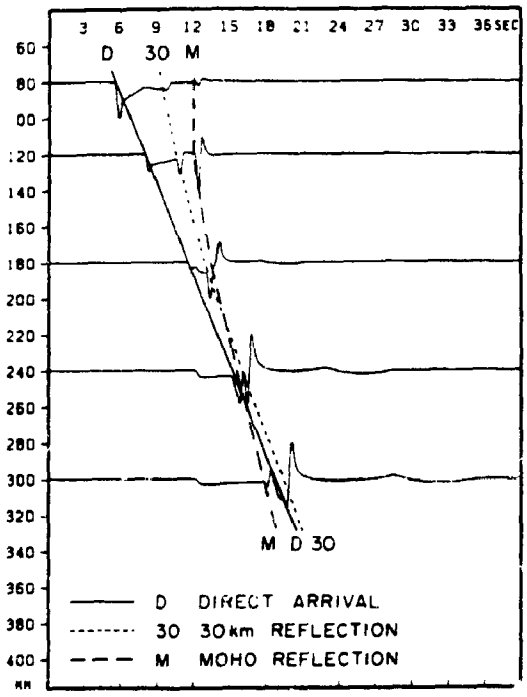

b

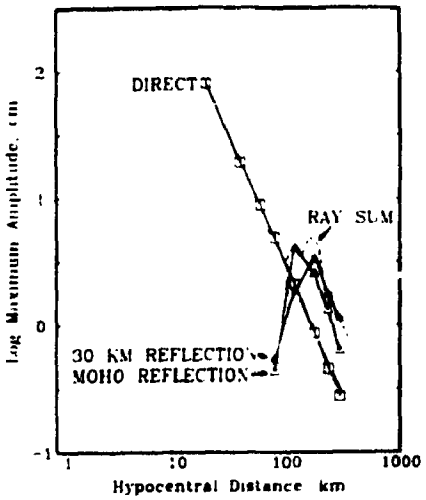

c

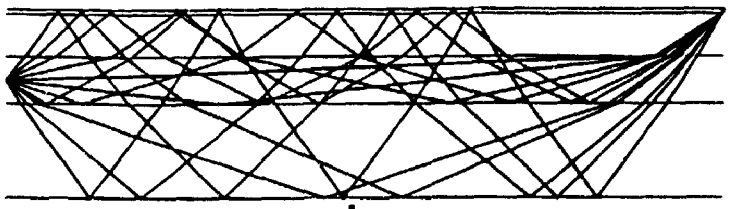

d

FIGURE 1.3 - Schematic illustration of wave propagation in a layered crust: (a) ray paths for distances of the order of 100 km, showing the direct and reflected ray paths (from Burger et al., 1987); (b) synthetic tangential displacement seismograms calculated for the three rays shown in (a) (from Burger et al., 1987); (c) peak ground displacement as a function of distance for the three individual rays (solid) and the ray sum (dashed) from the synthetic seismograms shown in (b) (from Burger et al., 1987); (d) ray diagram for a receiver at a distance of 300 km, for a mid-crustal source (from Ou and Herrmann, 1990).

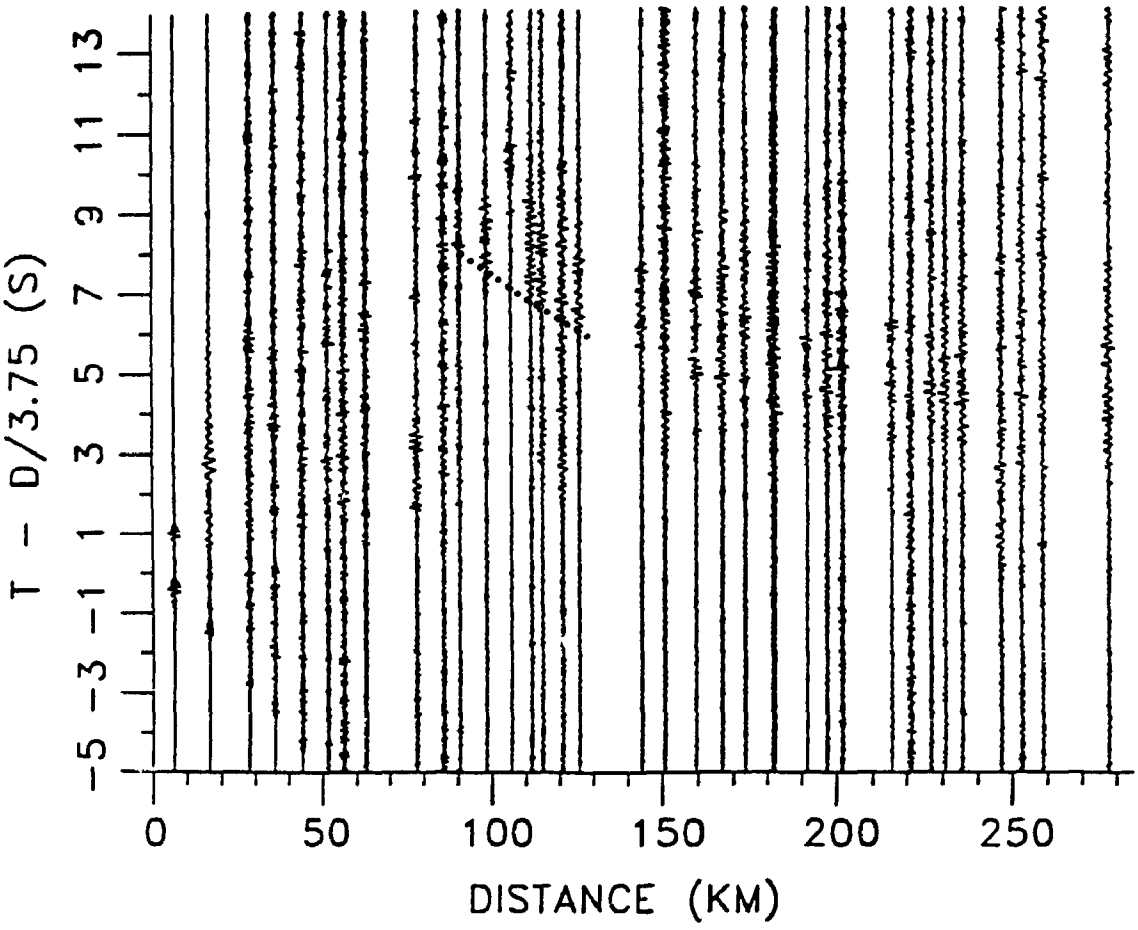

FIGURE 1.4 - S_mS information from line CD of the COCRUST experiment, located in the Baskatong Reservoir area of western Quebec; dotted line indicates S_mS arrival (after Mereu et al., 1986).

2 - DATABASE AND PROCESSING PROCEDURES

2.1 Earthquake Data

The earthquake database is comprised of approximately 100 events recorded on the ECTN. The locations of study events and ECTN stations are shown on Figure 2.1. The distribution of earthquakes in magnitude and distance is shown on Figure 2.2. Most stations record only vertical-component ground motions; a few record three components. The seismograms are digitally-recorded on instruments which have a velocity response that is approximately flat between 1 and 10 Hz. Frequencies above 15 Hz and below 1 Hz are sharply attenuated by band-pass filters (Munro et al., 1986). The amplitude of the required instrument correction to obtain the spectrum of ground acceleration from the Fourier transform of the recorded velocity time series is shown on Figure 2.3. Note that the plotted factors include the multiplication by $2\pi f$ (applied in Equations 2.1 and 2.2) which transforms velocity to acceleration; this factor was included on the plot to more accurately portray the net influence the instrument-correction procedure will have on both signal and noise.

Table 2.1 lists the station locations and instrumentation. Most instruments sample at 60 samples/sec; all but one (station WEO, near Toronto) are located on rock. The dynamic range allows the reliable recovery of ground motion spectra for events with peak ground velocity in the

approximate range 0.0001 to 2 mm/s. (Note: The minimum detectable ground velocity is a factor of 10 lower than 0.0001 mm/s, but spectral amplitudes for such small motions cannot be reliably estimated over the entire 1 to 10 Hz frequency band.)

2.2 Signal Window for Analysis

For each record the Fourier spectrum of ground acceleration for the shear wave phases (S, S_mS, Lg, S_n, etc.) is obtained, so that we can study the propagation of the shear wave energy that may cause damage to structures. The time interval containing all significant shear phases is referred to as the 'S-window'. The S-window includes the direct arrival for near distances. At greater distances it also includes reflections from internal crustal interfaces and the Moho discontinuity. At distances of several hundred km, it includes the S_n and Lg phases. For each record I determine the S-window as that which begins with the first discernable S-arrival and continues until approximately 90% of the total S-energy has been accumulated (as indicated by the cumulative square of the velocity). Figure 2.4 illustrates the typical content of the S-window for a range of hypocentral distances.

The inclusion of S_n in the shear wave spectrum is a departure from past practice, which has been to isolate Lg whenever possible (eg. Chun et al., 1987; Shin and Herrmann, 1987; Ou and Herrmann, 1990). The difficulty with

attempting to isolate Lg is that it follows the S_n arrival too closely in time to allow separation, for observations recorded at distances less than about 500 km. It is inconsistent to separate S_n where possible (ie. R > 500 km), while including it of necessity over a broad distance range (ie. 200 to 500 km); this inconsistency may bias attenuation estimates. Furthermore, the spectral amplitudes of the S_n phase sometimes exceed those of the Lg phase over a significant frequency band (5 to 10 Hz), implying that the phase may carry significant information concerning the overall energy content of the source (see station GGN on Figure 2.4, for example). I believe a less-biased 'snapshot' of the overall shear-wave spectrum is obtained by consistently including all discernable S-phases.

2.3 Computation of Fourier Spectra

Following Chael (1987), I use a lag-window spectral technique to obtain stable estimates of the Fourier spectrum. The S-window is subdivided into 256-sample intervals, with 50% overlap between segments. This segment length is about 4 seconds in duration for a sampling rate of 60 samples/sec, and was found to provide the optimal balance between greatest stability of spectral estimates, and reliable recovery of low-frequency (1 Hz) amplitudes. (For very short signals, 1 segment or less in duration, the segment length is halved.) For each segment, a 5% cosine-taper is applied to both ends of the time series and the

spectrum obtained by Fast Fourier Transform. The amplitude of the acceleration spectrum is obtained as:

$$a(f) = 2 \pi f \{(\Sigma v_i^2(f)) \cdot T / (n \cdot t)\}^{\frac{1}{2}} \qquad (2.1)$$

where v(f) is the amplitude of the Fourier velocity spectrum and T is the duration of the S-window, which includes n data segments of 256-samples, each with duration t. The averaging of spectral amplitudes over the segments is based on the square of the spectral velocities to ensure energy conservation.

The earthquake spectra were corrected for the complex instrument response using the well-calibrated ECTN transfer functions (Munro et al., 1986; see Figure 2.3). Finally, the resulting acceleration spectra were logarithmically-averaged over frequency intervals of 0.1 log units, enabling the tabulation of Fourier spectral acceleration for each record at log f = 0 0, 0.1, 0.2,..., 1.0. At this stage, signal-to-noise ratio was evaluated for each record. The noise spectrum, N(f), was estimated from a one-segment time interval immediately preceding the S-window, processed in the same way as the signal. The noise power was normalized to the same duration as the signal:

$$N(f) = 2 \pi f \{v_N^2(f) \cdot T / t\}^{\frac{1}{2}} \qquad (2.2)$$

where v_N is the amplitude of the Fourier velocity spectrum of the noise sample.

Records with a signal-to-noise ratio less than 2 were excluded from further analyses. For the included records, the noise power was subtracted from the signal power:

$$A(f) = \{a^2(f) - N^2(f)\}^{\frac{1}{2}} \qquad (2.3)$$

where A(f) is the noise-corrected Fourier amplitude of acceleration. Equation 2.3 was not applied for stations less than 100 km from the source, for which the noise segment would contain much of the P-signal, resulting in serious overestimation of the actual noise; for these close-in records the noise power was assumed to be negligible. Appendix A tabulates the computed spectral amplitudes of acceleration (A(f)) for all records.

Figure 2.5 shows the computed acceleration spectra (A(f)) as a function of frequency for a number of events. Observe that the processing has removed almost all of the random peak-to-trough variability. The acceleration spectra have the general shape that we expect based on the Brune model (Figure 1.1). For small events the corner frequency lies near the high-frequency end of the ECTN bandwidth, while for large events the corner is near the low-frequency end of the bandwidth.

Acceleration spectra are plotted as a function of distance for the same events on Figure 2.6, for two frequencies. Overall, there is a steady decrease in amplitudes with distance, although in some cases amplitudes appear to be elevated in certain distance ranges; this

result is expected in light of the wave propagation studies of Somerville et al. (1987). There is a large component of station-to-station variability in ground motions; this variability includes any relative differences in site response between the stations (factors S_j of Equation 1.6).

The ability of the processing procedures to reliably recover spectral amplitudes, and also determine the underlying source, path and site effects, was validated by application of the procedures to simulated records for which the underlying spectra are known. This exercise is described in Section 4.

2.4 H/V Ratio for Hard Rock Sites

The ratio of the horizontal to the vertical component of ground motion (H/V) is an important parameter for two reasons. First, most seismograph stations in ENA record only the vertical component, but the horizontal component is of primary interest in seismological and engineering studies. This often necessitates the conversion of observed vertical-component ground motion data to equivalent horizontal-component data. For example, Boore and Atkinson (1987) used an average H/V ratio (=1.4) to enable a comparison of horizontal-component ground motion relations with observed vertical-component data. A second use for the H/V ratio is in engineering design analyses: vertical-component 'design ground motions' are usually obtained from

the horizontal-component 'design ground motions', the latter being derived from a seismic hazard analysis.

Most ECTN stations record only the vertical component but there are six stations in the Charlevoix area and one in western Quebec recording three components. All of the three-component stations are located on hard rock. In this section the H/V ratio for hard-rock sites is derived using the three-component subset of the ECTN Fourier spectra database. The H/V ratio was calculated as a function of frequency from the Fourier spectra for each horizontal-component record; there are 130 three-component recordings, for a total of 260 frequency-dependent H/V values. The log of the H/V ratio for each horizontal component record was computed as the difference between the log of the Fourier amplitude of the horizontal component and the log of the Fourier amplitude of the corresponding vertical component. H/V was also calculated based on an alternate (energy-conservation) definition, in which $H = ((H_1^2 + H_2^2)/2)^{\frac{1}{2}}$ (where H_1 and H_2 are the values corresponding to each of two horizontal components), but this did not produce significantly different estimates.

The site-dependence of H/V was checked by averaging estimates on a site-by-site basis. Only one station had an H/V ratio that was significantly different (ie. by more than 0.05 log units) from the average over the entire group. The anomalous station, A61 in the Charlevoix region, had H/V

ratios that exceeded the average by 0.15 log units (factor of 1.4) at high frequencies.

The mean H/V ratio, and its 90% confidence limits, are shown on Figure 2.7 as a function of frequency (excluding station A61). The least-squares fit to the data is given by:

$$\log H/V = 0.0519 + 0.117 \log f \qquad (2.4)$$

The H/V ratio is independent of distance, as shown on Figure 2.8. Figure 2.8 also illustrates the large amount of scatter in H/V ratios. The standard deviation of H/V is 0.24 log units at 1 Hz, decreasing steadily with frequency to 0.17 log units at 10 Hz. Note that the confidence limits on the mean are small despite this scatter of individual estimates, due to the relatively large number of recordings.

I conclude that the H/V ratio for the hard-rock ECTN sites increases with frequency, from a value of 1.1 (0.05 log units) at 1 Hz to a value of 1.5 (0.17 log units) at 10 Hz. This result is in agreement with the study of Gupta and McLaughlin (1987); they found that H/V for average sites in the eastern United States increases with frequency from 1.5 at 1 Hz to 1.7 at 5 Hz, but that hard-rock sites had lower H/V ratios. Thus Equation 2.4 is probably applicable to most hard-rock sites in ENA.

2.5 The Distance-Dependence of Duration

The duration of ground motion plays an important role in predictive ground motion relations for ENA. Recent

relations (eg. Boore and Atkinson, 1987; Toro and McGuire, 1987; EPRI, 1988; Atkinson and Boore, 1990) have been based on a model in which time-domain amplitudes are predicted from frequency-domain amplitudes using Parseval's Theorem and random process theory. For a given Fourier spectrum, the peak ground motions and response spectral amplitudes are determined by the duration of motion, with longer durations resulting in smaller ground motion amplitudes in the time domain (because the total energy is spread out over a longer window).

Current ENA relations all assume that the duration of motion, at distances greater than 200 km, is given by:

$$T = 1/f_o + 0.05\ R \qquad (2.5)$$

where f_o is the corner frequency of the source spectrum (usually taken from the Brune (1970) source model), R is hypocentral distance in km, and T is duration in seconds. In Equation 2.5, the first term represents the source duration, while the second term represents the effects of wave propagation in a layered crust, according to theoretical studies (Herrmann, 1985).

There has been some controversy concerning the applicability of Equation 2.5 for distances less than about 60 km, for which the signal consists entirely of the direct wave. If scattering does not have a significant effect, then one might expect a constant duration in this distance range. Boore and Atkinson (1987) and Atkinson and Boore

(1990) (these papers will be referred to collectively as BA) assumed Equation 2.5 was valid over all distances, while Toro and McGuire (1987) and EPRI (1988) (these papers will be referred to collectively as EPRI) assumed a constant duration of $1/f_o$ for R < 100 km. As a result of this difference, the EPRI ground motion relations predict amplitudes that are significantly larger than those predicted by the BA relations, for distances less than 100 km.

In this section I compare the predictions of Equation 2.5 to the observed durations of the ECTN S-wave trains. The great majority of the observations are for M_N < 5, and so the source durations are small, generally less than 1 second. The distance term of Equation 2.5 will therefore swamp the source term in nearly all cases, allowing us to make the simplifying assumption of a constant source duration (about 0.5 seconds) for all events.

The duration of each record could be defined in a number of ways. My interest here is in defining the appropriate duration to use in the context of random process theory, as it is applied in the development of ground motion relations (BA, EPRI). I therefore compute the duration required to match the observed relationship between time-domain and frequency-domain amplitudes, at least for the central part of the ECTN's 1 to 10 Hz frequency band (ie.

characterized by velocity). I refer to this as the rms duration. From Parseval's Theorem:

$$v_{rms} = [2/T \int_0^{\infty} V^2(f)\ df]^{\frac{1}{2}} \qquad (2.6)$$

where v_{rms} is the root-mean-square velocity, V(f) is the absolute value of the Fourier spectrum of velocity, and f is frequency (Hz).

Most of the contributions to the integral in Equation 2.6 come from within the ECTN bandwidth of 1 to 10 Hz, since the velocity spectrum peaks at f_o, which is near the center of the bandwidth for most of the records. The remaining contributions to the integral are estimated by assuming that:

$$V(f) = V(f_1)\ f\ /\ f_1 \quad \text{for} \quad f < f_1 \qquad (2.7a)$$

$$V(f) = V(f_2)\ f_2\ /\ f \quad \text{for} \quad f > f_2 \qquad (2.7b)$$

where f_1 and f_2 are the lower and upper frequencies of the bandwidth. Equation 2.7 is based on the Brune spectral shape, for 1 Hz < f_o < 10 Hz. Examination of velocity spectra for a variety of records confirmed that Equation 2.7 is a reasonable extrapolation. Contributions to the integral may be assumed negligible for frequencies above 25 Hz.

From random process theory:

$$v_p = P\ v_{rms} \qquad (2.8)$$

where v_p is the peak ground velocity, and P is the peak factor, given by (Cartwright and Longuet-Higgins, 1956):

$$P = (2\ \ln(N))^{\frac{1}{2}} + 0.5772/(2\ \ln(N))^{\frac{1}{2}} \qquad (2.9)$$

N is the number of extrema, taken as:

$$N = 2 F T \qquad (2.10)$$

where F is the predominant frequency. I defined F as the frequency at which v_p was measured. F could also be defined from the number of zero-crossings in the strong portion of the record; use of this alternative definition provides nearly identical results in terms of implied durations.

For each record, the parameters v_p and F were measured from the instrument-corrected seismograms, while the integral over V(f) (Equation 2.6) was obtained from the Fourier velocity spectrum. With these parameters defined, T was computed using Equations 2.6 through 2.10. This is very similar to the strong-motion duration definition of Vanmarcke and Lai (1980), which was based on the rms acceleration.

The computed durations are plotted for distances of R < 500 km on Figure 2.9. The distance range from 10 to 100 km is shown in more detail on Figure 2.10 (a log scale has been used for duration on this figure, to improve the clarity of the T < 5 sec range). In each figure a line representing Equation 2.5 is plotted, for an assumed source duration of 0.5 seconds.

Durations scatter widely but clearly increase with distance for R > 10 km, in a manner which is consistent with the distance-dependent duration term of 0.05 R suggested on theoretical grounds by Herrmann (1985). Comparing the ratio

of the observed rms durations to Equation 2.5 (with $1/f_o$ = 0.5), the mean of the ratios is 1.1, and its standard deviation is 1.1. The mean trend of the duration data with distance is shown on Figure 2.11 for 10 < R < 1000 km. The overall trend is a steady increase in duration with distance, but there appears to be a distance range, from approximately 60 to 250 km, for which the duration is nearly constant (= 10 sec on average).

I conclude that Equation 2.5 is a reasonable approximation of observed durations in ENA over all distances from 10 to 1000 km, in the context of the random process model used in the development of ground motion relations.

TABLE 2.1 - ECTN station locations and instrumentation

Coordinates		Stn.	Instrument	
46.37	-75.97	MIQ	1	
53.81	-77.43	LDQ	2	but with dynamic range of 1
45.39	-75.72	OTT	1	
45.5	-73.62	MNT	1	
50.53	-68.77	MNQ	1	was 1, 2 after 5/3/86
46.36	-72.37	GNT	1	
45.46	-76.22	FHO	2	
45.7	-75.48	GAC	5	
47.34	-70.01	LPQ	2	
45.38	-71.93	SBQ	2	was 2, 3 after 3/1/87
48.23	-77.97	VDQ	2	
45.	-75.28	WBO	2	
45.99	-77.45	CKO	2	
46.22	-74.56	TRQ	2	
46.61	-75.86	GRQ	2	
53.8	-75.72	JAQ	2	
48.91	-67.11	GSQ	2	
47.54	-68.24	EBN	2	
45.12	-66.82	GGN	2	
45.85	-64.81	LMN	2	
46.84	-66.37	KLN	2	
49.19	-68.39	HTQ	2	
44.02	-78.37	WEO	2	was 2, 3 after 24/11/88
46.40	-81.01	SUO	3	
46.64	-79.07	EEO	1	was 1, 3 after 27/10/87
46.68	-72.78	DPQ	3	
46.44	-81.50	SZO	3	
46.73	-81.00	SWO	3	
47.24	-70.20	A11	4	
47.47	-70.01	A16	4	
47.70	-69.69	A21	4	
47.46	-70.41	A54	4	
47.69	-70.09	A61	4	
47.83	-69.89	A64	4	

Notes: 1 = Mark I, 60 samples/sec, vertical component
2 = Mark II, 60 samples/sec, vertical component
3 = Mark III, 60 samples/sec, vertical component
4 = Mark III, 80 samples/sec, 3 components
5 = SRO, 30 samples/sec, 3 components

Coordinates quoted are latitude (degrees N) and longitude (degrees W).

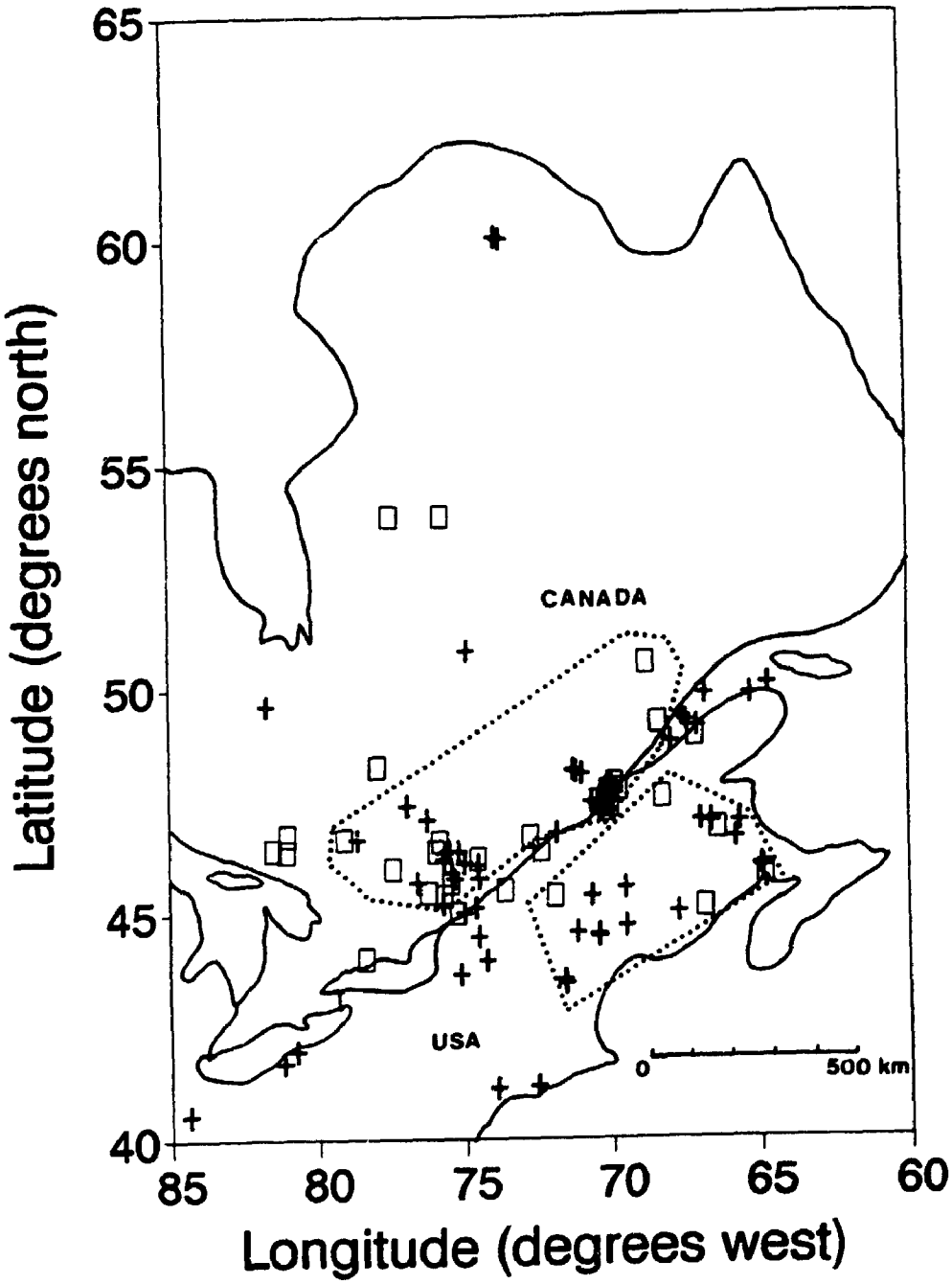

FIGURE 2.1 - Locations of ECTN stations (squares) and study earthquakes (crosses). Dotted lines delineate areas used for Grenville (north) and Appalachian (south) tectonic province travel path subsets, discussed in text.

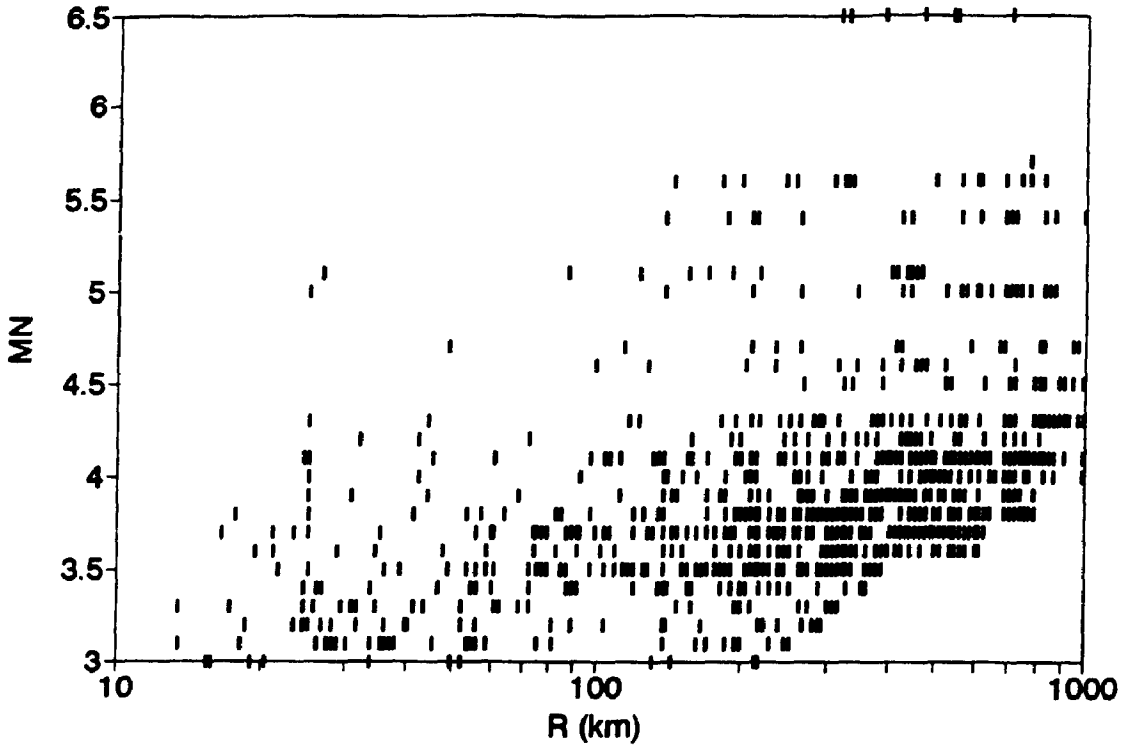

FIGURE 2.2 - Distribution of study earthquakes by magnitude (M_N) and distance (R).

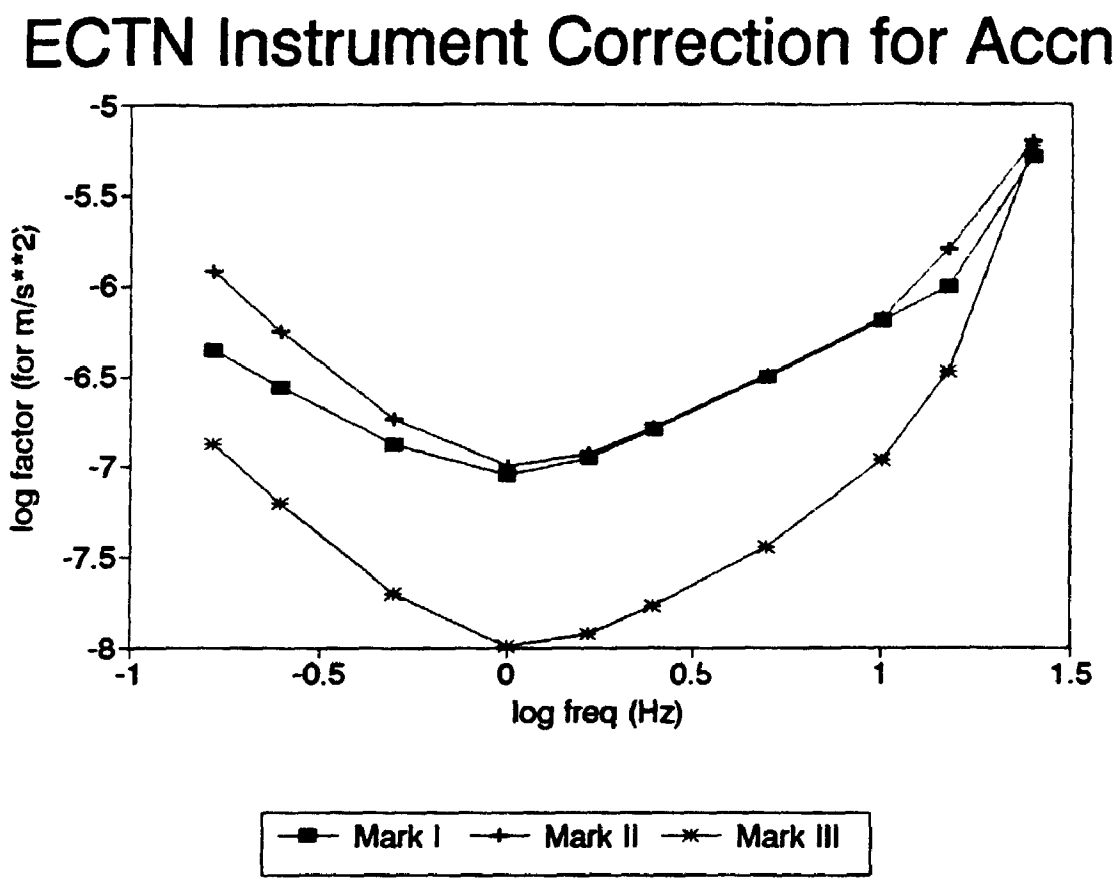

FIGURE 2.3 - Correction factor to obtain Fourier amplitude of ground acceleration from Fourier amplitude of recorded velocity (= instrument response x $2\pi f$), for the three types of ECTN instruments (Mark I, Mark II and Mark III).

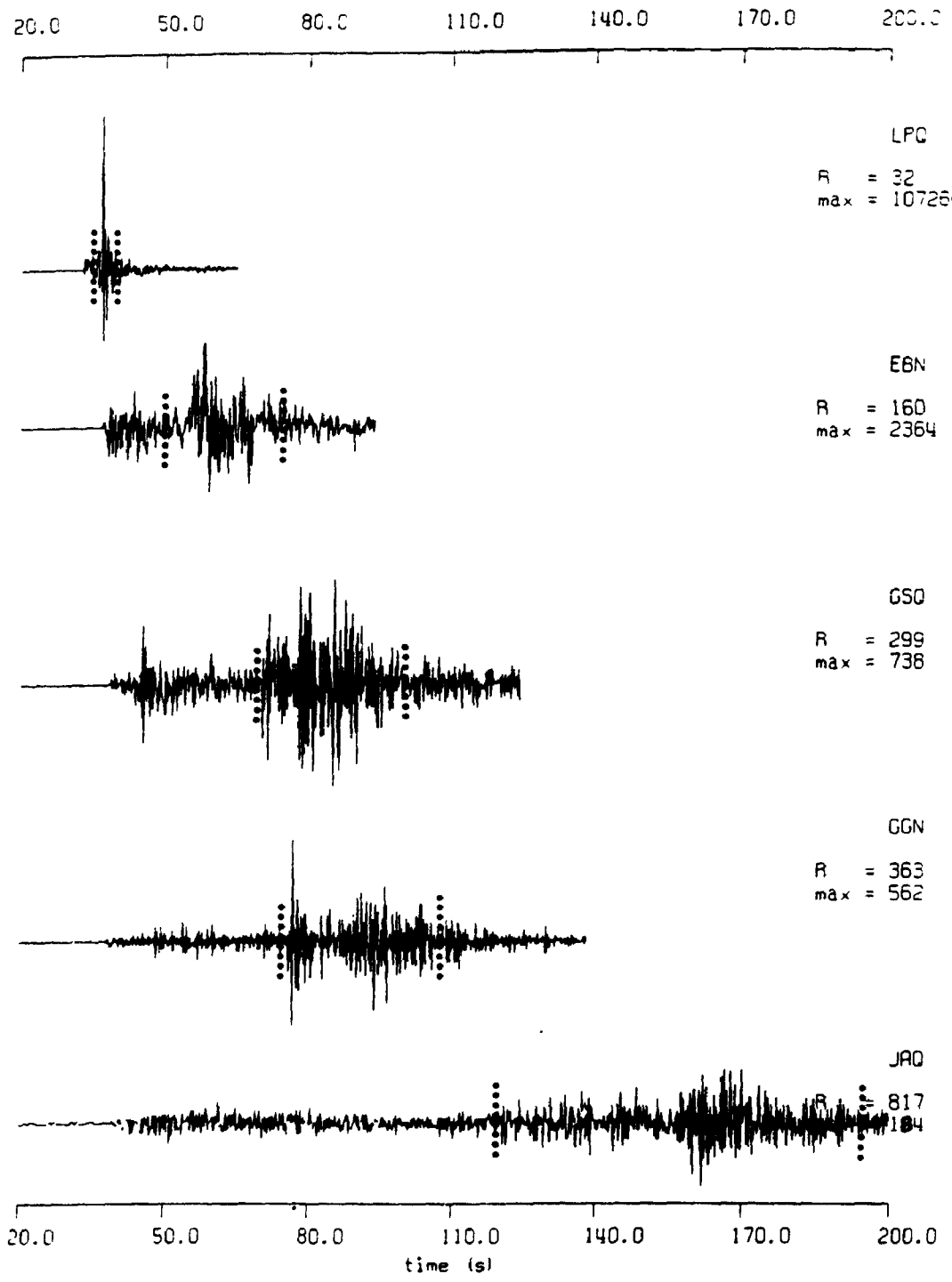

FIGURE 2.4 - Example seismograms for an event of M_N 4.2. Dotted lines show the S-window as defined by the 90% energy criterion. The right column gives the station name, hypocentral distance in km, and maximum amplitude in counts, where 100000 counts represents a velocity of 1 mm/s.

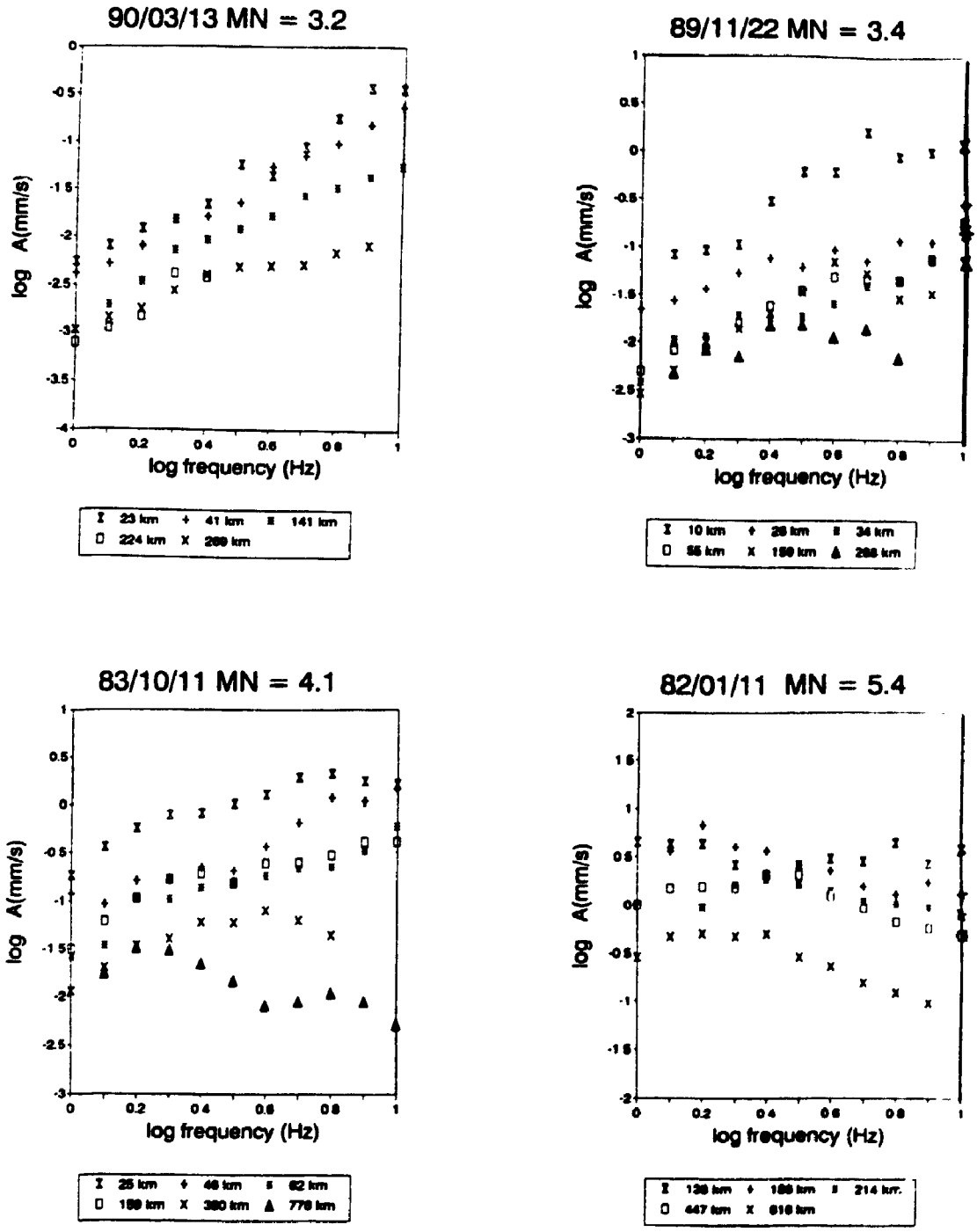

FIGURE 2.5 - Computed Fourier acceleration spectra for four example events, at selected distances.

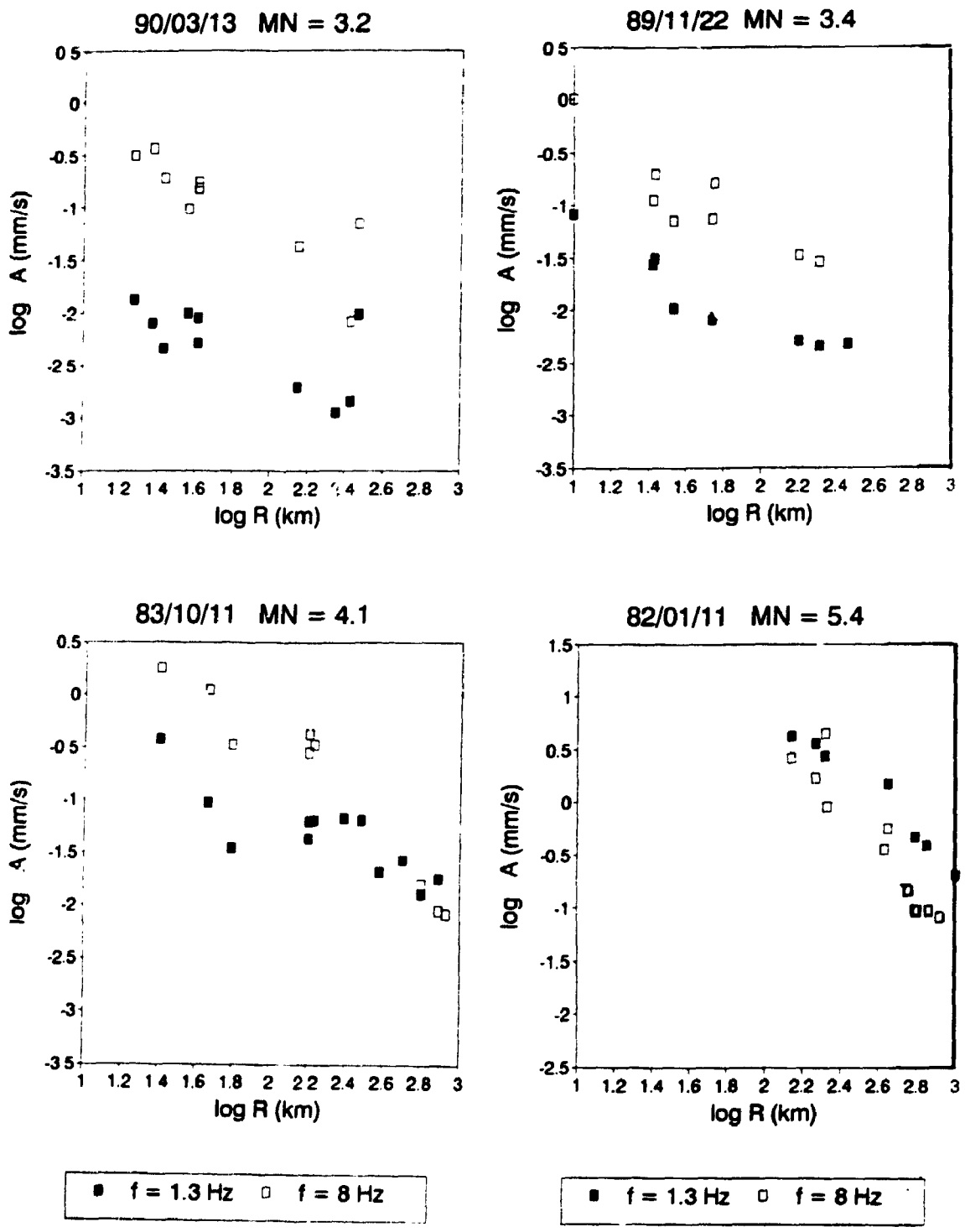

FIGURE 2.6 - Observed decay of spectral amplitude with distance, for frequencies of 1.3 and 8 Hz, for four example events.

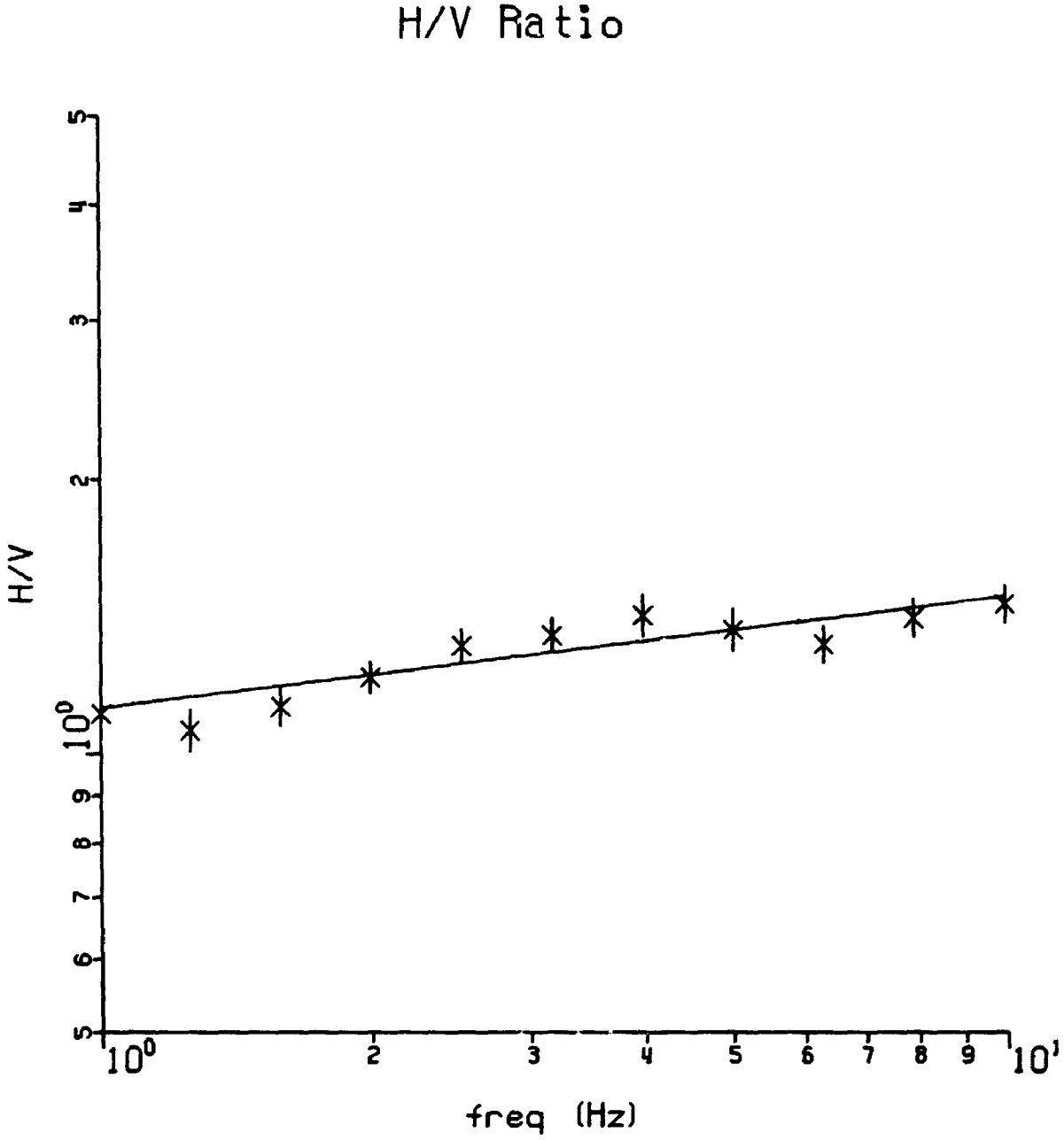

FIGURE 2.7 - Mean H/V ratio as a function of frequency. Vertical bars show 90% confidence limits. The line is the least-squares fit to the means. Station A61 has been excluded.

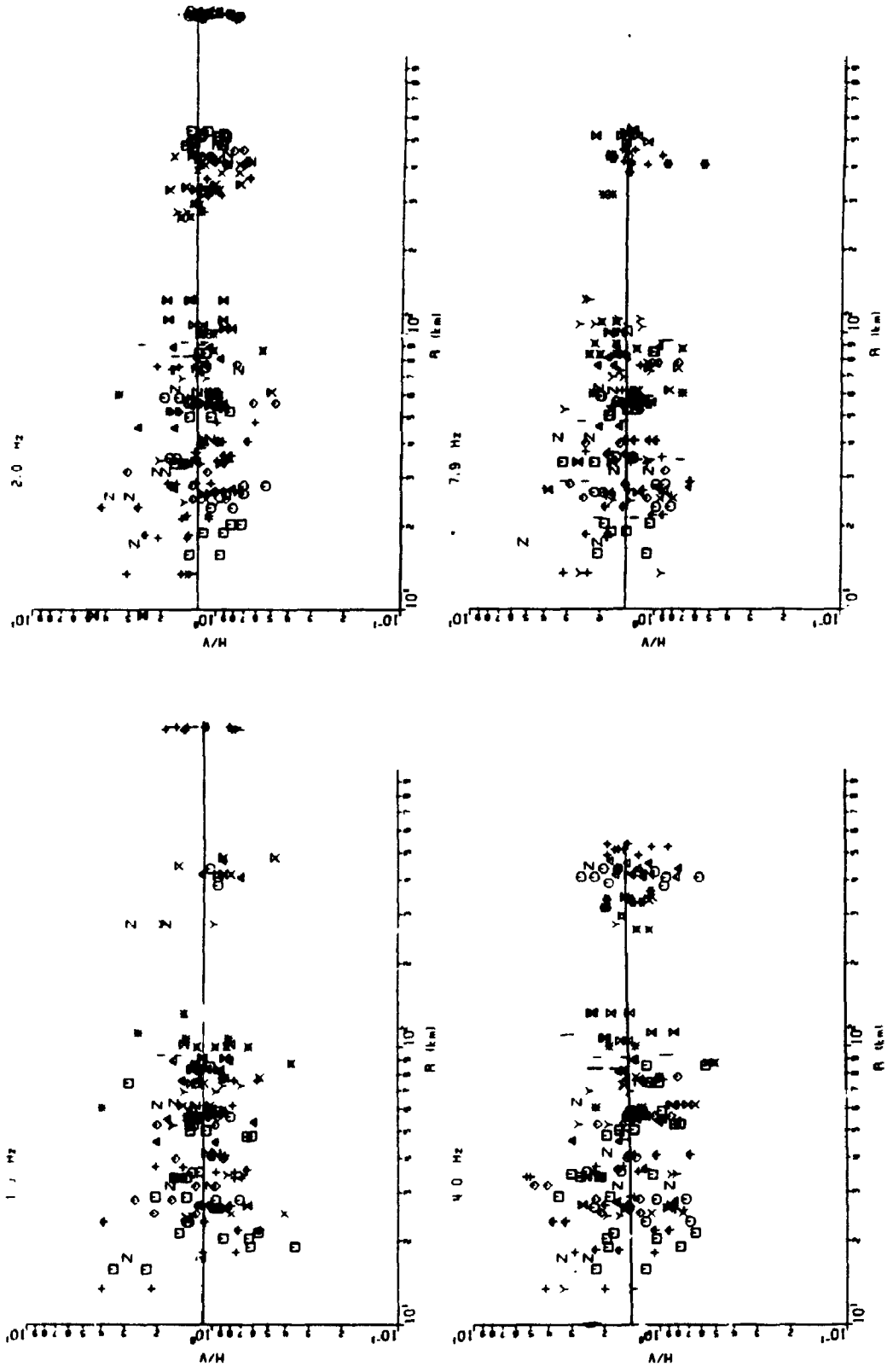

FIGURE 2.8 – Observed H/V ratios as a function of distance, for frequencies of 1, 2, 4 and 8 Hz. Horizontal lines show mean H/V ratio for each frequency. Observations from a single earthquake share the same symbol.

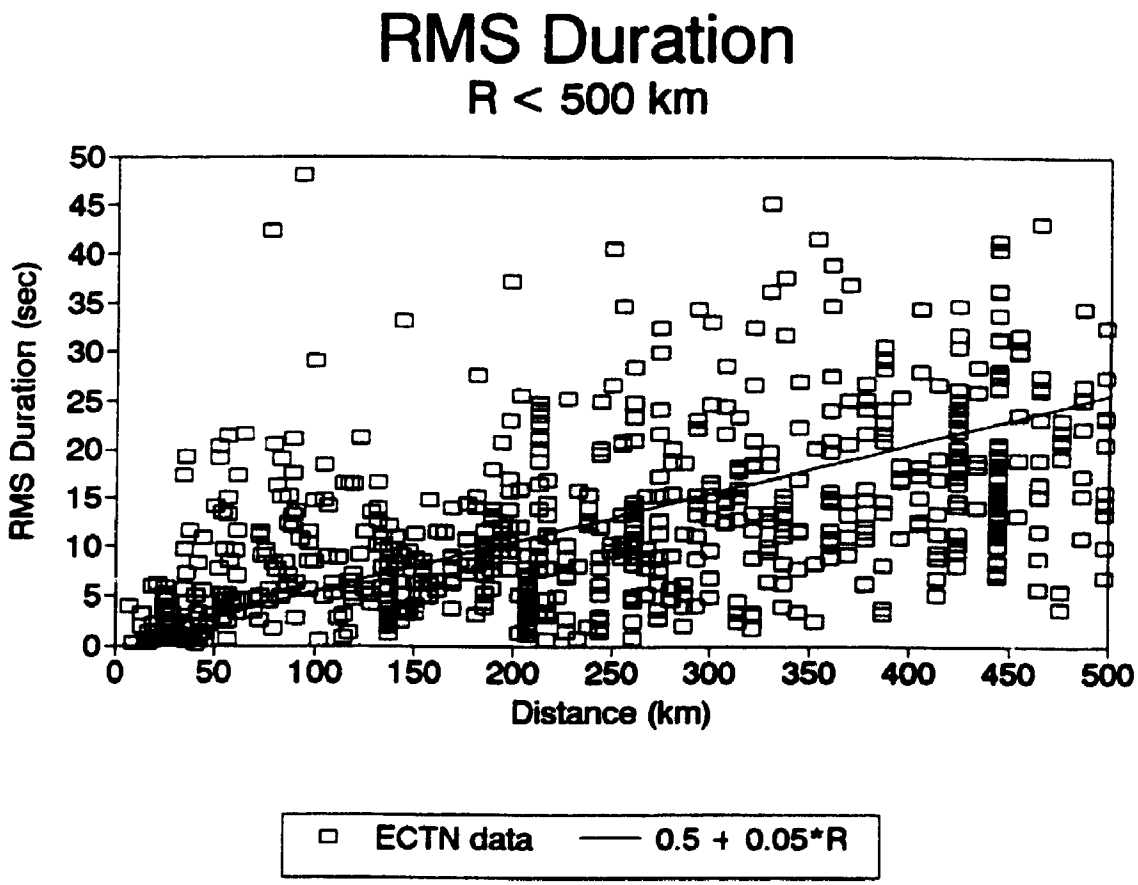

FIGURE 2.9 - Observed (rms) durations of ECTN velocity records for hypocentral distances less than 500 km.

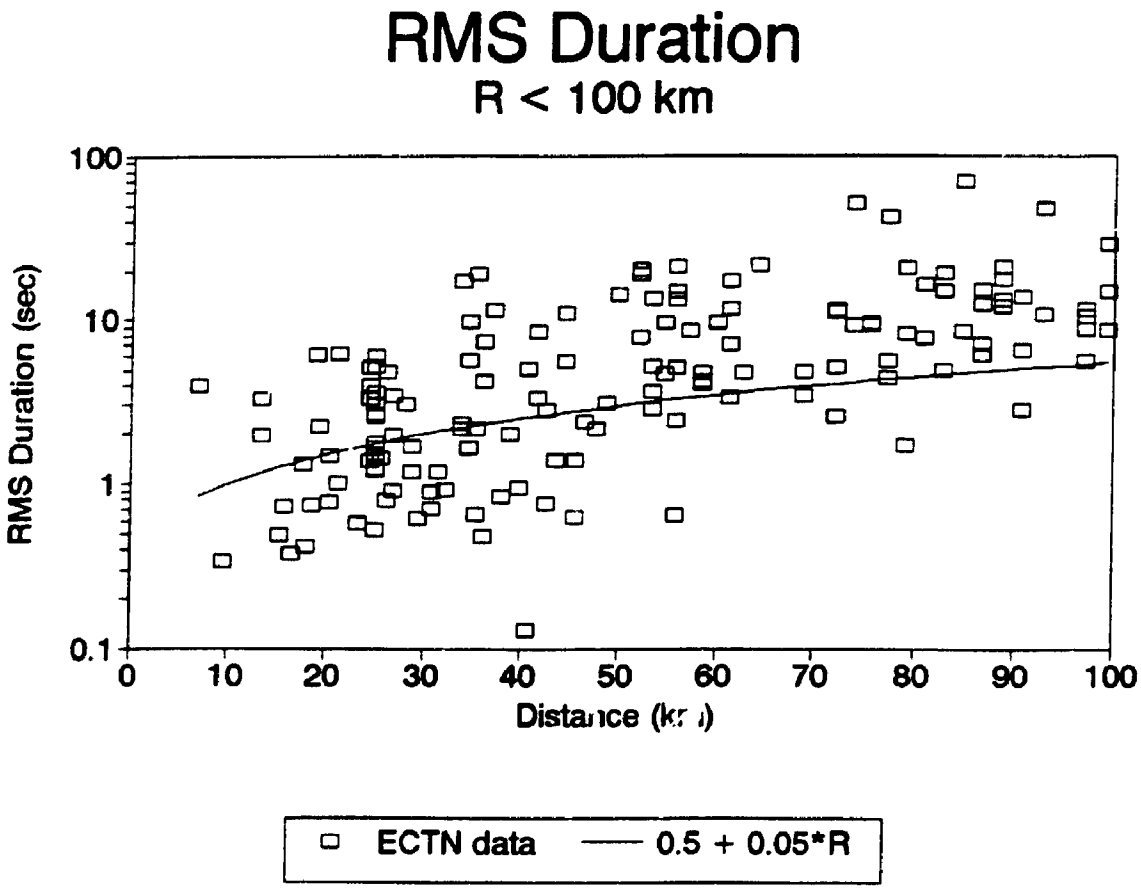

FIGURE 2.10 - Observed (rms) durations of ECTN velocity records for hypocentral distances less than 100 km.

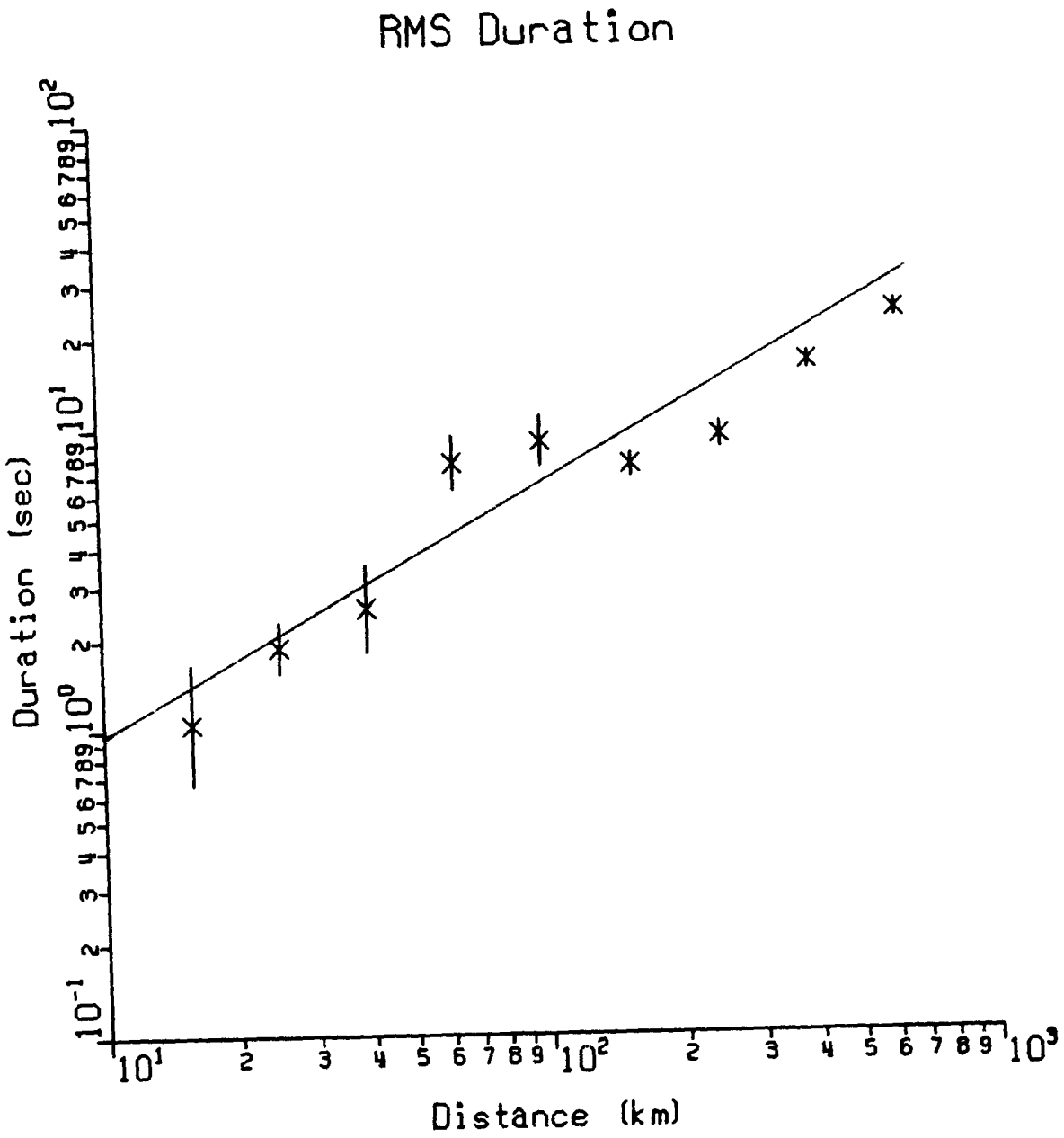

FIGURE 2.11 - Mean of the rms duration, averaged by distance bins. Vertical bars show 90% confidence limits on the estimate of the mean.

3 - ATTENUATION

3.1 Regression Technique for Hinged Trilinear Form

This chapter examines empirical evidence regarding the shape of the attenuation curve for the Fourier spectrum of ground acceleration in southeastern Canada. The analysis is based on regression of the ECTN spectral amplitudes to an equation of the form described by Equation 1.6 (see also Equation 3.1). To accommodate possible complexities in the shape of the attenuation curve (Chapter 1.2.3), the attenuation coefficient for the apparent geometric spreading (b) is allowed to vary with distance. Specifically, I allow 'b' to take separate frequency-dependent values in each of three distance ranges:

(i) $R \leq R_{o1}$, where R_{o1} = 50 km (initial trial value), corresponding to attenuation of the direct-wave;

(ii) $R_{o1} < R \leq R_{o2}$, where R_{o2} = 200 km (initial trial value), corresponding to a transition zone as the direct-wave is joined by postcritical reflections from mid-crustal interfaces and the Moho discontinuity;

(iii) $R > R_{o2}$, corresponding to attenuation of multiply-reflected and refracted S-waves.

The three-part form, with frequency-dependent coefficients, was chosen for the initial regression trials in order to provide maximum flexibility in fitting the observations, thereby reducing variability due to modeling error.

For the hinged trilinear form, the regression equations are:

(i) $R \leq R_{o1}$ (3.1a)

$$[\log A_{io}(f)]_j = \log A_{ij}(f) + b_1(f) \log R_{ij} + c(f) R_{ij} - \log S_j(f)$$

(ii) $R_{o1} < R \leq R_{o2}$ (3.1b)

$$[\log A_{io}(f)]_j = \log A_{ij}(f) + b_1(f) \log R_{o1} + b_2(f) \log (R_{ij}/R_{o1}) + c(f) R_{ij} - \log S_j(f)$$

(iii) $R > R_{o2}$ (3.1c)

$$[\log A_{io}(f)]_j = \log A_{ij}(f) + b_1(f) \log R_{o1} + b_2(f) \log (R_{o2}/R_{o1}) + b_3(f) \log (R_{ij}/R_{o2}) + c(f) R_{ij} - \log S_j(f)$$

The anelastic coefficient, c(f), is inversely proportional to the quality factor, Q:

$$Q = [0.4343\ \pi\ f] \ /\ (c\ \beta) \qquad (3.2)$$

where β is shear wave velocity (assumed = 3.8 km/sec).

The regression is performed iteratively, as illustrated in Figure 3.1. In the first iteration, assume that all site terms equal zero. For trial values of R_{o1} and R_{o2}, the regression program steps through all possible combinations of attenuation parameters ($b_1(f)$, $b_2(f)$, $b_3(f)$, $Q(f)$), searching for the combination that minimizes the average residual error. The constraints imposed on b are that it be 1.0 or greater for the direct wave, 0.5 or greater for the Lg-phase; it is unconstrained in the transition zone. Q is also assumed to be frequency-dependent, but is the same in

all three distance ranges (ie. apparent geometric spreading depends on the geometry of spreading in a layered crust, which is a function of distance, but anelasticity is independent of distance).

Each combination of attenuation parameters is used to calculate an implied average source term for each earthquake. The residual (misfit) for each observation is:

$$k_{ij} = [\log A_{io}(f)]_j - \overline{\log A_{io}(f)} \qquad (3.3)$$

,where $\overline{\log A_{io}(f)}$ is the mean source amplitude for earthquake i, obtained by averaging the $[\log A_{io}(f)]_j$ values over all stations recording the earthquake. The solution is the combination of b_1, b_2, b_3, and Q that minimizes the average absolute value of the residuals. The solution was based on the absolute value of the errors, rather than the least-squared error, in order to lessen the influence of outlying points on the solution (Press et al., 1986, p. 456, 501, 543). Site terms for each of the stations are obtained by averaging the residuals by station, applying the constraint that the average site term for rock sites be equal to zero. The above process is then repeated using these site terms in Equations 3.1. Iteration continues until no further reduction in residual error is possible. Finally, the values of R_{o1} and R_{o2} are perturbed to further minimize the residuals. These regressions provide, for each frequency, estimates of the site term for each station, the source term for each earthquake, and the coefficients b

and c . (Note: The source terms obtained for each event correspond to a distance of R = 1 km. The data cannot define amplitudes at hypocentral distances less than 10 km, since this generally represents a point at zero epicentral distance. In obtaining the source amplitudes at R = 1 km, a geometric spreading coefficient of 1.0 is assumed to apply in the distance range from R = 1 to R = 10 km. This assumption is not critical, since for practical purposes we are only interested in the distance range R > 10 km.)

The veracity of the regression program was tested as follows. For a given regression result (ie. all coefficients of Equations 3.1), I create a 'zero-variability' dataset by subtracting the source term, site term and residual from each observed spectral amplitude in the ECTN dataset. Regression of this modified dataset then yields (for a correct regression program) the exact attenuation function from the regression result, a zero source term for every event, a zero site term for every station, and zero residuals for all observations. The values of the attenuation coefficients are readily verified by inspection of the modified dataset.

3.2 Monte Carlo Tests of Regression Results

Initial trilinear regressions of the dataset showed, as expected, a strong trade-off between b_3 (geometric spreading of Lg) and Q. This is illustrated for a single frequency (8 Hz) on Figure 3.2. Observe that, for this frequency, a b_3

coefficient anywhere in the range from 0.9 to 1.7 appears to provide an equivalent fit to the data, although with different associated Q values. By contrast, there is relatively little trade-off between the b_1 and b_2 coefficients (slopes for the direct-wave and transition zone); however these coefficients are not tightly defined. Clearly, it is important to assess the significance of the indicated coefficients in light of these results.

To perform significance tests regarding the derived attenuation curve and obtain estimates of the errors in coefficients, Monte Carlo techniques are used (Press et al., 1986, p. 529-532). Starting with specified coefficients of Equation 3.1, I simulate synthetic realizations of these parameters as synthetic datasets. Each data point within a set is simulated by adding a random (log) residual to the predicted value from Equation 3.1. The residuals are selected by drawing random numbers from a normal distribution with zero mean; the variance is chosen to reproduce the observed average residual, as determined from the regression analysis (Equation 3.3). For any specified combination of attenuation coefficients, I generate ten datasets, each of which have the same number of observations as the ECTN dataset, the same distribution in distance, and the same degree of random variability. Regression of the simulated datasets provides insight into the combinations of

coefficients that may be obtained from a known underlying shape, in the face of random variability.

By investigating regression results for the Monte Carlo datasets using both frequency-dependent and frequency-independent hinged trilinear shapes, in conjunction with the observed random variability, the following conclusions are reached:

(i) there is no significant dependence of b_1, b_2 or b_3 on frequency in the ECTN dataset;

(ii) the best-fit value of b_3 from the ECTN data regressions is 1.0 when no constraints are placed on Q. If Q is constrained to be constant or increase with frequency (eg. Q of the form $Q = Q_o f^n$, where $n \geq 0$), then we obtain $b_3 = 0.7$. At first glance, this would appear to suggest that geometric attenuation is greater than the theoretical value of 0.5 that is attributed to surface-wave spreading in a half-space; such a discrepancy could be interpreted as evidence of leakage of energy from the crustal waveguide into the mantle. However, when we perform regressions on simulated datasets for which we have specified $b_3 = 0.5$, we often obtain this same result (eg. regressions of 10 simulated datasets, for which we know that $b_3 = 0.5$, yield b_3 values ranging from 0.5 to 1.0). The simulations thus demonstrate that the scatter of the data does not allow the true slope to be obtained, and that regressions

tend to favor higher values of b_3 (with less curvature) than were specified in the simulations. I therefore conclude that the b_3 coefficient for the ECTN dataset is not significantly different from a value of 0.5.

3.3 Regression Results for Trilinear Form

With the results of the significance tests in hand, the regressions are repeated, imposing the constraints that b_1, b_2, b_3 be independent of frequency, and that $b_3 = 0.5$, in accordance with the standard theoretical interpretation of the Lg phase as entirely trapped within the crust. The resulting coefficients are:

$b_1 = 1.1 \pm 0.1$

$b_2 = 0.0 \pm 0.2$

$b_3 = 0.5$

$Q = 670\ f^{0.33}\ (\pm 100)$

$R_{o1} = 70 \pm 5$ km

$R_{o2} = 130 \pm 10$ km

The average absolute value of the residual error in an observation is 0.14 ($\pm$ 0.01) log units. The (log) residuals are normally distributed with a standard deviation of approximately 0.20 ($\pm$ 0.03) log units, independent of distance and frequency. Considering both random errors and those remaining due to uncertainty in the true functional form, source and site terms are uncertain by approximately 0.1 log units.

Site terms are summarized in Table 3.1. For most rock stations they are within 0.2 log units (factor of 1.6) of unity; however some stations, particularly those in the Charlevoix area, have site response terms that exceed 0.3 log units (factor of two). The soil site (WEO) amplifies high-frequency motions by nearly a factor of ten. Source parameters for all events are listed in Appendix B; the tabulated values for the stress parameter were calculated by fitting the high-frequency level of the source spectrum to Equation 1.2 (for $f>>f_o$).

To facilitate visual comparisons of the fitted trilinear curve with the data, I use the source and site terms from the regressions to normalize the observed spectral amplitudes to a common level (ie. I remove the source and site effects, leaving just path effects in the data). I define:

$$\log A'_{ij}(f) = \log A_{ij}(f) - \log A_{io}(f) - \log S_j(f) \qquad (3.4)$$

where I will refer to the source-site-corrected amplitudes, $A'_{ij}(f)$, as 'normalized' amplitudes. Figure 3.3 provides an example of normalized spectral amplitudes for one frequency (f = 2 Hz). The figure was plotted for a subset of the data showing particularly good distance coverage; thus the scatter illustrates the minimum level of random variability observed for events with well-defined source terms. It is clear from Figure 3.3 that scatter makes distinction of the underlying shape of the attenuation curve difficult.

To better define the shape implied by the attenuation data, it is useful to plot the mean normalized amplitudes for a number of distance bins. Accordingly, the mean normalized (log) amplitudes, and their 90% confidence limits, are computed for distance bins of width 0.15 log units, and shown on Figure 3.4 for frequencies of 1, 2, 4 and 8 Hz. Figure 3.4 shows a remarkably stable attenuation pattern for the mean normalized amplitudes, which are very well described by the hinged trilinear form. Overall, the shape of the curve suggests that there is a significant flattening in the decay of spectral amplitudes in the transition zone between direct-wave and multiply-reflected and refracted waves.

3.4 Regression to Linear and Bilinear Forms

To test the influence of the assumed trilinear functional form on the shape indicated by the data points on Figure 3.4, I regress the data to more traditional forms of Equation (3.1), including:

(i) a 'linear' (as opposed to 'trilinear') form, with b=1.0 for all distances; and

(ii) a 'bilinear' form, with b=1.0 for distances less than R_o (determined to be 60 km by iteration of trial values from 50 to 150 km), and b=0.5 for distances greater than R_o.

These regressions give different Q values than the trilinear form. For the b=1.0 regression, I obtain a frequency-

independent Q of 2000. For the bilinear form, I obtain $Q = 790\ f^{0.27}$.

Normalizing the data to the source and site terms determined from these regressions indicates the same general flattening in the 70 to 130 km distance range as had been previously determined. This is illustrated in Figures 3.5 and 3.6. Observe from Figure 3.5 that 1/R is not a bad assumption over all distance ranges; it simply smooths through the disruption in the curve around 100 km. Interestingly, Figure 3.6 shows that the traditional bilinear form assumed in most previous studies does a very good job of matching the observed shape, when R_o = 60 km. This R_o value is significantly less than the usual assumed value of R_o = 100 km. The switch in slope from 1.0 to 0.5 reproduces much of the required flattening in the 70 to 130 km distance range.

Figures 3.5 and 3.6 raise a question as to the statistical significance of the apparent flattening in the transition zone. To address this issue, Monte Carlo simulations of datasets having an underlying bilinear form, with b_1=1.0, b_2=b_3=0.5, R_{o1}=60 km, are regressed to a trilinear form. Comparisons of these regressions with the results from our ECTN dataset indicate that the trilinear nature of the ECTN curve is statistically significant. For a 'true' value of b_2=0.5, the simulated datasets yielded an average b_2=0.4, with the lowest b_2 value from ten datasets

being 0.3. The ECTN dataset, by comparison, yielded the value b_2=0.0

3.5 Influence of Focal Depth

Theoretical studies (Ou and Herrmann, 1990; Somerville et al., 1990) show that crustal layering and velocity gradients should cause the rate of attenuation for the direct wave (ie. R < 60 km) to be dependent on focal depth; shallow-focus earthquakes should attenuate more rapidly than deep-focus events. To search for such an effect in the ECTN data, I subdivide the data into three subsets, having focal depths in the range 0 to 8 km (subset contains 422 observations), 8 to 16 km (283 observations), and 16 to 30 km (120 observations). Figure 3.7 plots mean normalized amplitudes for each of these depth ranges, in comparison to the attenuation curve for the dataset as a whole. There is little evidence for a focal depth effect, with the possible exception of the subset of events deeper than 16 km. The data for the deep subset is consistent with lesser attenuation at distances less than 40 km. However the discrepancies between the data and the average curve are not compelling, since there are only 12 observations for distances less than 40 km. It is possible that a better dataset would reveal systematic focal depth effects.

3.6 Influence of Tectonic Province

Previous authors (Gupta and McLaughlin, 1987; Woodgold, 1990) have mapped regional variations in Q, which are

presumably attributable to regional differences in crustal geology. For the ECTN study region, data subsets may be identified corresponding to Grenville and Appalachian tectonic province travel paths, as delineated on Figure 2.1 (ie. an Appalachian travel path corresponds to a data point for which both the source and receiver are in the Appalachian tectonic province). In my regressions, the site terms should reflect any systematic near-surface differences in crustal conditions, while the mean normalized amplitudes for the travel-path subsets should reveal any deeper influences of crustal conditions on attenuation. Looking first at the site terms (Table 3.1), there is no apparent influence of tectonic province. Most of the stations in the Charlevoix area (which includes all station names beginning with the letter 'A', plus station LPQ) have negative site terms of about 0.2 log units, but site terms in other parts of the Grenville province, and in the Appalachian province, vary randomly about 0. Turning to the travel path subsets, the mean normalized amplitudes for each of the tectonic provinces are in good agreement with the average regional curves shown in Figure 3.8. I conclude that there is little evidence of a difference in attenuation according to tectonic province.

TABLE 3.1 - ECTN site terms (log $S_j(f)$ from Equation 3.1) from trilinear regression.

Station		Coordinates		f=1 Hz	f=2 Hz	f=4 Hz	f=8 Hz
OTT	G	45.39	-75.72	0.00	0.08	0.07	0.13
MNT		45.50	-73.62	-0.14	-0.16	-0.06	0.02
MNQ	G	50.53	-68.77	-0.03	-0.01	0.03	0.13
GNT	G	46.36	-72.37	0.28	0.13	0.02	-0.08
FHO		45.46	-76.22	0.00	0.11	0.20	0.23
GAC	G	45.70	-75.48	-0.07	-0.20	-0.15	-0.15
LPQ	G	47.34	-70.01	0.26	0.20	0.20	0.15
SBQ	A	45.38	-71.93	0.21	0.18	0.18	0.15
VDQ		48.23	-77.97	0.03	0.07	0.11	0.10
WBO		45.00	-75.28	0.10	0.05	0.06	0.17
CKO	G	45.99	-77.45	0.05	0.20	0.17	0.22
TRQ	G	46.22	-74.56	0.09	0.13	0.10	0.17
GRQ	G	46.61	-75.86	0.11	0.18	0.23	0.20
JAQ		48.80	-75.72	0.00	0.10	0.34	0.50
GSQ		48.91	-67.11	0.16	0.03	-0.07	-0.13
EBN	A	47.54	-68.24	0.22	0.03	0.02	0.02
GGN	A	45.12	-66.82	0.04	0.10	0.12	-0.08
LMN	A	45.85	-64.81	0.21	-0.05	0.07	-0.09
KLN	A	46.84	-66.37	0.12	0.01	0.03	0.06
HTQ	G	49.19	-68.39	0.01	0.03	0.06	0.15
WEO		44.02	-78.37	0.07	0.10	0.34	0.84
SUO		46.40	-81.01	-0.34	-0.27	-0.23	-0.12
EEO	G	46.64	-79.07	0.00	0.20	0.27	0.23
DPQ	G	46.68	-72.78	-0.24	-0.18	-0.11	0.07
SZO		46.44	-81.50	-0.36	-0.07	-0.13	0.00
SWO		46.73	-81.00	-0.21	-0.12	0.00	0.00
A11	G	47.24	-70.20	-0.03	-0.08	-0.29	-0.36
A16	G	47.47	-70.01	-0.02	-0.11	-0.22	-0.33
A21	G	47.70	-69.69	-0.03	-0.04	-0.08	-0.06
A54	G	47.46	-70.41	-0.06	-0.08	-0.20	-0.15
A61	G	47.69	-70.09	-0.20	-0.25	-0.47	-0.37
A64	G	47.83	-69.89	-0.16	-0.20	-0.26	-0.28

Notes: G = Grenville Province; A = Appalachian Province
Coordinates quoted are latitude (degrees N) and longitude (degrees W).

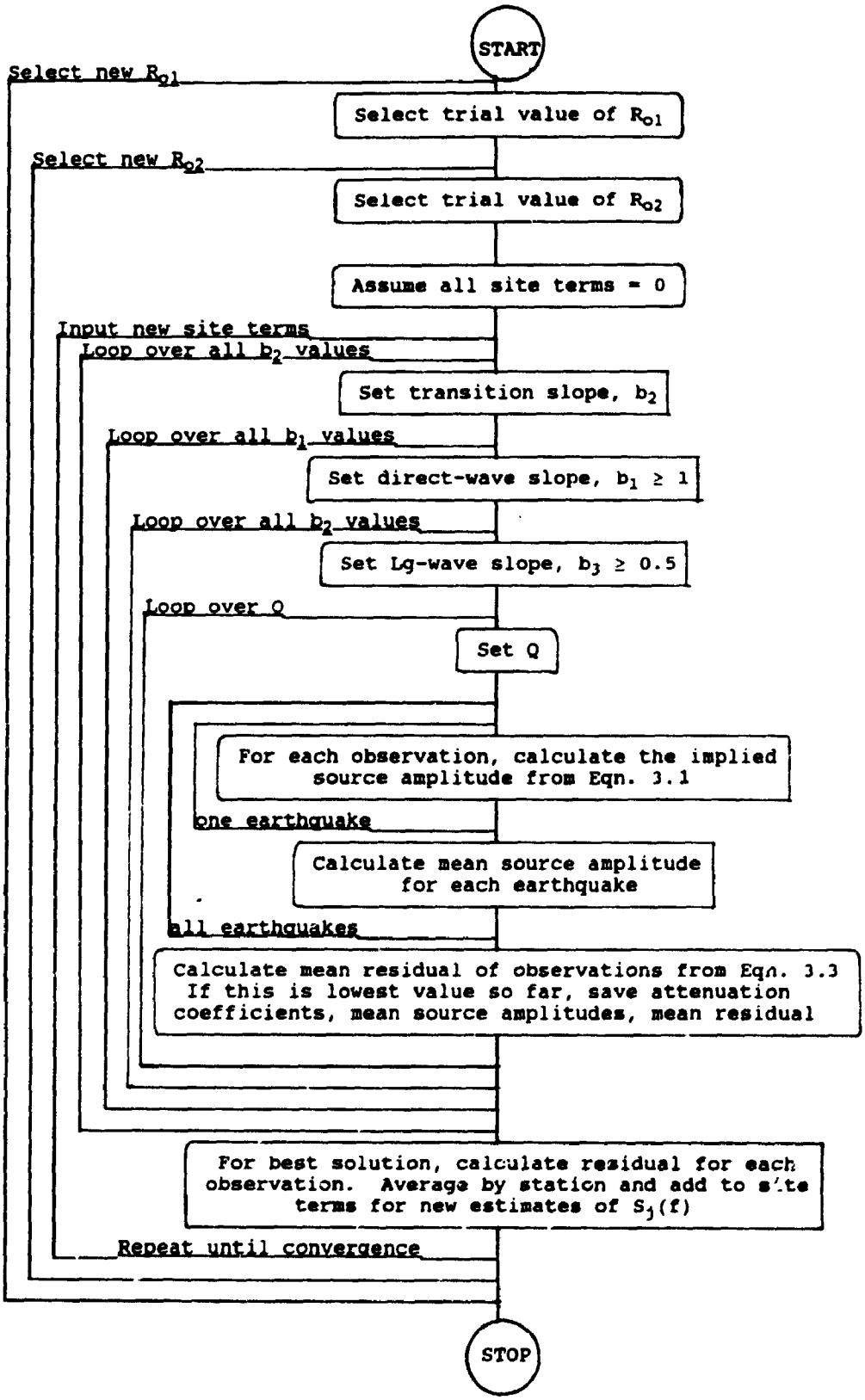

FIGURE 3.1 - Flowchart of regression analysis procedure (program FIT).

Q	b3=0.5	0.7	0.9	1.1	1.3	1.5	1.7
1000	211	233	256	281	308	335	363
1500	154	167	166	180	199	221	244
2000	165	154	150	152	161	176	194
2500	186	168	153	149	150	157	170
3000	205	183	166	154	149	151	159
3500	218	196	176	161	151	149	153
4000	229	206	185	167	153	150	151
4500	238	214	192	173	159	151	150
5000	245	221	198	179	163	153	150

b2	b1=1	1.1	1.2	1.3	1.4	1.5
-0.6	162	160	159	157	157	157
-0.4	157	155	154	154	154	155
-0.2	153	152	152	152	153	154
0	150	150	150	151	153	155
0.2	149	149	150	152	154	157
0.4	149	150	152	154	157	160
0.6	151	153	155	157	161	165

FIGURE 3.2 - Example of average regression residuals (f=8 Hz), in log units times 1000. Top frame shows strong trade-off between Q and Lg-wave spreading coefficient (b_3). Lower frame shows weak trade-off between direct-wave spreading coefficient (b_1) and transition slope (b_2).

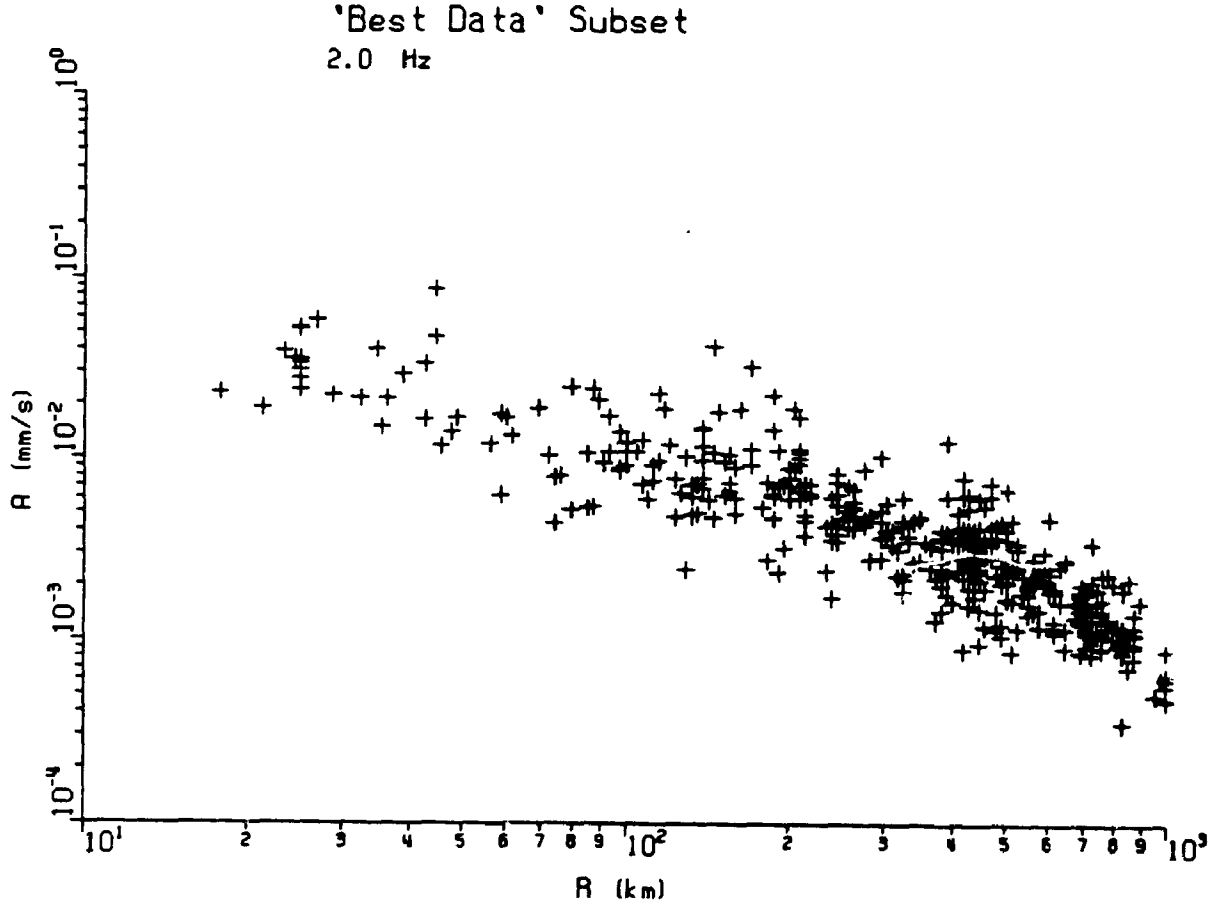

FIGURE 3.3 - Observed decay of normalized spectral amplitude (f = 2 Hz) in the S-window for a subset of the data having particularly good distance coverage (and therefore well-defined source levels). The normalization is based on source and site terms derived from trilinear regression to Equation (3.1).

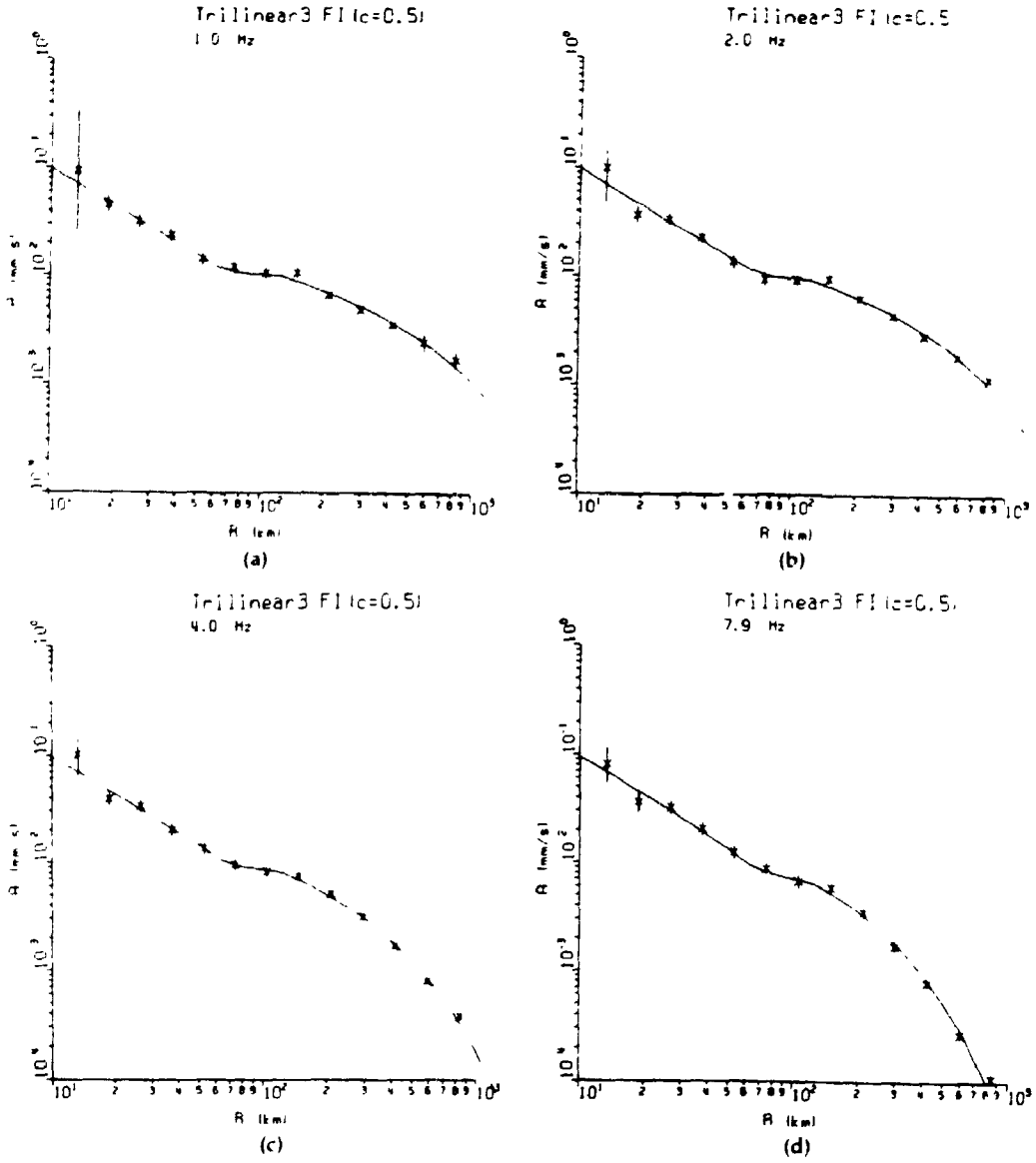

FIGURE 3.4 - Observed decay of the mean of the normalized spectral amplitudes in the S-window, for frequencies of 1, 2, 4 and 8 Hz. The normalization is based on source and site terms derived from trilinear regression to Equation (3.1). The height of the vertical bars shows the 90% confidence limits. The smooth lines are those determined by the regression.

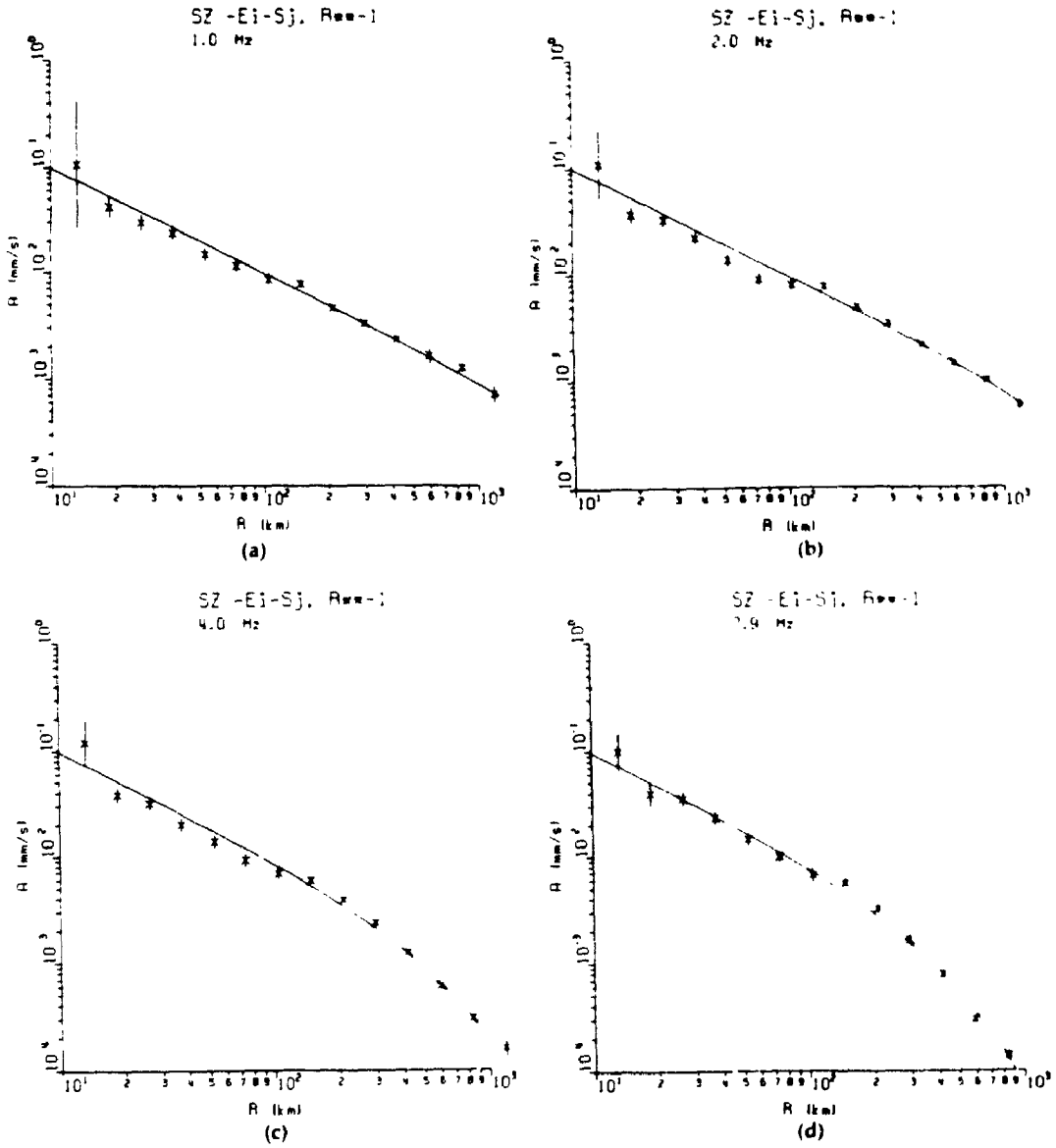

FIGURE 3.5 - Observed decay of the mean of the normalized spectral amplitudes in the S-window, for frequencies of 1, 2, 4 and 8 Hz. The normalization is based on source and site terms derived from linear regression to Equation (3.1), assuming b = 1.0 at all distances. The height of the vertical bars shows the 90% confidence limits. The smooth lines are those determined by the regression.

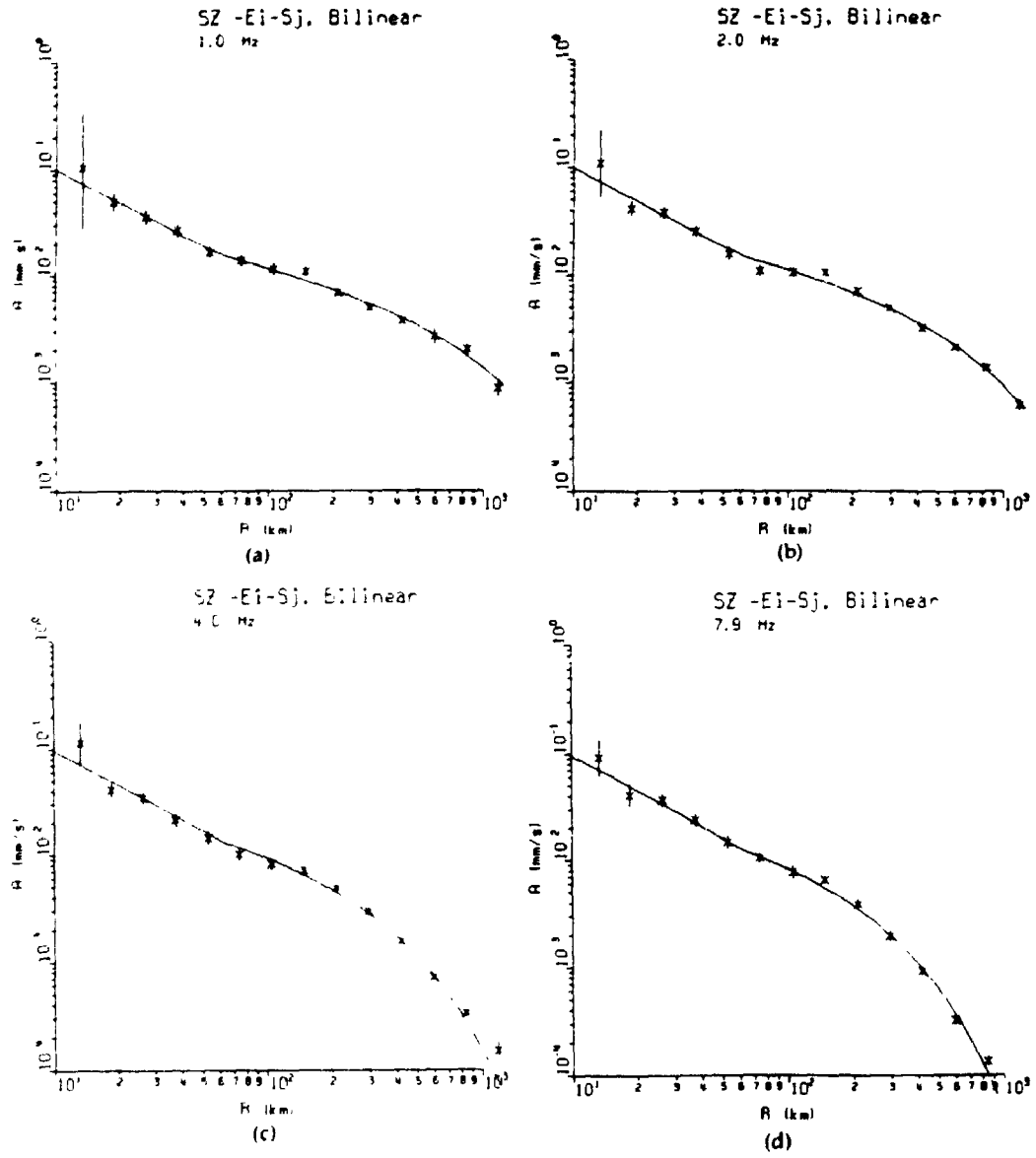

FIGURE 3.6 - Observed decay of the mean of the normalized spectral amplitudes in the S-window, for frequencies of 1, 2, 4 and 8 Hz. The normalization is based on source and site terms derived from bilinear regression to Equation (3.1), assuming b = 1.0 and 0.5, for near and regional distances, respectively. The height of the vertical bars shows the 90% confidence limits. The smooth lines are those determined by the regression.

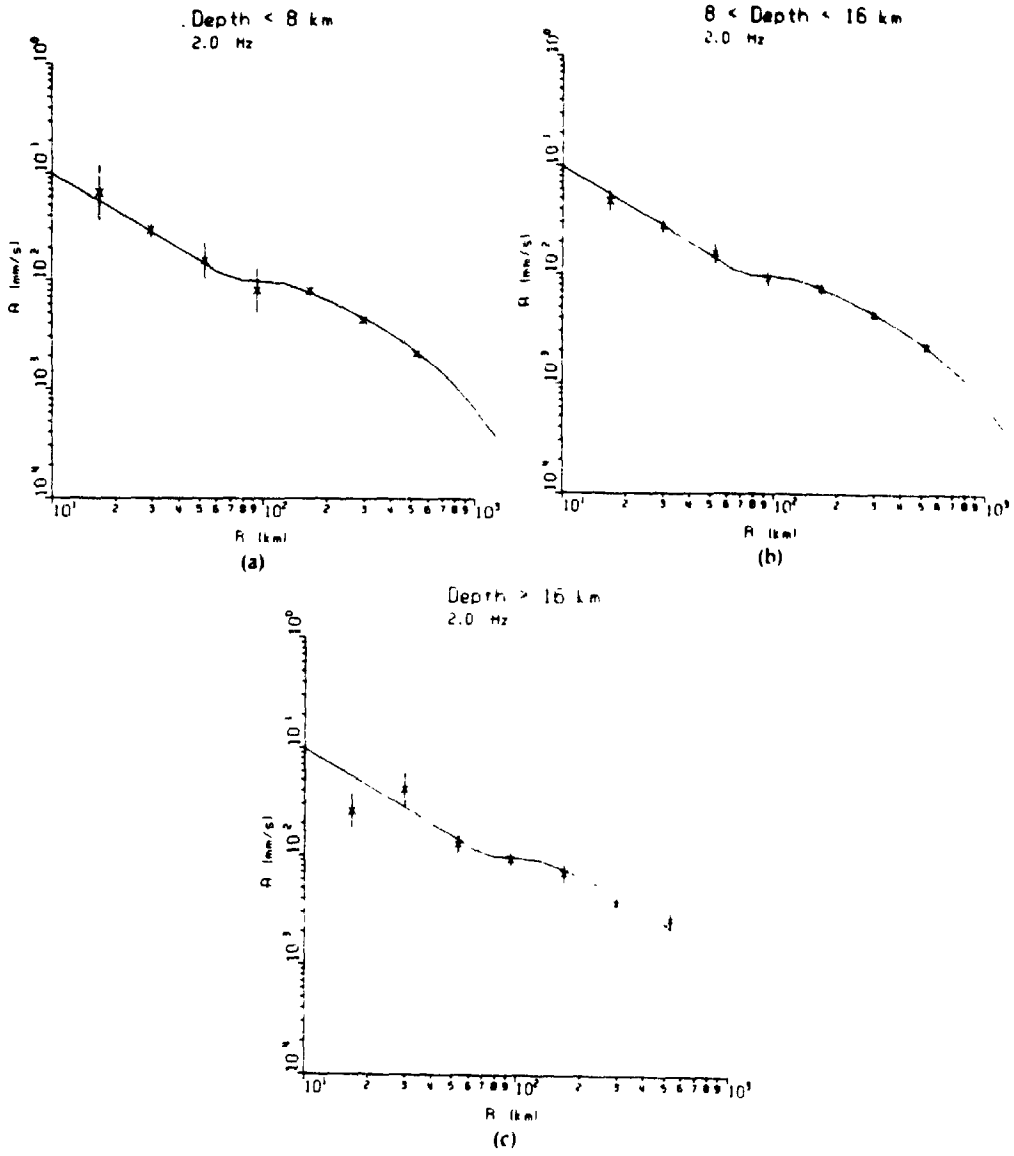

FIGURE 3.7 - Comparison of the mean of the normalized spectral amplitudes, for each of three focal-depth-subsets, with the attenuation curves for the dataset as a whole (ie. smooth curves same as in Figure 3.4). Plots are for f = 2 Hz; other frequencies show similar pattern.

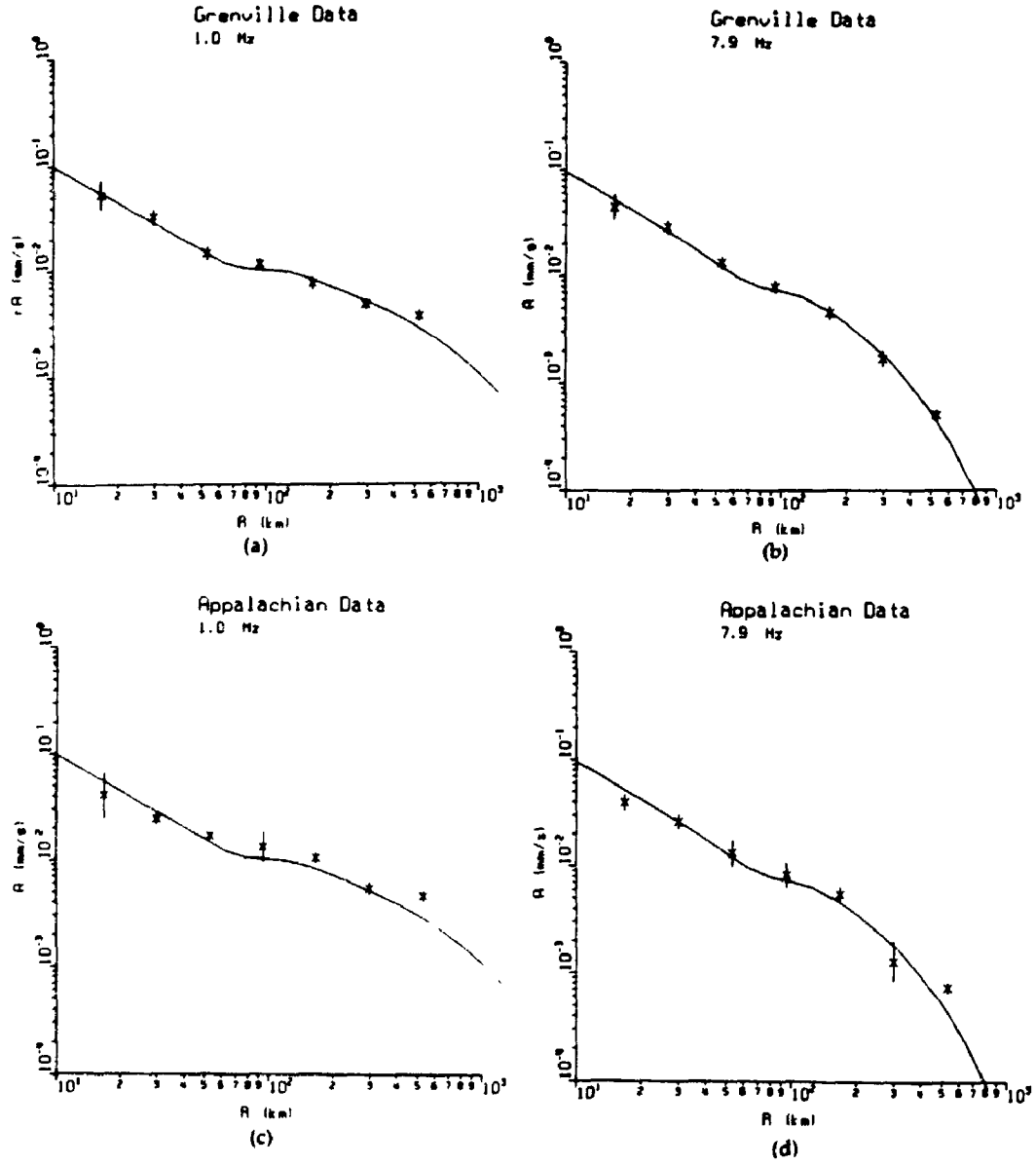

FIGURE 3.8 - Comparison of the mean of the normalized spectral amplitudes, for the Grenville and Appalachian travel-path-subsets, with the attenuation curves for the dataset as a whole (ie. smooth curves same as in Figure 3.4). Plots are for f = 1 Hz and f = 8 Hz; other frequencies show similar pattern.

4 - SIMULATION OF GROUND MOTIONS BASED ON REGRESSION RESULTS

4.1 Introduction

In this chapter I demonstrate the adequacy and utility of the regression results in describing ground motion amplitudes of engineering interest. This is accomplished by simulating ground motion records for four test events from the ECTN dataset, using the stochastic method (Chapter 1.2.1). The four test events are:

(i) Ottawa earthquake, 83/10/11, M_N = 4.2, h = 14 km

(ii) Charlevoix earthquake, 90/03/03, M_N = 3.6, h = 20 km

(iii) Mont Laurier earthquake, 90/10/19, M_N = 5.1, h = 7 km

(iv) Saguenay earthquake, 88/11/25, M_N = 6.5, h = 26 km

(where h is the focal depth). The simulations use as input the source, site and attenuation terms determined from the regression analyses. The simulations are then compared to the actual recordings. The comparison is based on peak ground acceleration and velocity, and response spectra for frequencies of 1, 2, 5 and 10 Hz. This comparison will demonstrate that the source, attenuation and site terms determined from the regression analysis can be used in conjunction with the stochastic simulation method to accurately predict average ground motion parameters of engineering interest.

4.2 Stochastic Simulations of Test Events

High-frequency ground motion is modeled as bandlimited Gaussian noise in which the radiated energy is distributed

over a specified duration. The results of the regression analyses describe the average source and propagation operators, which give the overall level and shape of the Fourier spectrum for each event as a function of distance.

The time domain implementation of this stochastic approach is illustrated in Figure 4.1. I first generate a windowed time series of random Gaussian noise with zero mean amplitude; the variance is chosen such that the spectral amplitude is unity on average. The spectrum of the windowed time series is multiplied by the desired amplitude spectrum (A_{ij} from Equation 3.1). (Note: To simulate the ECTN velocity records, an additional filter is applied at this stage to reproduce the ECTN instrument response.) The filtered spectrum is then transformed back into the time domain to yield the simulated earthquake record for that particular event and station.

The window applied to the initial random time series determines the shape of the envelope of the final time series. Most previous studies have used a simple tapered boxcar. This produces seismograms which have the correct amplitudes and frequency content, but they do not 'look realistic'. To obtain seismograms that have envelope shapes comparable to those of actual recordings, I use a Saragoni and Hart (1974) window, given by:

$$w(t) = a\, t^b \exp(-c\, t)\, H(t) \qquad (4.1)$$

where t is time, H(t) is the Heaviside step function (eg. H=0 for t<0, H=1 for t≥0), and a, b, and c are constants that determine the window shape. The choices for a, b and c are made such that the peak amplitude, which has a value of unity, is reached at 20% of the signal's duration; the amplitude at the end of the signal is 20% of the peak amplitude. This requires the values $a = 5.79T^{-b}$, $b = 0.673$ and $c = 3.37/T$, where T is duration in seconds. To avoid abrupt amplitude changes at the ends of the signal, a 2% cosine filter is applied to each end of the windowed time series. The resulting window shape can be seen in Figure 4.1. The choices for window shape were guided by visual inspection of a large number of ECTN seismograms, so that they match the Lg and direct-S envelopes on average. The window shape does not, however, include the additional phases of the seismogram that are apparent at some distance ranges (eg. S_n at distances of several hundred km).

The duration of the Saragoni and Hart window was selected as:

$$T = 1/f_A + 0.07\ R \qquad (4.2)$$

where f_A is the lowest corner frequency of the spectrum (assumed to represent the inverse of source duration) and R is hypocentral distance in km. The duration of 0.07 R with the shaped window used here is approximately equivalent to a duration of 0.05 R with a boxcar, in terms of predicted peak

velocities (Chapter 2.5). No attempt was made to 'fine-tune' the choice of window shape and duration.

Stochastic simulations were generated for each of the ECTN stations which recorded the four earthquakes. The source spectra for each of the four events, as obtained from the regression analyses, are shown in Figure 4.2. A sample of the simulated records is compared to the corresponding actual recordings in Figure 4.3. The stochastic simulations match the amplitude, frequency content and duration of the main portion of the S-wave train of the actual records reasonably well on average, including the significant effects of scattering on the character of the waveforms.

4.3 Comparisons of Ground Motion Parameters for Real and Simulated Records

To compare ground motion measures of the real versus the simulated records, I process both the real and simulated seismograms (which are velocity time histories) in exactly the same way:

(i) the peak ground velocity is estimated by dividing the observed peak amplitude of the velocity record by the appropriate ECTN response factor, for the frequency at which the peak velocity occurs.

(ii) the velocity record is tapered (5% taper), transformed to the frequency domain, then divided by the complex instrument response for acceleration. Cosine filters are applied to frequencies above 12 Hz (spectral amplitudes diminish to 0 for 18 Hz and above) and below

0.8 Hz (spectral amplitudes diminish to 0 for 0.5 Hz and below). These filters are necessary because of noise contamination outside the 1 to 10 Hz frequency band. The record is transformed back to the time domain to yield an instrument-corrected accelerogram.

(iii) the peak acceleration is obtained directly from the accelerogram. Note that this is not a true measure of peak acceleration because frequencies above 12 Hz have been removed.

(iv) the 5% damped response spectrum is computed from the accelerogram; values of pseudo-acceleration (PSA) are tabulated for frequencies of 1, 2, 5 and 10 Hz.

Figure 4.4 compares the response spectra of the simulated and real recordings on an event-by-event basis, for frequencies of 1 and 10 Hz. The simulated ground motions match the real ground motions very well on average. However the real records show considerable random variability, which I did not attempt to reproduce in the simulations. The Charlevoix earthquake, in particular, shows extreme amplitude variability. The reason for this is unknown; examination of many other ECTN recordings suggests that the variability shown by the Charlevoix event is atypical. Note that the near data (R<150 km) for the Saguenay event are from strong-motion recordings for which we have no knowledge of the site terms; these data were not used in the regressions that determined the source spectra.

The figure suggests that these stations may have a significant site response.

Figure 4.5 plots the differences between the real records and the simulations for several ground motion parameters, combining all events. The figure plots (log, base 10) residuals as a function of (log) distance, for PGA, PGV and PSA at 1, 2, 5, and 10 Hz; the log residuals are defined as the difference between the log of the observed record parameter and the log of the simulated record parameter. Thus a log residual of 0.3 for PGA, for example, would indicate that the observed PGA was a factor of 2 ($=10^{0.3}$) larger than the PGA of the simulated record for that event and station. The residual plots indicate that the simulations match the observations quite well over the entire distance range of 10 to 1000 km. For frequencies of 1 to 2 Hz, the simulations apparently underestimate the ground motions in the distance range from 100 to 400 km. For frequencies near 10 Hz, the simulations underestimate the ground motions at distances less than 100 km, and overestimate them at larger distances. This suggests that the attenuation form is not matching frequency dependencies in the actual attenuation. (Recall that a frequency-independent form war selected because the observed frequency-dependence is not statistically significant.) In particular, the flattening of the attenuation curve due to the first postcritical reflection from the Moho is more

pronounced at low frequencies than at high frequencies. These discrepancies could be resolved by fine-tuning the attenuation and other parameters. (They could also be reduced by eliminating the Saguenay strong-motion data, for which the site terms are unknown but appear to be significant.) Since the match between synthetics and recordings is quite good for distances less than 100 km, the range of most engineering interest, such fine-tuning may not be warranted for practical purposes.

Table 4.1 summarizes the differences between the real and simulated ground motion parameters, listing the mean residual and standard error of an estimate for three distance ranges ($R < 100$ km, $R < 200$ km, and $R < 1000$ km). The mean residual is a measure of model bias whereas the standard error measures variability of individual estimates. The near-zero-mean of the residuals indicate that the predictions are accurate on average, while the large standard errors (corresponding to more than a factor of two) indicate low precision for any given event and station. At distances less than 100 km, high-frequency (5 to 10 Hz) amplitudes are underpredicted by 20 to 35%. When distances up to 200 km or more are considered, the high frequencies have no net bias, but low frequencies (1 to 2 Hz) are underpredicted by 20 to 40%. These discrepancies could likely be eliminated by allowing a frequency-dependent attenuation form, but this additional complexity does not

appear warranted, particularly since the attenuation studies indicated that the apparent frequency-dependence is not statistically significant.

The variability of estimates is unexpectedly large considering that this represents only the intra-event variability (ie. the source spectra are known). The large variability can be attributed to the inclusion of two unusual events, the Charlevoix and Saguenay earthquakes, both of which were deep. The results of regression to the larger ECTN dataset, by comparison, indicates that the average standard deviation of data from regression predictions (intra-event variability) is about 0.20 log units (factor of 1.6).

I conclude that the agreement between simulations and recordings is excellent on average, although there is large station-to-station variability. This indicates that the regression results have provided a useful, albeit imprecise, characterization of the overall source, path and site effects that influence the ground motions in the frequency band from 1 to 10 Hz.

TABLE 4.1
Average Residual(Bias) and Standard Error: Stochastic Model
Comparison of Records to Simulations for Calibration Events

FREQ.	BIAS	(Factor)	STANDARD ERROR	(Factor)
a) All distances (R = 10 to 1000 km)				
1 Hz	0.15	1.41	0.32	2.09
2 Hz	0.11	1.29	0.33	2.14
5 Hz	0.02	1.05	0.33	2.14
10 Hz	-0.01	0.98	0.33	2.14
PGA	-0.01	0.98	0.34	2.19
PGV	0.09	1.23	0.38	2.40
b) Distances less than 200 km				
1 Hz	0.13	1.35	0.35	2.24
2 Hz	0.09	1.23	0.35	2.24
5 Hz	0.03	1.07	0.36	2.29
10 Hz	0.07	1.17	0.30	2.00
PGA	0.05	1.12	0.36	2.29
PGV	0.00	1.00	0.38	2.40
c) Distances less than 100 km				
1 Hz	0.07	1.17	0.36	2.29
2 Hz	0.06	1.15	0.35	2.24
5 Hz	0.09	1.23	0.38	2.40
10 Hz	0.12	1.32	0.30	2.00
PGA	0.14	1.38	0.31	2.04
PGV	0.06	1.15	0.36	2.29

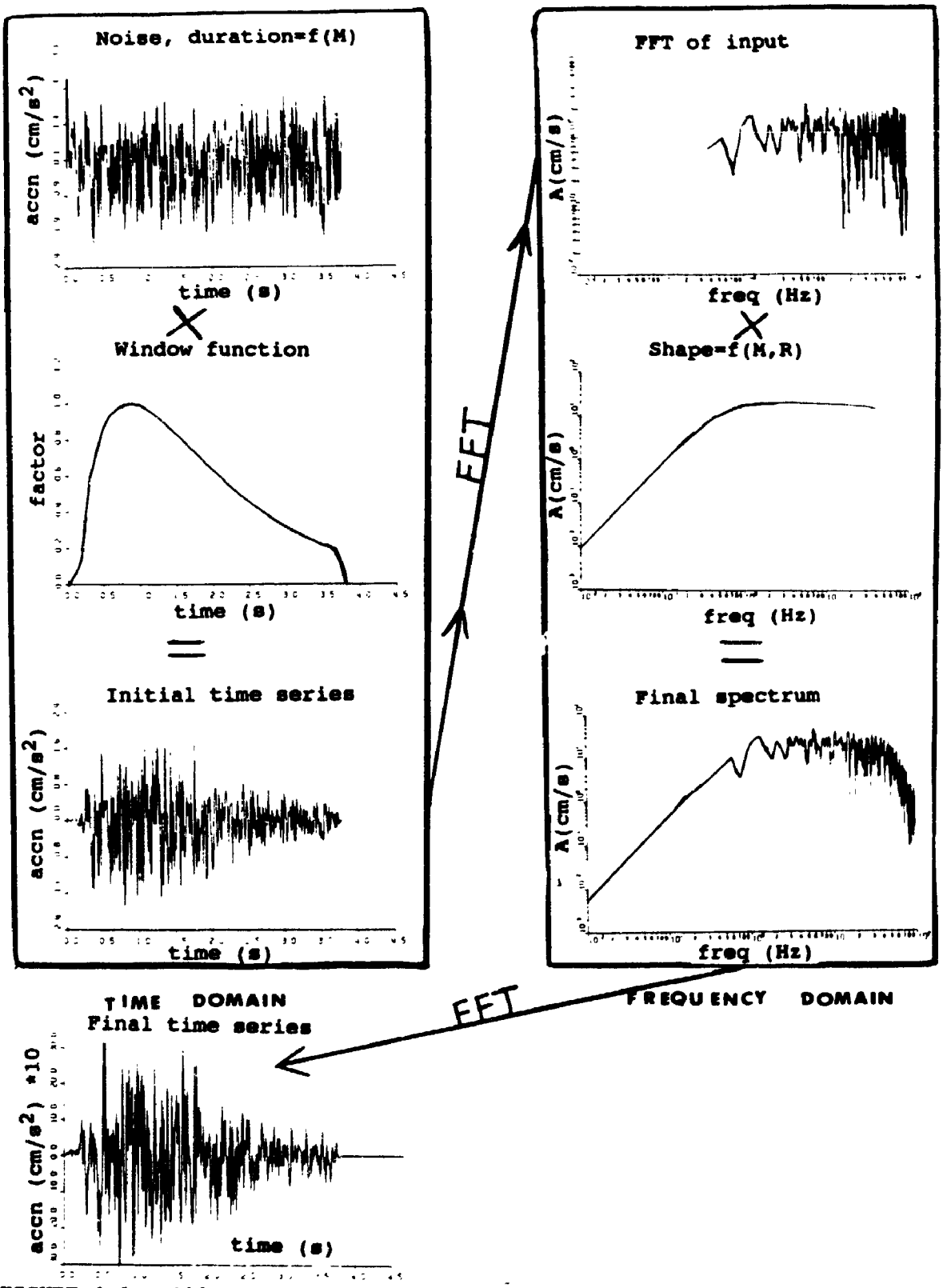

FIGURE 4.1 - Illustration of simulation technique (for Brune 200 bar event with M=6 at R=20 km). Finite-duration Gaussian noise is windowed (left), then transformed to frequency domain. The noise spectrum is multiplied by the desired spectral shape (right), then transformed back to the time domain to yield the final time series.

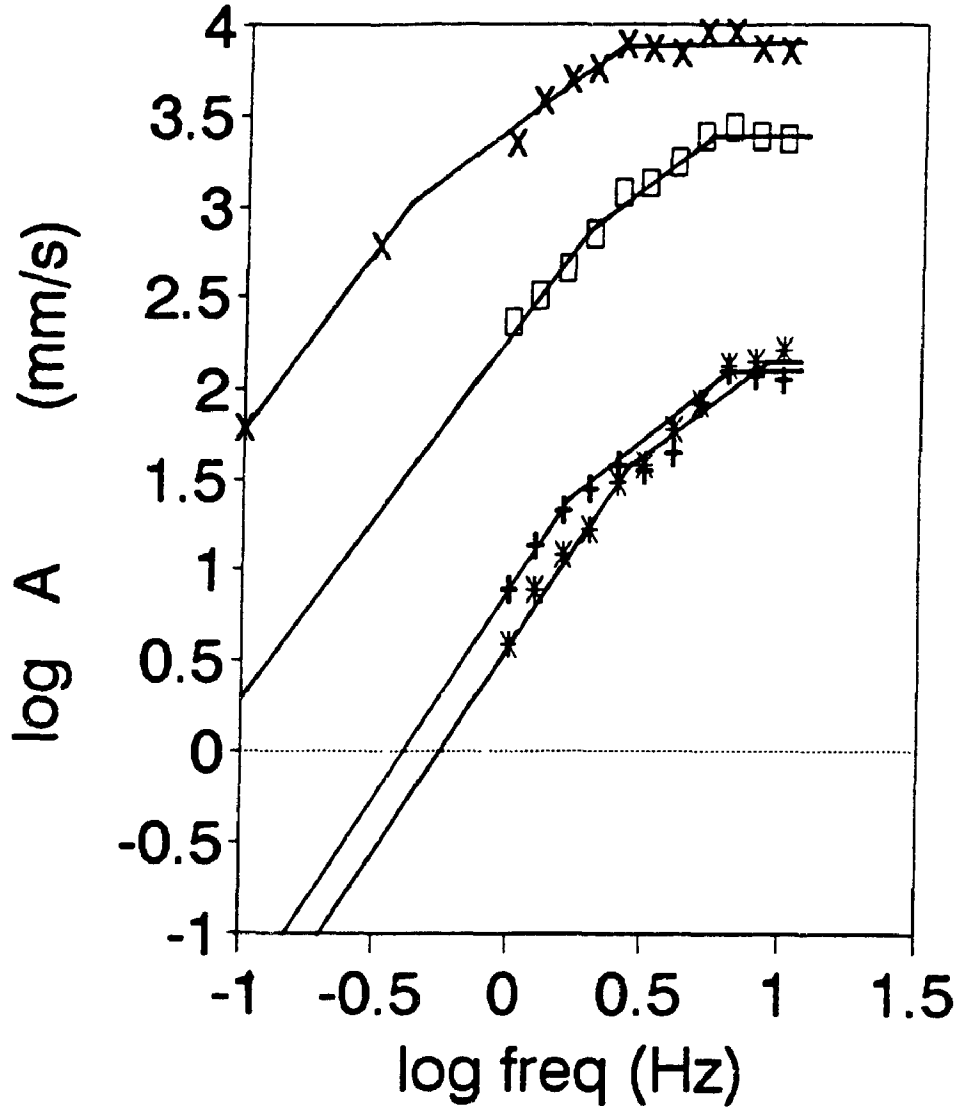

FIGURE 4.2 - Source Spectra for Study Events (vertical component of the Fourier acceleration spectrum, at a distance of R = 1 km)

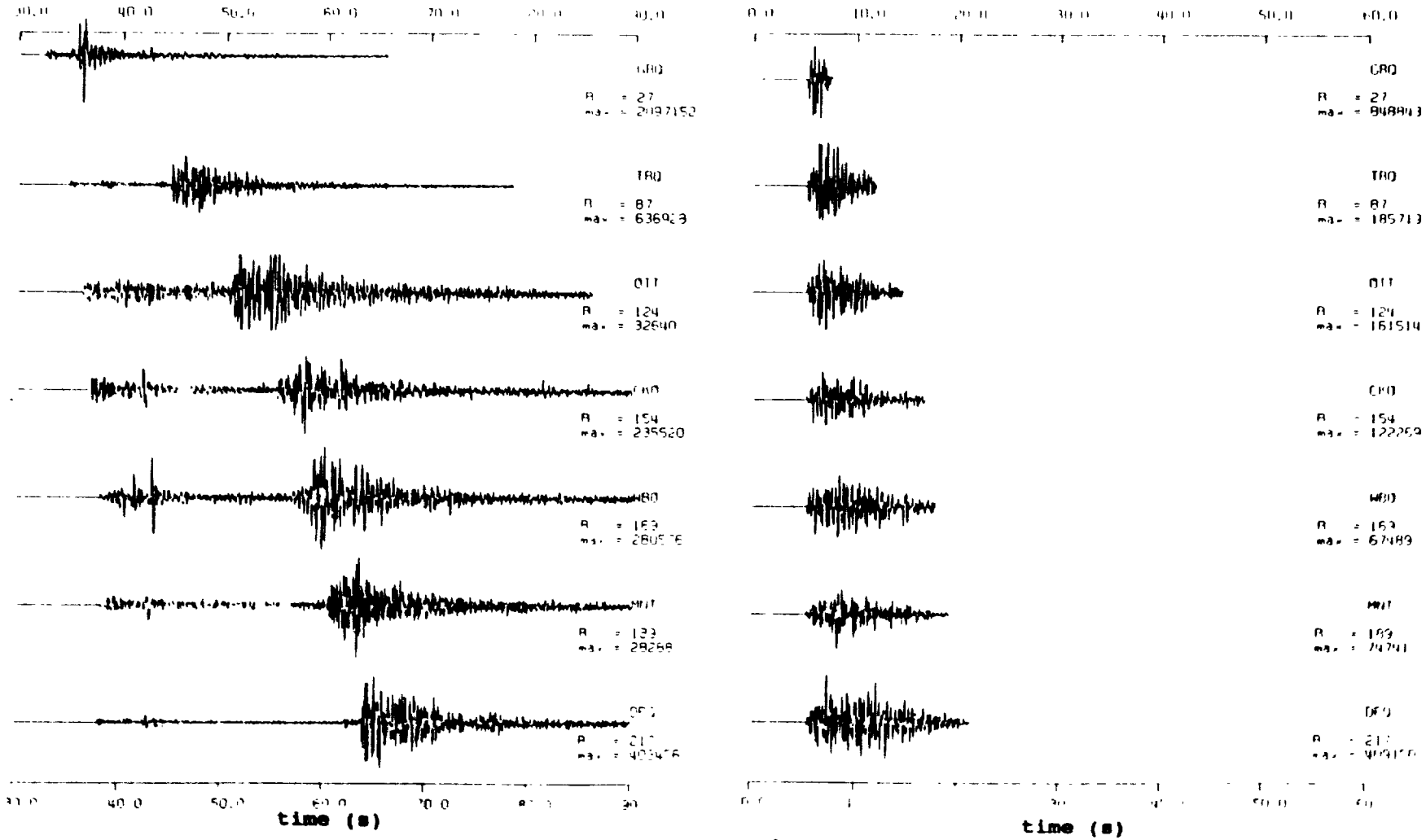

FIGURE 4.3 - Example comparison of Records (left) with Stochastic Synthetics (right) for Mont Laurier earthquake.

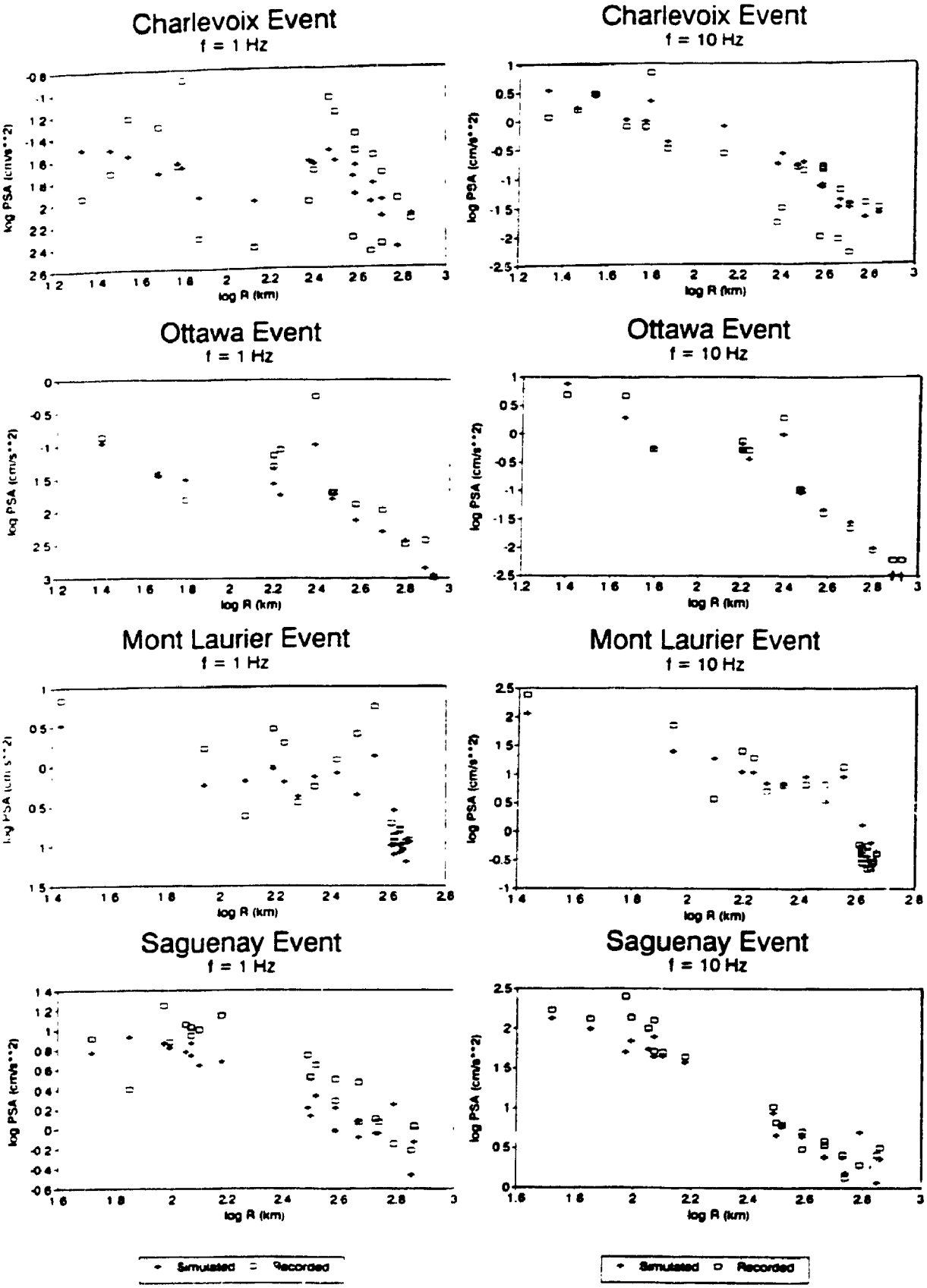

FIGURE 4.4 - Comparison of Stochastic Synthetics to Records: PSA at 1 and 10 Hz for Four Calibration Events.

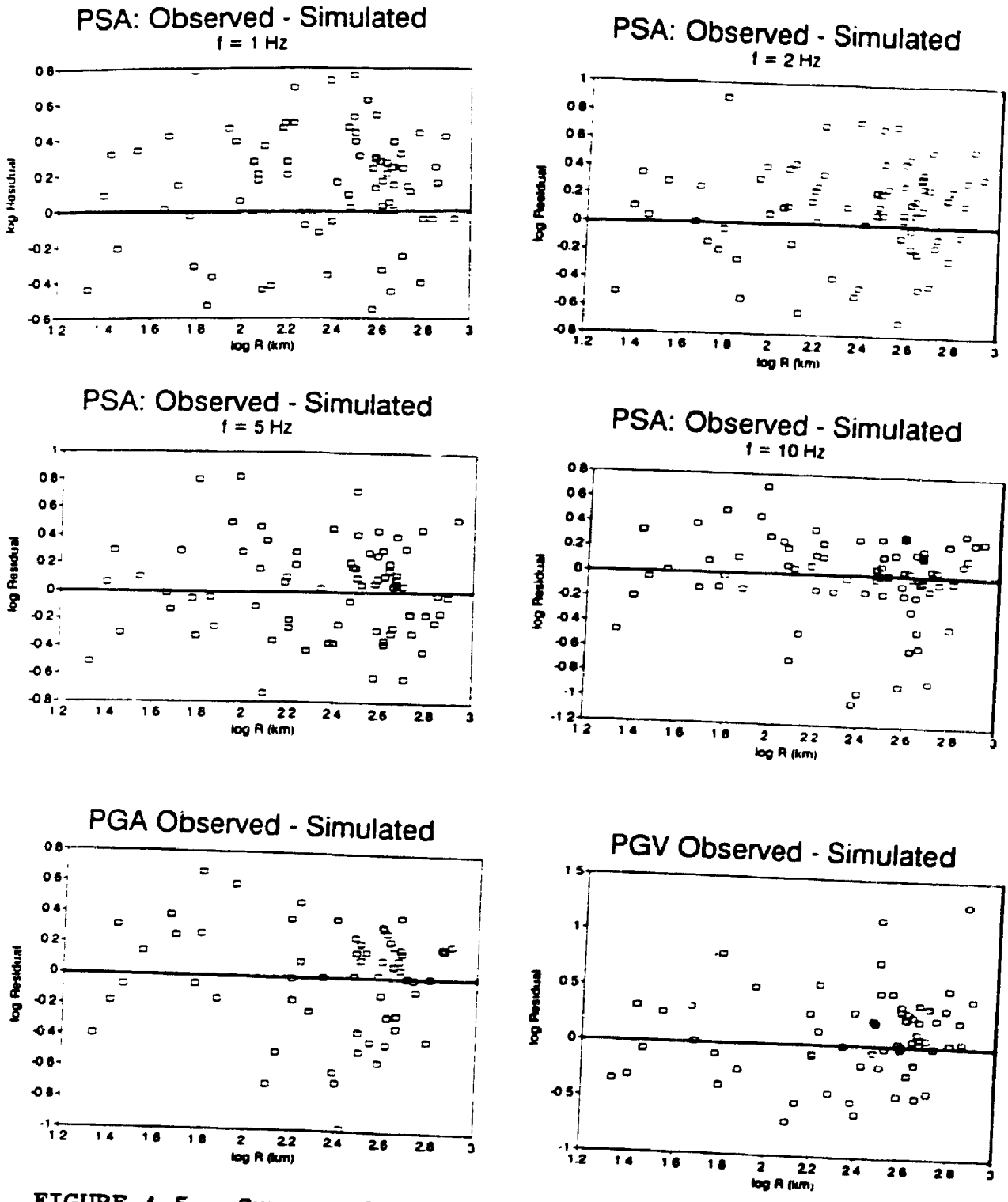

FIGURE 4.5 - Summary Comparison of the (log) differences between Records and Stochastic Synthetics (all events).

5 - EARTHQUAKE SOURCE SPECTRA IN EASTERN NORTH AMERICA

5.1 Introduction

It has been shown in Chapter 4 that ground motions in the frequency range from 1 to 10 Hz can be accurately, albeit imprecisely, predicted from a simple stochastic model, if the source spectrum of the earthquake is known. In Chapter 4, the source spectra for the events to be simulated were known from regression analysis of the observations. In order to predict ground motions for a future earthquake, we require a more general model for the average source spectrum, preferably as a function of its seismic moment (or some other simple magnitude measure).

In this chapter, I establish an average empirical source model for ENA earthquakes as a function of seismic moment. The model is based on acceleration source spectra data for ENA earthquakes of M 3 to 7 and contains no apriori assumptions concerning the source-spectral shape. The data include ECTN source spectra (Chapter 3), estimates obtained from historic ENA events using regional seismographic data (Street and Turcotte, 1977), teleseismic spectra (Boatwright and Choy, 1992), and spectral amplitudes obtained from correlations between Modified Mercalli Intensity (MMI) data and high-frequency spectral levels. These data allow definition of the Fourier spectrum of acceleration at 1 Hz and at high frequencies (ie. frequencies above the highest

corner frequency but below any high-frequency cut-off) for ENA sources of $4 \leq M \leq 7$.

5.2 Source Spectral Database

5.2.1 ECTN Source Spectra. The primary data for the model are the ECTN spectra of acceleration at the earthquake source (R = 1 km). The reliability of these source spectra, in light of large random variability and the unresolvable uncertainties in attenuation, is a significant issue, which I address in this section.

Boatwright (personal communication, 1993) applied the inversion procedure of Boatwright et al. (1991; also Fletcher and Boatwright, 1991) to the same ECTN spectral amplitude dataset. His inversion procedure contrasts with that of this study in the manner in which source and site terms are constrained, and in the way that the attenuation curve is modeled. Principally, the source terms in his data regression are constrained to fit the Brune spectral shape, while the site terms are unconstrained. Differences between the results from these two regression schemes are surprisingly small; on average moment magnitudes agree to within 0.1 units, corner frequencies agree within 10%, and Brune stress parameters agree within 30%. (For my regressions, the Brune stress parameter is computed from the high-frequency level of the source spectrum, using Equation 1.2 for $f >> f_o$.) There are two main reasons for the agreement: (i) most of the study events fit the Brune shape

reasonably well; and (ii) the average (unconstrained) site terms are not strongly dependent on frequency. I conclude that both of these two inversion methods provide equivalent information on the source spectrum, and imply similar spectral amplitudes.

Further confirmation of the reliability of the ECTN source spectra is provided by comparisons with spectra derived independently from strong-motion data. Such a comparison is shown by Boatwright (personal communication, 1993) for the March 31 aftershock of the 1982 Miramichi earthquake; he finds that the regional data satisfactorily predict the near-source amplitudes. The ECTN spectrum for the Saguenay earthquake, as obtained from this study using just the ECTN data, agrees well with that obtained by Boore and Atkinson (1992), which was largely based on the strong-motion data for that event. Finally, the seismic moments for events of $M < 4.5$ agree with published values which were based on other data sources. (There are three such events: 82/01/19, 82/03/31 and 82/06/16. Moment magnitudes for these events are listed in Boore and Atkinson (1987) as 4.3 - 4.5, 4.0 - 4.2, and 3.8, respectively. The ECTN data give a value of 4.0 for all three events.)

For events of $M > 4.5$, the seismic moment generally cannot be reliably determined from ECTN data due to the limited bandwidth; determination of the long-period displacement level for such events requires instrumentation

capable of recovering frequencies significantly less than 1 Hz. Therefore seismic moments for all events of M > 4.5 are based on other data sources, primarily those listed by Boore and Atkinson (1987). The one exception is the Mont Laurier earthquake of 1990, for which no independent estimates of moment are available. From the ECTN data, I estimate M = 4.7 from P-waves, and M = 4.5 from S-waves. By examining the spectrum of this event, and comparing it to others having similar amplitude at 1 Hz, I prefer the P-wave estimate of 4.7.

The limited ECTN bandwidth also places constraints on the reliability of the high-frequency spectral levels, and hence the Brune stress parameters, for events of M 3.5 and smaller. As shown in Figure 5.1, the corner frequency for events of M < 3.5 approaches 10 Hz (the upper limit of the recoverable ECTN bandwidth). For these events the 10 Hz amplitude is a lower bound for the high-frequency level. Consequently the Brune stress parameter will be systematically underestimated. This leads to an apparent dependence of stress parameter on seismic moment for events of M < 4 (Figure 5.1). For events of M > 4, we would infer that the average Brune stress is somewhat greater than 100 bars, independent of seismic moment. Note that two events (Saguenay and Mont Laurier) have much larger stress parameters, of the order of 500 bars.

Typical source spectra for some of the earthquakes are plotted as a function of frequency in Figure 5.2, in comparison to the Brune model for the event's seismic moment and high-frequency level. The figure also compares the inversions of this study (A model and data) to Boatwright's inversions (B model and data). Small events (M < 4.5) are well-matched by the Brune shape. For events larger than M 4.5, by contrast, there appears to be a deficit of intermediate-frequency energy relative to that which would be implied by the Brune model, for the given moment and high-frequency level. This is analogous to the 'The Case of the Missing Moment' described for the Saguenay earthquake by Boore and Atkinson (1992), and appears to be a feature of all of the larger events. A second corner frequency is required to reconcile the long-period level required by the seismic moment with the high-frequency level, in order to avoid grossly overestimating spectral levels for intermediate frequencies.

The ECTN spectral data provide a relatively complete picture of spectral amplitudes for small earthquakes, but there are only a dozen events for the magnitude range 4 < M < 7, which is of most engineering interest. I next describe data that can augment the source spectral database for M > 4. I focus on two spectral parameters: the 1 Hz spectral amplitude and the high-frequency level of the spectrum. Definition of these parameters as a function of seismic

moment (Table 5.1) will provide the basis for an empirical spectral model covering the entire frequency band.

5.2.2 Additional Seismographic Data. There are three additional seismographic data sources for ENA source spectral amplitudes. These data, and the frequency range over which they apply, are described below.

(i) Street and Turcotte (1977) digitized regional seismographic recordings from historic earthquakes in ENA and tabulated 1 Hz source spectral amplitudes. The attenuation correction they employed at 1 Hz agrees well with that determined by this study, so the 1 Hz source spectral estimates should be mutually-consistent.

(ii) Boatwright and Choy (1992) used teleseismic data to obtain acceleration source spectra, for frequencies less than 2 Hz, for several ENA events. Their 1 Hz spectral estimates agree with results based on ECTN or strong motion data, for the Saguenay, Ungava and Nahanni earthquakes; their 1 Hz amplitude levels are also consistent with Street and Turcotte's (1977) estimates for events of similar moment. However, the ECTN data give larger amplitudes than those found by Boatwright and Choy for the high-frequency spectral level. I suspect this discrepancy is due to the bandwidth of the teleseismic data for the Boatwright and Choy study ($f < 2$ Hz), combined with increasing

uncertainty in teleseismic attenuation corrections for frequencies in the 1 to 2 Hz range. Their spectra do not necessarily extend to sufficiently high frequencies to allow the high-frequency level to be observed. I therefore use the Boatwright and Choy source spectral amplitudes at 1 Hz, but do not consider their teleseismic estimates to be a reliable measure of the high-frequency spectral levels.

(iii) I consider the Nahanni earthquakes to be more nearly representative of midplate than western earthquakes: they occurred in a region of high compressive stresses in which thrust mechanisms are dominant, there was no surface rupture despite shallow focal depths, and the rocks in the focal region have high seismic velocities (Wetmiller et al., 1988). I therefore include them in the ENA dataset. The source spectrum for the largest event (M 6.8) was determined by near-source accelerograph data (Choy and Boatwright, 1988). The spectra of the smaller events were obtained from the spectral ratio of each event to that of the largest shock (Boore and Atkinson, 1989). The spectral ratios were based on regional seismographic data. The Nahanni source spectra are well-defined over the entire frequency band of interest.

These additional seismographic data provide sufficient information regarding 1 Hz spectral amplitudes to allow a

reasonably well-based spectral model to be defined for intermediate frequencies. Unfortunately, they do not provide much additional information on the high-frequency spectral level for large ENA events. Hanks and Johnston (1992) have suggested that the Modified Mercalli Intensity (MMI) data from historic earthquakes may contain such information. I therefore turn to this data source of uncertain value, in the hope that it may allow us to estimate the high-frequency level for large ENA earthquakes for which we have no instrumental data.

5.2.3 Modified Mercalli Intensity Data. I first examine the correlation between source spectral parameters and Modified Mercalli Intensity. Table 5.2 lists the areas enclosed by various MMI levels, for all felt events in ENA for which we have seismographic estimates of the source spectrum. The data are taken from the paper of Hanks and Johnston (1992), and from interpretation of intensity maps provided by the Geological Survey of Canada (J. Drysdale, personal communication, 1992). I examined the correlation between each of these intensity parameters and source-spectral amplitudes.

The correlation between felt area (MMI I to III) and high-frequency source spectral level is excellent. As shown in Figure 5.3 (upper frame), the felt area of an earthquake allows us to estimate the high-frequency level of the acceleration spectrum at the earthquake source with

surprising precision. The least-squares fit to the data is given by:

$$\log A_{HF} = -2.73 + 0.99 \log a_f \qquad (5.1)$$

where A_{HF} is the high-frequency source level of the vertical component at a distance of R = 1 km, in mm/s, and a_f is the felt area in km^2. The standard deviation of log A_{HF} residuals (sigma) is only 0.12. Equation 5.1 has therefore been used to estimate the high-frequency level for all large historic ENA events for which we have seismographic estimates of the seismic moment.

Interestingly, the felt area appears to be a slightly more accurate measure of the high-frequency source spectrum than is the area of stronger shaking (compare symbols for MMI V and felt areas on Figure 5.3). Felt area is probably less variable than areas of stronger shaking because soil effects are averaged over a larger region. I also find that the felt area is a better indicator of high-frequency level than of 1 Hz level (compare upper and lower frames of Figure 5.3). Finally, felt area is a better predictor of high-frequency level (sigma = 0.12) than is seismic moment (sigma = 0.17, to be shown later). This implies that felt area is more strongly controlled by stress drop than by seismic moment. It supports the contention of Hanks and Johnston (1992) that intensity data may be more diagnostic of real variations in stress drop than instrumental data (unless the

latter is obtained by modern systems capable of recovering high frequencies).

To understand why this is so, consider the idealized Brune spectra for events having the same seismic moment but different stress drops (eg. refer to Figure 1.1). If we assume that people (and many objects) are most sensitive to the peak of the acceleration spectrum, which controls the peak ground acceleration and/or velocity, then it is clear that the high-frequency source level controls the strength of the felt effects, even at large distances. It is also apparent that the felt area will be more closely related to the high-frequency spectral level than to the 1 Hz spectral level, since the 1 Hz amplitude does not necessarily measure the strongest part of the spectrum. Finally, it can be shown from Equation 1.2 (assuming $f>>f_o$) that the high-frequency source level is proportional to $M_o^{0.333}\Delta\sigma^{0.667}$; thus the felt area is more indicative of stress drop than of seismic moment.

5.3 ENA Spectral Model

5.3.1 Comparison of Data to Brune Model. The augmented source spectral database is given in Table 5.1. All tabulated data are for the vertical component; where necessary, conversion from horizontal components has been made by subtracting 0.17 log units from the high-frequency spectral level, or 0.05 units from the 1 Hz level (see Chapter 2.4).

Observed high-frequency spectral amplitude levels for all events are plotted as a function of moment magnitude in Figure 5.4, in comparison to the level predicted by the Brune model (at a frequency of 10 Hz) for stress parameters of 100 and 500 bars (Equation 1.2). For $M < 4$, the stress parameter appears to increase with M, as is expected due to the finite bandwidth of the ECTN instruments (Boore, 1986). For $M > 4$, the data are consistent with a constant Brune stress parameter of approximately 200 bars. Different data sources (indicated by different symbols) appear to be mutually consistent. Aftershock data appear to have lower stress parameters than mainshocks, as suggested by Boore and Atkinson (1989). The (unweighted) regression line to the mainshock data, for $M > 4$ (shown on the Figure) is:

$$\log A_{HF} = 0.33 + 0.51\ M \qquad (5.2)$$

where A_{HF} is in mm/s, at a distance of 1 km, for the vertical component. The standard deviation of the residuals (sigma) is 0.17 log units. Note that the slope of the line is essentially equal to the value of 0.5 that is required for a constant-stress model.

Figure 5.5 plots the 1 Hz spectral amplitudes against M. For $M < 4$ the amplitudes are independent of the stress parameter (we are on the 'moment-end' of the spectrum). For $M > 4$ the amplitudes are consistent with a constant Brune stress parameter of approximately 50 bars (although 1 Hz amplitudes are not particularly sensitive to the stress

parameter until large magnitudes are reached). All plotted data sources, including aftershocks, appear mutually consistent, and they have all been included in obtaining the least-squares fit to the 1 Hz spectral amplitude, which for $M > 4$ is:

$$\log A_{1Hz} = 1.13 + 1.23(M-4) - 0.14(M-4)^2 \qquad (5.3)$$

with sigma = 0.18. (Note: This regression excluded the highest point on Figure 5.5, which is Street and Turcotte's value of A_{1Hz} for the Timiskaming earthquake; this point exceeds the high-frequency level for this event estimated from the felt area, and is an outlier to the data. The data point is not sufficiently reliable to warrant allowing it to dominate the fit.)

The fact that a 50-bar stress parameter matches the 1 Hz spectral amplitude, while a 200-bar stress parameter matches the high-frequency level, is further evidence that two corners are required for the ENA spectral model. Interestingly, Smith et al. (1991) reached a similar conclusion from a set of ten interplate events ($M > 6$); their conclusions were also based on composite source spectra compiled from a variety of sources. The apparent need for two corner frequencies leads me to propose an empirical source model which will more accurately predict ENA source spectra in the 1 to 10 Hz frequency band.

5.3.2 Construction of Empirical Source Model. In Figure 5.6 I construct an empirical two-corner model for ENA source

spectra (horizontal component of the shear-wave spectrum), for M = 4, 5, 6 and 7, which reconciles all of the available spectral data. The primary constraints on the model are the fits to the 1 Hz and high-frequency amplitudes, given by Equations 5.2 and 5.3 and shown by the plus symbols in Figure 5.6. The other constraints on the model are that it must converge to the omega-squared source model (Equation 1.2) at low frequencies, at the level determined by the seismic moment. Spectral amplitudes are constant for high frequencies (above the second corner).

A secondary goal, which is not always compatible with those above, is to match spectral shape data by matching observed corner frequencies. For this purpose I have plotted interpreted lower and upper corner frequencies for the largest events (Figure 5.7; data in Table 5.3). The lower corner frequencies, f_A, are interpreted from teleseismic and strong-motion data. They include the implied corner frequencies from the source duration data of Somerville et al. (1987), under the assumption that $f_A = 1/(2T)$, where T is the observed teleseismic duration (Boatwright, personal communication, 1992). This assumption follows from the Brune model.

f_A is well-constrained by the data. A linear least-squares fit gives:

$$\log f_A = 2.41 - 0.533\ M \qquad (5.4)$$

This equation was used to obtain the f_A values plotted as vertical bars on Figure 5.6.

The upper corner frequencies, f_B, are from ECTN and strong-motion data. They were obtained by finding the frequency at which the source spectrum has attained 1/2 of its full high-frequency level; this definition is used for consistency with the Brune functional form (eg. in Equation 1.2, $A(f) = A_{HF}/2$ at $f = f_o$; see also Figure 1.1).

f_B is not well-constrained by data, due to the paucity of high-frequency data for large magnitudes. The fit to these data was therefore used only loosely in constraining the high-frequency shape of the spectrum. Consequently the f_B values implied by the constructed model (plotted on Figure 5.7 and given by Equation 5.7) do not match the data very closely.

In order to match both amplitude levels and corner frequencies, it is apparent that the spectral shape must be more complex than that of a single-corner-frequency Brune model. The data points on Figure 5.6 suggest that an appropriate functional form might be derived by adding two Brune spectra (Boore, personal communication, 1992). Accordingly, the functional form for the empirical model is:

$$A(f) = C\ (2\pi f)^2\ M_o\ \{(1-\epsilon)/[1+(f/f_A)^2] + \epsilon/[1+(f/f_B)^2]\} \qquad (5.5)$$

where ϵ represents some fraction of the total moment. To determine the parameters of the model, I fixed f_A to be

given by Equation 5.4. By trial-and-error, I determined that all data of $4 \leq M \leq 7$ can be sensibly fit when:

$$\log \epsilon = 2.52 - 0.637\ M \qquad (5.6)$$

$$\log f_B = 1.43 - 0.188\ M \qquad (5.7)$$

A measure of how well the model fits the empirical data is provided in Figure 5.8, which plots the residuals (defined as the difference, in log units, between observations and model predictions) as a function of magnitude, for the 1 Hz and high-frequency level. For these data the mean residual is -0.05 at 1 Hz and -0.01 at high frequencies, with standard deviations of 0.17 and 0.16 respectively. In Figure 5.9, the mean and standard deviation of residuals is plotted as a function of frequency, using just the ECTN data. There are only nine ECTN mainshocks with $M > 4$; two of these events, Saguenay and Mont Laurier, have stress parameters that are much larger than average, according to Figure 5.4. As shown in the upper part of the figure, their inclusion leads to significant positive residuals. If these two events are omitted (lower part of figure), the residuals are approximately zero. Thus the empirical model accommodates most ENA events, but will underpredict the high-frequency amplitudes from very high-stress events such as Saguenay.

5.4 Implications of Spectral Model

The complexity of spectral shape required to fit the empirical data suggests that ground motions from moderate to

large events may be significantly affected by 'roughness' (Gusev, 1983) on the fault plane. Equation 5.5 matches the shape proposed for large earthquakes (M > 6.5) by Gusev (1983), on the basis of observed magnitude relationships. Gusev noted that the radiation spectrum of large events may be considered the superposition of radiation from a 'main smooth source' and incoherently combined radiation from a 'subsource population'. He describes a subsource as any of a number of potentially significant elements of the main rupture, such as high-friction patches, local fault locking, bends in the fault surface, etc. Thus the empirical spectra could accommodate, in a general sense, any of a number of possible physical models incorporating some form of roughness. Examples include the Brune partial stress drop model (Brune, 1970), the asperity model (Hartzell and Brune, 1977; McGarr, 1981), the specific barrier model (Papageorgiou and Aki, 1983), and multiple-event models (Joyner and Boore, 1986; Boatwright, 1988). The spectra implied by these suggested physical models may vary substantially depending on both the model and the selected rupture parameters, but all share the characteristic of enhanced high-frequency energy. It is not the intent of Equation 5.5 to supplant these physical models, or discriminate amongst them. It is simply noted that a number of physical models are potentially consistent with the empirical model.

An interesting observation concerning the high-frequency source-spectral amplitudes, as shown on Figures 5.4 and 5.8, is that there appear to be two classes of events. Most earthquakes of M > 4 have high-frequency spectral amplitudes that are well-predicted (ie. within about 0.15 log units) by a Brune stress parameter of approximately 200 bars. By contrast, four events - the 1988 Saguenay, 1990 Mont Laurier, 1935 Timiskaming and 1968 Illinois earthquakes - are characterized by particularly high stress parameters, of the order of 500 bars. The high stress for the Timiskaming earthquake is rather speculative because its seismic moment is subject to considerable uncertainty; the high stresses for the other three events appear to be firmly established. The Saguenay and Illinois earthquakes were unusually deep (> 20 km), but the Mont Laurier and Timiskaming earthquakes occurred at 'normal' depths (about 10 km). It may be that ENA fault conditions, which are characterized by high horizontal compressive stresses and long earthquake repeat times, lead to patches of particularly high dynamic stress on the rupture surface in some cases. The possibility of the occurrence of high-stress events of this nature implies that the variability of high-frequency ground motions for ENA may be larger than previously estimated.

I explored the possibility of using Lg magnitude (M_N) rather than moment magnitude to predict the high-frequency

spectral level, thinking that this might reduce the standard deviation of the high-frequency residuals (ie. reduce variability). One might expect that high-stress events would be characterized by high M_N values. Perhaps surprisingly, I found that M_N does no better than **M** as a predictive parameter for the high-frequency level; the standard deviation of the spectral amplitude residuals, given M_N, is 0.19, compared to a standard deviation of 0.17, given **M**. Presumably this is because M_N is generally measured at frequencies lower than the highest corner frequency (except for very large magnitudes, which are sparsely represented in the dataset). I conclude that there is no advantage to using M_N rather than **M** in predictive equations for high-frequency spectral parameters. Since **M** is at least tied directly to a particular frequency range of the spectrum, and has a simple physical basis (Hanks and Kanamori, 1979), it remains the best magnitude measure for the spectral model. When **M** must be estimated from catalogue values of M_N, the empirical relation obtained from the database may be used:

$$\mathbf{M} = -0.39 + 0.98\ M_N \qquad (5.8)$$

(standard deviation = 0.15). As shown in Figure 5.10, the empirical data are sufficient to define the relationship well for $M_N \leq 6.5$.

TABLE 5.1 - Source-spectral parameters for M ≥ 4 events.

Event	MN	M	A_HF	stress	A_1Hz	Data Source
250301	7.0	6.4	3.60	177	3.32	S&T, MMI
290812	5.4	4.9	2.76	130	1.97	S&T, MMI
291118		6.7	3.88	278	3.60	S&T, MMI
351101	6.3	5.8	3.52	379	3.85	S&T, MMI
391019		5.3	2.96	130	2.65	S&T, MMI
401220	5.7	5.5	2.99	102	2.35	S&T, MMI
430114		4.2			1.26	S&T
440905	5.9	5.7	3.10	106	2.45	S&T, MMI
491005		4.4			1.45	S&T
521014		4.2			1.45	S&T
570426		4.6			1.65	S&T
681109		5.4	3.38	483		MMI
751006		4.3			1.21	S&T
800827		5.1	3.00	230		MMI
820109 *		4.6	2.32	48	2.02	ECTN
820109	5.7	5.5	2.91	77	2.80	B&C, MMI
820111 *	5.4	5.2	2.74	72	2.20	ECTN
820119	4.5	4.0	2.19	86	1.60	ECTN
831007	5.6	5.0	2.77	113	1.60	ECTN
851005		6.7	3.55	89	3.40	B&A
851223		6.8	3.45	53	3.40	B&A
851225 *		5.2	2.55	38	2.45	B&A
860131	5.0	4.8	2.75	149	1.60	ECTN
860712	4.5	4.5	2.61	154	1.60	ECTN
870610		5.0	2.88	177		MMI
880325		6.3	3.25	63	3.10	B&A
881123	4.6	4.1	2.47	190	1.60	ECTN
881125	6.5	5.8	3.61	517	1.60	ECTN
890316	5.7	5.0	2.80	126	2.60	ECTN
891225	6.1	5.9	3.30	149	3.00	ECTN
901019	5.1	4.7	3.06	517	1.60	ECTN

NOTES: Spectral levels are in log units, for mm/s, vertical component at R = 1 km. Stress is the required Brune stress, in bars, to match the observed high-frequency level(A_HF).
ECTN = this study; S&T = Street and Turcotte, 1977;
MMI = estimated from felt area; B&C = Boatwright and Choy, 1992;
B&A = Boore and Atkinson, 1989.
* indicates event was an aftershock.

TABLE 5.2 - MMI areas for events with seismographic source spectral data.

Event	MMI areas(km**2) log a_f	log a_{IV}	log a_V	log a_{VI}	M	log source A_HF	A A_1Hz
250301	6.41	5.83	5.14	4.8	6.4		3.32
290812	5.56		4.45	3.4	4.9		1.92
291118	6.7	6.32	5.95	5.43	6.7		3.55
351101	6.33	5.89	5.11	4.6	5.8		3.8
401220	5.79	5.34	4.67	3.42	5.5		2.3
440905	5.91	5.57	5.07	4.36	5.7		2.4
820109	5.14	4.05	3.7		4.6	2.32	2.02
820109	5.71	5.36	4.89	3.38	5.5		2.8
820111	5.45	4.91	4.5	3.45	5.2	2.74	2.2
820331	4.96	4.58	3.9		4.1	2.11	1.4
820402	4.5	3.9			3.7	1.64	
820616	4.85	4.5	3.9		4	2.06	1.2
820713	4.25	3.7			3.2	1.44	-0.1
820813	4.66	4.25			3.5	1.88	0.4
831007	5.81	5.3	4.79	3.42	5	2.77	2.2
851005	6.18	5.9	5		6.7	3.4	3.55
851223	6.18	6.08	5.26		6.8	3.4	3.45
860131	5.54	5.12	4.45	3.02	4.8	2.75	2.1
881125	6.52	6.16	5.68	5.12	5.8	3.61	3
891225	5.9	5.45	4.85		5.9	3.3	3
901019	5.81	6.1	4.85		4.7	3.06	2

Notes: a_f is felt area, a_{IV} is area experiencing MMI IV, etc. A_HF is vertical-component high-frequency source spectral amplitude (mm/s) at R=1 km. A_1Hz is 1 Hz source spectral amplitude (mm/s) at R=1km.

TABLE 5.3 - Observed corner frequencies.

Event	Moment M	fA(Hz)	fB(Hz)	Data Source
250301	6.4	0.1		S
351101	5.8	0.1		S
391019	5.3	0.3		S
401220	5.5	0.6		S
630303	4.7	1.0		S
630904	6.1	0.2		S
651021	4.6	1.0		S
681109	5.4	0.7		S
730615	4.5	0.6		S
790819	4.8	0.6		S
800727	5.1	0.5		S
820109	5.6	0.3		B&C
820111	5.2	0.6	1.6	B&C, ECTN
820119	4.0	2.5	2.6	ECTN
820331	4.1	1.0	3.2	ECTN
820616	4.0	2.0	3.3	ECTN
831007	5.0	0.8	1.4	S, ECTN
851005	6.7	0.1	0.8	B&C, B&A
851223	6.8	0.1	0.6	B&C, B&A
860131	4.8	0.8	2.1	ECTN
860712	4.5	1.0	2.2	ECTN
881123	4.1	1.3	3.2	ECTN
881125	5.8	0.2	1.7	B&C, ECTN
890316	5.0		1.0	ECTN
891225	5.9	0.2	1.0	B&C, ECTN
901019	4.7	0.8	2.6	ECTN

Notes: S=Somerville et al., 1987; B&C=Boatwright and Choy, 1992; ECTN=this study; B&A=Boore and Atkinson, 1989.
Corner fB is defined as the frequency at which the horizontal-component acceleration spectrum attains a value that is one-half of its high-frequency level.

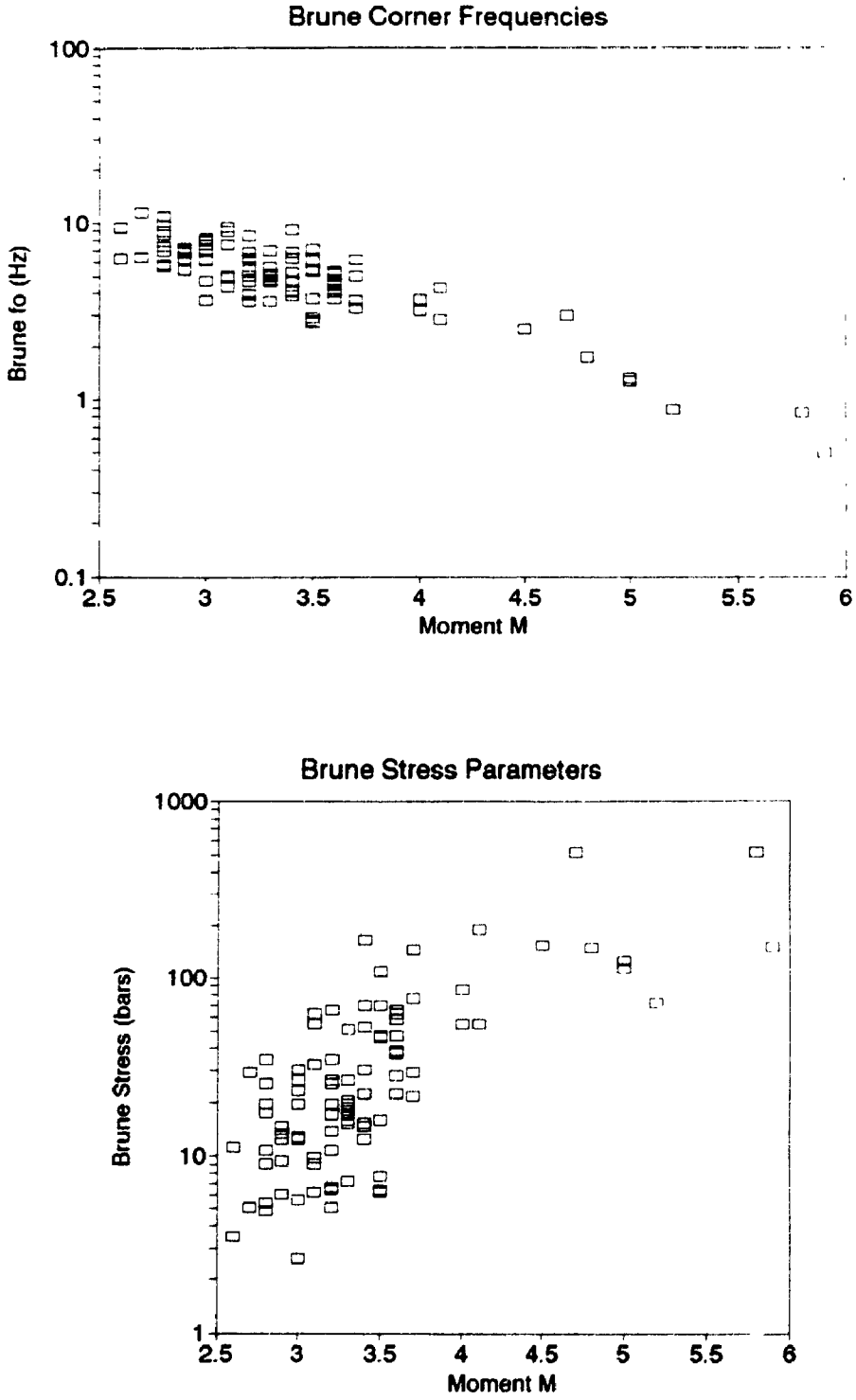

FIGURE 5.1 - Brune corner frequencies (top frame) and stress parameters (bottom frame) for the ECTN data, as a function of M.

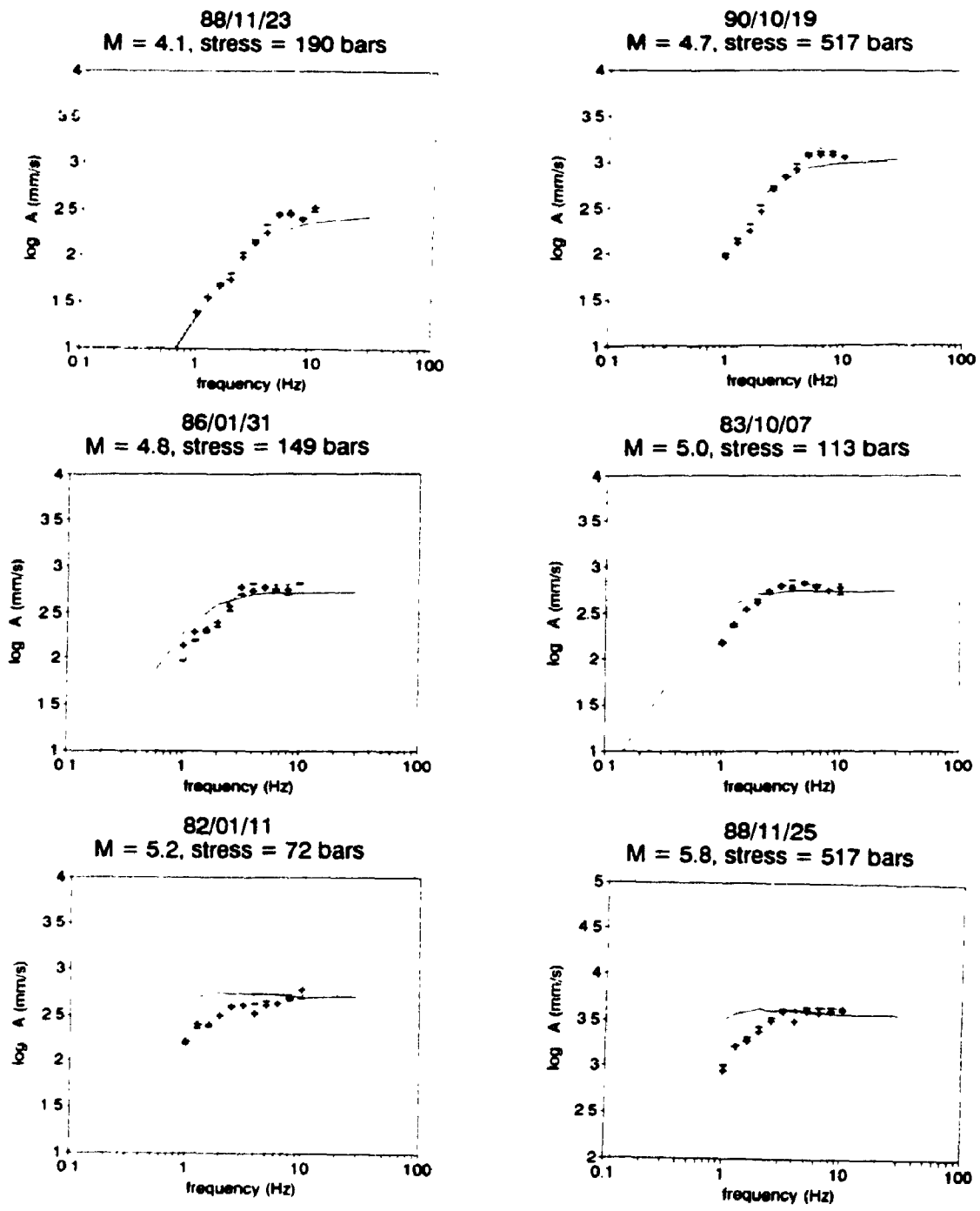

FIGURE 5.2 - Typical ECTN source spectra from this study (crosses) compared to corresponding Brune spectra for the seismic moment and high-frequency level (solid lines). Inversion results of Boatwright are also shown (horizontal bars for data and dotted lines for corresponding Brune model). For events of M < 4.5, the seismic moment was determined from the long-period level of the spectrum. For M > 4.5 the moment was obtained from other sources.

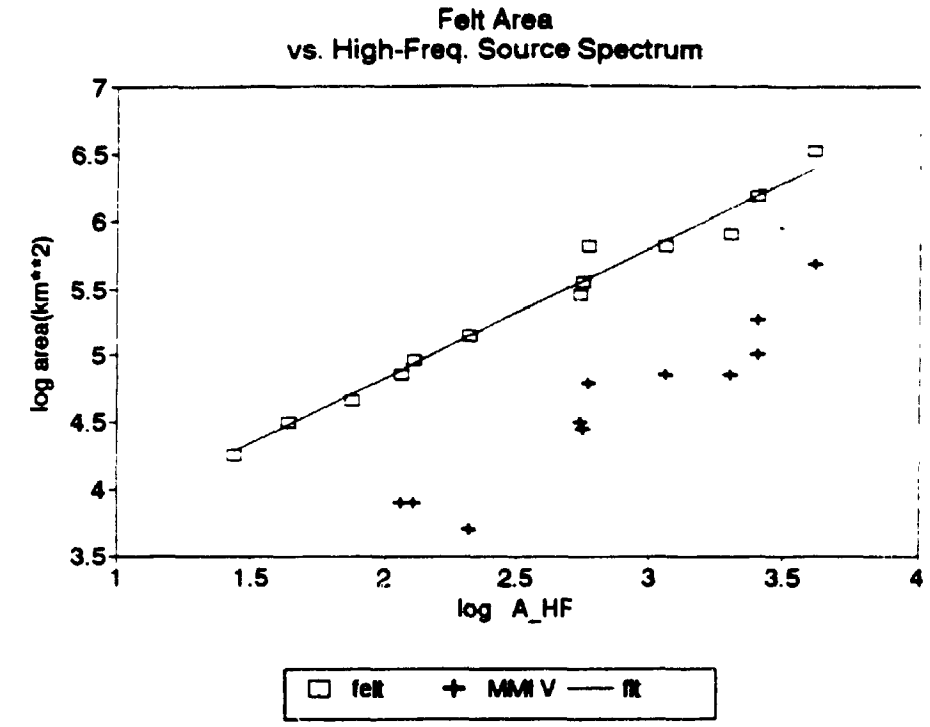

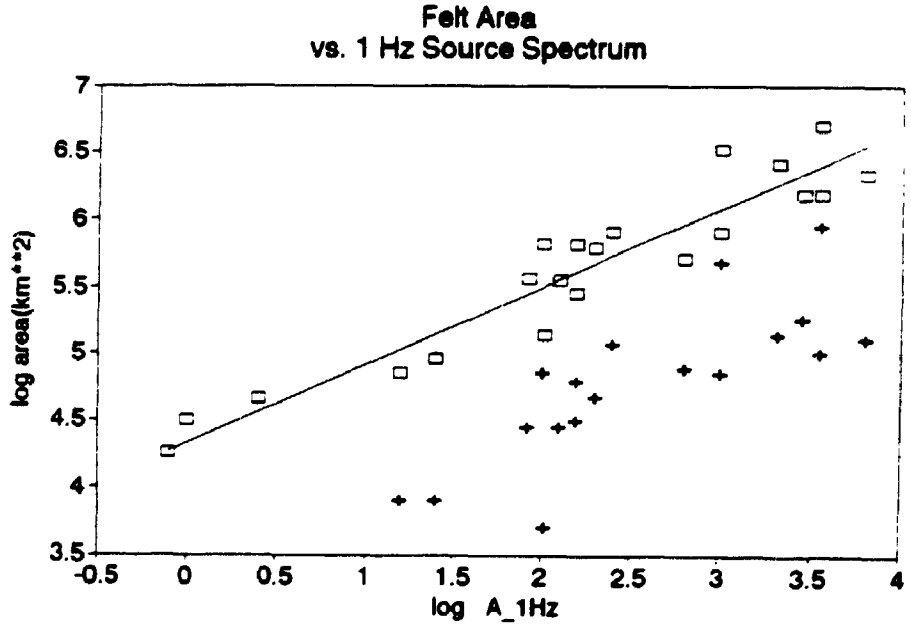

FIGURE 5.3 - Felt area (MMI intensity I - III) as a function of high-frequency source spectral amplitude (top frame), and 1 Hz source spectral amplitude (bottom frame). Data points for felt area are shown as squares, with lines indicating the least-squares fit. Corresponding areas for MMI V are also shown (plus symbols). All data are from ENA.

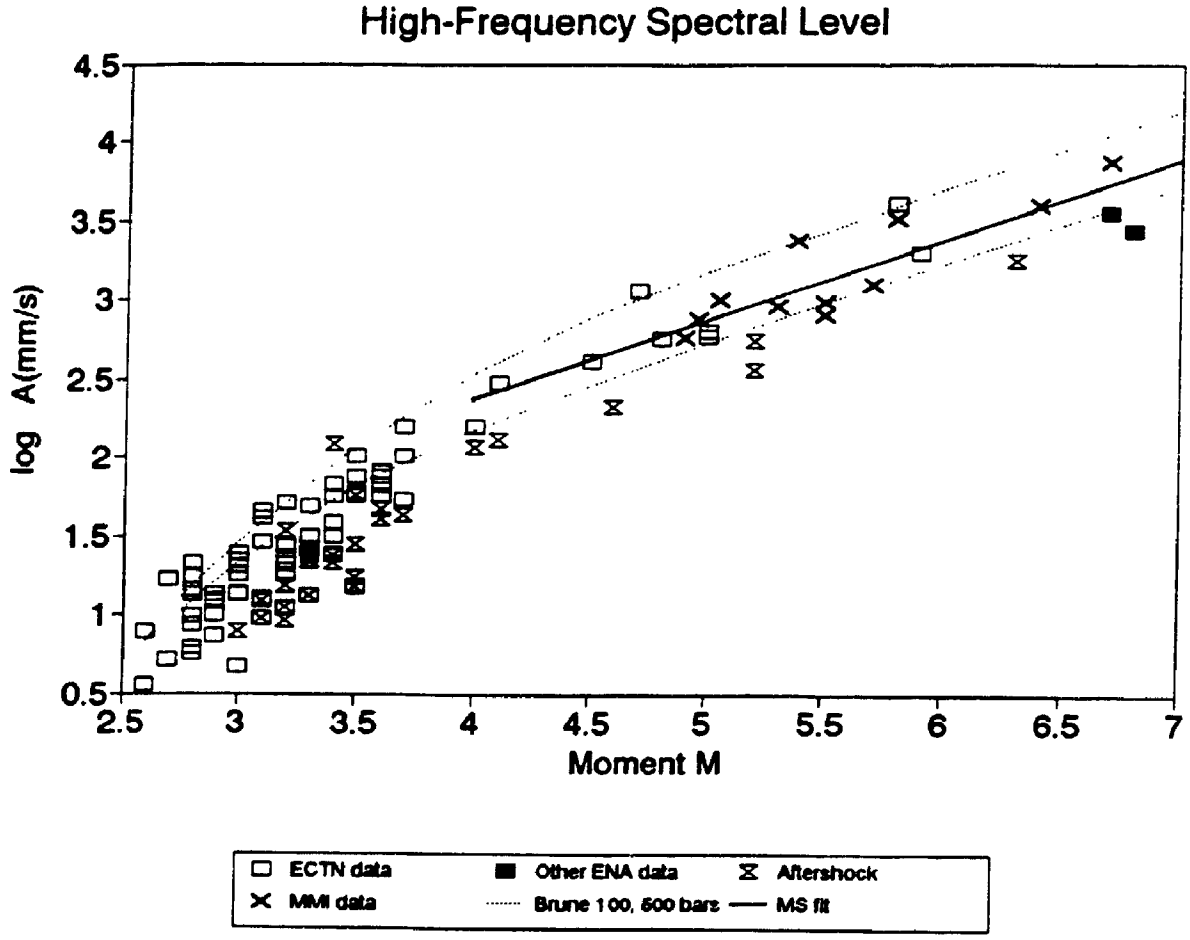

FIGURE 5.4 - High-frequency source spectral level (R = 1 km, for vertical component) in ENA, from ECTN data (open squares), MMI data (X's) and strong-motion data (filled squares); all aftershocks are denoted by hourglass symbols. Solid line shows least-squares fit to mainshock data of M > 4. Dotted lines show levels for Brune spectrum with stress parameters of 100 bars (lower line) and 500 bars (upper line).

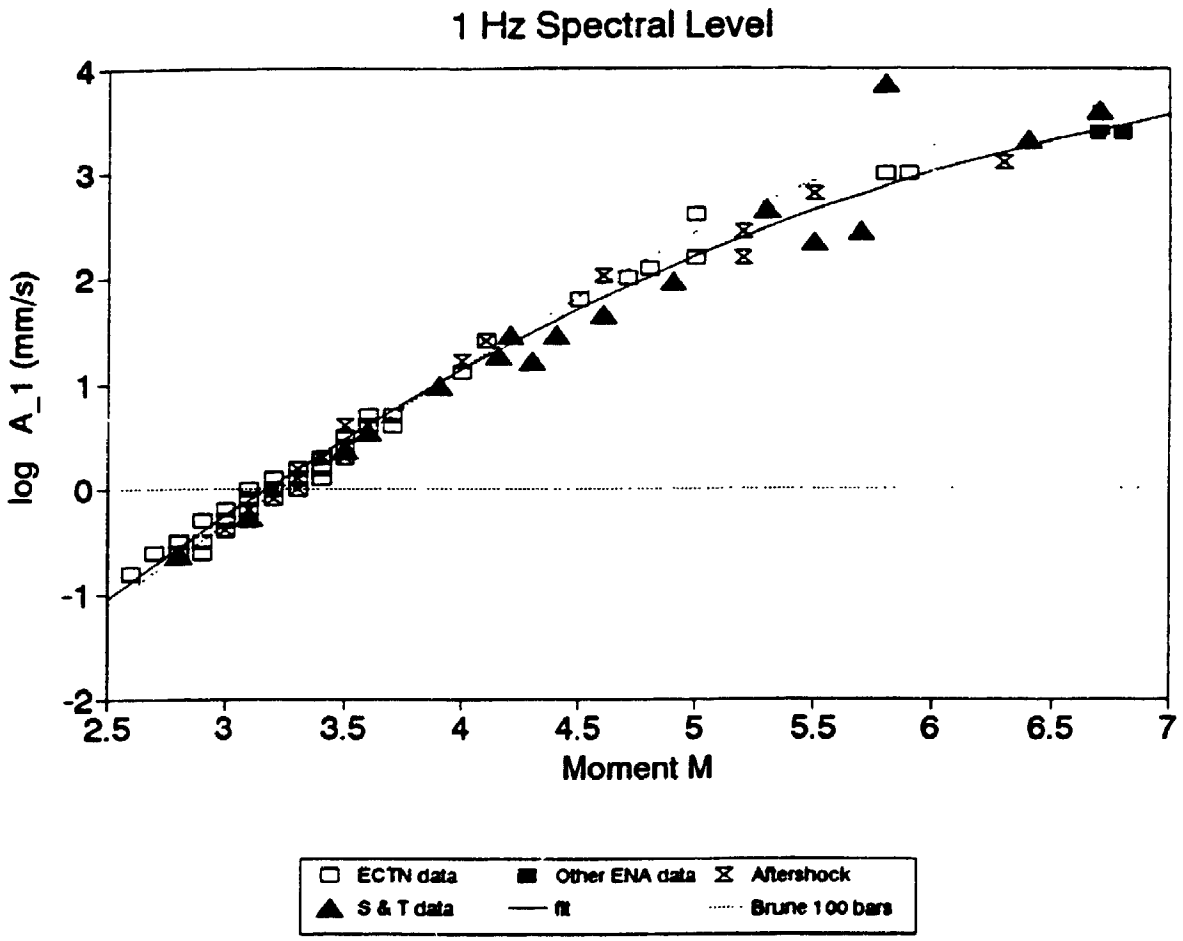

FIGURE 5.5 - Source spectral level (R = 1 km, for vertical component) in ENA, at a frequency of 1 Hz, from ECTN data (open squares), historical seismographic data of Street and Turcotte (triangles) and strong-motion data (filled squares); all aftershocks are denoted by hourglass symbols. Solid line shows least-squares fit to all data of M > 4. Dotted line shows level for Brune spectrum with stress parameter of 100 bars.

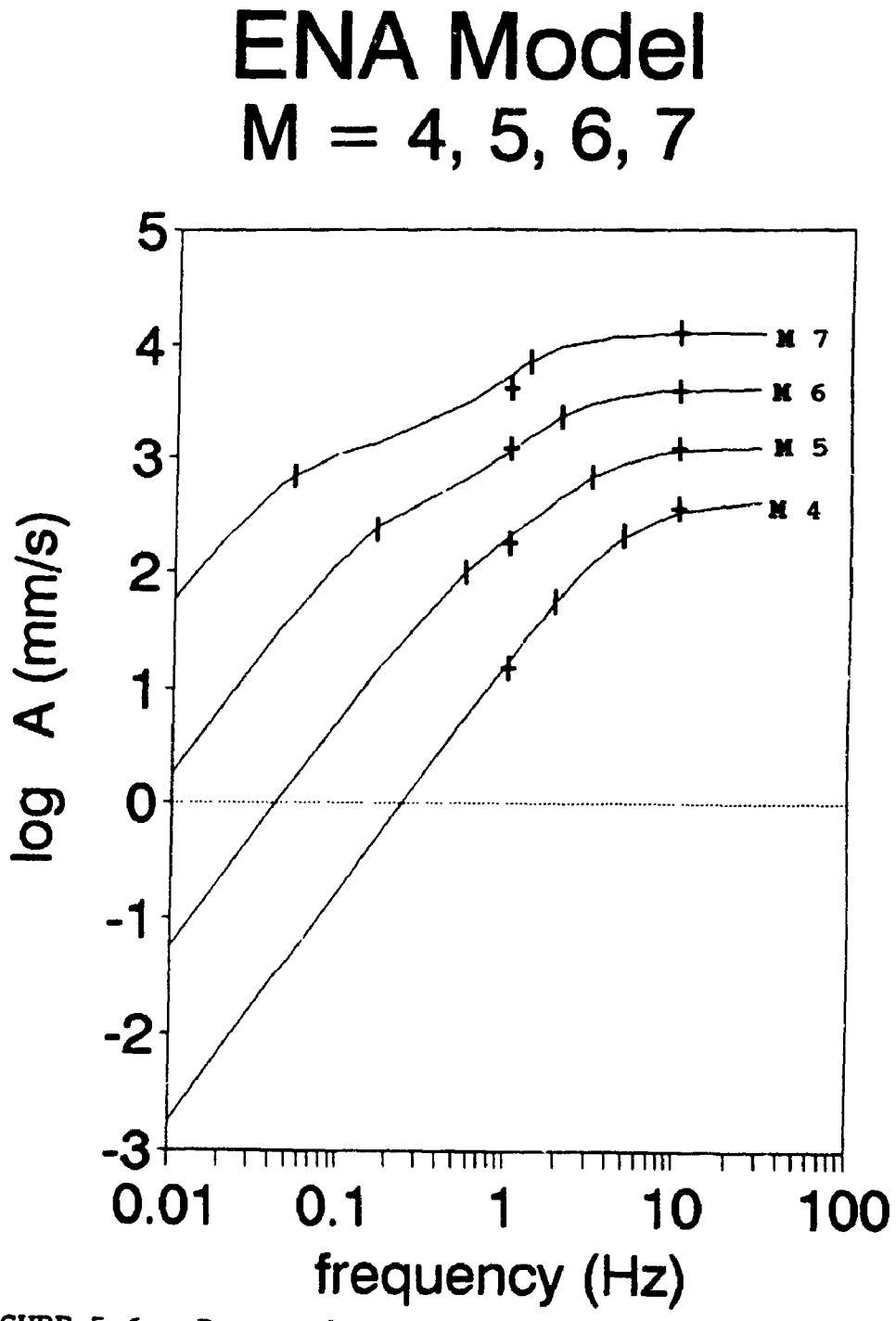

FIGURE 5.6 - Proposed two-corner model for ENA source spectral amplitudes (R = 1 km, horizontal component) as a function of frequency, for M = 4, 5, 6 and 7. Solid lines show the proposed model. Plus symbols show the target levels at 1 Hz and high frequency, obtained from least-squares fit to the data. Vertical bars show the target corner frequencies, f_A and f_B, obtained from least-squares fits to the data of Figure 5.7.

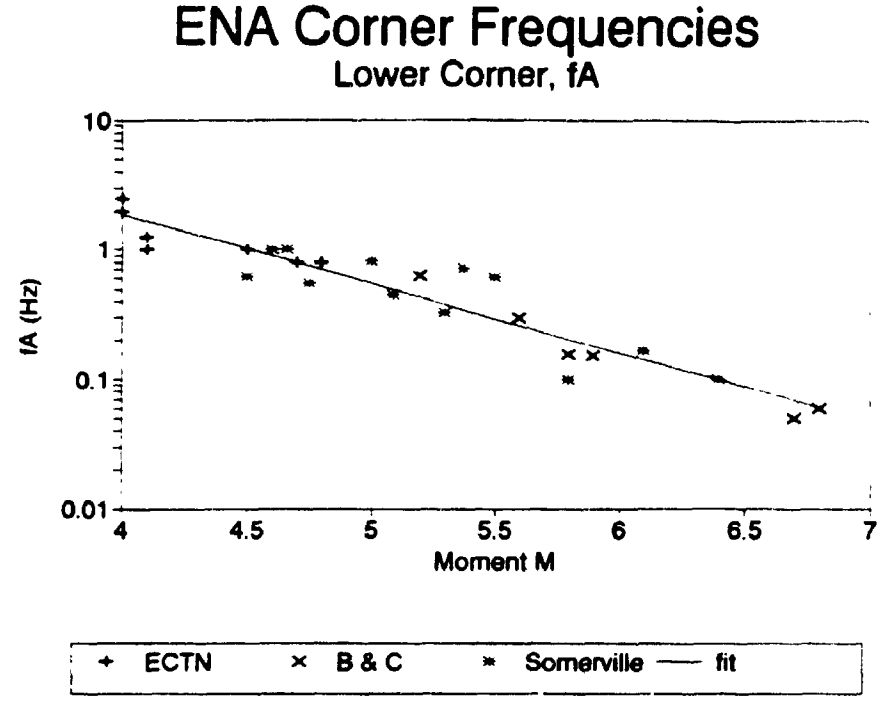

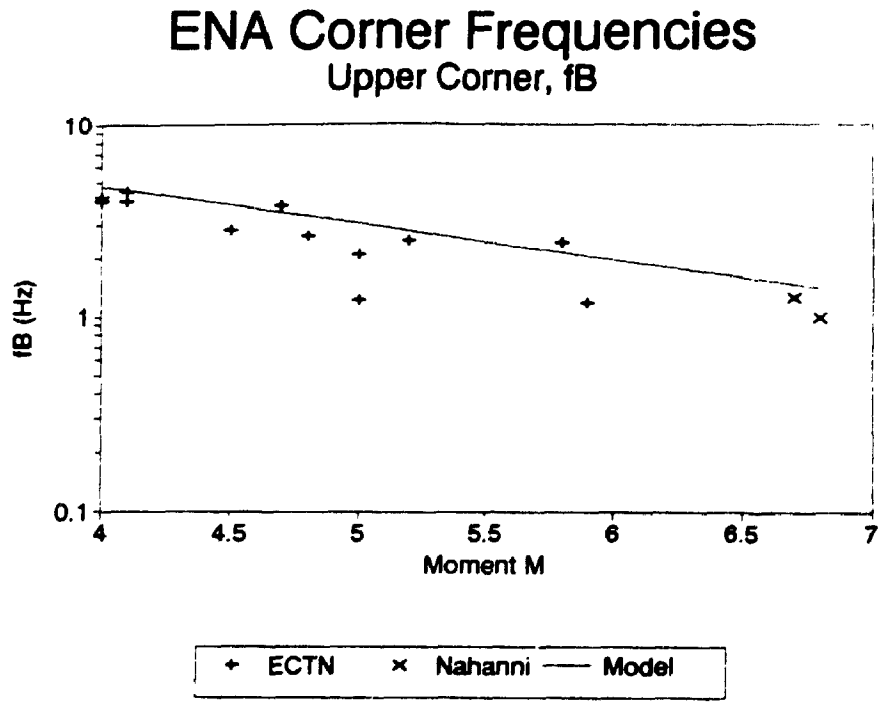

FIGURE 5.7 - ENA corner frequency data for the two-corner model. The solid line through the f_A data is the least-squares fit to the data. The solid line through the f_B data shows the values required by the empirical model (Equation 5.7), rather than the least-squares fit.

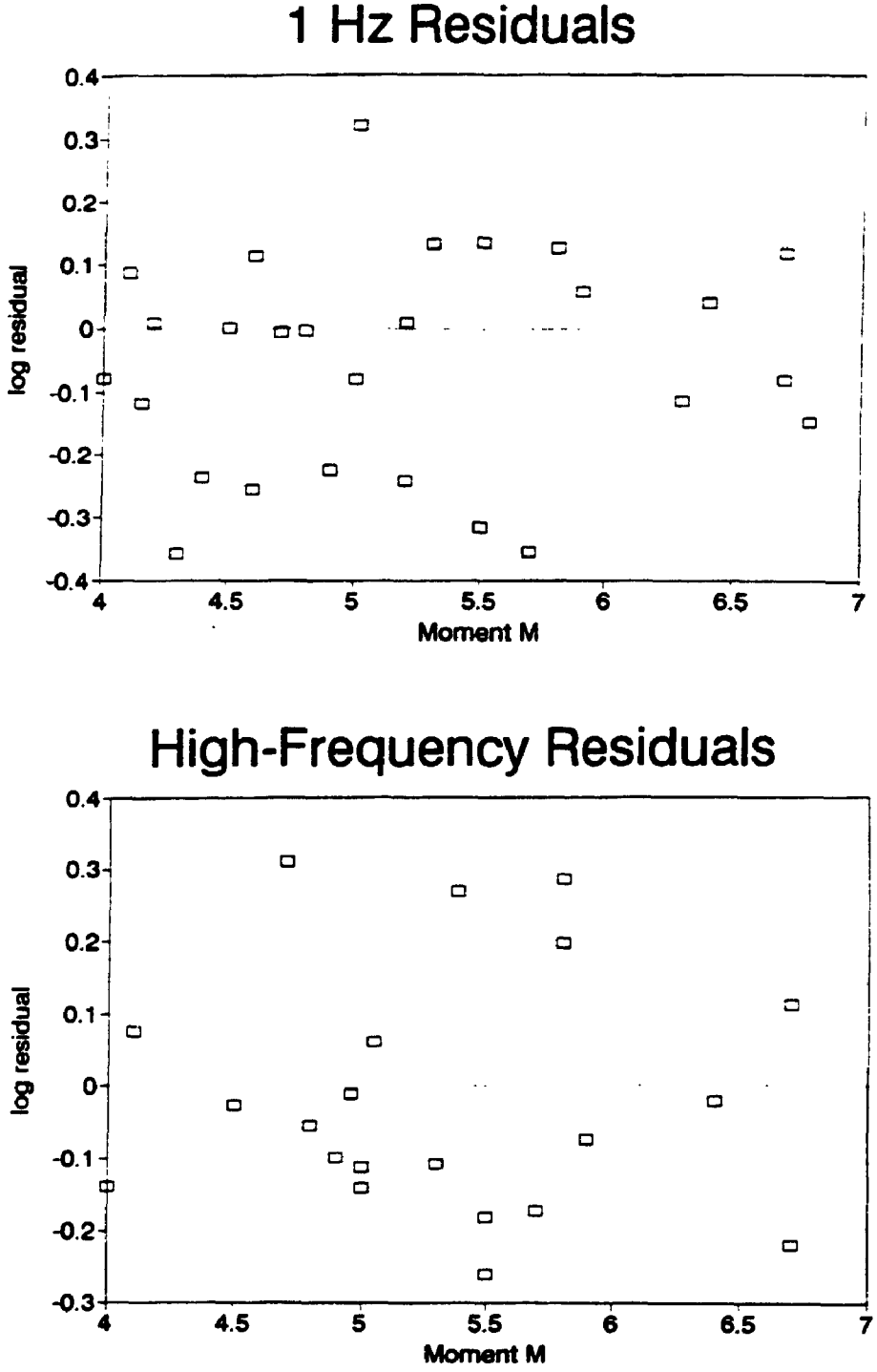

FIGURE 5.8 - Residuals for ENA source spectral model as a function of M, for a frequency of 1 Hz (top frame), and for the high-frequency level (bottom frame). (The residual is defined as the ratio of an observed amplitude to the model prediction.) All data used in deriving the model are included.

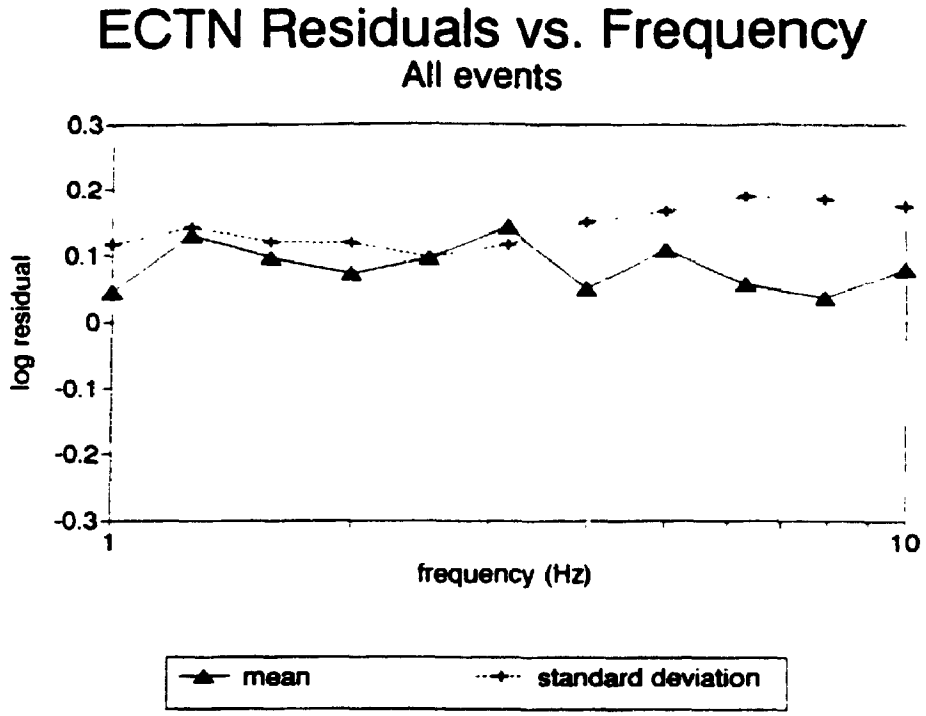

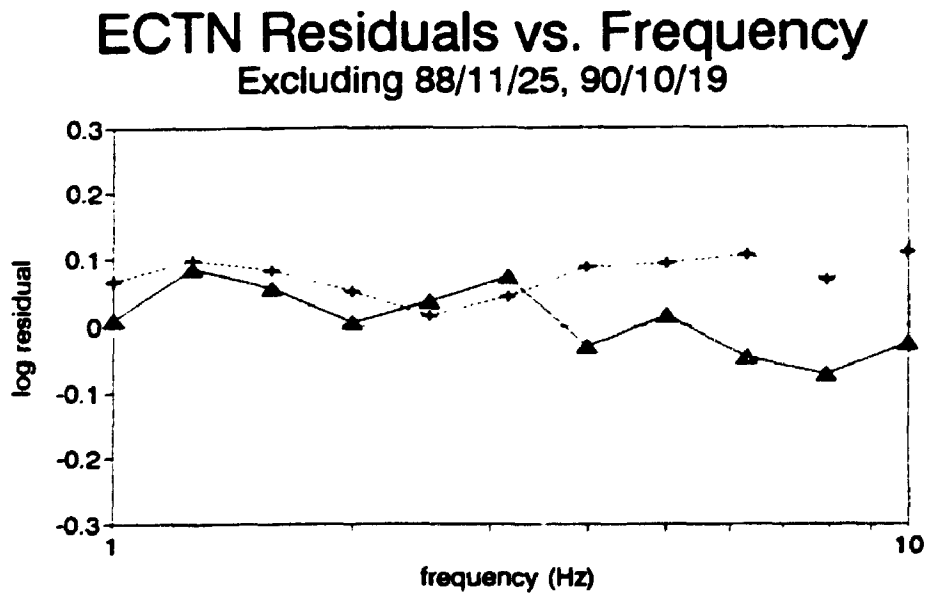

FIGURE 5.9 - Mean and standard deviation of residuals for ENA source spectral model, as a function of frequency. Top frame includes all ECTN data of M > 4 (nine events). Lower frame excludes the Saguenay and Mont Laurier earthquakes, which had particularly high stress drops.

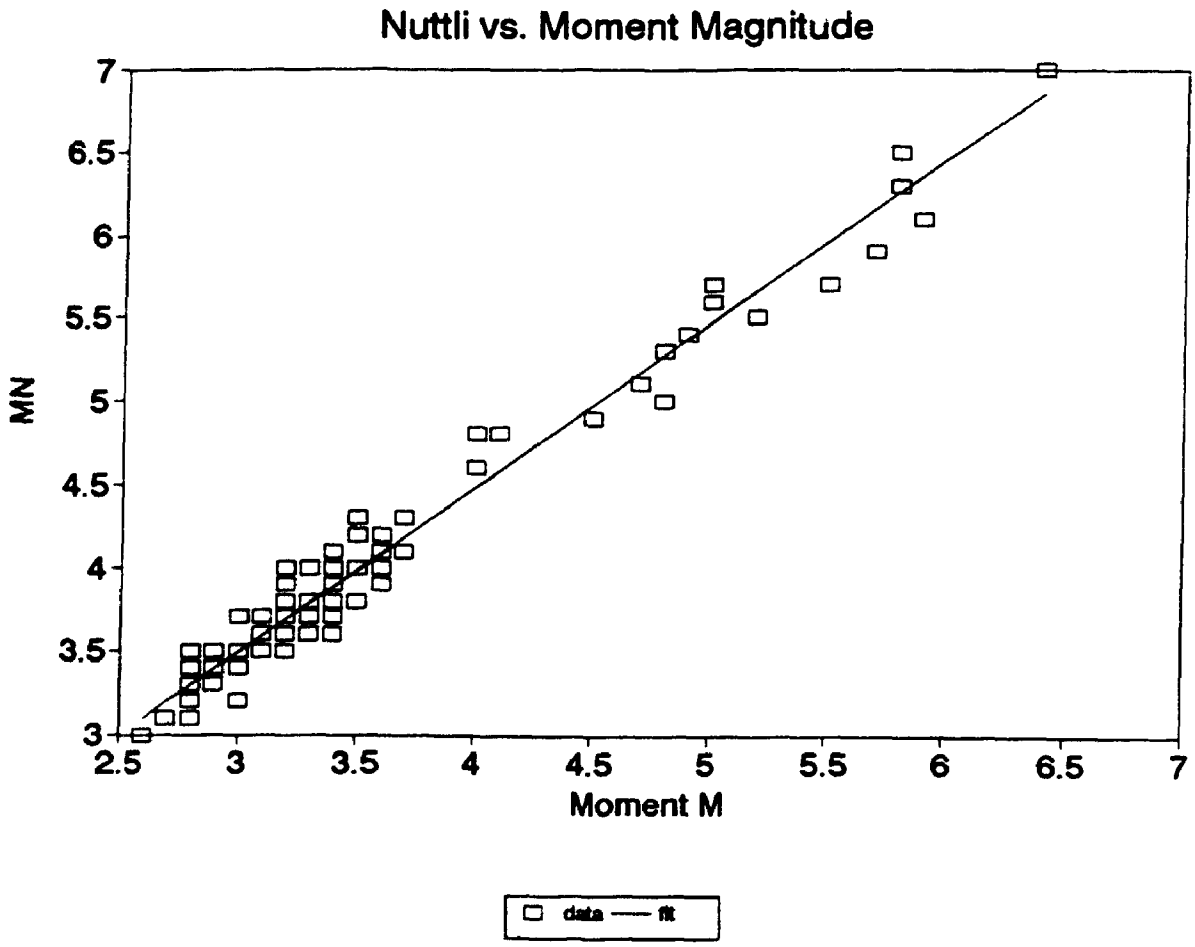

FIGURE 5.10 - Relationship between Lg magnitude (M_N) and moment magnitude (M). Data are from the ECTN (M values of this study; M_N values from Geophysics Division, Geological Survey of Canada), and from Boore and Atkinson (1987). Solid line is the least-squares fit to the data (see Equation 5.8).

6 - DISCUSSION OF RESULTS

6.1 Summary of Results

The results of this study indicate that the attenuation curve for ground motion amplitudes in the frequency domain, in southeastern Canada, has three distinct sections. At distances less than 70 km, amplitudes decay slightly more rapidly than 1/R. Between 70 and 130 km, spectral amplitudes are approximately constant. Beyond 130 km, amplitudes decay at a rate that is consistent with an apparent geometric spreading coefficient of 0.5, with $Q = 670\ f^{0.33}$. In essence, there is an offset in the attenuation curve, spanning the distance from 70 to 130 km. Thus events at a distance of 130 km produce spectral amplitudes which are comparable to those produced by events at a distance of 70 km. In the time domain, however, amplitudes may be significantly lower at 130 km due to the effects of increasing duration.

These findings are consistent with the hypothesis of Burger et al. (1987), that postcritical reflections from the Moho discontinuity play an important role in determining the shape of the attenuation curve. Because the feature is a subtle one and random variability is great, the attenuation curve can be parameterized in several ways. The data are most consistent with a hinged trilinear form. However a bilinear form, with R_o=60 km, can also reproduce much of the observed flattening in the transition zone from direct to

Lg-wave spreading. A linear form (R^{-1}, with constant Q=2000) also works well, albeit with larger residuals in the 50 to 100 km distance range; since the residuals are negative, it is a conservative interpretation. There is little evidence for a systematic dependence of attenuation on focal depth or tectonic province.

Based on regional seismographic data, teleseismic data, and MMI data from historical events, a two-corner source spectral model is proposed for events of $4 \leq M \leq 7$. The functional form (Equation 5.5) represents the addition of two Brune spectra, and is consistent with physical models in which 'roughness' (ie. abrupt fault locking, barriers, asperities, etc.) causes elevated high-frequency spectral levels. The shape of the spectrum features a mid-frequency 'sag', first proposed by Gusev (1983) on the basis of magnitude data for large earthquakes.

The high-frequency amplitude levels of the empirical model are roughly equivalent to a constant Brune stress parameter of 200 bars; amplitudes at frequencies near 1 Hz are equivalent to those for a 50-bar Brune model. For events of M 4 or smaller, the data are consistent with a simple Brune spectrum with a stress parameter of 200 bars; actual stress parameters are difficult to measure for small events due to finite bandwidth effects.

6.2 Implications for Ground Motion Relations

Ground motion relations can be developed with confidence if we know the appropriate source and attenuation models. The crux of the prediction methodology is the specification of the Fourier acceleration spectrum as a function of magnitude and distance. This study has developed a source model for the spectrum as a function of magnitude (Chapter 5), and described its attenuation with distance (Chapter 3). With the Fourier spectrum thus defined, peak ground motions and response spectra may be computed by the stochastic model as shown in Chapter 4.

Figure 6.1 compares empirical source spectra with the 100-bar Brune model, which is the assumption embodied in current relations (eg. Boore and Atkinson (1987), Atkinson and Boore (1990) - referred to here as AB90; Toro and McGuire (1987), EPRI, 1988 - referred to here as EPRI88). The empirical spectra exceed the Brune 100-bar spectra by a factor of about 1.4 in the 5 to 10 Hz frequency band, for M > 5. For frequencies near 1 Hz, spectral amplitudes are less than those of the 100-bar model, in some cases by as much as a factor of two. It should be noted, however, that the implied underestimation of the AB90 and EPRI88 ground motion relations at high frequencies is mitigated by the lower crustal constants that were used in those studies (ρ=2.7 gm/cm^3 and β=3.5 km/sec); the underestimation of the stress drop was largely offset by overestimation of the

scaling constant involving shear wave velocity (Equation 1.2). The net result is that the AB90 and EPRI88 relations are equivalent to using a Brune stress of about 150 bars, with the crustal constants of the current study. Thus the underestimation of the current ground motion relations at high frequencies is less pronounced than that implied by Figure 6.1, while the overestimation of low frequencies is even more pronounced.

Ground motion relations require significant revision to accommodate the differences between the empirical source model and the 100-bar Brune model. The impact of the revision on response spectra can be seen on Figure 6.2, which compares estimates of the ground motion parameters under the new model with those of the AB90 relations. The ground motion estimates for this figure are based on a limited number of stochastic simulations (10 trials for each magnitude and distance) using the method described in Chapter 4, with the source, attenuation and duration models of this study.

For moderate-to-large earthquakes, low-frequency ground motions are dramatically lower than predicted by the AB90 relations, as would be expected from Figure 6.1. For small events, however, the simulations indicate that the AB90 relations grossly underpredict the response of low-frequency oscillators at close distances. This unexpected result is due to limitations of the AB90 relations: (i) the AB90

equations were largely based on random process theory rather than simulations, and RPT is known to be subject to significant integration errors for low-frequency oscillations of short duration; and (ii) the AB90 regressions deliberately emphasized accuracy for moderate-to-large events at the expense of accuracy for small events.

For intermediate frequencies (near 1 Hz), the AB90 relations appear to be correct for small events, but will overestimate the simulated ground motions significantly for moderate-to-large events. For high frequencies (3 Hz to 8 Hz) the new simulations suggest that the AB90 relations are surprisingly accurate.

6.3 Implications for Seismic Hazard Estimates

The implications of revisions to the ground motion relations for seismic hazard estimates can be illustrated with a simple example. Consider the case of a site that lies well within the borders of a large homogeneous seismotectonic region; all contributions to the ground motion hazard come from within the zone in which the site is located. A simple analysis may be performed to obtain expected peak ground motions (acceleration and velocity) and response spectral parameters for exceedence probabilities of engineering interest, say 0.002 per annum (National Building Code probability level for ground motion parameters) and 0.0001 per annum (typical probability level used in analysis of critical structures).

An estimate of the probability of exceeding any ground motion parameter (ie. specified value of peak acceleration or specifed response spectral amplitude for a given natural frequency) can be computed by the well-known Cornell-McGuire method (Cornell, 1968; McGuire, 1977). Briefly, the method integrates contributions to the exceedence probability of the specified ground motion over all possible magnitudes and distances. The input to the calculations are the ground motion relations, the magnitude-recurrence relation giving the rates of earthquake occurrence (rate parameter, N_o, and slope, β, of the Gutenberg-Richter relation, $\log N(>M) = N_o - \beta M$), and the maximum magnitude, M_x (upper limit for integration over magnitude). The method is not discussed here; see EERI (1989) for a review.

For relatively inactive regions, such as most of Ontario, representative seismicity parameters for a hazard analysis might be $\beta = 2.0$, $N(\geq 5) = 0.02$ per annum (p.a.) for an area 200 km by 200 km, and $M_x = 7.5$ (or less). For this example, seismic hazard computations are performed using three different ground motion relations:

(i) the Atkinson and Boore (1990) relations for response spectral acceleration (PSA) and peak ground acceleration (PGA) and velocity (PGV) - these relations form the basis for recent seismic hazard estimates at most of Ontario's dam and nuclear sites;

(ii) the Hasegawa et al. (1981) relations for PGA and PGV, with corresponding spectral estimates as obtained by the National Building Code of Canada (NBCC) formulation for the spectral response factor (S) - these relations form the basis for the 1985 to 1995 editions of the NBCC; and

(iii) preliminary revised ground motion relations based on the stochastic model, using as input parameters the attenuation, source and duration models obtained in this study.

Expected response spectra for these three cases are compared on Figure 6.3 for a probability of 0.002 p.a. The impact of the revisions in the ground motion relations, for this probability, is a modest increase in high-frequency (5 to 10 Hz) ground motion levels (by about 20%) with a decrease in intermediate-frequency (1 to 2 Hz) motions by a factor of 1.5 to 2., relative to those that would be obtained with the Atkinson and Boore (1990) relations. For lower probability levels (not shown) the impact on high frequencies is similar to that shown while intermediate frequencies have even more dramatic reductions.

The spectral shape implied by the revised ground motion relations differs markedly from that used in the NBCC. The high-frequency level of the NBCC spectrum is appropriate but its 1 Hz level would appear to be conservative by nearly a factor of ten. It should be noted, however, that the NBCC

spectrum is intended to be applicable for multi-degree-of-freedom structures, so the comparison is not entirely consistent. Nevertheless, it is likely that the NBCC spectral shape warrants significant revision. The hazard to ENA structures of intermediate to long periods may have been seriously overestimated.

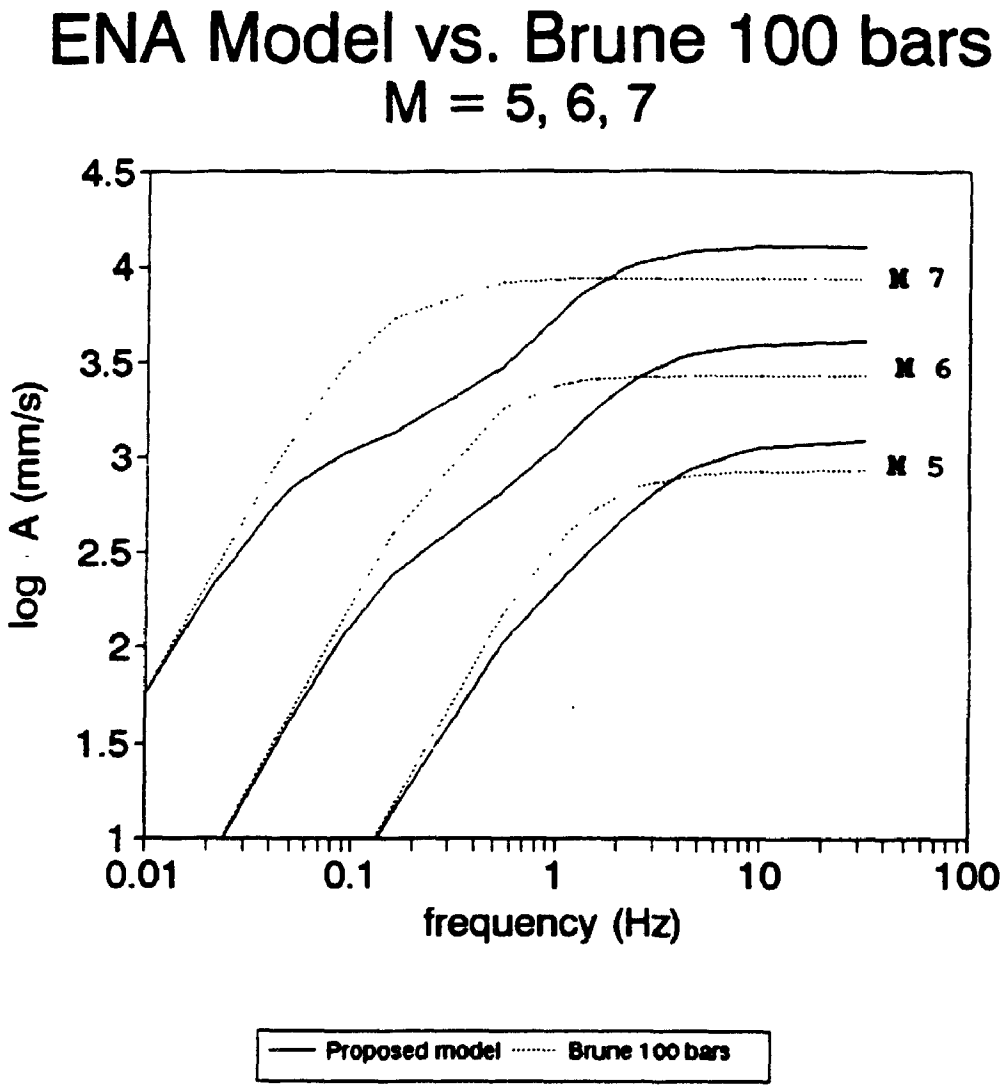

FIGURE 6.1 - Comparison of horizontal-component source spectra (R = 1 km) for the ENA empirical model with those of the 100-bar Brune model, for M 5, 6 and 7.

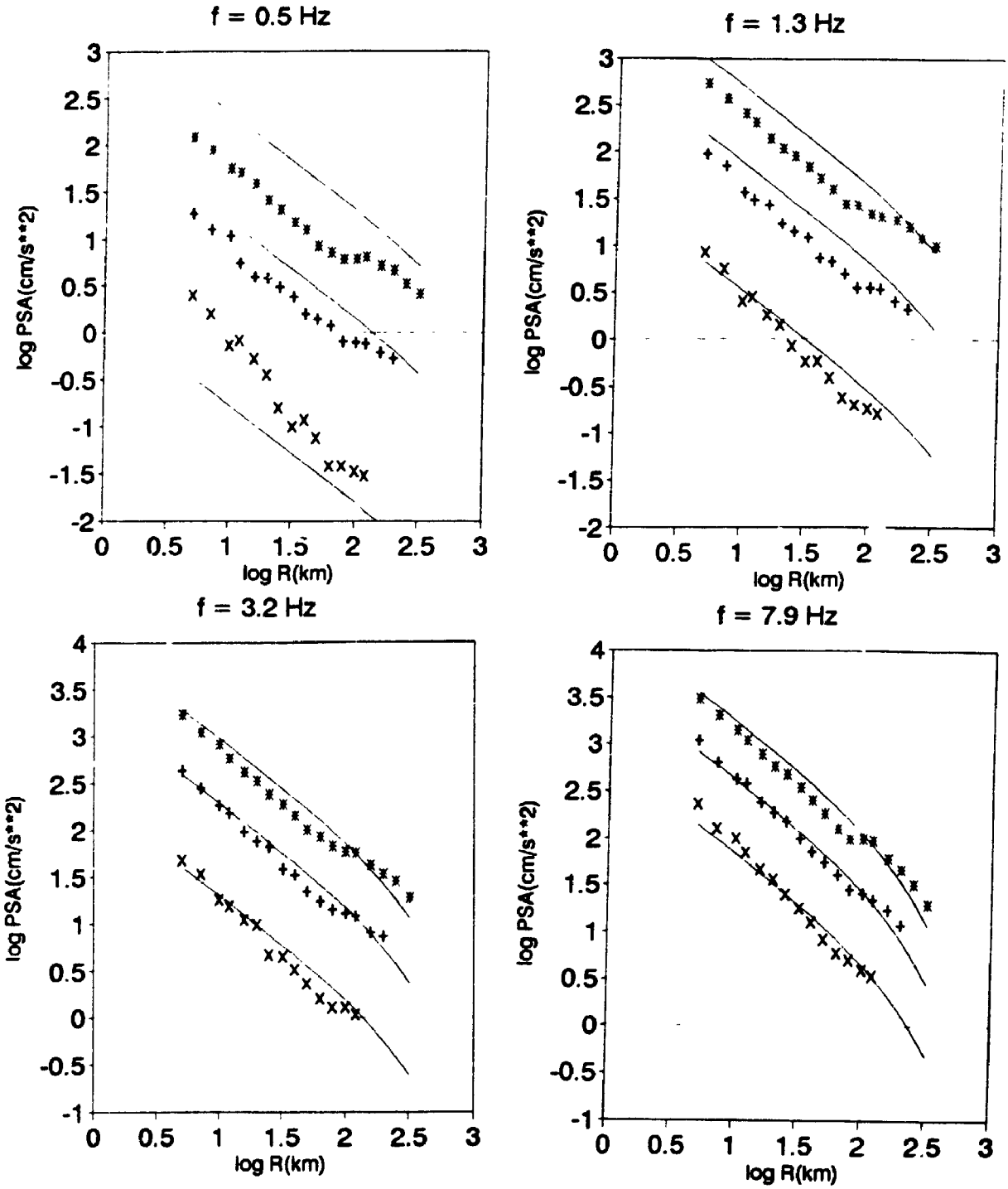

FIGURE 6.2 - Comparison of simulated response spectral values (horizontal component, 5% damping) using new model (symbols) with equations of Atkinson and Boore, 1990 (lines), for frequencies of 0.5, 1.3, 3.2 and 7.9 Hz. Results are shown for M 4, 5.5 and 7, by symbols x, + and *, respectively.

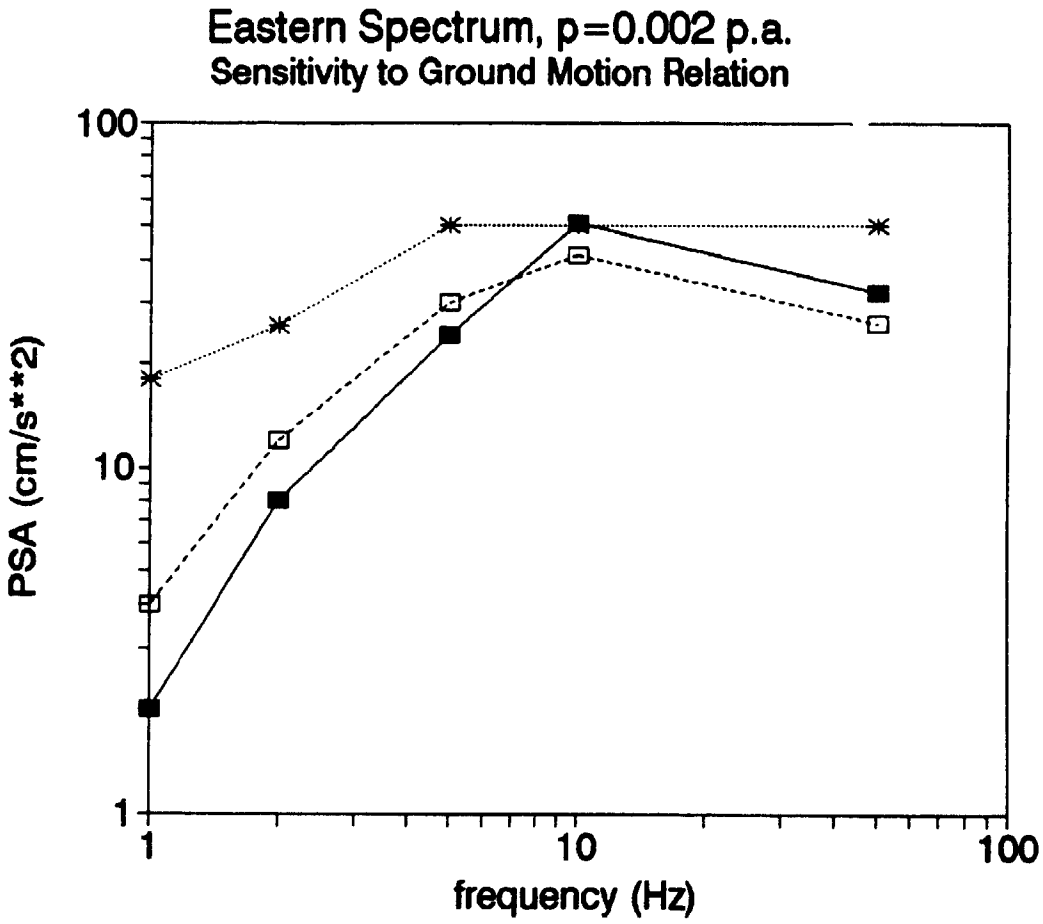

FIGURE 6.3 - Uniform Hazard Spectrum for ENA example, p = 0.002 per annum, showing sensitivity of design ground motions to assumed ground motion relations. Solid line shows spectrum implied by ground motion results of this study. Dashed line shows spectrum implied by Atkinson and Boore (1990) relations. Dotted line shows spectrum implied by National Building Code of Canada approach.

APPENDIX A

SPECTRAL AMPLITUDES OF ECTN RECORDS

APPENDIX A: Spectral Amplitudes of ECTN Records

Notes: Amplitudes in log units, mm/s. Distance (R) in km.
Value = 9.99 denotes undefined amplitude.

Event	MN	STN	log R	log A for log f(Hz) = 0.0	0.1	0.2	0.3	0.4	0.5	0.6	0.7	0.8	0.9	1.0
A860818.A	3.0	LPQ	1.31	-2.03	-2.10	-1.71	-1.77	-1.49	-1.25	-1.17	-0.88	-0.92	-0.82	-0.68
A860818.A	3.0	EBN	2.12	-2.65	-2.38	-2.30	-2.16	-2.02	-1.89	-1.67	-1.54	-1.53	-1.37	-1.29
A860818.A	3.0	HTQ	2.34	9.99	9.99	-2.77	-2.58	-2.36	-2.19	-2.08	-1.96	-1.90	-1.68	9.99
A900423.A	3.0	LPQ	1.19	-1.13	-0.84	9.99	-0.45	-0.40	-0.18	-0.13	0.10	0.10	-0.07	0.20
A900423.A	3.0	A16	1.20	-2.46	-2.20	-1.88	-1.57	-1.45	-1.26	-1.15	-0.93	-0.67	-0.68	-0.45
A900423.A	3.0	A11	1.28	-2.06	-2.13	-1.75	-1.68	-1.64	-1.53	-1.31	-1.48	-1.12	-1.07	-0.81
A900423.A	3.0	A54	1.31	-2.25	-1.86	-1.79	-1.71	-1.63	-1.33	-1.31	-1.15	-0.91	-0.75	-0.48
A900423.A	3.0	A61	1.53	-2.80	-2.78	-2.56	-2.51	-2.22	-2.07	-1.98	-1.79	-1.62	-1.32	-1.15
A900423.A	3.0	A21	1.70	-2.74	-2.78	-2.52	-2.33	-2.01	-1.70	-1.52	-1.40	-1.26	-1.11	-1.02
A900423.A	3.0	A64	1.72	-2.94	-2.74	-2.72	-2.30	-2.18	-2.04	-1.80	-1.74	-1.50	-1.24	-1.04
A900423.A	3.0	EBN	2.16	9.99	-2.81	-2.62	-2.52	-2.19	-2.01	-1.89	-1.83	-1.62	-1.67	9.99
A900423.A	3.0	DPQ	2.33	-3.36	-3.06	-2.91	-2.93	9.99	9.99	9.99	9.99	9.99	9.99	9.99
A850303.A	3.1	LPQ	1.58	-1.80	-1.67	-1.54	-1.40	-1.29	-1.02	-0.87	-0.60	-0.79	-0.68	-0.65
A850303.A	3.1	EBN	2.23	9.99	9.99	9.99	-2.36	-2.26	-2.10	-1.91	-2.05	-1.58	-1.55	9.99
A850303.A	3.1	GNT	2.27	-2.87	-2.61	-2.33	-2.21	-2.04	-1.67	-1.72	-1.59	-1.73	-1.71	-1.65
A850303.A	3.1	HTQ	2.40	9.99	9.99	-2.68	-2.37	-2.25	-2.15	-2.01	-1.82	-1.72	-1.59	9.99
A880124.A	3.1	LPQ	1.56	-2.37	-2.43	-2.05	-1.94	-1.70	-1.46	-1.22	-1.20	-1.03	-1.14	-0.98
A880124.A	3.1	DPQ	2.29	-2.84	-2.55	-2.64	-2.47	-2.31	-1.89	-1.87	-1.72	-1.59	-1.69	-1.46
A880124.A	3.1	HTQ	2.39	9.99	-2.85	-2.61	-2.55	-2.36	-2.15	-1.94	-1.85	-1.83	-1.78	-1.71
A880313.A	3.1	A54	0.85	9.99	-1.43	9.99	-1.06	-0.84	-0.66	-0.72	-0.14	-0.16	-0.17	-0.04
A880313.A	3.1	A11	1.42	-2.09	-1.66	-1.76	-1.47	-1.53	-1.48	-1.39	-1.36	-1.04	-1.10	-0.93
A880313.A	3.1	A16	1.45	-1.94	-1.57	-1.63	-1.57	-1.49	-1.32	-1.22	-0.99	-0.86	-0.74	-0.71
A880313.A	3.1	LPQ	1.48	-1.97	-1.96	-1.54	-1.60	-1.41	-1.04	-0.70	-0.52	-0.59	-0.72	-0.51
A880313.A	3.1	A61	1.55	-2.62	-2.40	-2.36	-2.25	-2.15	-1.83	-1.70	-1.47	-1.29	-1.08	-0.97
A880313.A	3.1	A64	1.75	-2.74	-2.63	-2.49	-2.23	-2.00	-1.83	-1.69	-1.59	-1.36	-1.16	-1.01
A880313.A	3.1	A21	1.77	-2.57	-2.37	-2.29	-2.23	-1.84	-1.66	-1.33	-1.16	-1.16	-1.04	-0.92
A880313.A	3.1	EBN	2.21	9.99	9.99	-2.50	-2.21	-2.13	-2.01	-1.69	-1.72	-1.56	-1.54	-1.59
A880313.A	3.1	DPQ	2.30	-2.99	-2.70	-2.75	-2.55	-2.31	-2.16	-1.97	-1.90	-1.69	-1.56	-1.45
A880313.A	3.1	HTQ	2.39	9.99	9.99	9.99	-2.43	-2.30	-2.04	-1.98	-1.91	-1.80	-1.61	-1.69

A890131.A	3.1	A54	1.44	9.99	-1.46	9.99	-1.23	-1.42	-1.03	-0.77	-0.64	-0.28	-0.09	-0.18
A890131.A	3.1	A11	1.66	-2.51	-2.32	-1.99	-2.00	-1.80	-1.79	-1.65	-1.30	-1.29	-1.10	-1.03
A890131.A	3.1	A16	1.73	-2.24	-2.29	-2.04	-2.02	-2.01	-1.78	-1.63	-1.52	-1.24	-1.13	-0.91
A890131.A	3.1	A61	1.74	-2.65	-2.48	-2.25	-2.14	-2.01	-1.96	-1.66	-1.60	-1.38	-1.07	-1.02
A890131.A	3.1	A64	1.88	-2.80	-2.57	-2.44	-2.35	-2.03	-2.00	-1.81	-1.72	-1.46	-1.33	-1.08
A890131.A	3.1	A21	1.91	-2.73	-2.69	-2.59	-2.21	-2.19	-1.81	-1.70	-1.52	-1.27	-1.08	-0.97
A900421.A	3.1	A16	1.13	-2.07	-1.72	-1.56	-1.46	-1.22	-1.20	-0.96	-0.76	-0.61	-0.62	-0.28
A900421.A	3.1	A61	1.26	-1.89	-1.84	-1.57	-1.68	-1.26	-1.30	-1.14	-1.16	-0.75	-0.41	-0.42
A900421.A	3.1	A54	1.46	9.99	-2.03	9.99	-1.65	-1.35	-1.28	-1.15	-1.08	-0.65	-0.42	-0.63
A900421.A	3.1	A21	1.53	-1.94	-1.82	-1.97	-1.41	-1.42	-1.25	-1.18	-0.64	-0.49	-0.40	-0.59
A900421.A	3.1	A64	1.55	-2.06	-1.95	-1.74	-1.56	-1.49	-1.23	-1.13	-0.96	-0.74	-0.72	-0.77
A900421.A	3.1	A11	1.57	-2.37	-2.17	-2.18	-1.80	-1.49	-1.32	-1.42	-1.34	-1.08	-1.07	-0.85
A900421.A	3.1	EBN	2.14	-2.67	-2.57	-2.54	-2.05	-1.95	-1.65	-1.56	-1.49	-1.40	-1.38	-1.20
A900421.A	3.1	DPQ	2.36	-2.80	-2.65	-2.61	-2.32	-2.14	-1.93	-1.72	-1.70	-1.71	9.99	9.99
A871111.A	3.2	GAC	1.40	-1.61	-1.68	-1.42	-1.41	-1.23	-0.79	-0.73	-0.55	-0.49	-0.28	-0.34
A871111.A	3.2	OTT	1.75	-2.31	-1.94	-1.65	-1.58	-1.14	-0.97	-0.79	-0.71	-0.58	-0.44	-0.34
A871111.A	3.2	TRQ	1.91	-2.19	-2.00	-1.81	-1.51	-1.47	-1.34	-1.02	-0.80	-0.78	-0.56	-0.58
A871111.A	3.2	WBO	1.95	-2.46	-2.00	-1.88	-1.71	-1.83	-1.51	-1.24	-1.16	-0.96	-0.73	-0.57
A871111.A	3.2	GRQ	2.02	9.99	-2.18	-1.97	-1.90	-1.57	-1.36	9.99	9.99	9.99	9.99	9.99
A871111.A	3.2	MNT	2.14	9.99	9.99	-2.29	-1.97	-1.84	-1.61	-1.57	-1.33	-1.11	-0.98	-0.93
A871111.A	3.2	CKO	2.22	-2.14	-1.94	-1.74	-1.56	-1.38	-1.51	-1.47	-1.31	-1.13	-0.99	-1.02
A891013.A	3.2	LPQ	1.39	-0.70	-0.60	9.99	-0.27	-0.24	0.02	0.25	0.47	0.57	0.54	0.78
A891013.A	3.2	A16	1.40	-1.96	-1.97	-1.63	-1.34	-1.32	-1.11	-0.97	-0.78	-0.64	-0.64	-0.42
A891013.A	3.2	A11	1.45	-2.00	-1.82	-1.58	-1.41	-1.17	-1.18	-1.09	-0.71	-0.63	-0.69	-0.49
A891013.A	3.2	A54	1.50	-1.64	-1.64	-1.37	-1.29	-1.08	-0.74	-0.95	-0.63	-0.51	-0.24	-0.37
A891013.A	3.2	A61	1.60	-2.10	-1.93	-1.95	-1.57	-1.35	-1.18	-1.27	-1.19	-1.02	-0.86	-0.89
A891013.A	3.2	A21	1.72	-2.37	-2.06	-2.14	-1.99	-1.52	-1.42	-1.26	-1.07	-0.91	-0.67	-0.80
A891013.A	3.2	A64	1.75	-2.42	-2.08	-1.84	-1.72	-1.70	-1.43	-1.34	-1.24	-1.06	-0.95	-0.81
A891013.A	3.2	DPQ	2.34	-2.91	-2.65	-2.38	-2.37	-2.17	-1.99	-2.01	9.99	9.99	9.99	9.99
A891013.A	3.2	GSQ	2.45	9.99	-2.74	-2.36	-2.25	-2.19	-2.05	-1.92	-1.92	-1.99	9.99	9.99
A891013.A	3.2	KLN	2.46	9.99	9.99	-2.70	-2.49	-2.28	-2.22	-1.98	-1.99	9.99	9.99	9.99
A900313.A	3.2	A16	1.27	9.99	-1.88	9.99	-1.60	-1.42	-1.28	-1.01	-0.77	-0.73	-0.50	-0.32
A900313.A	3.2	A61	1.37	-2.27	-2.10	-1.92	-1.82	-1.66	-1.24	-1.35	-1.06	-0.76	-0.44	-0.45
A900313.A	3.2	A54	1.43	-2.19	-2.34	-2.08	-1.76	-1.45	-1.59	-1.50	-1.11	-0.96	-0.72	-0.59
A900313.A	3.2	A11	1.56	-2.10	-2.01	-1.73	-1.49	-1.59	-1.62	-1.33	-1.23	-1.19	-1.02	-0.96
A900313.A	3.2	A64	1.61	-2.39	-2.29	-2.10	-1.82	-1.79	-1.64	-1.26	-1.15	-1.03	-0.82	-0.64

A900313.A	3.2	A21	1.61	-2.30	-2.05	-2.02	-1.68	-1.39	-1.24	-1.10	-1.01	-0.91	-0.76	-0.71
A900313.A	3.2	EBN	2.15	9.99	-2.71	-2.47	-2.15	-2.03	-1.92	-1.77	-1.57	-1.48	-1.37	-1.25
A900313.A	3.2	DPQ	2.35	-3.10	-2.95	-2.83	-2.38	-2.42	9.99	9.99	9.99	9.99	9.99	9.99
A900313.A	3.2	GSQ	2.43	-2.97	-2.84	-2.75	-2.56	-2.40	-2.32	-2.30	-2.29	-2.16	-2.08	9.99
A900313.A	3.2	KLN	2.47	-2.17	-2.02	-1.89	-1.75	-1.73	-1.50	-1.35	-1.26	-1.18	-1.16	-1.23
A870318.A	3.3	LPQ	1.64	-2.15	-2.04	-1.76	-1.59	-1.42	-1.42	-1.13	-1.11	-0.98	-0.76	-0.57
A870318.A	3.3	EBN	2.17	9.99	9.99	9.99	-2.34	-2.00	-1.86	-1.71	-1.54	-1.46	-1.43	-1.32
A870318.A	3.3	HTQ	2.32	-2.85	-2.44	-2.13	-2.14	9.99	9.99	9.99	9.99	9.99	9.99	9.99
A870318.A	3.3	GSQ	2.42	9.99	-2.60	-2.31	-2.19	-2.04	-2.02	-1.87	-1.83	-1.84	9.99	9.99
A870318.A	3.3	KLN	2.48	9.99	9.99	-2.96	-2.80	-2.68	-2.45	-2.34	-2.12	-2.07	-1.99	9.99
A880515.A	3.3	OTT	1.47	-2.20	-2.12	-2.07	-1.43	-1.24	-1.03	-0.91	-0.76	-0.66	-0.66	-0.72
A880515.A	3.3	WBO	1.49	-2.07	-1.69	9.99	-1.55	-1.32	-1.29	-0.92	-1.04	-0.65	-0.49	-0.31
A880515.A	3.3	GAC	1.79	-2.56	-2.49	-2.02	-1.92	-1.80	-1.70	-1.42	-1.48	-1.46	-1.37	-1.35
A880515.A	3.3	MNT	2.20	-2.74	-2.33	-2.02	-1.85	-1.67	-1.65	-1.48	-1.37	-1.31	-1.35	-1.39
A880515.A	3.3	DPQ	2.44	9.99	-2.52	-2.40	-2.28	-1.91	-1.74	-1.82	9.99	9.99	9.99	9.99
A901021.A	3.3	A54	1.24	-1.90	-1.67	-1.82	-1.50	-1.18	-1.09	-0.86	-0.79	-0.42	-0.51	-0.21
A901021.A	3.3	A11	1.41	9.99	-1.74	9.99	-1.52	-1.14	-1.07	-0.77	-0.76	-0.45	-0.14	-0.15
A901021.A	3.3	A16	1.50	-2.15	-1.90	-1.79	-1.55	-1.55	-1.02	-0.91	-0.87	-0.69	-0.70	-0.32
A901021.A	3.3	A61	1.62	-2.51	-2.44	-2.20	-2.01	-1.85	-1.92	-1.72	-1.49	-1.24	-1.13	-0.83
A901021.A	3.3	A64	1.79	-2.73	-2.45	-2.49	-2.22	-1.94	-1.76	-1.47	-1.41	-1.24	-1.01	-0.76
A901021.A	3.3	A21	1.80	-2.49	-2.28	-2.11	-1.94	-1.65	-1.52	-1.48	-1.23	-1.02	-0.83	-0.65
A901021.A	3.3	DPQ	2.30	-2.77	-2.48	-2.37	-2.20	-1.92	-1.63	-1.43	-1.48	-1.34	-1.32	-1.17
A901021.A	3.3	KLN	2.49	-2.05	-1.92	-1.86	-1.70	-1.69	-1.59	-1.34	-1.27	-1.22	-1.24	9.99
A901218.A	3.3	A11	1.13	9.99	-1.44	9.99	-1.04	-0.74	-0.69	-0.57	-0.49	-0.45	-0.51	-0.52
A901218.A	3.3	A54	1.39	-1.94	-1.52	-1.53	-1.35	-1.31	-1.16	-1.07	-0.90	-0.97	-0.95	-0.75
A901218.A	3.3	A16	1.54	-2.07	-1.84	-1.83	-1.68	-1.35	-1.17	-1.06	-1.05	-1.26	-1.15	-0.85
A901218.A	3.3	A61	1.72	-2.72	-2.65	-2.37	-2.20	-2.01	-1.83	-1.81	-1.70	-1.57	-1.45	-1.33
A901218.A	3.3	A21	1.84	-2.34	-2.21	-2.03	-1.95	-1.54	-1.39	-1.34	-1.35	-1.29	-1.28	-1.13
A901218.A	3.3	A64	1.86	-2.52	-2.55	-2.23	-2.10	-1.81	-1.70	-1.69	-1.44	-1.40	-1.38	-1.25
A901218.A	3.3	DPQ	2.29	-2.79	-2.52	-2.27	-2.17	-1.76	-1.50	-1.61	-1.52	-1.46	-0.99	-1.10
A901218.A	3.3	KLN	2.48	9.99	9.99	-1.48	-1.31	-1.26	-1.26	-1.00	-1.00	-1.17	-1.44	9.99
A901218.A	3.3	MNT	2.50	-3.00	-2.84	-2.57	-2.58	9.99	9.99	9.99	9.99	9.99	9.99	9.99
A870806.A	3.4	LPQ	1.39	-2.08	-1.67	-1.46	-1.35	-1.21	-1.03	-0.82	-0.64	-0.38	-0.39	-0.24
A870806.A	3.4	EBN	2.19	9.99	-2.56	-2.39	-2.19	-1.94	-1.75	-1.61	-1.30	-1.29	-1.24	-1.13
A870806.A	3.4	GNT	2.30	9.99	-2.13	-1.89	-1.86	-1.85	-1.64	-1.65	-1.68	-1.60	-1.68	9.99
A870806.A	3.4	HTQ	2.38	-2.68	-2.46	-2.24	-2.16	-1.98	-1.77	-1.54	-1.48	-1.43	-1.35	9.99

A870806.A	3.4	GSQ	2.46	-2.52	-2.32	-2.18	-1.86	-1.84	-1.89	9.99	9.99	9.99	9.99	9.99
A870806.A	3.4	MNT	2.52	-3.05	-2.83	-2.70	-2.48	-2.35	-2.10	-1.87	-1.88	9.99	9.99	9.99
A870806.A	3.4	TRQ	2.55	-2.85	-2.49	-2.18	-2.38	9.99	9.99	9.99	9.99	9.99	9.99	9.99
A870806.A	3.4	MNQ	2.56	9.99	9.99	-2.53	-2.26	-2.16	-1.95	-1.95	-1.82	-1.73	-1.69	-1.66
A880809.A	3.4	WBO	1.39	-1.73	-1.76	9.99	-1.77	-1.44	-1.23	-1.09	-0.87	-0.61	-0.40	-0.40
A880809.A	3.4	OTT	1.86	-2.77	-2.53	-2.19	-2.26	-1.94	-1.81	-1.46	-1.24	-1.07	-0.88	-0.76
A880809.A	3.4	GAC	1.94	-2.61	-2.52	-2.24	-2.16	-1.93	-1.82	-1.32	-1.52	-1.33	-1.35	-1.30
A880809.A	3.4	MNT	2.08	9.99	-2.80	-2.50	-2.26	-2.03	-1.72	-1.58	-1.51	-1.40	-1.40	-1.14
A880809.A	3.4	TRQ	2.15	9.99	-2.37	-2.15	-2.02	-1.87	-1.49	-1.42	-1.36	-1.03	-1.04	-1.02
A880809.A	3.4	GRQ	2.28	-2.63	-2.39	-2.26	-1.81	-1.75	-1.68	-1.53	-1.52	-1.52	-1.32	-1.24
A880809.A	3.4	CKO	2.34	-3.00	-2.74	-2.56	-2.38	-2.15	-1.96	-1.78	-1.66	-1.62	-1.53	-1.44
A880809.A	3.4	DPQ	2.40	-2.96	-2.72	-2.56	-2.49	-2.32	-1.91	-1.83	-1.72	-1.66	-1.51	-1.45
A891104.A	3.4	GRQ	1.67	-1.53	-1.26	-1.00	-0.89	-0.71	-0.61	-0.47	-0.28	-0.24	-0.04	-0.07
A891104.A	3.4	GAC	1.78	-2.88	-2.91	-2.59	-2.55	-2.31	-2.02	-1.96	-1.64	-1.60	-1.38	-1.24
A891104.A	3.4	TRQ	1.95	-2.16	-1.80	-1.52	-1.48	-1.24	-1.18	-0.91	-0.84	-0.53	-0.40	-0.34
A891104.A	3.4	OTT	1.96	-2.80	-2.66	-2.57	-2.23	-2.06	-1.75	-1.48	-1.36	-1.27	-1.11	-1.18
A891104.A	3.4	CKO	2.13	9.99	-2.00	-1.74	-1.39	-1.14	-1.12	-0.86	-0.76	-0.60	-0.41	-0.41
A891104.A	3.4	WBO	2.14	9.99	-1.95	-1.77	-1.58	-1.41	-1.07	-0.98	-0.96	-0.71	-0.58	-0.67
A891104.A	3.4	MNT	2.26	-3.29	-3.14	-2.89	-2.69	-2.52	-2.28	-2.08	-1.98	-1.78	-1.68	-1.54
A891104.A	3.4	DPQ	2.36	-3.04	-2.84	-2.73	-2.62	-2.38	-2.02	-2.05	9.99	9.99	9.99	9.99
A891122.A	3.4	A54	0.98	9.99	-1.08	9.99	-0.97	-0.51	-0.22	-0.23	0.19	-0.06	0.01	0.07
A891122.A	3.4	A16	1.42	-1.66	-1.57	-1.44	-1.27	-1.11	-1.21	-1.04	-1.16	-0.95	-0.96	-0.55
A891122.A	3.4	A11	1.43	-1.75	-1.51	-1.18	-1.14	-1.16	-1.23	-0.88	-0.77	-0.57	-0.71	-0.67
A891122.A	3.4	A61	1.53	-2.42	-1.98	-1.94	-1.71	-1.74	-1.72	-1.59	-1.41	-1.36	-1.15	-0.81
A891122.A	3.4	A64	1.74	-2.31	-2.09	-2.06	-1.80	-1.61	-1.45	-1.32	-1.34	-1.36	-1.13	-0.75
A891122.A	3.4	A21	1.75	-2.25	-2.05	-1.88	-1.56	-1.30	-1.17	-1.04	-1.07	-1.10	-0.79	-0.60
A891122.A	3.4	EBN	2.20	-2.54	-2.30	-1.99	-1.85	-1.69	-1.46	-1.16	-1.28	-1.55	-1.49	-1.16
A891122.A	3.4	DPQ	2.31	-2.63	-2.35	-2.18	-2.04	-2.00	-1.70	-1.61	-1.53	-1.39	-1.55	9.99
A800311.A	3.7	GNT	1.79	-1.47	-1.44	-1.26	-0.96	-0.90	-0.74	-0.71	-0.58	-0.60	-0.57	-0.57
A800311.A	3.7	MNT	2.29	-2.15	-1.93	-1.79	-1.69	-1.38	-1.09	-0.91	-0.78	-0.67	-0.64	-0.52
A800311.A	3.7	MIQ	2.50	-1.75	-1.59	-1.48	-1.53	9.99	9.99	9.99	9.99	9.99	9.99	9.99
A800311.A	3.7	OTT	2.53	-2.26	-1.91	-1.80	-1.68	-1.49	-1.38	-1.22	-1.07	-1.02	-1.01	-1.04
A800311.A	3.7	FHO	2.56	9.99	9.99	-1.79	-1.60	-1.38	-1.22	-1.03	-1.02	-0.93	-0.95	-1.03
A800311.A	3.7	MNQ	2.68	-1.93	-1.81	-1.81	-1.60	-1.48	-1.42	-1.31	-1.37	-1.36	-1.30	-1.42
A800403.A	4.0	MNQ	2.31	9.99	-1.77	-1.40	-1.33	-1.38	9.99	9.99	9.99	9.99	9.99	9.99
A800403.A	4.0	GNT	2.63	9.99	-1.72	-1.62	-1.47	-1.48	9.99	9.99	9.99	9.99	9.99	9.99

A800403.A	4.0	MNT	2.75	9.99	9.99	-1.78	-1.66	-1.54	-1.44	-1.34	-1.39	-1.31	-1.41	-1.47
A800403.A	4.0	MIQ	2.82	9.99	-1.80	-1.57	-1.57	-1.60	-1.48	-1.48	-1.58	-1.59	-1.71	-1.78
A800403.A	4.0	OTT	2.84	9.99	-1.84	-1.73	-1.58	-1.44	-1.47	-1.46	-1.52	-1.60	9.99	9.99
A800403.A	4.0	FHO	2.86	9.99	9.99	-1.75	-1.64	-1.54	-1.40	-1.44	-1.47	-1.60	-1.74	-1.81
A810616.A	3.7	LPQ	1.22	-0.99	-0.70	9.99	-0.48	-0.25	0.06	0.05	0.25	0.32	0.41	0.22
A810616.A	3.7	GNT	2.34	9.99	-1.97	-1.81	-1.55	-1.52	-1.61	9.99	9.99	9.99	9.99	9.99
A810616.A	3.7	SBQ	2.44	-2.31	-2.07	-1.99	-1.82	-1.77	-1.48	-1.52	9.99	9.99	9.99	9.99
A810616.A	3.7	MNQ	2.55	-2.60	-2.41	-2.40	-2.00	-1.90	-1.77	-1.60	-1.59	-1.55	-1.47	9.99
A810616.A	3.7	MNT	2.55	9.99	-2.50	-2.30	-2.18	-2.03	-1.81	-1.76	-1.67	-1.53	-1.50	-1.54
A810616.A	3.7	TRQ	2.57	-2.57	-2.29	-2.12	-1.94	-1.93	-1.77	-1.80	9.99	9.99	9.99	9.99
A810616.A	3.7	GRQ	2.66	-2.81	-2.66	-2.39	-2.05	-1.66	-1.52	-1.54	-1.67	9.99	9.99	9.99
A810616.A	3.7	OTT	2.69	-2.63	-2.48	-2.27	-2.00	-1.92	-1.77	-1.82	9.99	9.99	9.99	9.99
A810616.A	3.7	FHO	2.72	9.99	-2.40	-2.20	-2.10	-2.03	-1.90	-1.82	-1.75	-1.78	-1.92	-2.01
A810616.A	3.7	CKO	2.77	9.99	-2.32	-2.15	-2.03	-1.98	-1.91	-1.95	-2.04	-2.11	9.99	9.99
A810704.A	3.7	WBO	1.75	-1.32	-1.38	-1.29	-1.36	-1.28	-0.94	-0.74	-0.79	-0.71	-0.41	-0.25
A810704.A	3.7	MNT	1.95	-1.78	-1.76	-1.43	-1.33	-1.28	-1.02	-1.05	-0.97	-0.84	-0.72	-0.58
A810704.A	3.7	OTT	1.96	-2.06	-1.82	-1.77	-1.44	-1.19	-0.96	-0.71	-0.45	-0.44	-0.47	-0.34
A810704.A	3.7	GAC	1.97	-2.26	-2.22	-1.90	-1.66	-1.54	-1.35	-1.18	-0.99	-0.75	-0.73	-0.62
A810704.A	3.7	TRQ	2.08	9.99	9.99	9.99	9.99	-1.41	-1.10	-0.75	-0.81	-0.89	-0.66	-0.69
A810704.A	3.7	FHO	2.12	-1.89	-1.66	-1.64	-1.70	-1.42	-1.10	-0.72	-0.61	-0.47	-0.47	-0.60
A810704.A	3.7	GRQ	2.28	9.99	-2.12	-1.86	-1.47	-1.21	-1.00	-0.88	-0.70	-0.87	-0.84	-0.73
A810704.A	3.7	SBQ	2.33	-1.89	-1.71	-1.36	-1.45	9.99	9.99	9.99	9.99	9.99	9.99	9.99
A810704.A	3.7	GNT	2.34	9.99	9.99	-1.83	-1.56	-1.51	-1.40	-1.31	-1.16	-1.23	-1.28	-1.34
A810704.A	3.7	CKO	2.38	-2.26	-1.97	-1.69	-1.65	-1.55	-1.53	-1.42	-1.34	-1.14	-1.10	-1.14
A810704.A	3.7	LPQ	2.63	-2.22	-2.06	-2.03	-1.86	-1.52	-1.49	-1.49	-1.54	-1.75	9.99	9.99
A810713.A	3.7	MNQ	2.21	-1.70	-1.40	-1.38	-1.43	-1.25	-1.15	-0.82	-0.72	-0.59	-0.51	-0.34
A810713.A	3.7	LPQ	2.56	-2.09	-1.84	-1.71	-1.69	-1.58	-1.45	-1.27	-1.38	9.99	9.99	9.99
A810713.A	3.7	GNT	2.75	9.99	9.99	-1.97	-1.86	-1.88	-1.80	-1.80	-1.78	-1.94	9.99	9.99
A810918.A	3.5	TRQ	1.59	-1.73	-1.38	9.99	-1.14	-1.11	-0.94	-0.84	-0.62	-0.41	-0.29	-0.28
A810918.A	3.5	GAC	1.77	-2.30	-2.14	-1.75	-1.69	-1.50	-1.35	-1.26	-1.10	-1.06	-1.05	-0.91
A810918.A	3.5	GRQ	1.93	-2.52	-2.20	-2.00	-1.83	-1.77	-1.49	-1.38	-1.21	-1.26	-1.12	-0.84
A810918.A	3.5	OTT	1.99	-2.10	-2.06	-2.05	-1.71	-1.42	-1.28	-1.20	-1.06	-0.83	-0.80	-0.82
A810918.A	3.5	FHO	2.07	9.99	-2.11	-1.56	-1.35	-1.00	-0.93	-1.03	-0.71	-0.61	-0.92	-0.87
A810918.A	3.5	WBO	2.10	-2.39	-2.29	-1.90	-1.87	-1.58	-1.43	-1.44	-1.20	-1.20	-0.84	-0.82
A810918.A	3.5	MNT	2.11	-2.42	-2.27	-2.27	-1.88	-1.68	-1.57	-1.28	-1.22	-1.07	-0.80	-0.69
A810918.A	3.5	CKO	2.27	9.99	-2.10	-1.77	-1.73	-1.57	-1.50	-1.43	-1.32	-1.36	-1.37	-1.19

A810918.A	3.5	GNT	2.31	-2.03	-1.82	-1.70	-1.67	-1.51	-1.41	-1.39	-1.16	-1.18	-1.21	9.99
A810918.A	3.5	VDQ	2.51	-2.85	-2.58	-2.42	-2.30	-2.07	-1.97	-1.85	-1.88	-2.02	-2.13	9.99
A810930.A	3.5	GRQ	1.56	-2.08	-1.87	-1.36	-1.35	-1.50	-1.45	-1.17	-0.98	-0.88	-0.70	-0.53
A810930.A	3.5	GAC	1.88	-2.23	-2.18	-1.90	-2.16	-1.94	-1.69	-1.43	-1.35	-1.28	-1.05	-1.03
A810930.A	3.5	TRQ	1.90	-1.57	-1.56	-1.44	-1.34	-1.23	-1.17	-1.08	-1.01	-0.91	-0.76	-0.74
A810930.A	3.5	OTT	2.04	-2.39	-2.23	-2.09	-2.01	-1.55	-1.31	-1.02	-0.93	-0.98	-1.00	-0.79
A810930.A	3.5	FHO	2.06	-2.36	-2.07	-1.70	-1.77	-1.71	-1.43	-1.38	-1.25	-0.95	-0.73	-0.75
A810930.A	3.5	CKO	2.18	-2.23	-2.03	-1.70	-1.68	-1.59	-1.24	-1.25	-1.26	-0.97	-0.88	-0.76
A810930.A	3.5	WBO	2.19	-2.52	-2.37	-2.04	-1.99	-1.83	-1.49	-1.46	-1.39	-1.32	-1.06	-1.10
A810930.A	3.5	MNT	2.25	9.99	-2.68	-2.24	-2.29	-1.98	-1.87	-1.69	-1.63	-1.53	-1.28	-1.21
A810930.A	3.5	GNT	2.39	-2.50	-2.17	-1.95	-1.82	-1.82	-1.70	-1.59	-1.49	-1.46	-1.70	9.99
A810930.A	3.5	VDQ	2.44	-2.72	-2.47	-2.36	-2.14	-1.97	-1.98	9.99	9.99	9.99	9.99	9.99
A811028.A	3.9	GSQ	2.23	-1.50	-1.35	-1.16	-1.03	-0.76	-0.67	-0.54	-0.56	-0.63	-0.68	9.99
A811028.A	3.9	EBN	2.53	-2.13	-1.96	-1.71	-1.61	-1.38	-1.35	-1.44	9.99	9.99	9.99	9.99
A811028.A	3.9	LPQ	2.65	-2.08	-1.79	-1.60	-1.56	-1.42	-1.38	-1.44	-1.40	-1.46	-1.57	9.99
A811028.A	3.9	TRQ	2.90	9.99	-2.05	-1.81	-1.85	-1.85	-1.94	-2.05	-2.10	-2.17	-2.26	9.99
A811128.A	3.7	LMN	2.28	-1.66	-1.45	-1.17	-1.33	-1.05	-1.04	-1.01	-1.17	-1.23	-1.18	-1.44
A811128.A	3.7	GSQ	2.33	9.99	9.99	-1.85	-1.46	-1.44	-1.20	-1.28	-1.37	-1.44	9.99	9.99
A811128.A	3.7	LPQ	2.41	-2.05	-1.70	-1.40	-1.30	-1.30	-1.16	-1.29	-1.36	9.99	9.99	9.99
A811128.A	3.7	MNQ	2.62	-2.39	-2.21	-2.05	-1.84	-1.77	-1.69	-1.65	-1.69	-1.70	-1.87	-1.97
A811128.A	3.7	GNT	2.65	9.99	9.99	-1.73	-1.65	-1.71	-1.83	-1.81	-1.97	-2.08	9.99	9.99
A811128.A	3.7	SBQ	2.65	-1.93	-1.79	-1.65	-1.60	-1.56	-1.47	-1.50	-1.53	-1.61	9.99	9.99
A811128.A	3.7	MNT	2.75	9.99	-2.38	-2.25	-2.18	-2.01	-1.96	-2.04	9.99	9.99	9.99	9.99
A820109.B	3.8	EBN	2.14	-1.40	-1.15	-1.27	-1.27	-0.89	-0.77	-0.74	-0.71	-0.65	-0.52	-0.57
A820109.B	3.8	LMN	2.27	-1.74	-1.50	-1.32	-1.38	-1.05	-1.00	-1.07	-1.11	-1.26	-1.38	-1.37
A820109.B	3.8	LPQ	2.42	9.99	-1.78	-1.67	-1.54	-1.33	-1.34	-1.18	-1.35	9.99	9.99	9.99
A820109.B	3.8	MNQ	2.63	-2.53	-2.22	-2.03	-1.96	-1.79	-1.61	-1.63	9.99	9.99	9.99	9.99
A820109.B	3.8	SBQ	2.65	-2.03	-1.92	-1.80	-1.66	-1.55	-1.54	-1.55	-1.56	-1.63	-1.83	-1.95
A820109.C	3.7	EBN	2.14	-1.43	-1.17	-1.20	-1.12	-1.07	-0.98	-1.20	-0.90	-0.95	-0.99	9.99
A820109.C	3.7	LMN	2.27	-1.73	-1.55	-1.37	-1.44	-1.15	-1.15	-1.08	-1.34	-1.44	-1.26	-1.06
A820109.C	3.7	GSQ	2.33	9.99	9.99	9.99	-1.71	-1.60	-1.52	-1.74	9.99	9.99	9.99	9.99
A820109.C	3.7	LPQ	2.42	9.99	-1.80	-1.62	-1.33	-1.40	9.99	9.99	9.99	9.99	9.99	9.99
A820109.C	3.7	MNQ	2.63	-2.48	-2.25	-2.14	-2.08	-2.07	-2.09	-2.07	-2.05	-2.07	-2.45	9.99
A820109.C	3.7	GNT	2.65	-1.98	-1.87	-1.82	-1.76	-1.75	-1.82	-1.92	9.99	9.99	9.99	9.99
A820109.C	3.7	SBQ	2.65	9.99	-1.91	-1.72	-1.56	-1.47	-1.40	-1.45	-1.38	-1.46	-1.53	-1.70
A820111.A	5.4	EBN	2.14	0.66	0.63	0.63	0.41	0.32	0.41	0.48	0.45	0.64	0.42	0.58

A820111.A	5.4	LMN	2.27	9.99	0.56	0.83	0.60	0.56	0.41	0.35	0.19	0.10	0.23	0.10
A820111.A	5.4	GGN	2.32	9.99	0.44	0.85	0.82	0.90	0.70	0.74	0.76	0.78	0.65	0.50
A820111.A	5.4	GSQ	2.33	9.99	9.99	-0.03	0.20	0.26	0.20	0.14	0.03	0.00	-0.04	-0.10
A820111.A	5.4	LPQ	2.42	9.99	9.99	0.07	0.31	0.25	0.21	0.14	0.01	-0.14	9.99	9.99
A820111.A	5.4	MNQ	2.63	9.99	9.99	-0.33	-0.24	-0.26	-0.30	-0.38	-0.35	-0.42	-0.45	-0.53
A820111.A	5.4	SBQ	2.65	0.00	0.17	0.19	0.17	0.31	0.31	0.08	-0.04	-0.19	-0.25	-0.32
A820111.A	5.4	MNT	2.75	9.99	9.99	-0.51	-0.37	-0.24	-0.44	-0.54	-0.67	-0.78	-0.82	-0.87
A820111.A	5.4	TRQ	2.79	-0.54	-0.33	-0.30	-0.33	-0.31	-0.54	-0.64	-0.81	-0.92	-1.02	9.99
A820111.A	5.4	WBO	2.85	-0.52	-0.41	-0.45	-0.42	-0.52	-0.52	-0.65	9.99	9.99	9.99	9.99
A820111.A	5.4	OTT	2.86	9.99	9.99	-0.33	-0.29	-0.29	-0.46	-0.71	-0.89	-1.00	-1.02	-1.08
A820111.A	5.4	CKO	2.92	9.99	9.99	-0.41	-0.32	-0.41	-0.59	-0.82	-0.95	-1.03	-1.08	9.99
A820111.A	5.4	VDQ	2.94	9.99	9.99	9.99	-0.46	-0.40	-0.73	-0.89	-1.00	-1.14	9.99	9.99
A820111.A	5.4	JAQ	3.00	9.99	-0.69	-0.64	-0.73	-0.86	-0.92	-1.11	9.99	9.99	9.99	9.99
A820113.A	4.0	EBN	2.14	9.99	9.99	9.99	-1.26	-1.14	-1.01	-1.18	-0.97	-0.76	-0.69	9.99
A820113.A	4.0	LMN	2.27	-1.73	-1.61	-1.65	-1.47	-1.66	-1.32	-1.31	-1.36	-1.42	-1.36	-1.30
A820113.A	4.0	GGN	2.32	9.99	-1.90	-1.58	-1.31	-1.51	9.99	9.99	9.99	9.99	9.99	9.99
A820113.A	4.0	GSQ	2.33	-2.14	-1.91	-1.83	-1.80	-1.53	-1.52	-1.46	-1.61	9.99	9.99	9.99
A820113.A	4.0	LPQ	2.42	-2.18	-1.98	-1.81	-1.87	9.99	9.99	9.99	9.99	9.99	9.99	9.99
A820113.A	4.0	MNQ	2.63	9.99	-2.40	-2.30	-2.26	-2.03	-2.02	-1.91	-1.93	9.99	9.99	9.99
A820115.A	3.8	LMN	2.27	9.99	-1.14	-1.02	-1.07	-0.80	-0.90	-0.78	-0.87	-0.68	-0.72	-0.62
A820115.A	3.8	GGN	2.32	9.99	-1.36	-1.04	-0.84	-1.02	9.99	9.99	9.99	9.99	9.99	9.99
A820115.A	3.8	GSQ	2.33	9.99	9.99	-1.59	-1.37	-1.29	-1.25	-1.31	-1.34	9.99	9.99	9.99
A820115.A	3.8	MNQ	2.63	-2.29	-2.02	-1.82	-1.78	-1.79	9.99	9.99	9.99	9.99	9.99	9.99
A820115.A	3.8	GNT	2.65	9.99	9.99	-1.78	-1.61	-1.77	-1.88	9.99	9.99	9.99	9.99	9.99
A820115.A	3.8	SBQ	2.65	9.99	-1.71	-1.51	-1.52	-1.49	-1.63	9.99	9.99	9.99	9.99	9.99
A820115.A	3.8	TRQ	2.79	9.99	-2.03	-1.82	-1.81	-2.03	-2.12	-2.21	-2.29	-2.25	-2.35	9.99
A820115.A	3.8	WBO	2.85	9.99	9.99	9.99	-2.09	-2.06	-2.27	-2.32	-2.46	-2.50	-2.40	-2.56
A820115.A	3.8	GRQ	2.85	9.99	-1.94	-1.79	-1.76	-1.82	-1.92	-2.07	-2.19	-2.25	-2.26	-2.30
A820117.A	3.6	EBN	2.14	-1.56	-1.44	-1.40	-1.26	-1.11	-0.86	-0.92	-0.89	-0.69	-0.68	9.99
A820117.A	3.6	GGN	2.32	-1.89	-1.75	-1.58	-1.29	-1.20	-1.33	9.99	9.99	9.99	9.99	9.99
A820117.A	3.6	GSQ	2.33	9.99	-2.05	-1.87	-1.78	-1.53	-1.48	-1.49	-1.56	-1.55	-1.65	9.99
A820117.A	3.6	LPQ	2.42	-2.10	-1.89	-1.74	-1.75	9.99	9.99	9.99	9.99	9.99	9.99	9.99
A820117.A	3.6	MNQ	2.63	-2.66	-2.37	-2.30	-2.13	-2.04	-1.95	-1.90	-1.84	-1.89	-1.93	-2.05
A820117.A	3.6	GNT	2.65	9.99	-2.01	-1.91	-1.91	-2.02	9.99	9.99	9.99	9.99	9.99	9.99
A820117.A	3.6	SBQ	2.65	-2.22	-2.04	-1.84	-1.89	9.99	9.99	9.99	9.99	9.99	9.99	9.99
A820119.A	4.5	MNT	2.43	-1.29	-0.94	-0.91	-0.69	-0.38	-0.44	9.99	9.99	9.99	9.99	9.99

A820119.A	4.5	GNT	2.51	-1.00	-0.73	-0.64	-0.80	9.99	9.99	9.99	9.99	9.99	9.99	9.99
A820119.A	4.5	WBO	2.53	9.99	-1.08	-0.88	-0.68	-0.78	9.99	9.99	9.99	9.99	9.99	9.99
A820119.A	4.5	OTT	2.59	-1.28	-0.99	-0.70	-0.45	-0.41	-0.38	-0.29	-0.42	-0.34	-0.44	-0.57
A820119.A	4.5	EBN	2.72	-1.25	-1.11	-1.14	-0.98	-1.04	-1.11	-1.14	-1.10	-1.28	-1.36	-1.48
A820119.A	4.5	CKO	2.73	-1.31	-1.07	-0.95	-0.82	-0.84	-0.71	-0.76	-0.69	-0.85	-0.96	-1.13
A820119.A	4.5	VDQ	2.86	-1.60	-1.23	-0.93	-1.01	-1.01	-1.12	-1.08	-1.21	-1.37	-1.54	-1.66
A820119.A	4.5	MNQ	2.91	-1.59	-1.43	-1.38	-1.44	-1.34	-1.42	-1.56	-1.57	-1.69	-1.85	-2.03
A820316.A	3.5	KLN	1.40	-1.71	-1.35	-0.95	-0.85	-0.92	-0.70	-0.63	-0.42	-0.59	-0.70	-0.43
A820316.A	3.5	EBN	2.14	-1.82	-1.65	-1.47	-1.48	-1.16	-0.97	-1.25	-1.06	-1.01	-1.02	-1.14
A820316.A	3.5	LMN	2.27	-1.74	-1.63	-1.56	-1.67	-1.57	-1.26	-1.34	-1.35	-1.59	-1.84	-1.56
A820316.A	3.5	GGN	2.32	9.99	-2.05	-1.65	-1.42	-1.42	-1.26	-1.27	-1.27	-1.36	-1.49	9.99
A820316.A	3.5	GSQ	2.33	-2.06	-1.94	-1.86	-1.84	-1.55	-1.50	-1.45	-1.44	-1.43	-1.34	-1.28
A820331.A	5.0	KLN	1.40	-0.04	0.16	0.23	0.38	0.35	0.27	0.62	0.65	0.58	0.57	0.62
A820331.A	5.0	EBN	2.14	9.99	9.99	-0.47	-0.33	-0.04	-0.16	-0.20	0.21	-0.08	-0.13	-0.05
A820331.A	5.0	GGN	2.32	9.99	-0.57	-0.23	-0.20	-0.14	-0.21	-0.12	0.12	-0.14	-0.36	9.99
A820331.A	5.0	LPQ	2.42	9.99	9.99	-0.68	-0.38	-0.42	-0.57	9.99	9.99	9.99	9.99	9.99
A820331.A	5.0	MNQ	2.63	-0.91	-0.66	-0.73	-0.64	-0.65	-0.73	-0.69	-0.68	-0.77	-0.88	-0.99
A820331.A	5.0	GNT	2.65	9.99	-0.89	-0.85	-0.85	-1.00	-1.17	9.99	9.99	9.99	9.99	9.99
A820331.A	5.0	SBQ	2.65	9.99	-0.95	-0.75	-0.80	-0.85	-0.84	-0.79	-0.67	-0.76	-0.95	-1.10
A820331.A	5.0	TRQ	2.79	9.99	-1.32	-1.18	-1.12	-1.19	-1.42	9.99	9.99	9.99	9.99	9.99
A820331.A	5.0	WBO	2.85	9.99	9.99	-1.39	-1.33	-1.37	-1.48	-1.51	-1.56	-1.68	-1.71	-1.78
A820331.A	5.0	GRQ	2.85	9.99	9.99	-1.15	-1.08	-1.09	-1.24	-1.20	-1.23	-1.42	-1.54	9.99
A820331.A	5.0	OTT	2.86	-1.45	-1.34	-1.31	-1.35	-1.29	-1.42	9.99	9.99	9.99	9.99	9.99
A820331.A	5.0	CKO	2.92	9.99	-1.40	-1.29	-1.22	-1.27	-1.45	-1.54	-1.49	-1.70	-1.83	9.99
A820331.A	5.0	VDQ	2.94	9.99	9.99	9.99	-1.38	-1.29	-1.44	-1.53	-1.47	-1.64	-1.86	9.99
A820402.A	4.3	KLN	1.40	-0.78	-0.52	-0.34	-0.25	-0.16	-0.06	-0.13	-0.09	-0.03	-0.14	0.22
A820402.A	4.3	GGN	2.32	9.99	-1.24	-0.92	-0.72	-0.72	-0.65	-0.77	9.99	9.99	9.99	9.99
A820402.A	4.3	LPQ	2.42	-1.46	-1.14	-1.10	-0.90	-0.88	-0.91	-0.78	-0.96	-1.01	-1.14	9.99
A820402.A	4.3	MNQ	2.63	9.99	-1.52	-1.39	-1.22	-1.27	-1.09	-1.12	-1.12	-1.14	-1.23	-1.31
A820402.A	4.3	GNT	2.65	9.99	-1.27	-1.25	-1.27	-1.41	-1.50	9.99	9.99	9.99	9.99	9.99
A820402.A	4.3	SBQ	2.65	9.99	-1.36	-1.25	-1.11	-1.07	-1.09	-1.19	-1.24	-1.32	-1.47	-1.60
A820402.A	4.3	MNT	2.75	9.99	9.99	-1.91	-1.79	-1.63	-1.69	-1.64	-1.69	-1.84	9.99	9.99
A820402.A	4.3	TRQ	2.79	9.99	-1.73	-1.60	-1.62	-1.61	-1.66	-1.66	-1.76	-1.93	-2.02	-2.12
A820402.A	4.3	WBO	2.85	9.99	9.99	9.99	9.99	-1.75	-1.74	-1.86	-1.97	-2.23	9.99	9.99
A820402.A	4.3	GRQ	2.85	9.99	-1.70	-1.53	-1.46	-1.50	-1.43	-1.51	-1.63	-1.78	-1.95	9.99
A820402.A	4.3	OTT	2.86	9.99	-1.85	-1.68	-1.72	-1.67	-1.65	-1.75	9.99	9.99	9.99	9.99

A820402.A	4.3	CKO	2.92	9.99	-1.84	-1.73	-1.61	-1.65	-1.66	-1.80	-2.01	-2.07	-2.24	-2.34
A820402.A	4.3	VDQ	2.94	9.99	9.99	9.99	-1.69	-1.59	-1.73	-1.89	-1.97	-2.06	-2.20	-2.34
A820402.A	4.3	JAQ	3.00	9.99	9.99	-1.88	-1.75	-1.89	-1.80	-1.88	-1.94	-2.13	9.99	9.99
A820411.A	4.0	KLN	1.40	-1.18	-0.90	9.99	-0.54	-0.38	-0.21	-0.05	-0.03	0.00	0.09	0.26
A820411.A	4.0	EBN	2.14	-0.95	-0.63	-0.64	-0.80	-0.73	-0.66	-0.97	-0.56	-0.50	-0.67	-0.68
A820411.A	4.0	GGN	2.32	-1.46	-1.17	-1.11	-1.04	-0.86	-0.80	-0.61	-0.44	-0.37	-0.43	-0.53
A820411.A	4.0	GSQ	2.33	9.99	9.99	-1.53	-1.39	-1.17	-1.04	9.99	9.99	9.99	9.99	9.99
A820411.A	4.0	LPQ	2.42	-1.54	-1.31	-1.23	-1.05	-1.05	-1.07	9.99	9.99	9.99	9.99	9.99
A820411.A	4.0	GNT	2.65	9.99	9.99	-1.44	-1.40	-1.40	-1.71	9.99	9.99	9.99	9.99	9.99
A820411.A	4.0	SBQ	2.65	-1.59	-1.43	-1.36	-1.36	-1.24	-1.25	-1.19	-1.17	-1.17	-1.24	-1.35
A820411.A	4.0	MNT	2.75	9.99	-2.05	-1.91	-1.82	-1.75	-1.74	-1.85	9.99	9.99	9.99	9.99
A820411.A	4.0	WBO	2.85	9.99	9.99	-1.91	-1.84	-1.84	-1.92	-2.02	-2.15	-2.08	-2.10	-2.23
A820411.A	4.0	GRQ	2.85	9.99	9.99	9.99	-1.60	-1.57	-1.68	-1.81	-1.77	-1.81	-2.06	9.99
A820411.A	4.0	OTT	2.86	9.99	9.99	-1.89	-1.77	-1.77	-1.84	-1.91	-1.97	9.99	9.99	9.99
A820411.A	4.0	CKO	2.92	9.99	-1.89	-1.75	-1.72	-1.82	-1.93	-2.05	-2.09	-2.12	-2.23	-2.33
A820411.A	4.0	VDQ	2.94	9.99	-1.90	-1.79	-1.88	-1.89	-2.02	-2.06	-2.14	-2.27	-2.29	-2.40
A820411.A	4.0	JAQ	3.00	9.99	-2.17	-2.16	-2.22	-2.29	9.99	9.99	9.99	9.99	9.99	9.99
A820418.A	4.1	KLN	1.40	-0.75	-0.75	9.99	-0.53	-0.39	-0.44	-0.09	0.08	0.06	0.16	0.25
A820418.A	4.1	EBN	2.14	-1.25	-1.09	-1.11	-0.93	-0.83	-0.63	-0.96	-0.87	-0.92	-0.89	-0.90
A820418.A	4.1	GGN	2.32	-1.63	-1.38	-1.15	-0.90	-0.74	-0.70	-0.69	-0.49	-0.50	-0.37	-0.53
A820418.A	4.1	GSQ	2.33	9.99	9.99	9.99	9.99	-1.14	-1.27	-1.31	-1.41	-1.50	9.99	9.99
A820418.A	4.1	MNQ	2.63	9.99	-1.76	-1.61	-1.57	-1.66	-1.62	-1.70	-1.78	-1.90	9.99	9.99
A820418.A	4.1	GNT	2.65	9.99	9.99	-1.50	-1.48	-1.60	-1.72	-1.80	-1.90	-1.96	9.99	9.99
A820418.A	4.1	SBQ	2.65	-1.64	-1.47	-1.44	-1.37	-1.30	-1.29	-1.34	-1.38	-1.31	-1.51	-1.71
A820418.A	4.1	MNT	2.75	9.99	9.99	-2.20	-2.03	-1.87	-1.83	-2.02	9.99	9.99	9.99	9.99
A820418.A	4.1	TRQ	2.79	9.99	-1.97	-1.78	-1.83	-1.81	-2.00	-2.00	-2.17	-2.29	9.99	9.99
A820418.A	4.1	WBO	2.85	9.99	9.99	-2.10	-1.92	-1.93	-1.94	-2.10	-2.23	-2.35	-2.44	9.99
A820418.A	4.1	GRQ	2.85	9.99	-1.90	-1.73	-1.69	-1.68	-1.75	-1.84	-2.03	-2.17	-2.25	9.99
A820418.A	4.1	CKO	2.92	9.99	-2.05	-1.93	-1.82	-1.86	-2.02	-2.22	-2.39	-2.49	-2.57	9.99
A820418.A	4.1	VDQ	2.94	9.99	-1.95	-1.83	-2.00	-1.92	-2.09	-2.27	-2.36	-2.52	9.99	9.99
A820506.A	4.0	KLN	1.40	-1.31	-1.22	9.99	-0.69	-0.57	-0.63	-0.60	-0.53	-0.50	0.18	0.30
A820506.A	4.0	EBN	2.14	9.99	-1.06	-0.84	-0.88	-0.63	-0.60	-0.73	-0.56	-0.60	-0.53	-0.59
A820506.A	4.0	GGN	2.32	9.99	-1.66	-1.26	-1.16	-1.32	9.99	9.99	9.99	9.99	9.99	9.99
A820506.A	4.0	GSQ	2.33	9.99	-1.53	-1.33	-1.24	-1.12	-0.91	-1.04	-1.18	9.99	9.99	9.99
A820506.A	4.0	HTQ	2.44	9.99	-1.75	-1.62	-1.42	-1.12	-1.11	-0.99	-1.09	-1.20	-1.29	9.99
A820506.A	4.0	SBQ	2.65	-1.91	-1.68	-1.48	-1.43	-1.45	-1.46	-1.45	-1.53	-1.60	-1.65	9.99

A820506.A	4.0	TRQ	2.79	9.99	-2.06	-1.95	-1.85	-1.91	-1.95	-2.04	-2.08	-2.15	-2.21	9.99
A820506.A	4.0	WBO	2.85	9.99	9.99	9.99	-1.96	-1.95	-2.01	-2.11	-2.31	9.99	9.99	9.99
A820506.A	4.0	GRQ	2.85	9.99	-1.88	-1.77	-1.65	-1.69	-1.71	-1.77	-1.91	-2.06	-2.15	9.99
A820506.A	4.0	VDQ	2.94	9.99	9.99	9.99	-1.94	-1.86	-1.92	-2.10	-2.25	-2.38	-2.45	9.99
A820506.A	4.0	JAQ	3.00	9.99	9.99	-2.37	-2.20	-2.13	-2.11	-2.13	-2.27	9.99	9.99	9.99
A820616.A	4.7	KLN	1.69	-0.42	-0.26	-0.11	-0.16	-0.11	-0.02	0.11	0.39	0.46	0.35	0.50
A820616.A	4.7	EBN	2.06	-0.27	-0.03	-0.04	0.00	0.08	0.10	-0.23	-0.23	-0.20	-0.12	-0.04
A820616.A	4.7	LMN	2.32	9.99	9.99	9.99	9.99	-0.66	-0.56	-0.32	-0.33	-0.39	-0.59	9.99
A820616.A	4.7	GGN	2.32	9.99	-0.75	-0.52	-0.51	-0.28	-0.07	0.08	0.23	0.31	-0.02	9.99
A820616.A	4.7	LPQ	2.37	-0.92	-0.75	-0.69	-0.56	-0.46	-0.62	9.99	9.99	9.99	9.99	9.99
A820616.A	4.7	HTQ	2.42	-1.28	-0.99	-0.77	-0.53	-0.50	-0.78	9.99	9.99	9.99	9.99	9.99
A820616.A	4.7	GNT	2.62	-0.84	-0.81	-0.83	-0.92	-0.98	-1.09	9.99	9.99	9.99	9.99	9.99
A820616.A	4.7	SBQ	2.63	-0.98	-0.82	-0.60	-0.64	-0.81	-0.74	-0.71	-0.66	-0.73	-0.99	9.99
A820616.A	4.7	TRQ	2.77	-1.76	-1.58	-1.18	-0.95	-1.07	-1.23	-1.29	-1.29	-1.43	-1.52	-1.57
A820616.A	4.7	GRQ	2.83	-1.39	-1.16	-1.02	-1.01	-1.04	-1.11	-1.16	-1.23	-1.40	-1.60	9.99
A820616.A	4.7	WBO	2.83	9.99	9.99	-1.31	-1.21	-1.34	-1.36	-1.40	-1.44	-1.55	-1.69	-1.82
A820616.A	4.7	OTT	2.84	9.99	-1.39	-1.15	-1.22	-1.22	-1.39	-1.38	-1.47	-1.59	9.99	9.99
A820616.A	4.7	CKO	2.91	9.99	9.99	-1.28	-1.22	-1.31	-1.52	-1.60	-1.58	-1.68	-1.78	-1.88
A820616.A	4.7	VDQ	2.92	-1.41	-1.26	-1.26	-1.27	-1.31	-1.46	-1.66	-1.73	-1.79	-1.84	9.99
A820616.A	4.7	WEO	2.98	9.99	-1.48	-1.44	-1.59	-1.64	-1.65	-1.70	9.99	9.99	9.99	9.99
A820616.A	4.7	JAQ	2.99	9.99	-1.45	-1.39	-1.50	-1.51	-1.47	-1.63	9.99	9.99	9.99	9.99
A820623.A	3.5	GRQ	2.08	9.99	9.99	-2.31	-1.93	-1.71	-1.77	-1.52	-1.26	-1.15	-1.01	-0.89
A820623.A	3.5	VDQ	2.08	9.99	-2.44	-2.16	-2.07	-1.87	-1.76	-1.62	-1.42	-1.45	-1.30	-1.25
A820623.A	3.5	CKO	2.21	-2.46	-2.21	-2.04	-1.79	-1.61	-1.41	-1.37	-1.32	-0.89	-0.92	-0.78
A820623.A	3.5	TRQ	2.35	-3.01	-2.76	-2.67	-2.21	-1.84	-1.73	-1.76	9.99	9.99	9.99	9.99
A820623.A	3.5	OTT	2.38	-2.74	-2.53	-2.15	-2.08	-1.79	-1.69	-1.56	-1.40	-1.39	-1.22	9.99
A820623.A	3.5	WBO	2.47	-2.80	-2.54	-2.38	-2.29	-2.17	-1.88	-1.90	-1.92	9.99	9.99	9.99
A820623.A	3.5	MNT	2.52	-2.99	-2.72	-2.53	-2.50	-2.31	-1.99	-1.96	-1.83	-1.77	-1.66	-1.65
A820623.A	3.5	GNT	2.56	-2.46	-2.28	-2.19	-2.00	-1.98	-1.72	-1.82	9.99	9.99	9.99	9.99
A820623.A	3.5	WEO	2.59	-2.71	-2.40	-2.18	-2.18	-2.00	-1.85	-1.69	-1.47	-1.03	-0.94	-0.99
A820713.A	3.8	TRQ	1.25	-1.47	-1.17	-0.97	-0.91	-0.87	-0.54	-0.36	-0.45	-0.34	-0.33	-0.31
A820713.A	3.8	GAC	1.93	-2.06	-1.80	-1.73	-1.58	-1.20	-1.09	-0.94	-0.79	-0.77	-0.58	-0.41
A820713.A	3.8	MNT	1.99	-2.01	-1.86	-1.83	-1.63	-1.57	-1.39	-1.14	-1.12	-1.05	-0.88	-0.70
A820713.A	3.8	OTT	2.08	-1.75	-1.56	-1.38	-1.25	-1.23	-0.91	-0.78	-0.73	-0.53	-0.37	-0.43
A820713.A	3.8	WBO	2.13	9.99	-2.02	-1.60	-1.49	-1.46	-1.23	-1.03	-1.00	-0.77	-0.71	-0.66
A820713.A	3.8	GNT	2.23	-2.07	-1.56	-1.48	-1.31	-1.27	-1.32	-1.09	-1.07	-1.02	-1.00	-0.84

A820713.A	3.8	SBQ	2.34	-1.88	-1.70	-1.42	-1.43	9.99	9.99	9.99	9.99	9.99	9.99	9.99
A820713.A	3.8	VDQ	2.55	-2.54	-2.18	-2.00	-1.79	-1.68	-1.54	-1.42	-1.50	-1.50	-1.59	-1.70
A820713.A	3.8	WEO	2.58	-2.46	-2.09	-1.87	-1.86	-1.61	-1.37	-1.17	-1.11	-0.61	-0.64	9.99
A820713.A	3.8	EBN	2.70	-2.51	-2.30	-2.11	-2.05	-1.87	-1.93	-1.80	-1.84	-2.03	9.99	9.99
A820713.A	3.8	GSQ	2.81	9.99	-2.28	-2.05	-1.93	-1.95	-2.00	-2.15	9.99	9.99	9.99	9.99
A820713.A	3.8	MNQ	2.81	9.99	-2.25	-2.11	-1.98	-1.86	-1.89	-1.85	-1.81	-1.86	-1.88	-1.92
A820728.A	3.7	EBN	2.14	-1.47	-1.24	-1.12	-1.16	-1.16	-0.87	-0.98	-1.02	-1.10	-0.92	-0.73
A820728.A	3.7	LMN	2.27	-1.83	-1.58	-1.34	-1.46	-1.17	-1.06	-0.98	-1.16	-1.14	-1.29	-1.25
A820728.A	3.7	GGN	2.32	9.99	-1.75	-1.52	-1.14	-1.15	9.99	9.99	9.99	9.99	9.99	9.99
A820728.A	3.7	GSQ	2.33	9.99	9.99	-2.00	-1.67	-1.63	-1.73	9.99	9.99	9.99	9.99	9.99
A820728.A	3.7	LPQ	2.42	-2.07	-1.81	-1.67	-1.37	9.99	9.99	9.99	9.99	9.99	9.99	9.99
A820728.A	3.7	MNQ	2.63	9.99	9.99	-2.24	-2.06	-2.05	-2.16	9.99	9.99	9.99	9.99	9.99
A820728.A	3.7	GNT	2.65	-2.00	-1.87	-1.79	-1.82	-1.82	-1.85	-1.86	-1.95	9.99	9.99	9.99
A820728.A	3.7	SBQ	2.65	9.99	-1.84	-1.61	-1.49	-1.49	-1.45	-1.48	-1.46	-1.50	-1.66	-1.75
A820728.A	3.7	TRQ	2.79	9.99	-2.40	-1.98	-1.89	-1.93	-2.01	9.99	9.99	9.99	9.99	9.99
A820806.A	3.7	GAC	1.37	-2.14	-1.78	-1.43	-1.26	-1.06	-1.01	-0.79	-0.63	-0.62	-0.47	-0.38
A820806.A	3.7	OTT	1.78	-2.34	-2.15	-1.67	-1.35	-1.13	-1.13	-0.82	-0.93	-0.68	-0.53	-0.49
A820806.A	3.7	TRQ	1.90	-2.14	-2.04	-1.87	-1.81	-1.64	-1.37	-1.29	-1.08	-0.92	-0.77	-0.69
A820806.A	3.7	WBO	2.00	-2.44	-2.10	-1.90	-1.56	-1.52	-1.43	-1.17	-1.18	-1.02	-0.81	-0.77
A820806.A	3.7	MNT	2.17	-2.48	-2.01	-1.76	-1.55	-1.35	-0.92	-1.20	-1.06	-0.98	-0.92	-0.73
A820806.A	3.7	CKO	2.19	-2.34	-2.06	-1.70	-1.59	-1.41	-1.44	-1.21	-1.25	-1.02	-1.05	-0.97
A820806.A	3.7	GNT	2.39	9.99	-1.93	-1.76	-1.66	-1.50	-1.31	-1.17	-1.20	-1.09	-1.24	9.99
A820806.A	3.7	SBQ	2.45	-2.47	-2.07	-1.90	-1.7[illegible]	-1.72	-1.57	-1.54	-1.29	-1.27	-1.36	9.99
A820806.A	3.7	WEO	2.49	-2.45	-2.11	-1.98	-2.03	9.99	9.99	9.99	9.99	9.99	9.99	9.99
A820806.A	3.7	VDQ	2.51	-2.60	-2.41	-2.25	-2.32	9.99	9.99	9.99	9.99	9.99	9.99	9.99
A820806.A	3.7	LPQ	2.65	9.99	-2.22	-2.00	-2.00	-1.57	-1.54	-1.50	-1.52	-1.66	-1.77	9.99
A820806.A	3.7	EBN	2.76	9.99	9.99	-2.53	-2.25	-2.09	-2.05	-1.99	-1.98	-2.02	-2.13	9.99
A820813.A	4.3	CKO	2.07	-1.83	-1.66	-1.44	-0.98	-0.83	-0.63	-0.44	-0.43	-0.12	-0.04	0.02
A820813.A	4.3	VDQ	2.26	-1.43	-1.13	-1.11	-1.11	-0.89	-0.78	-0.72	-0.62	-0.64	-0.59	-0.65
A820813.A	4.3	OTT	2.42	-1.78	-1.58	-1.24	-1.25	9.99	9.99	9.99	9.99	9.99	9.99	9.99
A820813.A	4.3	WEO	2.47	-1.70	-1.52	-1.41	-1.12	-0.91	-0.72	-0.59	-0.46	-0.13	-0.09	-0.12
A820813.A	4.3	WBO	2.50	-1.83	-1.71	-1.40	-1.24	-1.12	-0.95	-0.85	-0.78	-0.77	-0.70	-0.75
A820813.A	4.3	MNT	2.61	-2.09	-1.86	-1.49	-1.47	-1.37	-1.09	-1.06	-1.07	-1.05	-1.05	-1.11
A820813.A	4.3	SBQ	2.73	9.99	-1.63	-1.49	-1.37	-1.37	-1.25	-1.22	-1.19	-1.29	-1.43	9.99
A820813.A	4.3	JAQ	2.91	9.99	-1.75	-1.51	-1.54	-1.52	-1.49	-1.56	-1.73	9.99	9.99	9.99
A820903.A	3.7	OTT	1.89	-2.03	-2.00	-1.49	-1.58	-1.26	-1.13	-1.22	-0.96	-0.66	-0.44	-0.50

A820903.A	3.7	GAC	1.95	-1.97	-2.01	-1.91	-1.64	-1.36	-1.21	-1.14	-1.02	-0.98	-0.91	-0.80
A820903.A	3.7	WBO	2.11	-2.15	-1.89	-1.89	-1.44	-1.38	-1.35	-1.19	-1.00	-0.97	-0.78	-0.75
A820903.A	3.7	TRQ	2.23	-2.05	-1.73	-1.52	-1.55	-1.32	-1.30	-1.04	-1.12	-0.93	-0.91	-1.01
A820903.A	3.7	WEO	2.37	9.99	-1.87	-1.69	-1.51	-1.29	-1.11	-0.83	-0.85	9.99	9.99	9.99
A820903.A	3.7	VDQ	2.48	-2.18	-1.92	-1.89	-1.96	9.99	9.99	9.99	9.99	9.99	9.99	9.99
A820903.A	3.7	SBQ	2.56	-2.33	-2.02	-1.86	-1.74	-1.79	9.99	9.99	9.99	9.99	9.99	9.99
A820903.A	3.7	LPQ	2.73	9.99	9.99	9.99	-1.76	-1.60	-1.58	-1.47	-1.67	-1.78	-1.91	9.99
A821026.A	3.5	KLN	1.40	-1.76	-1.74	-1.07	-1.25	-0.96	-0.97	-0.72	-0.59	-0.68	-0.66	-0.58
A821026.A	3.5	EBN	2.14	9.99	-1.69	-1.58	-1.49	-1.42	-1.21	-1.18	-1.05	9.99	9.99	9.99
A821026.A	3.5	GGN	2.32	-2.49	-2.27	-1.84	-1.61	-1.62	9.99	9.99	9.99	9.99	9.99	9.99
A821026.A	3.5	GSQ	2.33	-2.28	-2.10	-1.97	-1.91	-1.76	-1.64	-1.62	-1.56	-1.58	-1.60	9.99
A821026.A	3.5	LPQ	2.42	-2.50	-2.19	-2.02	-1.71	-1.73	9.99	9.99	9.99	9.99	9.99	9.99
A821204.A	3.9	LPQ	1.49	-0.91	-0.48	9.99	-0.18	0.06	0.26	0.32	0.49	0.43	0.35	0.37
A821204.A	3.9	EBN	2.17	-1.85	-1.58	-1.53	-1.22	-1.09	-1.08	-0.82	-0.44	-0.41	-0.42	-0.46
A821204.A	3.9	GNT	2.32	-2.01	-1.78	-1.58	-1.20	-1.19	-1.06	-0.96	-1.01	-1.10	9.99	9.99
A821204.A	3.9	HTQ	2.36	-2.26	-2.12	-1.81	-1.67	-1.39	-1.27	-1.02	-0.94	-0.96	9.99	9.99
A821204.A	3.9	SBQ	2.44	-2.11	-1.82	-1.65	-1.55	-1.46	-1.22	-1.17	-1.13	-1.02	-1.04	-1.08
A821204.A	3.9	GSQ	2.44	9.99	9.99	-1.85	-1.57	-1.42	-1.36	-1.36	-1.17	-1.27	9.99	9.99
A821204.A	3.9	KLN	2.48	-2.18	-1.94	-1.76	-1.66	-1.72	9.99	9.99	9.99	9.99	9.99	9.99
A821204.A	3.9	MNT	2.54	-2.37	-2.23	-2.22	-1.83	-1.71	-1.48	-1.39	-1.25	-1.23	-1.25	9.99
A821204.A	3.9	MNQ	2.54	-2.30	-2.03	-1.70	-1.65	-1.46	-1.45	-1.26	-1.16	-1.16	-1.11	9.99
A821204.A	3.9	GGN	2.57	9.99	-1.87	-1.76	-1.64	-1.55	-1.50	-1.57	9.99	9.99	9.99	9.99
A821204.A	3.9	GRQ	2.64	-2.29	-2.17	-1.69	-1.62	-1.39	-1.15	-1.18	-1.29	9.99	9.99	9.99
A821204.A	3.9	LMN	2.66	9.99	9.99	-2.24	-2.11	-2.05	-1.95	-2.04	-2.12	9.99	9.99	9.99
A821204.A	3.9	WBO	2.68	-2.45	-2.31	-2.08	-2.06	-1.78	-1.64	-1.61	-1.65	9.99	9.99	9.99
A821204.A	3.9	OTT	2.68	-2.44	-2.17	-1.99	-1.85	-1.56	-1.44	-1.44	-1.48	9.99	9.99	9.99
A821204.A	3.9	CKO	2.76	9.99	9.99	-1.98	-1.82	-1.56	-1.48	-1.58	-1.58	-1.55	-1.63	-1.69
A821204.A	3.9	WEO	2.87	9.99	-2.48	-2.29	-2.22	-2.02	-1.92	-1.79	-1.63	-1.40	9.99	9.99
A830117.A	4.1	GSQ	1.39	-0.71	-0.44	9.99	-0.22	0.04	0.29	0.26	0.53	0.48	0.63	0.77
A830117.A	4.1	HTQ	1.99	-1.39	-1.22	-0.83	-0.63	-0.72	-0.68	-0.72	-0.62	-0.52	-0.44	-0.27
A830117.A	4.1	MNQ	2.30	-1.60	-1.20	-1.04	-0.97	-1.03	-0.83	-0.77	-0.82	-0.67	-0.65	-0.61
A830117.A	4.1	EBN	2.29	-1.33	-1.00	-0.99	-0.91	-0.89	-1.02	-0.96	-0.62	-0.59	-0.55	9.99
A830117.A	4.1	KLN	2.41	-1.80	-1.47	-1.12	-1.08	-1.06	-1.04	-0.98	-1.08	9.99	9.99	9.99
A830117.A	4.1	LMN	2.60	-1.64	-1.49	-1.34	-1.31	-1.43	9.99	9.99	9.99	9.99	9.99	9.99
A830117.A	4.1	GGN	2.65	-1.86	-1.69	-1.46	-1.37	-1.25	-1.40	9.99	9.99	9.99	9.99	9.99
A830117.A	4.1	GNT	2.70	-1.45	-1.26	-1.26	-1.45	-1.58	-1.72	9.99	9.99	9.99	9.99	9.99

A830117.A	4.1	MNT	2.80	9.99	-1.80	-1.70	-1.75	-1.88	-1.98	9.99	9.99	9.99	9.99	9.99
A830117.A	4.1	WBO	2.89	9.99	9.99	-1.72	-1.68	-1.77	-1.93	-1.97	-2.01	9.99	9.99	9.99
A830117.A	4.1	OTT	2.89	9.99	-1.76	-1.65	-1.61	-1.66	-1.85	-2.00	9.99	9.99	9.99	9.99
A830117.A	4.1	VDQ	2.91	9.99	9.99	-1.77	-1.65	-1.59	-1.77	-1.88	-1.94	-2.04	9.99	9.99
A830117.A	4.1	CKO	2.93	9.99	9.99	-1.79	-1.75	-1.77	-1.91	-2.02	-2.05	-2.06	-2.02	-2.12
A830513.A	3.5	KLN	1.40	-1.88	-1.60	-1.32	-1.07	-0.84	-0.91	-0.92	-0.71	-0.67	-0.73	-0.56
A830513.A	3.5	EBN	2.14	9.99	9.99	9.99	-1.43	-1.19	-1.10	-1.01	-0.98	-0.73	-0.93	-0.78
A830513.A	3.5	LMN	2.27	9.99	-1.82	-1.70	-1.86	-1.65	-1.57	-1.50	-1.69	-1.77	9.99	9.99
A830513.A	3.5	GGN	2.32	-2.05	-1.92	-1.90	-1.76	-1.60	-1.36	-1.36	-1.00	-1.02	-1.18	9.99
A830513.B	3.9	KLN	1.40	-0.91	-0.63	9.99	-0.52	-0.08	0.10	0.22	0.22	0.30	0.20	0.32
A830513.B	3.9	EBN	2.14	-0.90	-0.57	-0.57	-0.76	-0.45	-0.45	-0.67	-0.71	9.99	9.99	9.99
A830513.B	3.9	LMN	2.27	-1.32	-0.95	-0.79	-0.98	-0.79	-0.71	-0.58	-0.68	-0.78	-0.91	-0.94
A830513.B	3.9	GGN	2.32	-1.40	-1.15	-1.04	-0.96	-0.70	-0.59	-0.45	-0.17	-0.08	-0.20	9.99
A830513.B	3.9	LPQ	2.42	-1.47	-1.26	-1.12	-0.89	-0.84	-0.80	-0.85	-0.91	-0.99	-1.11	9.99
A830513.B	3.9	MNQ	2.63	-1.99	-1.80	-1.64	-1.47	-1.49	-1.62	-1.67	-1.85	9.99	9.99	9.99
A830513.B	3.9	GNT	2.65	-1.55	-1.42	-1.44	-1.35	-1.32	-1.45	-1.52	-1.40	-1.58	9.99	9.99
A830513.B	3.9	SBQ	2.65	-1.51	-1.31	-1.23	-1.26	9.99	9.99	9.99	9.99	9.99	9.99	9.99
A830513.B	3.9	MNT	2.75	9.99	-1.86	-1.75	-1.66	-1.55	-1.44	-1.49	-1.47	-1.61	-1.73	9.99
A830513.B	3.9	TRQ	2.79	9.99	-2.01	-1.71	-1.60	-1.40	-1.45	-1.50	-1.56	-1.69	-1.89	9.99
A830513.B	3.9	WBO	2.85	9.99	9.99	9.99	9.99	-1.66	-1.63	-1.75	-1.82	-1.90	-2.06	-2.15
A830513.B	3.9	GRQ	2.85	9.99	-1.67	-1.53	-1.34	-1.26	-1.34	-1.49	-1.54	-1.77	-1.92	9.99
A830513.B	3.9	OTT	2.86	9.99	9.99	-1.76	-1.60	-1.57	-1.65	-1.61	-1.74	9.99	9.99	9.99
A830516.A	3.8	LPQ	1.62	-1.46	-1.03	-0.82	-0.80	-0.80	-0.74	-0.33	-0.20	-0.36	-0.34	-0.33
A830516.A	3.8	EBN	2.10	9.99	-1.77	-1.20	-1.22	-0.78	-0.67	-0.80	-0.56	-0.61	-0.59	-0.62
A830516.A	3.8	HTQ	2.30	-1.93	-1.46	-1.30	-1.41	-1.30	-0.81	-0.73	-0.58	-0.63	-0.31	-0.47
A830516.A	3.8	GNT	2.38	-1.76	-1.66	-1.63	-1.38	-1.42	9.99	9.99	9.99	9.99	9.99	9.99
A830516.A	3.8	GSQ	2.39	-1.67	-1.30	-1.30	-1.12	-0.81	-0.94	9.99	9.99	9.99	9.99	9.99
A830516.A	3.8	KLN	2.45	-2.02	-1.78	-1.78	-1.46	-1.49	9.99	9.99	9.99	9.99	9.99	9.99
A830516.A	3.8	SBQ	2.48	-1.85	-1.65	-1.63	-1.28	-1.21	-1.19	-1.20	-1.03	-1.11	-1.26	-1.35
A830516.A	3.8	MNQ	2.51	-2.12	-1.95	-1.57	-1.54	-1.30	-1.19	-1.11	-0.97	-0.93	-0.92	-1.02
A830516.A	3.8	GGN	2.57	-2.25	-2.11	-1.76	-1.71	-1.52	-1.51	-1.56	-1.30	-1.39	-1.71	9.99
A830516.A	3.8	MNT	2.57	-2.38	-2.13	-2.07	-1.87	-1.67	-1.45	-1.48	-1.34	-1.42	-1.47	-1.50
A830516.A	3.8	TRQ	2.59	-2.50	-2.17	-1.72	-1.64	-1.42	-1.39	-1.54	9.99	9.99	9.99	9.99
A830516.A	3.8	GRQ	2.67	-2.36	-2.04	-1.80	-1.61	-1.35	-1.31	-1.27	-1.34	-1.40	-1.55	-1.65
A830516.A	3.8	WBO	2.71	9.99	9.99	9.99	-1.92	-1.63	-1.64	-1.59	-1.77	-1.72	-1.80	-1.92
A830516.A	3.8	OTT	2.71	9.99	-2.04	-1.76	-1.71	-1.57	-1.51	-1.60	-1.60	-1.63	-1.66	9.99

A830516.A	3.8	VDQ	2.78	9.99	-2.16	-1.87	-1.84	-1.59	-1.57	-1.61	-1.63	-1.73	-1.82	-1.91
A830516.A	3.8	CKO	2.78	9.99	-1.99	-1.80	-1.76	-1.62	-1.65	-1.66	-1.75	-1.79	-1.88	-2.01
A830516.A	3.8	WEO	2.89	9.99	-2.41	-2.19	-2.15	-2.00	-1.96	-1.95	-1.83	-1.56	9.99	9.99
A830529.A	4.1	SBQ	2.19	-1.19	-0.84	-0.59	-0.56	-0.42	-0.45	-0.44	-0.35	-0.20	-0.27	-0.45
A830529.A	4.1	GNT	2.41	9.99	-1.10	-0.99	-0.96	-0.85	-1.11	9.99	9.99	9.99	9.99	9.99
A830529.A	4.1	MNT	2.44	-1.88	-1.50	-1.13	-0.98	-0.94	-0.86	-0.73	-0.77	-0.80	-0.78	-0.88
A830529.A	4.1	GGN	2.47	9.99	-1.31	-1.19	-0.95	-0.72	-0.64	-0.49	-0.46	-0.32	-0.63	9.99
A830529.A	4.1	LPQ	2.50	-1.62	-1.44	-1.24	-1.06	-0.99	-0.96	-1.02	-1.29	9.99	9.99	9.99
A830529.A	4.1	EBN	2.58	-1.57	-1.45	-1.32	-1.16	-1.15	-1.09	-0.97	-0.99	-1.07	-1.32	-1.54
A830529.A	4.1	TRQ	2.58	-1.99	-1.68	-1.41	-1.24	-1.10	-1.09	-1.09	-1.05	-1.16	-1.29	-1.40
A830529.A	4.1	WBO	2.59	-1.76	-1.38	-1.30	-1.35	9.99	9.99	9.99	9.99	9.99	9.99	9.99
A830529.A	4.1	KLN	2.61	-1.36	-1.03	-1.03	-1.05	-0.95	-0.97	-0.97	-0.90	-1.00	-1.11	9.99
A830529.A	4.1	OTT	2.63	-1.82	-1.41	-1.26	-1.13	-1.08	-0.99	-1.01	-0.97	-1.10	-1.19	-1.41
A830529.A	4.1	GRQ	2.69	-1.89	-1.60	-1.42	-1.17	-1.08	-1.07	-1.06	-1.10	-1.33	-1.45	-1.53
A830529.A	4.1	HTQ	2.74	9.99	-1.74	-1.57	-1.59	-1.43	-1.39	-1.48	-1.63	-1.65	-1.76	-1.93
A830529.A	4.1	GSQ	2.74	9.99	9.99	9.99	-1.43	-1.34	-1.45	-1.46	-1.59	9.99	9.99	9.99
A830529.A	4.1	CKO	2.76	9.99	-1.70	-1.48	-1.49	-1.23	-1.38	-1.51	-1.43	-1.60	-1.78	-1.93
A830529.A	4.1	VDQ	2.85	9.99	9.99	-1.56	-1.41	-1.47	-1.59	-1.66	-1.81	-1.97	-2.10	-2.25
A830812.A	3.5	GGN	1.86	-2.42	-2.00	-2.05	-1.99	-1.37	-1.20	-1.02	-0.81	-0.67	-0.35	-0.29
A830812.A	3.5	KLN	2.36	9.99	-2.46	-2.08	-1.86	-1.71	-1.71	-1.53	-1.37	-1.36	-1.29	-1.07
A830812.A	3.5	EBN	2.46	-2.64	-2.21	-1.98	-2.02	9.99	9.99	9.99	9.99	9.99	9.99	9.99
A830812.A	3.5	LPQ	2.50	9.99	9.99	-2.28	-2.06	-1.99	-1.71	-1.98	9.99	9.99	9.99	9.99
A831007.A	5.6	WBO	2.16	9.99	0.07	0.37	0.33	0.60	0.62	0.65	0.59	0.45	0.55	0.56
A831007.A	5.6	MNT	2.26	-0.08	0.33	0.17	0.32	0.45	0.51	0.51	0.61	0.55	0.49	0.32
A831007.A	5.6	OTT	2.30	0.05	0.17	0.52	0.46	0.55	0.44	0.46	0.41	0.53	0.43	0.28
A831007.A	5.6	SBQ	2.39	9.99	0.40	0.50	0.59	0.65	0.56	0.56	0.30	0.38	0.28	0.15
A831007.A	5.6	TRQ	2.41	-0.09	0.18	0.46	0.36	0.52	0.59	0.67	0.66	0.50	0.31	9.99
A831007.A	5.6	GNT	2.49	9.99	0.31	0.41	0.34	0.19	0.08	0.17	-0.02	-0.22	-0.26	-0.33
A831007.A	5.6	GRQ	2.51	-0.22	0.00	0.26	0.12	0.33	0.38	0.43	0.30	0.28	0.02	9.99
A831007.A	5.6	WEO	2.52	-0.03	0.07	0.30	0.28	9.99	9.99	9.99	9.99	9.99	9.99	9.99
A831007.A	5.6	CKO	2.53	-0.26	0.07	0.27	0.46	0.42	0.25	0.18	0.02	0.14	-0.06	-0.25
A831007.A	5.6	LPQ	2.70	9.99	-0.09	0.22	0.14	0.17	0.24	-0.01	-0.18	-0.39	-0.55	-0.66
A831007.A	5.6	VDQ	2.75	9.99	-0.19	-0.04	-0.01	-0.02	-0.09	-0.18	-0.29	-0.50	-0.69	9.99
A831007.A	5.6	GGN	2.78	-0.37	-0.13	-0.02	0.08	0.04	0.01	-0.07	-0.27	-0.41	-0.64	-0.77
A831007.A	5.6	EBN	2.79	9.99	9.99	-0.27	-0.07	-0.16	-0.33	-0.39	-0.52	-0.74	-0.89	9.99
A831007.A	5.6	KLN	2.84	9.99	-0.17	-0.11	-0.14	-0.15	-0.47	-0.55	-0.65	-0.83	-0.97	-1.06

A831007.A	5.6	HTQ	2.87	-0.40	-0.29	-0.20	-0.16	-0.24	-0.35	-0.39	-0.56	-0.77	-0.95	9.99
A831007.A	5.6	GSQ	2.89	-0.33	-0.20	-0.18	-0.26	-0.31	-0.48	-0.68	-0.82	-1.08	-1.21	9.99
A831007.A	5.6	MNQ	2.92	9.99	9.99	-0.27	-0.13	-0.28	-0.35	-0.51	-0.68	-0.86	-0.97	-1.06
A831007.B	3.6	WBO	2.16	9.99	9.99	-1.74	-1.39	-1.23	-0.96	-1.00	-0.98	-0.73	-0.58	-0.42
A831007.B	3.6	MNT	2.25	-2.17	-1.85	-1.97	-1.61	-1.42	-1.36	-1.13	-1.07	-1.06	-0.86	-0.74
A831007.B	3.6	OTT	2.30	-2.04	-1.70	-1.72	-1.54	-1.41	-1.10	-1.07	-0.88	-0.74	-0.64	-0.73
A831007.B	3.6	SBQ	2.39	-2.15	-1.85	-1.48	-1.42	-1.34	-1.17	-1.06	-1.08	9.99	9.99	9.99
A831007.B	3.6	TRQ	2.40	-2.38	-2.03	-1.79	-1.61	-1.46	-1.28	-1.23	-1.02	-0.99	-0.93	-1.00
A831007.B	3.6	GNT	2.49	9.99	9.99	-1.87	-1.76	-1.75	-1.66	-1.52	-1.51	9.99	9.99	9.99
A831007.B	3.6	GRQ	2.51	-2.42	-2.19	-1.99	-1.66	-1.39	-1.19	-1.29	9.99	9.99	9.99	9.99
A831007.B	3.6	WEO	2.52	-2.25	-2.06	-1.87	-1.71	-1.41	-1.44	9.99	9.99	9.99	9.99	9.99
A831007.B	3.6	CKO	2.53	-2.41	-2.15	-2.10	-1.76	-1.51	-1.42	-1.42	-1.28	-1.20	-1.17	-1.29
A831007.B	3.6	LPQ	2.70	9.99	-2.22	-2.03	-1.94	-1.75	-1.69	-1.70	-1.78	-1.90	9.99	9.99
A831007.B	3.6	VDQ	2.74	9.99	9.99	-2.43	-2.10	-1.97	-1.92	-1.88	-1.76	-1.90	-1.96	-2.08
A831007.B	3.6	GGN	2.78	9.99	9.99	9.99	-2.28	-1.78	-1.64	-1.68	-1.74	9.99	9.99	9.99
A831007.B	3.6	EBN	2.79	9.99	-2.46	-2.31	-2.20	-2.25	-2.39	9.99	9.99	9.99	9.99	9.99
A831011.A	4.1	OTT	1.40	-0.73	-0.43	-0.24	-0.11	-0.09	0.01	0.10	0.28	0.32	0.25	0.22
A831011.A	4.1	WBO	1.66	-0.93	-1.03	-0.79	-0.78	-0.65	-0.68	-0.43	-0.19	0.07	0.04	0.16
A831011.A	4.1	GAC	1.79	-1.59	-1.46	-0.97	-0.98	-0.86	-0.80	-0.74	-0.67	-0.64	-0.48	-0.22
A831011.A	4.1	GRQ	2.20	-1.50	-1.21	-0.97	-0.77	-0.72	-0.81	-0.61	-0.60	-0.52	-0.38	-0.38
A831011.A	4.1	CKO	2.20	-1.63	-1.37	-1.17	-1.01	-0.92	-0.48	-0.73	-0.67	-0.62	-0.55	-0.50
A831011.A	4.1	MNT	2.23	-1.48	-1.20	-1.23	-1.01	-1.00	-0.89	-1.07	-0.62	-0.51	-0.48	-0.70
A831011.A	4.1	WEO	2.39	-1.35	-1.17	-1.03	-1.06	9.99	9.99	9.99	9.99	9.99	9.99	9.99
A831011.A	4.1	GNT	2.47	9.99	9.99	-1.38	-1.33	-1.33	-1.40	9.99	9.99	9.99	9.99	9.99
A831011.A	4.1	SBQ	2.48	-1.52	-1.19	-0.97	-1.15	-1.03	-1.31	9.99	9.99	9.99	9.99	9.99
A831011.A	4.1	VDQ	2.58	-1.94	-1.69	-1.46	-1.40	-1.22	-1.23	-1.10	-1.20	-1.36	9.99	9.99
A831011.A	4.1	LPQ	2.70	9.99	-1.58	-1.40	-1.33	-1.17	-1.39	-1.45	-1.50	9.99	9.99	9.99
A831011.A	4.1	EBN	2.80	9.99	-1.89	-1.74	-1.66	-1.64	-1.71	-1.93	-1.79	-1.68	-1.80	-2.07
A831011.A	4.1	GSQ	2.89	9.99	-1.75	-1.49	-1.51	-1.65	-1.83	-2.09	-2.05	-1.96	-2.05	-2.28
A831011.A	4.1	LMN	2.93	9.99	9.99	-2.17	-1.97	-1.87	-1.69	-1.72	-1.65	-1.73	-2.08	9.99
A831117.A	3.7	KLN	1.40	-1.61	-1.39	-1.16	-0.89	-0.60	-0.64	-0.43	-0.37	-0.41	-0.23	-0.11
A831117.A	3.7	EBN	2.14	-1.49	-1.15	-1.09	-1.26	-0.86	-0.82	-0.93	9.99	9.99	9.99	9.99
A831117.A	3.7	LMN	2.27	-1.79	-1.51	-1.18	-1.40	-1.19	-1.15	-1.07	-1.19	-1.16	-1.22	-1.29
A831117.A	3.7	GGN	2.32	-2.43	-2.15	-2.08	-1.75	-1.29	-1.07	9.99	9.99	9.99	9.99	9.99
A831117.A	3.7	HTQ	2.44	-2.21	-2.05	-1.94	-1.67	-1.55	-1.51	-1.28	-1.35	-1.59	9.99	9.99
A831117.A	3.7	MNQ	2.63	9.99	-2.29	-2.17	-1.91	-1.85	-1.84	-1.74	-1.66	-1.66	-1.64	-1.67

A831117.A	3.7	GNT	2.65	9.99	-2.13	-1.99	-1.94	-1.92	-1.82	9.99	9.99	9.99	9.99	9.99
A831117.A	3.7	SBQ	2.65	-2.11	-1.91	-1.81	-1.78	-1.61	-1.59	-1.51	-1.55	-1.53	-1.65	-1.75
A831117.A	3.7	MNT	2.75	9.99	-2.45	-2.35	-2.27	-2.09	-1.98	-2.04	-1.99	-2.01	-2.08	9.99
A831228.A	3.5	GRQ	1.79	-2.13	-2.00	9.99	-1.95	-1.85	-1.57	-1.40	-1.18	-0.94	-0.90	-0.87
A831228.A	3.5	CKO	2.18	9.99	-2.32	-1.98	-1.80	-1.65	-1.41	-1.32	-1.25	-1.08	-0.93	-0.80
A831228.A	3.5	VDQ	[illegible]26	-2.71	-2.40	-2.08	-2.06	-1.89	-1.75	-1.58	-1.42	-1.34	-1.34	-1.31
A831228.A	3.5	OTT	2.28	-2.46	-2.13	-1.87	-1.76	-1.67	-1.61	-1.47	-1.40	-1.09	-1.06	-1.17
A831228.A	3.5	WBO	2.39	-2.61	-2.35	-2.17	-2.08	-1.99	-2.04	9.99	9.99	9.99	9.99	9.99
A831228.A	3.5	MNT	2.43	-3.15	-2.93	-2.73	-2.61	-2.37	-2.02	-1.91	-1.91	-1.79	-1.66	-1.68
A831228.A	3.5	GNT	2.49	-2.61	-2.35	-2.24	-2.24	-2.13	-2.03	-1.85	9.99	9.99	9.99	9.99
A831228.A	3.5	WEO	2.58	9.99	9.99	-2.52	-2.16	-2.14	-1.83	-1.65	-1.49	-1.04	-1.02	-0.90
A840224.A	3.7	KLN	1.40	-1.25	-0.86	9.99	-1.00	-0.36	-0.46	-0.19	-0.16	-0.06	-0.11	-0.05
A840224.A	3.7	EBN	2.14	-1.55	-1.22	-1.11	-1.16	-1.01	-0.86	-0.91	-0.79	-0.87	-0.83	-0.71
A840224.A	3.7	LMN	2.27	-1.70	-1.57	-1.43	-1.52	-1.28	-1.33	-1.27	-1.26	-1.32	-1.34	-1.27
A840224.A	3.7	GGN	2.32	9.99	-1.71	-1.51	-1.18	-1.17	-1.15	-1.07	-0.85	-0.82	-0.94	-1.05
A840224.A	3.7	GSQ	2.33	9.99	9.99	-1.86	-1.63	-1.52	-1.47	-1.42	-1.49	9.99	9.99	9.99
A840224.A	3.7	LPQ	2.42	-2.00	-1.85	-1.69	-1.52	-1.36	-1.32	-1.30	-1.35	9.99	9.99	9.99
A840224.A	3.7	HTQ	2.44	-2.43	-2.11	-1.91	-1.73	-1.57	-1.57	-1.65	9.99	9.99	9.99	9.99
A840224.A	3.7	MNQ	2.63	-2.45	-2.33	-2.04	-2.01	-2.03	9.99	9.99	9.99	9.99	9.99	9.99
A840224.A	3.7	GNT	2.65	9.99	-1.86	-1.76	-1.75	-1.84	9.99	9.99	9.99	9.99	9.99	9.99
A840224.A	3.7	SBQ	2.65	9.99	-1.92	-1.71	-1.66	-1.51	-1.44	-1.54	-1.45	-1.55	-1.67	-1.85
A840224.A	3.7	MNT	2.75	9.99	-2.48	-2.24	-2.24	-2.08	-2.01	-2.07	-2.13	-2.13	-2.17	9.99
A840224.A	3.7	TRQ	2.79	9.99	-2.21	-2.05	-2.01	-1.98	-2.01	-2.00	-2.06	-2.17	9.99	9.99
A840411.A	3.8	GSQ	1.73	-1.60	-1.37	-1.15	-1.07	-0.97	-0.74	-0.33	-0.15	-0.34	-0.24	-0.20
A840411.A	3.8	HTQ	1.81	-1.69	-1.56	-1.37	-1.22	-0.89	-0.85	-0.69	-0.70	-0.50	-0.44	-0.27
A840411.A	3.8	EBN	2.31	-1.98	-1.66	-1.59	-1.49	-1.30	-1.24	-1.11	-1.11	-1.05	-1.08	9.99
A840411.A	3.8	LPQ	2.46	-1.86	-1.61	-1.58	-1.32	-1.15	-1.20	9.99	9.99	9.99	9.99	9.99
A840411.A	3.8	KLN	2.46	9.99	-1.94	-1.71	-1.54	-1.41	-1.17	-1.24	9.99	9.99	9.99	9.99
A840411.A	3.8	GGN	2.67	9.99	9.99	-2.08	-1.85	-1.70	-1.70	-1.94	9.99	9.99	9.99	9.99
A840411.A	3.8	SBQ	2.74	9.99	9.99	-1.87	-1.70	-1.73	-1.68	-1.68	-1.64	-1.73	-1.77	-1.79
A840411.A	3.8	MNT	2.79	9.99	9.99	9.99	-2.04	-1.91	-1.77	-1.75	-1.78	-1.81	9.99	9.99
A840411.A	3.8	TRQ	2.80	9.99	9.99	9.99	9.99	-1.71	-1.65	-1.72	-1.79	-1.85	9.99	9.99
A840411.A	3.8	GRQ	2.84	9.99	-2.45	-1.97	-1.77	-1.47	-1.38	-1.53	-1.58	-1.77	-1.89	9.99
A840411.A	3.8	JAQ	2.88	9.99	-2.25	-2.08	-2.00	-1.83	-1.67	-1.66	-1.74	-1.86	9.99	9.99
A840411.A	3.8	VDQ	2.89	9.99	9.99	-2.05	-1.82	-1.70	-1.63	-1.79	-1.88	-1.97	-2.08	-2.16
A840923.A	3.6	LMN	1.29	-0.94	-0.81	9.99	-0.71	-0.52	-0.48	-0.40	-0.27	-0.48	-0.19	-0.16

A840923.A	3.6	KLN	2.18	-1.75	-1.53	-1.28	-1.19	-1.17	-0.94	-0.97	-1.05	-0.83	-0.85	-0.72
A840923.A	3.6	EBN	2.49	9.99	-2.02	-1.69	-1.60	-1.58	-1.42	-1.49	9.99	9.99	9.99	9.99
A840923.A	3.6	GSQ	2.56	-2.12	-1.98	-1.59	-1.62	-1.57	-1.59	-1.58	-1.67	9.99	9.99	9.99
A840923.A	3.6	LPQ	2.62	-2.23	-2.01	-1.90	-1.98	9.99	9.99	9.99	9.99	9.99	9.99	9.99
A840923.A	3.6	HTQ	2.65	-2.58	-2.29	-2.06	-1.89	-1.83	-1.80	-1.79	-1.79	9.99	9.99	9.99
A840923.A	3.6	SBQ	2.74	9.99	9.99	-1.99	-1.71	-1.65	-1.60	-1.67	-1.69	-1.69	-1.81	-1.92
A840923.A	3.6	GNT	2.76	9.99	9.99	9.99	9.99	-2.17	-2.14	-2.14	-2.21	-2.31	9.99	9.99
A840923.A	3.6	MNQ	2.76	9.99	-2.33	-2.15	-2.04	-2.04	-1.93	-2.00	9.99	9.99	9.99	9.99
A841130.A	3.8	KLN	1.40	-1.12	-0.90	9.99	-0.84	-0.49	-0.41	-0.25	-0.18	-0.12	-0.08	-0.05
A841130.A	3.8	EBN	2.14	-1.17	-0.87	-0.95	-1.18	-1.10	-1.11	-1.31	-1.18	-0.98	9.99	9.99
A841130.A	3.8	LMN	2.27	-1.54	-1.28	-1.07	-1.27	-1.19	-1.13	-1.03	-1.12	-1.20	9.99	9.99
A841130.A	3.8	GGN	2.32	9.99	-1.62	-1.37	-1.23	-1.03	-1.03	-0.86	-0.78	-0.72	-0.82	-0.88
A841130.A	3.8	GSQ	2.33	9.99	9.99	-1.94	-1.73	-1.69	-1.72	9.99	9.99	9.99	9.99	9.99
A841130.A	3.8	MNQ	2.63	-2.37	-2.20	-2.20	-2.14	-2.17	-2.23	9.99	9.99	9.99	9.99	9.99
A841130.A	3.8	GNT	2.65	-1.77	-1.64	-1.71	-1.67	-1.77	9.99	9.99	9.99	9.99	9.99	9.99
A841130.A	3.8	MNT	2.75	9.99	-2.24	-2.05	-2.04	-2.02	-2.00	-2.14	-2.17	-2.23	9.99	9.99
A841130.A	3.8	OTT	2.86	9.99	9.99	-2.09	-1.99	-2.01	-2.04	-2.26	-2.36	-2.43	9.99	9.99
A850412.A	3.5	SBQ	1.99	-2.28	-2.10	-2.05	-2.03	-1.62	-1.33	-1.22	-1.12	-0.95	-0.74	-0.61
A850412.A	3.5	GNT	2.23	-2.43	-2.29	-2.10	-1.80	-1.65	-1.63	-1.47	-1.21	-1.44	-1.50	-1.24
A850412.A	3.5	MNT	2.36	-2.70	-2.54	-2.33	-2.37	9.99	9.99	9.99	9.99	9.99	9.99	9.99
A850412.A	3.5	EBN	2.48	9.99	9.99	9.99	-2.13	-1.98	-1.88	-1.77	-1.63	-1.58	-1.64	9.99
A850412.A	3.5	GGN	2.48	9.99	9.99	9.99	-2.42	-2.07	-1.91	-1.76	-1.53	-1.57	9.99	9.99
A850412.A	3.5	WBO	2.56	9.99	9.99	-2.59	-2.20	-2.15	-2.13	-1.95	-1.90	-1.83	-1.78	9.99
A850412.A	3.5	KLN	2.57	9.99	9.99	9.99	-2.20	-2.05	-1.99	-1.92	-1.78	-1.76	-1.70	-1.66
A850412.A	3.5	OTT	2.59	-2.75	-2.62	-2.37	-2.29	-2.00	-2.07	9.99	9.99	9.99	9.99	9.99
A851005.A	4.0	KLN	1.40	-1.21	-0.99	9.99	-0.57	-0.64	-0.50	-0.26	-0.04	-0.14	-0.27	-0.04
A851005.A	4.0	EBN	2.14	-1.26	-1.14	-1.06	-1.27	-0.95	-0.90	-0.73	-0.87	-0.97	-0.89	9.99
A851005.A	4.0	LMN	2.27	-1.51	-1.29	-1.13	-1.39	-1.05	-0.96	-0.86	-1.10	-1.11	-1.13	-1.10
A851005.A	4.0	GGN	2.32	9.99	-1.55	-1.17	-1.03	-1.00	-0.91	-0.84	-0.84	-0.89	-1.06	9.99
A851005.A	4.0	GSQ	2.33	9.99	9.99	-1.60	-1.45	-1.21	-1.17	-1.15	-1.27	-1.52	9.99	9.99
A851005.A	4.0	LPQ	2.42	-1.72	-1.46	-1.45	-1.20	-1.12	-1.10	-1.13	9.99	9.99	9.99	9.99
A851005.A	4.0	HTQ	2.44	-2.16	-1.90	-1.78	-1.47	-1.20	-1.28	9.99	9.99	9.99	9.99	9.99
A851005.A	4.0	MNQ	2.63	9.99	-2.11	-1.99	-1.74	-1.68	-1.60	-1.58	-1.58	-1.67	9.99	9.99
A851005.A	4.0	GNT	2.65	9.99	9.99	-1.59	-1.54	-1.67	-1.68	-1.74	-1.79	9.99	9.99	9.99
A851005.A	4.0	SBQ	2.65	9.99	-1.64	-1.41	-1.33	-1.30	-1.28	-1.33	-1.34	-1.44	-1.74	-1.95
A851005.A	4.0	MNT	2.75	9.99	9.99	-2.22	-1.95	-1.82	-1.78	-1.84	-1.84	-2.12	9.99	9.99

A851005.A	4.0	TRQ	2.79	9.99	-1.92	-1.80	-1.74	-1.76	-1.84	-1.88	-1.94	-2.04	-2.23	-2.33
A851005.A	4.0	WBO	2.85	9.99	-2.12	-1.98	-2.01	-1.90	-1.91	-2.05	-2.16	-2.30	-2.42	9.99
A851005.A	4.0	GRQ	2.85	9.99	-2.38	-2.16	-1.78	-1.50	-1.55	-1.64	-1.79	-1.93	-2.19	9.99
A851005.A	4.0	OTT	2.86	9.99	-2.24	-2.12	-1.94	-1.88	-1.88	-2.01	-2.10	9.99	9.99	9.99
A851005.A	4.0	CKO	2.92	9.99	9.99	9.99	-1.97	-1.90	-2.03	-2.13	-2.28	9.99	9.99	9.99
A851005.A	4.0	VDQ	2.94	9.99	9.99	9.99	-1.99	-1.94	-1.99	-2.16	-2.29	-2.38	-2.54	9.99
A851005.A	4.0	JAQ	3.00	9.99	9.99	-2.43	-2.28	-2.28	-2.19	-2.17	-2.39	-2.52	9.99	9.99
A851019.A	4.1	WBO	2.65	-1.59	-1.46	-1.28	-1.29	-1.36	9.99	9.99	9.99	9.99	9.99	9.99
A851019.A	4.1	WEO	2.69	-2.17	-1.99	-1.67	-1.79	9.99	9.99	9.99	9.99	9.99	9.99	9.99
A851019.A	4.1	MNT	2.69	-1.70	-1.43	-1.62	-1.42	-1.43	-1.37	-1.31	-1.37	-1.52	-1.63	-1.81
A851019.A	4.1	OTT	2.70	-1.76	-1.61	-1.29	-1.47	9.99	9.99	9.99	9.99	9.99	9.99	9.99
A851019.A	4.1	SBQ	2.70	-1.58	-1.35	-1.31	-1.37	-1.30	-1.52	9.99	9.99	9.99	9.99	9.99
A851019.A	4.1	GNT	2.78	9.99	-1.21	-1.17	-1.52	-1.60	-1.73	-1.71	-1.70	-1.78	-2.01	9.99
A851019.A	4.1	GGN	2.86	9.99	9.99	9.99	-1.79	-1.65	-1.75	-1.71	-1.76	-1.78	-1.95	-2.14
A851019.A	4.1	EEO	2.87	9.99	-1.95	-1.82	-1.66	-1.70	-1.62	-1.71	-1.67	-1.66	-1.71	-1.94
A851019.A	4.1	LPQ	2.88	9.99	-1.84	-1.72	-1.75	-1.74	-1.93	-1.98	-2.06	9.99	9.99	9.99
A851019.A	4.1	EBN	2.93	9.99	-1.94	-1.81	-1.84	-1.96	-2.10	-2.09	-2.16	-2.29	-2.55	-2.73
A851019.A	4.1	VDQ	2.93	9.99	-1.77	-1.67	-1.81	-1.79	-1.94	9.99	9.99	9.99	9.99	9.99
A851019.A	4.1	KLN	2.94	9.99	9.99	-1.82	-1.76	-1.80	-2.06	-1.98	-2.02	-2.20	-2.40	9.99
A851019.A	4.1	HTQ	3.00	9.99	-2.12	-2.01	-2.07	-2.17	-2.32	-2.38	-2.49	9.99	9.99	9.99
A860111.A	4.0	LPQ	1.63	-1.05	-1.00	9.99	-0.85	-0.71	-0.42	-0.27	-0.17	0.16	0.35	0.13
A860111.A	4.0	EBN	2.15	9.99	-1.82	-1.64	-1.47	-1.27	-1.01	-0.87	-0.96	-0.88	-0.90	-0.93
A860111.A	4.0	GSQ	2.41	-1.95	-1.72	-1.41	-1.39	-1.23	-1.32	-1.45	9.99	9.99	9.99	9.99
A860111.A	4.0	SBQ	2.47	-2.15	-1.95	-1.73	-1.53	-1.53	-1.39	-1.22	-1.24	9.99	9.99	9.99
A860111.A	4.0	MNT	2.56	-2.32	-2.21	-2.07	-1.91	-1.54	-1.36	-1.34	-1.27	-1.29	-1.32	-1.37
A860111.A	4.0	GGN	2.58	9.99	-2.29	-1.92	-1.87	-1.74	-1.68	-1.51	-1.23	-1.45	-1.66	9.99
A860111.A	4.0	OTT	2.70	-2.12	-2.00	-1.65	-1.59	-1.40	-1.54	-1.45	-1.49	-1.50	-1.60	-1.67
A360111.A	4.0	VDQ	2.77	9.99	9.99	-1.98	-1.81	-1.49	-1.55	-1.61	-1.58	-1.79	-1.91	9.99
A860111.A	4.0	CKO	2.77	9.99	-1.98	-1.68	-1.59	-1.46	-1.52	-1.49	-1.58	-1.66	-1.73	-1.87
A860111.A	4.0	EEO	2.84	9.99	9.99	9.99	-1.77	-1.65	-1.58	-1.55	-1.65	-1.78	-1.96	-2.11
A860111.A	4.0	WEO	2.88	9.99	-2.14	-1.99	-1.95	-1.86	-1.74	-1.70	-1.65	-1.47	-1.62	-1.77
A860111.A	4.0	JAQ	2.89	9.99	9.99	9.99	-2.10	-1.92	-1.79	-1.90	-2.03	9.99	9.99	9.99
A860111.A	4.0	SUO	2.92	9.99	9.99	-3.24	-2.99	-3.00	-2.92	-2.90	-2.92	-3.05	-3.10	-3.13
A860131.A	5.0	WEO	2.54	-0.39	0.00	0.11	-0.04	9.99	9.99	9.99	9.99	9.99	9.99	9.99
A860131.A	5.0	SUO	2.72	-1.16	-1.07	-1.09	-1.11	-1.10	-1.08	-1.05	-1.20	-1.37	-1.51	9.99
A860131.A	5.0	EEO	2.76	9.99	-0.23	-0.06	-0.08	-0.01	-0.03	-0.04	-0.24	-0.39	-0.55	-0.67

A860131.A	5.0	OTT	2.78	-0.49	-0.23	-0.18	-0.26	-0.19	0.00	0.01	-0.24	-0.30	-0.51	-0.63
A860131.A	5.0	MNT	2.87	-0.66	-0.53	-0.47	-0.52	-0.41	-0.44	-0.47	-0.73	-0.81	-1.01	9.99
A860131.A	5.0	VDQ	2.89	-0.50	-0.28	-0.31	-0.38	-0.37	-0.32	-0.41	-0.58	-0.77	-0.91	9.99
A860131.A	5.0	SBQ	2.93	9.99	9.99	-0.55	-0.48	-0.59	-0.70	-0.73	-0.89	-1.08	-1.25	9.99
A860131.A	5.0	GNT	2.94	-0.43	-0.33	-0.45	-0.57	-0.52	-0.55	-0.68	-0.90	-1.07	-1.22	9.99
A860131.A	5.0	LPQ	3.04	9.99	-0.61	-0.55	-0.64	-0.66	-0.68	9.99	9.99	9.99	9.99	9.99
A860131.A	5.0	GGN	3.09	9.99	9.99	-1.07	-1.06	-1.20	-1.34	9.99	9.99	9.99	9.99	9.99
A860131.A	5.0	HTQ	3.11	-0.65	-0.62	-0.64	-0.73	-0.78	-0.95	9.99	9.99	9.99	9.99	9.99
A860131.A	5.0	KLN	3.12	-1.00	-0.97	-1.14	-1.20	-1.36	-1.45	9.99	9.99	9.99	9.99	9.99
A860131.A	5.0	GSQ	3.13	9.99	-0.75	-0.72	-0.77	-0.95	-1.13	9.99	9.99	9.99	9.99	9.99
A860131.A	5.0	LMN	3.14	-1.13	-1.16	-1.24	-1.48	-1.63	-1.77	9.99	9.99	9.99	9.99	9.99
A860131.A	5.0	JAQ	3.15	-0.87	-0.72	-0.68	-0.79	-0.83	-0.92	9.99	9.99	9.99	9.99	9.99
A860712.A	4.5	WEO	2.80	-1.00	-0.84	-0.45	-0.53	-0.51	-0.55	-0.36	-0.47	-0.41	-0.44	-0.60
A860712.A	4.5	SUO	2.85	9.99	9.99	9.99	-1.64	-1.55	-1.72	-1.78	-1.85	-2.09	9.99	9.99
A860712.A	4.5	EEO	2.90	-1.03	-0.76	-0.76	-0.73	-0.75	-0.77	-0.97	-1.09	-1.31	-1.46	-1.59
A860712.A	4.5	CKO	2.92	-1.01	-0.90	-0.63	-0.68	-0.76	-0.80	-0.86	-1.05	-1.16	-1.30	-1.37
A860712.A	4.5	OTT	2.95	9.99	9.99	-0.86	-0.76	-0.81	-0.91	-1.18	9.99	9.99	9.99	9.99
A860712.A	4.5	WBO	2.95	-1.03	-0.89	-0.80	-0.89	-0.85	-0.89	-1.01	-1.16	-1.25	-1.37	-1.48
A860712.A	4.5	GRQ	2.98	9.99	-1.13	-0.85	-0.73	-0.76	-0.88	-0.97	-1.17	-1.38	-1.56	9.99
A860712.A	4.5	TRQ	3.00	-1.13	-0.90	-0.70	-0.82	-0.90	-1.06	-1.15	-1.28	-1.44	-1.57	-1.64
A860712.A	4.5	MNT	3.01	9.99	9.99	-1.03	-1.01	-1.06	-1.06	9.99	9.99	9.99	9.99	9.99
A860712.A	4.5	SBQ	3.06	-1.12	-0.93	-0.92	-1.07	-1.07	-1.25	9.99	9.99	9.99	9.99	9.99
A860712.A	4.5	GNT	3.06	-1.00	-0.92	-0.96	-0.96	-1.07	-1.28	9.99	9.99	9.99	9.99	9.99
A860712.A	4.5	LPQ	3.14	-1.21	-1.06	-1.00	-1.06	-1.13	-1.29	9.99	9.99	9.99	9.99	9.99
A860712.A	4.5	HTQ	3.20	-1.27	-1.14	-1.20	-1.27	-1.34	-1.63	9.99	9.99	9.99	9.99	9.99
A860712.A	4.5	KLN	3.20	-1.60	-1.58	-1.64	-1.70	-1.92	-2.13	9.99	9.99	9.99	9.99	9.99
A860712.A	4.5	JAQ	3.21	-1.34	-1.24	-1.32	-1.41	-1.52	-1.63	9.99	9.99	9.99	9.99	9.99
A860712.A	4.5	MNQ	3.21	-1.34	-1.15	-1.11	-1.12	-1.33	-1.45	9.99	9.99	9.99	9.99	9.99
A860806.A	3.5	TRQ	1.73	-2.14	-1.89	-1.48	-1.33	-1.16	-1.18	-0.93	-0.81	-0.80	-0.70	-0.63
A860806.A	3.5	GRQ	1.75	-1.96	-1.75	-1.60	-1.21	-1.20	-1.01	-0.87	-0.72	-0.63	-0.71	-0.45
A860806.A	3.5	GAC	1.89	-1.97	-1.93	-1.91	-1.67	-1.59	-1.34	-1.42	-1.32	-1.21	-1.21	-1.03
A860806.A	3.5	OTT	2.06	-1.95	-1.58	-1.38	-1.32	-1.39	-1.59	-1.52	-1.62	-1.84	-1.86	-1.76
A860806.A	3.5	WBO	2.18	9.99	-1.92	-1.81	-1.58	-1.33	-1.24	-1.34	-1.39	-1.26	-1.17	-1.21
A860806.A	3.5	CKO	2.25	-2.23	-2.03	-1.93	-1.61	-1.44	-1.31	-1.17	-1.20	-1.17	-1.10	-0.97
A860806.A	3.5	GNT	2.34	-1.92	-1.72	-1.72	-1.31	-1.27	-1.21	-1.25	-1.11	-1.19	-1.27	9.99
A860806.A	3.5	SBQ	2.44	-2.50	-2.15	-2.02	-1.87	-1.88	9.99	9.99	9.99	9.99	9.99	9.99

A860806.A	3.5	WEO	2.56	9.99	-2.36	-2.06	-1.92	-1.77	-1.64	-1.61	-1.29	-1.06	-1.02	-1.01
A860919.A	4.2	LPQ	1.51	-0.50	-0.56	9.99	-0.39	0.20	0.44	0.57	0.52	0.39	0.59	0.52
A860919.A	4.2	EBN	2.20	-1.55	-1.27	-1.28	-1.12	9.99	9.99	9.99	9.99	9.99	9.99	9.99
A860919.A	4.2	GNT	2.28	-1.54	-1.22	-1.12	-0.76	-0.80	-0.79	-0.73	-0.66	-0.66	9.99	9.99
A860919.A	4.2	SBQ	2.39	-1.66	-1.34	-1.25	-1.21	-0.85	-0.94	9.99	9.99	9.99	9.99	9.99
A860919.A	4.2	HTQ	2.41	-1.83	-1.57	-1.27	-1.23	-1.05	-1.02	-0.9[illegible]	-0.87	9.99	9.99	9.99
A860919.A	4.2	GSQ	2.48	-1.60	-1.46	-1.18	-1.15	-1.08	-1.05	-0.96	-0.97	-1.21	9.99	9.99
A860919.A	4.2	KLN	2.48	9.99	-1.56	-1.41	-1.32	-1.28	-1.16	-1.20	9.99	9.99	9.99	9.99
A860919.A	4.2	MNT	2.51	-2.01	-1.88	-1.75	-1.43	-1.21	-1.07	-0.97	-0.84	-0.76	-0.75	-0.68
A860919.A	4.2	TRQ	2.54	-1.66	-1.33	-1.02	-1.13	9.99	9.99	9.99	9.99	9.99	9.99	9.99
A860919.A	4.2	GGN	2.56	9.99	-1.79	-1.58	-1.43	-1.16	-1.25	-1.37	-1.43	-1.66	-1.95	-2.11
A860919.A	4.2	MNQ	2.58	-2.02	-1.81	-1.64	-1.39	-1.30	-1.23	-1.10	-1.14	-1.09	-1.15	-1.30
A860919.A	4.2	GRQ	2.63	-2.05	-1.68	-1.30	-1.14	-0.93	-0.80	-0.85	-0.81	-0.84	-0.89	9.99
A860919.A	4.2	LMN	2.65	-2.00	-1.88	-1.82	-1.81	-1.77	-1.70	9.99	9.99	9.99	9.99	9.99
A860919.A	4.2	WBO	2.66	-1.90	-1.73	-1.52	-1.41	-1.30	-1.17	-1.20	-1.22	9.99	9.99	9.99
A860919.A	4.2	OTT	2.67	-1.77	-1.64	-1.50	-1.40	-1.36	-1.36	-1.50	-1.64	9.99	9.99	9.99
A860919.A	4.2	CKO	2.[illegible]5	9.99	-1.63	-1.51	-1.29	-1.24	-1.17	-1.20	-1.29	-1.27	-1.29	-1.35
A860919.A	4.2	JAQ	2.91	9.99	-2.01	-1.78	-1.76	-1.66	-1.55	9.99	9.99	9.99	9.99	9.99
A861025.A	3.9	MNT	2.45	-1.97	-1.78	-1.85	-1.93	9.99	9.99	9.99	9.99	9.99	9.99	9.99
A861025.A	3.9	TRQ	2.59	9.99	9.99	9.99	-2.09	-2.01	-2.07	-2.14	9.99	9.99	9.99	9.99
A861025.A	3.9	OTT	2.60	-1.65	-1.54	-1.55	-1.82	-1.97	-2.11	-2.31	-2.29	-2.39	-2.44	9.99
A861025.A	3.9	GGN	2.62	-1.98	-1.73	-1.82	-1.95	-1.93	-1.93	-1.82	-2.07	-2.27	-2.56	9.99
A861025.A	3.9	GRQ	2.69	-1.98	-1.84	-1.70	-1.95	-1.95	-2.01	-1.99	-2.02	-2.13	-2.31	-2.42
A861025.A	3.9	EBN	2.72	9.99	9.99	-2.32	-2.23	-2.30	-2.36	9.99	9.99	9.99	9.99	9.99
A861025.A	3.9	CKO	2.74	9.99	-1.97	-1.80	-1.84	-1.89	-2.13	9.99	9.99	9.99	9.99	9.99
A861025.A	3.9	WEO	2.74	9.99	-1.79	-1.55	-1.48	-1.61	-1.71	9.99	9.99	9.99	9.99	9.99
A861109.A	4.2	GSQ	1.63	-0.86	-0.80	-0.42	-0.23	-0.12	-0.07	-0.19	-0.02	-0.10	-0.17	0.00
A861109.A	4.2	HTQ	1.86	-1.26	-1.13	-0.97	-0.74	-0.52	-0.39	-0.45	-0.22	-0.20	-0.19	-0.20
A861109.A	4.2	EBN	2.30	-1.51	-1.19	-0.85	-0.86	-0.77	-0.89	-0.77	-0.84	-0.99	-0.90	-0.72
A861109.A	4.2	KLN	2.44	-1.68	-1.46	-1.17	-1.11	-1.05	-1.00	-0.89	-1.00	9.99	9.99	9.99
A861109.A	4.2	LMN	2.63	-1.86	-1.73	-1.60	-1.64	-1.70	9.99	9.99	9.99	9.99	9.99	9.99
A861109.A	4.2	GGN	2.66	-1.99	-1.85	-1.57	-1.40	-1.30	-1.40	-1.47	-1.68	-1.97	-2.17	9.99
A861109.A	4.2	GNT	2.69	-1.43	-1.32	-1.31	-1.29	-1.19	-1.24	-1.31	9.99	9.99	9.99	9.99
A861109.A	4.2	SBQ	2.74	9.99	-1.63	-1.32	-1.36	-1.40	-1.31	-1.35	-1.42	-1.57	-1.63	-1.68
A861109.A	4.2	MNT	2.80	9.99	9.99	9.99	9.99	-1.56	-1.44	-1.42	-1.46	-1.60	9.99	9.99
A861109.A	4.2	TRQ	2.80	9.99	-1.52	-1.41	-1.25	-1.29	-1.27	-1.49	-1.54	-1.54	-1.64	9.99

A861109.A 4.2 GRQ	2.84	9.99	9.99	9.99	-1.50	-1.29	-1.28	-1.30	-1.41	-1.63	-1.79	9.99
A861109.A 4.2 OTT	2.88	9.99	9.99	9.99	-1.56	-1.47	-1.74	-1.94	-2.13	-2.29	-2.46	9.99
A861109.A 4.2 WBO	2.88	9.99	-1.79	-1.63	-1.56	-1.52	-1.57	-1.63	-1.84	-1.90	-1.93	-2.02
A861109.A 4.2 JAQ	2.88	9.99	9.99	-1.87	-1.65	-1.45	-1.29	-1.30	-1.30	-1.49	9.99	9.99
A870713.A 4.1 WEO	2.48	-1.84	-1.64	-1.43	-1.09	-1.14	9.99	9.99	9.99	9.99	9.99	9.99
A870713.A 4.1 SUO	2.70	9.99	-1.57	-1.33	-1.23	-1.25	-1.41	-1.40	-1.51	-1.54	-1.64	9.99
A870713.A 4.1 SZO	2.70	9.99	-1.63	-1.53	-1.31	-1.51	-1.49	-1.54	-1.65	-1.68	-1.74	-1.80
A870713.A 4.1 CKO	2.72	9.99	-1.79	-1.66	-1.53	-1.36	-1.41	9.99	9.99	9.99	9.99	9.99
A870713.A 4.1 SWO	2.73	9.99	9.99	9.99	-1.65	-1.45	-1.57	-1.55	-1.65	9.99	9.99	9.99
A870713.A 4.1 WBO	2.74	9.99	-1.84	-1.72	-1.54	-1.46	-1.35	-1.41	-1.36	-1.36	-1.37	-1.48
A870713.A 4.1 OTT	2.74	9.99	-1.89	-1.59	-1.43	-1.38	-1.20	-1.30	-1.24	-1.24	-1.31	-1.43
A870713.A 4.1 GRQ	2.81	9.99	-1.80	-1.65	-1.55	-1.46	-1.42	-1.45	-1.42	-1.52	-1.61	-1.70
A870713.A 4.1 TRQ	2.84	9.99	-1.80	-1.62	-1.55	-1.62	-1.60	-1.56	-1.53	-1.72	9.99	9.99
A870713.A 4.1 MNT	2.84	9.99	-2.01	-1.81	-1.69	-1.64	-1.61	-1.61	-1.60	-1.73	-1.90	9.99
A870713.A 4.1 GNT	2.92	9.99	9.99	-1.84	-1.69	-1.83	-1.83	-1.83	-1.91	-2.15	9.99	9.99
A870926.A 3.8 WBO	1.92	-1.82	-1.75	-1.56	-1.40	-1.07	-1.02	-0.69	-0.65	-0.65	-0.59	-0.54
A870926.A 3.8 MNT	2.13	-2.10	-1.55	-1.58	-1.63	-1.38	-1.06	-1.01	-0.83	-0.97	-0.96	-0.60
A870926.A 3.8 OTT	2.14	-1.98	-1.72	-1.72	-1.42	-1.26	-1.20	-1.17	-1.04	-0.74	-0.66	-0.82
A870926.A 3.8 TRQ	2.29	-1.91	-1.66	-1.57	-1.31	-1.34	-1.20	-0.99	-0.85	-0.93	-0.92	-0.88
A870926.A 3.8 GRQ	2.41	9.99	-2.26	-1.96	-1.86	-1.47	-1.38	-1.22	-1.17	-1.24	-1.30	9.99
A870926.A 3.8 CKO	2.45	-2.18	-1.90	-1.65	-1.48	-1.48	-1.52	9.99	9.99	9.99	9.99	9.99
A870926.A 3.8 WEO	2.49	-2.25	-2.00	-1.77	-1.62	-1.49	-1.29	-1.08	-0.80	-0.52	-0.51	-0.56
A870926.A 3.8 LPQ	2.67	-2.30	-2.04	-1.94	-1.79	-1.56	-1.54	-1.59	-1.76	-1.81	-1.85	9.99
A870926.A 3.8 SUO	2.74	9.99	-2.19	-2.00	-1.94	-1.74	-1.63	-1.76	-1.70	-1.74	-1.91	-2.05
A870926.A 3.8 SWO	2.75	9.99	-2.35	-2.13	-2.06	-1.94	-1.80	-1.67	-1.72	-1.83	-1.82	-1.93
A870926.A 3.8 SZO	2.77	9.99	9.99	9.99	-2.03	-1.90	-1.77	-1.78	-1.77	-1.85	-1.99	-2.10
A870926.A 3.8 EBN	2.77	9.99	-2.43	-2.20	-2.13	-2.13	-2.11	-2.06	-1.98	-2.12	-2.26	-2.33
A870926.A 3.8 GGN	2.79	9.99	-2.29	-2.17	-2.08	-1.97	-1.93	-2.04	-2.26	-2.62	-2.86	9.99
A870926.A 3.8 KLN	2.84	9.99	-2.46	-2.08	-2.18	-2.12	-2.21	-2.20	-2.18	-2.35	-2.57	9.99
A870926.A 3.8 GSQ	2.87	9.99	-2.35	-2.22	-2.22	-2.24	-2.20	-2.29	-2.45	-2.51	-2.58	9.99
A870926.A 3.8 MNQ	2.90	9.99	-2.41	-2.22	-2.18	-2.06	-2.05	-2.13	-2.26	-2.23	-2.34	9.99
A871023.A 3.7 MNT	1.88	-2.13	-2.06	-2.00	-1.91	-1.66	-1.30	-1.27	-1.12	-1.05	-0.67	-0.74
A871023.A 3.7 GAC	1.89	-1.97	-1.93	-1.72	-1.57	-1.32	-1.14	-1.10	-0.96	-0.75	-0.71	-0.66
A871023.A 3.7 OTT	2.02	-2.22	-1.97	-1.89	-1.44	-1.34	-1.36	-1.21	-0.95	-0.71	-0.63	-0.58
A871023.A 3.7 WBO	2.02	-2.07	-1.74	-1.76	-1.49	-1.44	-1.23	-1.09	-0.89	-0.76	-0.46	-0.46
A871023.A 3.7 GNT	2.25	9.99	-1.86	-1.73	-1.71	-1.36	-1.20	-1.09	-1.05	-0.95	-1.09	-1.05

A871023.A	3.7	CKO	2.36	-2.55	-2.25	-2.01	-1.89	-1.46	-1.54	9.99	9.99	9.99	9.99	9.99
A871023.A	3.7	WEO	2.56	9.99	-2.36	-2.20	-2.13	-1.79	-1.59	-1.47	-1.14	-0.86	-0.79	-0.74
A871023.A	3.7	SUO	2.70	-2.69	-2.53	-2.31	-2.14	-2.01	-1.97	-1.91	-1.88	-1.85	-1.90	-1.97
A871023.A	3.7	SWO	2.71	9.99	-2.34	-2.15	-2.12	-2.13	9.99	9.99	9.99	9.99	9.99	9.99
A871023.A	3.7	EBN	2.71	9.99	9.99	-2.35	-2.23	-2.20	-2.02	9.99	9.99	9.99	9.99	9.99
A871023.A	3.7	SZO	2.74	9.99	-2.44	-2.34	-2.28	-2.09	-1.96	-1.90	-1.92	-1.96	9.99	9.99
A871023.A	3.7	HTQ	2.78	9.99	9.99	9.99	-2.07	-1.85	-1.83	-1.74	-1.77	-1.85	-1.96	-2.04
A871023.A	3.7	GGN	2.78	9.99	9.99	-2.71	-2.39	-2.36	-2.35	-2.53	9.99	9.99	9.99	9.99
A871111.A	3.5	GAC	1.34	-1.68	-1.63	-1.42	-1.41	-1.23	-0.78	-0.70	-0.58	-0.47	-0.33	-0.31
A871111.A	3.5	OTT	1.73	-2.31	-1.95	-1.65	-1.58	-1.14	-0.97	-0.79	-0.71	-0.58	-0.44	-0.34
A871111.A	3.5	TRQ	1.90	-2.12	-1.90	-1.67	-1.47	-1.45	-1.24	-0.98	-0.80	-0.72	-0.55	-0.58
A871111.A	3.5	WBO	1.94	-2.26	-1.98	-1.84	-1.66	-1.66	-1.45	-1.17	-1.15	-0.95	-0.68	-0.55
A871111.A	3.5	GRQ	2.02	9.99	-2.18	-1.97	-1.90	-1.57	-1.36	-1.25	9.99	9.99	9.99	9.99
A871111.A	3.5	MNT	2.14	-2.51	-2.36	-2.26	-1.94	-1.94	-1.56	-1.59	-1.28	-1.11	-1.00	-0.91
A871111.A	3.5	CKO	2.22	-2.14	-1.94	-1.74	-1.57	-1.38	-1.51	-1.47	-1.31	-1.13	-1.00	-1.02
A871111.A	3.5	WEO	2.49	-2.45	-2.21	-2.14	-1.94	-1.79	-1.52	-1.35	-1.13	-0.73	-0.59	-0.64
A880102.A	3.6	LPQ	1.54	-1.72	-1.59	-1.32	-1.25	-1.01	-0.77	-0.73	-0.50	-0.43	-0.35	-0.50
A880102.A	3.6	GNT	2.28	-2.25	-2.03	-2.19	-1.86	-1.79	-1.51	-1.38	-1.45	-1.45	-1.37	-1.46
A880102.A	3.6	HTQ	2.39	-2.54	-2.37	-1.95	-1.77	-1.79	9.99	9.99	9.99	9.99	9.99	9.99
A880102.A	3.6	GSQ	2.47	-2.67	-2.37	-1.98	-1.93	-1.73	-1.61	-1.53	-1.54	-1.64	-1.78	9.99
A880102.A	3.6	KLN	2.50	-2.44	-2.33	-2.21	-2.01	-1.94	-1.90	-1.71	-1.65	-1.71	-1.72	-1.75
A880102.A	3.6	MNT	2.51	-2.66	-2.54	-2.48	-2.15	-2.02	-1.80	-1.68	-1.57	-1.47	-1.63	9.99
A880102.A	3.6	TRQ	2.53	-2.66	-2.32	-1.96	-1.88	-1.90	9.99	9.99	9.99	9.99	9.99	9.99
A880102.A	3.6	MNQ	2.56	-2.56	-2.22	-2.18	-1.91	-1.91	-1.69	-1.61	-1.63	-1.63	-1.63	-1.73
A880102.A	3.6	GRQ	2.62	9.99	9.99	9.99	-2.16	-1.89	-1.74	-1.67	-1.66	-1.66	-1.73	9.99
A880102.A	3.6	OTT	2.67	-2.68	-2.58	-2.44	-2.09	-1.89	-1.89	-1.82	-1.83	-1.87	-1.81	-1.94
A880102.A	3.6	CKO	2.75	9.99	-2.53	-2.36	-2.14	-2.01	-1.94	-2.01	-2.06	-2.05	-2.04	-2.17
A880128.A	3.8	KLN	1.76	-1.38	-1.25	-1.12	-1.05	-1.01	-0.87	-1.10	-1.00	-0.93	-0.80	-0.90
A880128.A	3.8	GSQ	2.38	9.99	-1.36	-1.26	-0.94	-1.06	9.99	9.99	9.99	9.99	9.99	9.99
A880128.A	3.8	EBN	2.31	-1.69	-1.48	-1.30	-1.06	-0.97	-1.01	-0.97	-0.86	-1.09	-1.25	9.99
A880128.A	3.8	HTQ	2.50	9.99	-1.69	-1.37	-1.27	-1.04	-1.04	-0.89	-1.13	-1.02	-1.16	-1.37
A880128.A	3.8	A21	2.50	9.99	-1.61	-1.43	-1.40	-1.25	-1.46	9.99	9.99	9.99	9.99	9.99
A880128.A	3.8	A64	2.52	9.99	-1.96	-1.78	-1.68	-1.72	9.99	9.99	9.99	9.99	9.99	9.99
A880128.A	3.8	A16	2.52	9.99	9.99	-1.75	-1.45	-1.40	-1.37	9.99	9.99	9.99	9.99	9.99
A880128.A	3.8	GGN	2.36	-1.86	-1.76	-1.59	-1.42	-1.46	-1.42	-1.51	-1.82	-2.01	-2.23	9.99
A880128.A	3.8	A61	2.53	9.99	-1.88	-1.69	-1.65	-1.45	-1.50	-1.46	-1.59	9.99	9.99	9.99

A880128.A	3.8	A11	2.54	9.99	9.99	-1.62	-1.26	-1.41	-1.40	-1.57	-1.58	-1.75	9.99	9.99
A880128.A	3.8	MNQ	2.66	-2.19	-1.87	-1.62	-1.52	-1.35	-1.40	9.99	9.99	9.99	9.99	9.99
A880128.A	3.8	DPQ	2.73	9.99	-2.14	-2.00	-1.98	-2.06	-1.83	-1.92	-1.98	-2.10	-2.12	-2.19
A880128.A	3.8	MNT	2.80	9.99	9.99	-2.29	-2.16	-2.10	-2.05	-2.09	-2.13	-2.24	-2.33	9.99
A880128.A	3.8	TRQ	2.84	9.99	-2.20	-1.96	-1.87	-2.01	-2.03	-2.09	-2.21	9.99	9.99	9.99
A880128.A	3.8	GRQ	2.89	9.99	9.99	9.99	9.99	-2.00	-1.94	-2.06	-2.24	-2.40	-2.51	9.99
A880128.A	3.8	WBO	2.89	9.99	9.99	-2.19	-2.13	-2.17	-2.28	-2.39	-2.43	-2.56	9.99	9.99
A880310.A	3.7	GRQ	1.55	-1.55	-1.57	-1.18	-1.03	-0.93	-0.65	-0.70	-0.39	-0.32	-0.04	0.03
A880310.A	3.7	GAC	1.87	-2.15	-2.00	-1.79	-1.69	-1.60	-1.18	-1.17	-0.93	-0.85	-0.64	-0.64
A880310.A	3.7	TRQ	1.94	-2.10	-1.93	-1.79	-1.52	-1.41	-1.20	-1.06	-0.82	-0.52	-0.44	-0.31
A880310.A	3.7	OTT	2.03	-2.09	-1.96	-1.58	-1.45	-1.19	-0.94	-0.73	-0.68	-0.52	-0.33	-0.32
A880310.A	3.7	CKO	2.16	-1.99	-1.79	-1.30	-1.15	-0.88	-0.68	-0.76	-0.88	-0.66	-0.57	-0.53
A880310.A	3.7	MNT	2.27	-2.52	-2.05	-1.83	-1.87	-1.72	-1.30	-1.11	-1.00	-0.89	-0.90	-0.78
A880310.A	3.7	WEO	2.52	-2.23	-1.98	-1.83	-1.74	-1.56	-1.43	-1.20	-1.01	-0.59	-0.50	-0.35
A880310.A	3.7	LPQ	2.65	9.99	9.99	-2.03	-1.80	-1.62	-1.54	-1.43	-1.54	-1.60	-1.68	9.99
A880310.A	3.7	EBN	2.76	9.99	9.99	9.99	-2.18	-2.01	-2.00	-1.97	-1.91	-1.92	9.99	9.99
A880310.A	3.7	HTQ	2.80	9.99	-2.39	-2.18	-2.14	-1.98	-1.92	-1.91	-1.93	9.99	9.99	9.99
A880310.A	3.7	SUO	2.61	9.99	-2.42	-2.26	-2.11	-2.01	-1.79	-1.61	-1.60	-1.48	-1.47	-1.50
A880310.A	3.7	SWO	2.61	-2.55	-2.38	-2.28	-1.93	-1.86	-1.67	-1.61	-1.49	-1.40	-1.36	-1.38
A880310.A	3.7	A54	2.62	-2.36	-2.13	-1.94	-1.66	-1.57	-1.53	-1.57	9.99	9.99	9.99	9.99
A880310.A	3.7	A16	2.65	9.99	9.99	-2.29	-2.02	-1.81	-1.81	-1.81	-1.61	-1.62	-1.70	9.99
A880310.A	3.7	A61	2.65	-2.61	-2.36	-2.06	-1.85	-1.78	-1.83	9.99	9.99	9.99	9.99	9.99
A880310.A	3.7	A21	2.68	-2.31	-2.16	-1.90	-1.79	-1.83	9.99	9.99	9.99	9.99	9.99	9.99
A880424.A	3.7	LMN	1.33	-1.39	-1.15	-1.16	-0.93	-0.79	-0.55	-0.31	-0.30	-0.31	-0.19	0.07
A880424.A	3.7	KLN	2.16	-1.57	-1.36	-1.37	-1.53	-1.18	-1.07	-1.08	-0.92	-0.85	-0.70	-0.72
A880424.A	3.7	GGN	2.25	-2.04	-1.81	-1.50	-1.50	-1.15	-1.11	-1.13	-1.27	-1.38	-1.66	-1.87
A880424.A	3.7	GSQ	2.56	-2.39	-2.21	-2.09	-1.85	-1.72	-1.68	-1.64	-1.76	9.99	9.99	9.99
A880424.A	3.7	LPQ	2.62	-2.06	-1.93	-1.85	-1.76	-1.73	-1.70	-1.79	-1.84	-1.95	9.99	9.99
A880424.A	3.7	HTQ	2.64	-2.62	-2.51	-2.17	-2.08	-1.99	-1.89	-1.85	-1.90	9.99	9.99	9.99
A880424.A	3.7	MNQ	2.76	9.99	-2.51	-2.34	-2.27	-2.26	-2.08	-2.05	-1.99	-1.92	-2.01	9.99
A880509.A	3.5	KLN	1.40	-1.75	-1.82	-1.43	-1.26	-0.93	-0.75	-0.76	-0.60	-0.69	-0.32	0.10
A880509.A	3.5	EBN	2.14	-1.80	-1.54	-1.42	-1.29	-1.24	-1.21	-1.05	-1.04	-0.93	-0.90	-0.63
A880509.A	3.5	LMN	2.27	-2.01	-1.83	-1.87	-1.70	-1.85	-1.58	-1.47	-1.65	-1.59	9.99	9.99
A880509.A	3.5	GGN	2.32	-2.42	-2.26	-1.81	-1.59	-1.81	-1.59	-1.52	-1.64	-1.94	-2.14	9.99
A880509.A	3.5	GSQ	2.33	-2.29	-2.18	-2.06	-1.96	-1.68	-1.66	-1.56	-1.62	9.99	9.99	9.99
A880509.A	3.5	LPQ	2.42	-2.37	-2.20	-2.00	-1.86	-1.74	-1.64	-1.53	9.99	9.99	9.99	9.99

A880509.A	3.5	A11	2.44	-2.51	-2.29	-2.23	-1.97	-1.81	-1.72	-1.68	-1.59	-1.60	-1.70	9.99
A880509.A	3.5	A61	2.44	9.99	-2.43	-2.11	-1.98	-1.78	-1.79	9.99	9.99	9.99	9.99	9.99
A880509.A	3.5	HTQ	2.44	9.99	-2.40	-2.11	-1.97	-1.76	-1.77	9.99	9.99	9.99	9.99	9.99
A880826.A	3.8	KLN	1.40	-1.22	-1.00	9.99	-0.74	-0.68	-0.82	-0.74	-0.46	-0.46	-0.36	-0.20
A880826.A	3.8	EBN	2.14	9.99	-1.20	-0.99	-0.94	-0.82	-0.94	-1.03	-0.96	-0.84	-0.86	-0.44
A880826.A	3.8	LMN	2.27	9.99	9.99	9.99	-1.36	-1.30	-1.53	-1.54	-1.27	-1.18	9.99	9.99
A880826.A	3.8	GGN	2.32	9.99	-2.49	-2.23	-2.09	-1.63	-1.49	-1.25	-1.09	-1.28	-1.85	-2.14
A880826.A	3.8	LPQ	2.42	-1.76	-1.64	-1.44	-1.22	-1.31	9.99	9.99	9.99	9.99	9.99	9.99
A880826.A	3.8	MNQ	2.63	-2.33	-1.98	-1.85	-1.79	-1.67	-1.74	-1.71	-1.72	-1.87	9.99	9.99
A880826.A	3.8	DPQ	2.67	9.99	-2.16	-1.95	-1.87	-1.71	-1.78	-1.92	9.99	9.99	9.99	9.99
A880826.A	3.8	MNT	2.75	9.99	-2.17	-2.06	-2.00	-2.00	-1.95	-2.13	9.99	9.99	9.99	9.99
A880826.A	3.8	TRQ	2.79	9.99	-1.99	-1.88	-1.82	-1.85	-1.98	-2.12	-2.19	9.99	9.99	9.99
A880826.A	3.8	WBO	2.85	9.99	9.99	-2.12	-2.03	-2.04	-2.16	-2.41	9.99	9.99	9.99	9.99
A880826.A	3.8	GRQ	2.85	9.99	9.99	-1.93	-1.78	-1.84	-1.87	-2.05	-2.26	9.99	9.99	9.99
A880826.A	3.8	A21	2.39	9.99	-1.52	-1.37	-1.27	-1.12	-1.12	-1.24	9.99	9.99	9.99	9.99
A880826.A	3.8	A16	2.42	9.99	-1.69	-1.46	-1.47	-1.21	-1.32	-1.34	-1.60	9.99	9.99	9.99
A880826.A	3.8	A11	2.44	-1.78	-1.63	-1.46	-1.41	-1.39	9.99	9.99	9.99	9.99	9.99	9.99
A880826.A	3.8	A54	2.47	-2.01	-1.75	-1.63	-1.62	-1.43	-1.36	-1.47	9.99	9.99	9.99	9.99
A881020.A	3.9	MNT	2.34	-1.86	-1.50	-1.30	-1.32	9.99	9.99	9.99	9.99	9.99	9.99	9.99
A881020.A	3.9	DPQ	2.43	-2.23	-1.89	-1.75	-1.68	-1.58	-1.45	-1.49	-1.53	9.99	9.99	9.99
A881020.A	3.9	LPQ	2.51	-2.12	-1.56	-1.46	-1.56	9.99	9.99	9.99	9.99	9.99	9.99	9.99
A881020.A	3.9	TRQ	2.51	-2.07	-1.77	-1.48	-1.54	9.99	9.99	9.99	9.99	9.99	9.99	9.99
A881020.A	3.9	WBO	2.52	-1.97	-1.62	-1.62	-1.46	-1.30	-1.28	-1.35	9.99	9.99	9.99	9.99
A881020.A	3.9	GGN	2.54	-1.90	-1.72	-1.38	-1.34	-1.26	-1.19	-1.23	-1.43	-1.54	-1.84	-2.01
A881020.A	3.9	EBN	2.60	9.99	-1.85	-1.66	-1.65	-1.60	-1.61	-1.49	-1.39	-1.34	-1.44	-1.62
A881020.A	3.9	GRQ	2.63	-2.06	-1.85	-1.67	-1.53	-1.50	-1.50	-1.44	-1.43	-1.54	-1.55	-1.65
A881020.A	3.9	KLN	2.65	-1.86	-1.72	-1.58	-1.43	-1.33	-1.51	9.99	9.99	9.99	9.99	9.99
A881020.A	3.9	CKO	2.71	9.99	-1.89	-1.75	-1.66	-1.55	-1.66	-1.78	-1.86	-1.78	-1.80	-1.92
A881020.A	3.9	LMN	2.71	9.99	-1.86	-1.74	-1.79	-1.68	-1.58	-1.76	-1.89	-1.83	-1.81	-1.96
A881020.A	3.9	HTQ	2.75	9.99	9.99	-2.04	-1.90	-1.80	-1.87	-1.99	9.99	9.99	9.99	9.99
A881020.A	3.9	GSQ	2.76	9.99	9.99	9.99	-1.84	-1.79	-1.93	-2.02	-2.03	-2.10	9.99	9.99
A881020.A	3.9	WEO	2.76	9.99	-2.08	-1.84	-1.76	-1.62	-1.65	9.99	9.99	9.99	9.99	9.99
A881020.A	3.9	MNQ	2.84	9.99	9.99	-2.20	-2.08	-2.13	-2.10	-2.19	-2.11	-2.11	-2.15	-2.26
A881123.A	4.6	A54	2.00	-0.57	-0.27	-0.23	-0.25	-0.17	-0.01	0.04	0.20	0.26	0.18	0.32
A881123.A	4.6	A61	2.00	-0.56	9.99	9.99	-0.55	-0.33	9.99	9.99	-0.03	-0.03	0.13	0.20
A881123.A	4.6	LPQ	2.11	-0.57	-0.41	-0.48	-0.67	-0.41	-0.34	-0.07	9.99	9.99	9.99	9.99

A881123.A	4.6	DPQ	2.31	-0.88	-0.60	-0.30	-0.16	-0.25	9.99	9.99	9.99	9.99	9.99	9.99
A881123.A	4.6	EBN	2.37	-0.77	-0.72	-0.78	-0.85	9.99	9.99	9.99	9.99	9.99	9.99	9.99
A881123.A	4.6	GSQ	2.50	9.99	-0.98	-0.88	-0.88	-0.71	-0.82	-0.84	-0.87	-0.87	-0.91	9.99
A881123.A	4.6	MNT	2.54	-1.22	-0.93	-0.81	-0.74	-0.62	-0.33	-0.24	-0.32	-0.30	-0.35	-0.41
A881123.A	4.6	GRQ	2.59	-0.96	-0.67	-0.46	-0.49	9.99	9.99	9.99	9.99	9.99	9.99	9.99
A881123.A	4.6	OTT	2.66	-1.05	-0.89	-0.67	-0.45	-0.30	-0.3[illegible]	-0.21	-0.32	-0.39	-0.59	9.99
A881123.A	4.6	WBO	2.67	-1.13	-0.91	-0.85	-0.59	-0.55	-0.47	-0.46	-0.47	-0.54	-0.64	-0.74
A881123.A	4.6	GGN	2.68	-1.13	-1.08	-1.09	-1.10	9.99	9.99	9.99	9.99	9.99	9.99	9.99
A881123.A	4.6	CKO	2.72	-1.01	-0.85	-0.52	-0.56	-0.31	-0.33	-0.40	-0.45	-0.63	-0.76	-0.83
A881123.A	4.6	WEO	2.86	-1.13	-1.01	-0.87	-0.84	-0.76	-0.65	-0.54	-0.59	-0.41	-0.59	-0.77
A881125.A	6.5	GSQ	2.50	0.77	0.95	1.27	1.12	1.37	1.08	1.02	1.00	0.81	0.74	0.62
A881125.A	6.5	TRQ	2.52	0.68	1.17	1.21	1.06	1.09	1.14	1.10	1.06	1.13	0.96	9.99
A881125.A	6.5	KLN	2.59	0.82	0.92	0.77	1.01	0.91	0.84	0.69	0.64	0.51	0.47	0.40
A881125.A	6.5	GRQ	2.59	0.59	0.81	0.96	0.98	1.02	1.11	0.98	0.97	0.89	0.83	0.77
A881125.A	6.5	WBO	2.67	0.55	0.85	1.09	1.00	1.16	0.97	0.94	0.79	0.71	0.73	0.56
A881125.A	6.5	GGN	2.67	9.99	9.99	0.72	0.88	0.86	0.92	0.68	0.78	0.53	0.36	0.26
A881125.A	6.5	CKO	2.73	0.48	0.74	0.80	0.86	0.87	0.87	0.71	0.62	0.57	0.50	0.39
A881125.A	6.5	LMN	2.74	0.67	0.89	0.52	0.51	0.43	0.40	0.33	0.14	0.08	0.04	9.99
A881125.A	6.5	JAQ	2.85	0.10	0.24	0.41	0.60	0.65	0.81	0.68	0.55	0.46	9.99	9.99
A881126.A	4.1	A54	2.02	9.99	-1.59	-1.24	-1.07	-0.89	-0.65	-0.61	-0.56	-0.30	-0.24	-0.11
A881126.A	4.1	A61	2.03	-1.77	-1.64	-1.55	-1.18	-1.03	-0.97	-0.85	-0.55	-0.54	-0.32	-0.19
A881126.A	4.1	A64	2.05	-1.90	-1.68	-1.59	-1.27	-1.16	-0.74	-0.60	-0.58	-0.50	-0.34	-0.30
A881126.A	4.1	A21	2.12	9.99	-1.77	-1.49	-1.22	-1.15	-0.74	-0.71	-0.69	-0.34	-0.30	-0.16
A881126.A	4.1	A11	2.12	-1.92	-1.69	-1.46	-1.32	-1.33	-1.12	-0.99	-0.90	-0.68	9.99	9.99
A881126.A	4.1	LPQ	2.13	9.99	-1.60	-1.37	-1.13	-0.84	-0.74	-0.58	-0.68	-0.55	-0.30	-0.26
A881126.A	4.1	DPQ	2.30	9.99	-1.72	-1.46	-1.26	-0.99	-0.79	-0.77	-0.64	-0.50	-0.43	-0.34
A881126.A	4.1	EBN	2.38	-2.11	-1.67	-1.64	-1.45	-1.20	-1.14	-0.94	-0.93	-1.01	9.99	9.99
A881126.A	4.1	HTQ	2.39	-1.92	-1.70	-1.51	-1.42	-1.29	-1.07	-0.96	-0.86	-0.89	9.99	9.99
A881126.A	4.1	GSQ	2.51	-1.88	-1.57	-1.32	-1.22	-1.25	-1.25	-1.29	-1.22	-1.38	9.99	9.99
A881126.A	4.1	TRQ	2.51	-1.76	-1.59	-1.25	-1.27	9.99	9.99	9.99	9.99	9.99	9.99	9.99
A881126.A	4.1	MNT	2.54	-1.97	-1.84	-1.70	-1.75	9.99	9.99	9.99	9.99	9.99	9.99	9.99
A881126.A	4.1	GRQ	2.58	-2.18	-1.76	-1.54	-1.25	-1.18	-0.97	-0.83	-0.89	9.99	9.99	9.99
A881126.A	4.1	KLN	2.60	-2.20	-2.04	-1.95	-1.81	-1.76	-1.62	-1.44	-1.57	9.99	9.99	9.99
A881126.A	4.1	OTT	2.66	-1.86	-1.74	-1.66	-1.40	-1.11	-1.07	-1.09	-1.04	-0.96	-1.03	-1.14
A881126.A	4.1	WBO	2.67	-2.01	-1.78	-1.49	-1.45	-1.19	-1.16	-1.07	-1.15	9.99	9.99	9.99
A881126.A	4.1	GGN	2.68	-2.31	-2.17	-2.03	-1.77	-1.80	-1.83	9.99	9.99	9.99	9.99	9.99

A881126.A	4.1	CKO	2.72	9.99	-1.88	-1.67	-1.44	-1.31	-1.24	-1.23	-1.18	-1.22	-1.20	-1.24
A881126.A	4.1	SWO	2.87	9.99	-2.11	-1.87	-1.87	-1.78	-1.62	-1.53	-1.58	9.99	9.99	9.99
A881126.A	4.1	SUO	2.88	9.99	-2.22	-1.97	-1.94	-1.86	-1.70	-1.65	-1.70	-1.64	-1.69	-1.74
A881126.A	4.1	SZO	2.90	9.99	-2.15	-2.01	-1.79	-1.83	9.99	9.99	9.99	9.99	9.99	9.99
A890119.A	3.6	A61	1.92	-2.03	-1.78	-1.76	-1.52	-1.28	-1.17	-1.18	-0.76	-1.00	-0.79	-0.54
A890119.A	3.6	A54	1.92	-2.10	-1.85	-1.75	-1.62	-1.24	-1.20	-1.13	-0.86	-0.68	-0.70	-0.56
A890119.A	3.6	A64	1.96	-2.00	-1.91	-1.71	-1.72	-1.44	-1.09	-1.13	-1.04	-0.84	-0.81	-0.60
A890119.A	3.6	A16	2.01	-2.07	-1.80	-1.47	-1.42	-1.55	9.99	9.99	9.99	9.99	9.99	9.99
A890119.A	3.6	A21	2.04	9.99	9.99	9.99	9.99	-1.33	-1.15	-1.07	-0.85	-0.79	-0.63	-0.56
A890119.A	3.6	EBN	2.33	-2.26	-2.12	-1.97	-1.78	-1.75	-1.43	-1.24	-1.28	9.99	9.99	9.99
A890119.A	3.6	HTQ	2.36	-2.28	-2.16	-2.03	-1.83	-1.47	-1.31	-1.08	-1.14	9.99	9.99	9.99
A890119.A	3.6	GSQ	2.48	9.99	9.99	-2.05	-1.71	-1.57	-1.65	9.99	9.99	9.99	9.99	9.99
A890119.A	3.6	MNQ	2.50	-2.22	-1.98	-1.81	-1.77	-1.60	-1.56	-1.41	-1.30	-1.19	-1.14	-1.25
A890119.A	3.6	TRQ	2.53	-2.51	-2.22	-2.01	-1.92	-1.66	-1.54	-1.55	9.99	9.99	9.99	9.99
A890119.A	3.6	MNT	2.54	-2.66	-2.35	-2.11	-2.16	9.99	9.99	9.99	9.99	9.99	9.99	9.99
A890119.A	3.6	GRQ	2.60	-2.55	-2.26	-2.06	-1.89	-1.72	-1.54	-1.40	-1.44	9.99	9.99	9.99
A890119.A	3.6	OTT	2.67	-2.64	-2.39	-2.32	-1.83	-1.82	-1.68	-1.71	9.99	9.99	9.99	9.99
A890119.A	3.6	CKO	2.73	9.99	-2.35	-2.23	-2.12	-1.83	-1.69	-1.77	9.99	9.99	9.99	9.99
A890210.A	4.3	GSQ	2.34	-1.17	-0.96	-0.68	-0.61	-0.46	-0.34	-0.23	-0.24	-0.36	-0.46	9.99
A890210.A	4.3	HTQ	2.46	9.99	-1.28	-0.96	-0.73	-0.87	9.99	9.99	9.99	9.99	9.99	9.99
A890210.A	4.3	KLN	2.58	-1.64	-1.44	-1.28	-1.25	-1.13	-0.96	-1.12	9.99	9.99	9.99	9.99
A890210.A	4.3	EBN	2.59	-1.62	-1.49	-1.21	-1.20	-1.04	-0.97	-1.00	-1.12	-1.08	-1.19	9.99
A890210.A	4.3	GGN	2.76	9.99	-1.67	-1.56	-1.46	-1.45	-1.33	-1.36	-1.38	-1.43	9.99	9.99
A890210.A	4.3	TRQ	2.93	9.99	9.99	-1.57	-1.42	-1.47	-1.43	-1.51	-1.59	-1.62	-1.71	9.99
A890210.A	4.3	JAQ	2.94	9.99	-1.60	-1.46	-1.42	-1.27	-1.10	-1.08	-1.15	-1.17	-1.19	9.99
A890210.A	4.3	GRQ	2.96	9.99	9.99	-1.60	-1.46	-1.42	-1.34	-1.40	-1.57	-1.67	-1.89	9.99
A890210.A	4.3	WBO	2.99	9.99	-1.89	-1.68	-1.66	-1.60	-1.65	-1.73	-1.87	-2.07	9.99	9.99
A890210.A	4.3	OTT	2.99	9.99	9.99	-1.74	-1.61	-1.54	-1.55	-1.67	-1.87	9.99	9.99	9.99
A890210.A	4.3	CKO	3.02	9.99	-1.82	-1.59	-1.70	-1.63	-1.67	9.99	9.99	9.99	9.99	9.99
A890309.A	4.3	LPQ	1.65	-0.36	-0.02	0.23	0.48	0.49	0.70	0.74	0.96	0.80	0.65	0.58
A890309.A	4.3	EBN	2.09	-1.38	-1.28	-1.20	-0.95	-0.66	9.99	9.99	9.99	9.99	9.99	9.99
A890309.A	4.3	DPQ	2.40	-1.75	-1.39	-1.25	-1.17	-0.87	-0.68	-0.51	-0.44	-0.62	9.99	9.99
A890309.A	4.3	HTQ	2.29	-1.45	-1.21	-1.18	-1.13	-0.89	-0.79	-0.66	-0.60	-0.85	-0.65	-0.66
A890309.A	4.3	KLN	2.45	-1.56	-1.37	-1.29	-1.21	-1.27	-1.31	9.99	9.99	9.99	9.99	9.99
A890309.A	4.3	GSQ	2.38	-1.34	-1.11	-0.94	-0.85	-0.94	-0.84	-0.96	-0.92	-1.14	-1.27	9.99
A890309.A	4.3	GGN	2.57	-1.98	-1.68	-1.53	-1.45	-1.39	-1.24	-1.28	-1.23	-1.30	-1.46	-1.55

A890309.A	4.3	OTT	2.71	9.99	-1.72	-1.42	-1.20	-1.16	-1.07	-1.12	-1.29	-1.21	-1.28	-1.49
A890309.A	4.3	JAQ	2.90	9.99	9.99	-1.82	-1.55	-1.49	-1.40	-1.43	-1.55	-1.72	9.99	9.99
A890309.A	4.3	SUO	2.93	9.99	-1.89	-1.75	-1.60	-1.60	-1.54	-1.62	-1.69	-1.84	-1.91	-2.04
A890309.A	4.3	SZO	2.95	9.99	-1.91	-1.60	-1.52	-1.53	-1.60	-1.56	-1.69	-1.84	-1.90	-1.97
A890316.A	5.7	JAQ	2.89	-0.37	-0.27	-0.21	-0.22	-0.10	-0.24	-0.42	9.99	9.99	9.99	9.99
A890316.A	5.7	HTQ	3.08	-0.43	-0.30	-0.36	-0.51	-0.70	-0.81	9.99	9.99	9.99	9.99	9.99
A890316.A	5.7	GSQ	3.10	9.99	9.99	-0.37	-0.32	-0.52	-0.59	9.99	9.99	9.99	9.99	9.99
A890316.A	5.7	A64	3.13	9.99	-0.41	-0.40	-0.54	-0.76	-0.88	9.99	9.99	9.99	9.99	9.99
A890316.A	5.7	A61	3.14	-0.41	-0.31	-0.45	-0.53	-0.77	-0.99	9.99	9.99	9.99	9.99	9.99
A890316.A	5.7	A16	3.15	-0.35	-0.36	-0.54	-0.61	-0.90	-1.04	9.99	9.99	9.99	9.99	9.99
A890316.A	5.7	A54	3.15	-0.49	-0.35	-0.35	-0.57	-0.73	-0.92	9.99	9.99	9.99	9.99	9.99
A890316.A	5.7	EBN	3.14	-0.50	-0.57	-0.66	-0.73	-0.87	-1.09	9.99	9.99	9.99	9.99	9.99
A890316.A	5.7	A11	3.15	-0.31	-0.52	-0.52	-0.61	-0.88	-1.08	9.99	9.99	9.99	9.99	9.99
A890316.A	5.7	KLN	3.17	9.99	9.99	-0.83	-0.78	-1.01	-1.26	9.99	9.99	9.99	9.99	9.99
A890316.A	5.7	DPQ	3.17	-0.71	-0.58	-0.57	-0.75	-0.90	-1.06	9.99	9.99	9.99	9.99	9.99
A890316.A	5.7	GRQ	3.19	-0.54	-0.62	-0.66	-0.66	-0.84	-1.06	9.99	9.99	9.99	9.99	9.99
A890316.A	5.7	TRQ	3.19	9.99	-0.67	-0.57	-0.61	-0.75	-1.07	9.99	9.99	9.99	9.99	9.99
A890316.A	5.7	MNT	3.21	-0.66	-0.66	-0.73	-0.85	-1.07	-1.23	9.99	9.99	9.99	9.99	9.99
A890316.A	5.7	CKO	3.21	9.99	-0.75	-0.72	-0.74	-0.87	-1.07	9.99	9.99	9.99	9.99	9.99
A890316.A	5.7	SWO	3.22	-0.64	-0.64	-0.75	-0.87	-1.11	-1.31	9.99	9.99	9.99	9.99	9.99
A890316.A	5.7	OTT	3.22	-0.73	-0.66	-0.69	-0.70	-0.86	-1.17	9.99	9.99	9.99	9.99	9.99
A890316.A	5.7	GGN	3.22	-0.69	-0.77	-0.96	-0.96	-1.15	-1.33	9.99	9.99	9.99	9.99	9.99
A890316.A	5.7	SUO	3.22	-0.70	-0.73	-0.79	-0.81	-0.99	-1.23	9.99	9.99	9.99	9.99	9.99
A890316.A	5.7	SZO	3.23	9.99	-0.77	-0.74	-0.82	-1.04	-1.29	9.99	9.99	9.99	9.99	9.99
A890316.A	5.7	WBO	3.23	-0.78	-0.66	-0.72	-0.81	-1.04	-1.30	9.99	9.99	9.99	9.99	9.99
A890810.A	3.5	KLN	1.69	-1.72	-1.79	-1.38	-1.31	-1.32	-1.05	-0.75	-0.79	-0.71	-0.62	-0.47
A890810.A	3.5	LMN	2.07	-1.78	-1.57	-1.57	-1.65	-1.44	-1.39	9.99	9.99	9.99	9.99	9.99
A890810.A	3.5	EBN	2.32	-2.10	-1.71	-1.68	-1.60	-1.29	-1.26	-1.30	9.99	9.99	9.99	9.99
A890810.A	3.5	GSQ	2.43	9.99	-2.06	-1.90	-1.78	-1.54	-1.41	-1.48	9.99	9.99	9.99	9.99
A890810.A	3.5	A21	2.50	9.99	9.99	-1.91	-1.72	-1.69	-1.67	-1.56	-1.54	-1.52	-1.65	9.99
A890810.A	3.5	A16	2.52	9.99	9.99	-1.98	-1.79	-1.78	-1.68	-1.70	9.99	9.99	9.99	9.99
A890810.A	3.5	A64	2.53	9.99	-2.33	-2.11	-2.00	-1.91	-1.81	-1.83	9.99	9.99	9.99	9.99
A890810.A	3.5	HTQ	2.53	9.99	-2.19	-1.97	-1.68	-1.70	-1.66	-1.54	-1.77	9.99	9.99	9.99
A890810.A	3.5	A54	2.56	9.99	-2.44	-2.17	-2.00	-1.89	-1.83	-1.83	-1.90	9.99	9.99	9.99
A891116.A	4.0	CKO	1.97	-1.00	-0.83	-0.61	-0.46	-0.06	-0.02	0.24	0.11	0.38	0.46	0.57
A891116.A	4.0	OTT	2.18	-1.88	-1.63	-1.18	-1.02	-0.87	-0.67	-0.62	-0.41	-0.48	-0.27	-0.51

A891116.A	4.0	TRQ	2.21	-0.99	-0.62	-0.61	-0.49	-0.29	-0.16	-0.12	-0.07	0.05	-0.07	-0.09
A891116.A	4.0	DPQ	2.47	-2.07	-1.82	-1.60	-1.41	-1.41	-1.16	-1.14	-1.03	-0.74	-0.86	-0.93
A891116.A	4.0	SWO	2.53	9.99	-2.15	-1.83	-1.58	-1.53	-1.23	-1.25	9.99	9.99	9.99	9.99
A891116.A	4.0	SUO	2.53	-2.22	-1.92	-1.77	-1.50	-1.51	9.99	9.99	9.99	9.99	9.99	9.99
A891116.A	4.0	SZO	2.57	-2.07	-1.79	-1.79	-1.62	-1.36	-1.30	-1.24	-1.20	-1.09	-1.12	-1.18
A891116.A	4.0	A54	2.68	9.99	-2.05	-1.71	-1.61	-1.46	-1.48	9.99	9.99	9.99	9.99	9.99
A891116.A	4.0	A11	2.69	9.99	-1.91	-1.78	-1.66	-1.53	-1.75	-1.61	-1.60	-1.66	-1.78	-1.93
A891116.A	4.0	A61	2.71	9.99	-1.97	-1.87	-1.70	-1.68	-1.70	-1.66	-1.67	-1.77	-1.82	-1.86
A891116.A	4.0	A16	2.71	9.99	9.99	-1.90	-1.79	-1.69	-1.77	-1.72	-1.56	-1.72	-1.77	-1.88
A891116.A	4.0	A64	2.72	9.99	-2.14	-1.76	-1.68	-1.65	-1.55	-1.47	-1.63	-1.65	-1.79	9.99
A891116.A	4.0	A21	2.73	9.99	9.99	-1.86	-1.58	-1.45	-1.45	-1.43	-1.54	-1.50	-1.54	-1.73
A891116.A	4.0	EBN	2.81	9.99	-2.26	-1.98	-1.90	-1.85	-1.70	-1.82	-1.83	-2.01	9.99	9.99
A891116.A	4.0	GSQ	2.88	9.99	-2.09	-1.84	-1.90	-1.83	-2.04	-2.04	-2.19	9.99	9.99	9.99
A891116.A	4.0	GGN	2.89	9.99	-1.71	-1.44	-1.43	-1.30	-1.31	-1.39	9.99	9.99	9.99	9.99
A891225.W	5.0	GSQ	3.12	9.99	9.99	-1.00	-0.95	-1.09	-1.12	9.99	9.99	9.99	9.99	9.99
A891225.W	5.0	LPQ	3.16	9.99	9.99	-0.27	-0.16	-0.20	-0.17	9.99	9.99	9.99	9.99	9.99
A891225.W	5.0	EBN	3.16	9.99	-1.32	-1.27	-1.33	-1.43	-1.52	9.99	9.99	9.99	9.99	9.99
A891225.W	5.0	KLN	3.19	9.99	9.99	-1.55	-1.48	-1.57	-1.71	9.99	9.99	9.99	9.99	9.99
A891225.W	5.0	MNT	3.21	9.99	9.99	-1.35	-1.27	-1.37	-1.54	9.99	9.99	9.99	9.99	9.99
A891225.W	5.0	GGN	3.24	9.99	9.99	-0.82	-0.67	-0.81	-0.90	9.99	9.99	9.99	9.99	9.99
A891225.W	5.0	A64	3.14	9.99	-1.26	-1.21	-1.24	-1.25	-1.35	9.99	9.99	9.99	9.99	9.99
A891225.W	5.0	A61	3.14	9.99	9.99	-1.23	-1.20	-1.31	-1.42	9.99	9.99	9.99	9.99	9.99
A891225.W	5.0	A21	3.15	-0.91	-1.08	-1.08	-1.11	-1.16	-1.25	9.99	9.99	9.99	9.99	9.99
A891225.W	5.0	A16	3.15	-1.01	-1.24	-1.30	-1.30	-1.34	-1.46	9.99	9.99	9.99	9.99	9.99
A891225.W	5.0	A11	3.16	9.99	-1.36	-1.25	-1.22	-1.35	-1.54	9.99	9.99	9.99	9.99	9.99
A891225.W	5.0	SWO	3.19	-1.44	-1.24	-1.28	-1.27	-1.31	-1.42	9.99	9.99	9.99	9.99	9.99
A891225.W	5.0	SUO	3.20	-1.52	-1.37	-1.39	-1.29	-1.30	-1.33	9.99	9.99	9.99	9.99	9.99
A891225.W	5.0	SZO	3.20	9.99	9.99	-1.36	-1.22	-1.36	-1.41	9.99	9.99	9.99	9.99	9.99
A891225.Y	6.1	GSQ	3.11	0.15	0.30	0.30	0.12	-0.16	-0.33	9.99	9.99	9.99	9.99	9.99
A891225.Y	6.1	EBN	3.15	-0.20	-0.10	-0.06	-0.22	-0.52	-0.68	9.99	9.99	9.99	9.99	9.99
A891225.Y	6.1	DPQ	3.17	-0.28	-0.12	-0.14	-0.30	-0.46	-0.61	9.99	9.99	9.99	9.99	9.99
A891225.Y	6.1	KLN	3.19	-0.28	-0.17	-0.26	-0.35	-0.62	-0.81	9.99	9.99	9.99	9.99	9.99
A891225.Y	6.1	MNT	3.21	-0.21	-0.12	-0.38	-0.46	-0.67	-0.74	9.99	9.99	9.99	9.99	9.99
A891225.Y	6.1	OTT	3.21	-0.35	-0.17	-0.25	-0.30	-0.48	-0.64	9.99	9.99	9.99	9.99	9.99
A891225.Y	6.1	LMN	3.22	-0.52	-0.48	-0.61	-0.76	-1.02	-1.18	9.99	9.99	9.99	9.99	9.99
A891225.Y	6.1	GGN	3.23	0.49	0.58	0.45	0.34	0.08	-0.13	9.99	9.99	9.99	9.99	9.99

A891225.Y	6.1	A64	3.14	-0.11	0.03	-0.12	-0.19	-0.42	-0.55	9.99	9.99	9.99	9.99
A891225.Y	6.1	A61	3.14	-0.09	-0.01	-0.03	-0.15	-0.47	-0.63	9.99	9.99	9.99	9.99
A891225.Y	6.1	A21	3.14	0.01	0.19	0.13	-0.05	-0.24	-0.45	9.99	9.99	9.99	9.99
A891225.Y	6.1	A54	3.15	-0.16	0.01	-0.03	-0.23	-0.36	-0.57	9.99	9.99	9.99	9.99
A891225.Y	6.1	A16	3.15	-0.05	0.02	0.00	-0.25	-0.52	-0.72	9.99	9.99	9.99	9.99
A891225.Y	6.1	A11	3.16	9.99	-0.13	-0.08	-0.16	-0.47	-0.69	9.99	9.99	9.99	9.99
A900303.A	3.6	A64	1.33	-1.50	-1.32	-1.17	-1.08	-0.76	-0.67	-0.47	-0.58	-0.33	-0.28	-0.25
A900303.A	3.6	A61	1.46	-1.68	-1.43	-1.16	-1.06	-0.92	-0.79	-0.68	-0.66	-0.59	-0.49	-0.32
A900303.A	3.6	A21	1.54	9.99	-1.02	9.99	-0.60	-0.39	-0.43	-0.32	-0.10	0.22	0.09	0.09
A900303.A	3.6	A16	1.68	-1.51	-1.27	-1.17	-1.13	-1.15	-0.91	-0.78	-0.54	-0.65	-0.62	-0.43
A900303.A	3.6	A54	1.77	-1.92	-1.72	-1.41	-1.44	-1.20	-0.98	-0.89	-0.74	-0.71	-0.53	-0.43
A900303.A	3.6	A11	1.87	-2.04	-1.78	-1.71	-1.60	-1.35	-1.31	-0.99	-1.04	-0.82	-0.84	-0.69
A900303.A	3.6	GSQ	2.38	-2.32	-2.13	-1.99	-1.90	-1.69	-1.60	-1.44	-1.52	9.99	9.99	9.99
A900303.A	3.6	KLN	2.47	-1.64	-1.37	-1.21	-1.14	-1.09	-0.81	-0.76	-0.72	-0.63	-0.69	-0.73
A900303.A	3.6	MNT	2.58	-2.79	-2.59	-2.29	-2.16	-2.04	-1.99	-1.80	-1.68	-1.70	9.99	9.99
A900303.A	3.6	GGN	2.59	9.99	-1.54	-1.36	-1.27	-1.01	-0.97	-0.86	-0.78	-0.84	-0.94	9.99
A900303.A	3.6	TRQ	2.59	-1.63	-1.38	-1.05	-0.94	-0.88	-0.88	-0.85	-0.75	-0.68	-0.73	-0.86
A900303.A	3.6	GRQ	2.67	-1.62	-1.42	-1.25	-1.12	-0.95	-0.81	-0.71	-0.76	-0.87	-0.94	-0.99
A900303.A	3.6	WBO	2.71	9.99	-1.71	-1.45	-1.45	-1.04	-1.06	-1.08	-1.09	-1.13	-1.10	-1.26
A900303.A	3.6	OTT	2.71	9.99	9.99	-2.45	-2.15	-1.91	-1.88	-1.90	-2.00	9.99	9.99	9.99
A900303.A	3.6	CKO	2.78	9.99	-1.61	-1.49	-1.29	-1.09	-1.03	-1.05	-1.01	-1.12	-1.22	-1.35
A901007.A	3.9	TRQ	1.65	-0.84	-0.53	-0.38	-0.13	-0.23	0.14	0.12	0.32	0.45	0.36	0.39
A901007.A	3.9	GRQ	1.84	-0.99	-0.81	-0.60	-0.48	-0.15	-0.18	0.10	0.21	0.33	0.42	0.45
A901007.A	3.9	OTT	2.05	9.99	-1.71	-1.43	-0.98	-0.79	-0.82	9.99	9.99	9.99	9.99	9.99
A901007.A	3.9	WBO	2.16	-0.87	-0.58	-0.21	-0.26	-0.12	-0.23	-0.17	0.06	0.11	-0.13	-0.18
A901007.A	3.9	CKO	2.27	-1.09	-0.92	-0.68	-0.38	-0.05	-0.10	-0.25	9.99	9.99	9.99	9.99
A901007.A	3.9	DPQ	2.26	-1.97	-1.75	-1.62	-1.67	-1.33	-1.00	-0.91	-0.65	-0.57	-0.53	-0.66
A901007.A	3.9	A54	2.58	-2.07	-1.82	-1.76	-1.50	-1.43	-1.40	-1.37	-1.27	-1.22	-1.28	-1.35
A901007.A	3.9	A11	2.59	9.99	9.99	-1.89	-1.76	-1.67	-1.55	-1.57	-1.56	-1.44	-1.55	-1.69
A901007.A	3.9	A16	2.61	9.99	-2.05	-1.93	-1.59	-1.43	-1.28	-1.29	-1.27	-1.34	-1.35	-1.43
A901007.A	3.9	A61	2.61	-2.24	-2.11	-1.88	-1.80	-1.73	-1.70	-1.67	-1.54	-1.60	9.99	9.99
A901007.A	3.9	A64	2.63	-2.07	-1.92	-1.90	-1.68	-1.64	-1.44	-1.47	-1.40	-1.46	-1.56	9.99
A901007.A	3.9	A21	2.64	-2.16	-1.82	-1.82	-1.74	-1.58	-1.36	-1.34	-1.33	-1.31	-1.46	9.99
A901007.A	3.9	SWO	2.66	-2.31	-2.16	-1.92	-1.97	9.99	9.99	9.99	9.99	9.99	9.99	9.99
A901007.A	3.9	SZO	2.69	-2.40	-2.07	-1.96	-1.92	-1.77	-1.69	-1.62	-1.53	-1.56	-1.59	-1.67
A901019.A	5.1	GRQ	1.43	1.03	1.37	9.99	1.39	1.50	1.73	1.54	1.96	1.81	1.71	1.81

A901019.A	5.1	TRQ	1.94	0.32	0.78	0.93	0.96	1.37	1.39	1.68	1.61	1.68	1.60	1.56
A901019.A	5.1	OTT	2.09	-0.50	-0.27	0.13	0.41	0.48	0.43	0.36	0.50	0.51	0.33	0.43
A901019.A	5.1	CKO	2.19	9.99	9.99	9.99	9.99	0.70	0.92	1.11	1.15	1.19	1.35	1.03
A901019.A	5.1	WBO	2.23	0.45	0.57	1.00	1.01	1.24	1.39	1.07	1.15	1.37	1.27	1.01
A901019.A	5.1	MNT	2.28	-0.74	-0.59	-0.62	-0.34	-0.03	0.16	0.30	0.14	0.31	0.36	0.38
A901019.A	5.1	DPQ	2.34	-0.52	-0.35	-0.07	0.13	0.30	0.30	0.51	0.69	0.66	0.65	0.53
A901019.A	5.1	A54	2.61	-0.63	-0.45	-0.30	-0.01	0.10	-0.03	0.05	-0.01	-0.08	-0.16	-0.26
A901019.A	5.1	SUO	2.62	-0.78	-0.65	-0.55	-0.87	9.99	9.99	9.99	9.99	9.99	9.99	9.99
A901019.A	5.1	A11	2.62	-0.57	-0.34	-0.42	-0.08	-0.04	-0.07	-0.23	-0.21	-0.28	-0.43	-0.52
A901019.A	5.1	A16	2.64	-0.52	-0.37	-0.37	-0.32	-0.07	0.08	0.07	0.03	-0.07	-0.24	-0.39
A901019.A	5.1	A61	2.64	9.99	-0.70	-0.44	-0.28	-0.27	-0.30	-0.24	-0.30	-0.52	9.99	9.99
A901019.A	5.1	SZO	2.65	-0.80	-0.66	-0.65	-0.64	-0.58	-0.52	-0.50	-0.35	-0.47	9.99	9.99
A901019.A	5.1	A64	2.66	-0.66	-0.51	-0.37	-0.21	-0.20	-0.17	-0.21	-0.21	-0.30	-0.44	-0.53
A901019.A	5.1	A21	2.67	-0.62	-0.50	-0.36	-0.13	-0.08	-0.11	-0.02	-0.08	-0.1?	-0.31	-0.44

APPENDIX B

SOURCE PARAMETERS OF ECTN EARTHQUAKES

SOURCE PARAMETERS OF ECTN STUDY EVENTS
Notes: Depth of 9.9 denotes unknown depth.
GSC M = magnitude listed by the Geological Survey of Canada.

Date	Lat.	Long.	GSC M		Moment m	Stress(bars)	Focal Depth(km)
A800311.A	46.79	-71.87	3.7	MN	3.4	53	9.9
A800403.A	48.77	-67.95	4.0	MN	3.5	109	9.9
A800413.A	49.64	-81.64	4.1	MN			9.9
A800606.A	43.64	-75.14	3.5	MN			9.9
A810616.A	47.47	-70.00	3.7	MN	3.0	27	8.0
A810704.A	45.14	-74.62	3.7	MN	3.2	27	13.0
A810713.A	49.82	-66.80	3.7	MN	3.2	17	9.9
A810918.A	46.11	-75.02	3.5	MN	3.0	13	9.9
A810930.A	46.37	-75.56	3.5	MN	2.9	15	9.9
A811021.A	41.15	-72.58	3.8	MN			6.0
A811028.A	49.83	-65.25	3.9	MN	3.4	30	9.9
A811128.A	47.03	-66.61	3.7	MN	3.3	7	5.0
A820109.B	47.00	-66.60	3.8	MN	3.3	16	5.0
A820109.C	47.00	-66.60	3.7	MN	3.3	7	5.0
A820111.A	47.00	-66.60	5.4	MB	5.2	72	5.0
A820112.A	47.00	-66.60	3.5	MN			5.0
A820113.A	47.00	-66.60	4.0	MN	3.2	5	5.0
A820115.A	47.00	-66.60	3.8	MN	3.5	16	5.0
A820117.A	47.00	-66.60	3.6	MN	3.2	11	5.0
A820119.A	43.51	-71.62	4.5	MB	4.0	86	7.0
A820316.A	47.00	-66.60	3.5	MN	3.2	7	5.0
A820331.A	47.00	-66.60	5.0	MB	4.1	55	5.0
A820402.A	47.00	-66.60	4.3	MN	3.7	22	5.0
A820411.A	47.00	-66.60	4.0	MN	3.5	46	5.0
A820418.A	47.00	-66.60	4.1	MN	3.6	22	5.0
A820506.A	47.00	-66.60	4.0	MN	3.4	15	5.0
A820616.A	47.01	-66.95	4.7	MB	4.0	55	8.0
A820623.A	47.39	-76.95	3.5	MN	2.8	18	9.9
A820713.A	46.09	-74.54	3.8	MN	3.2	26	9.9
A820728.A	47.00	-66.60	3.7	MN	3.3	17	5.0
A820806.A	45.89	-75.46	3.7	MN	3.0	19	9.9
A820813.A	46.66	-78.61	4.3	MN	3.5	70	9.9
A820903.A	45.69	-76.61	3.7	MN	3.2	19	9.9
A821026.A	47.00	-66.60	3.5	MN	3.0	6	5.0
A821204.A	47.54	-70.22	3.9	MN	3.2	65	15.0
A830117.A	49.11	-67.06	4.1	MN	3.6	63	9.9
A830314.A	50.82	-74.90	3.6	MN			9.9
A830513.A	47.00	-66.60	3.5	MN	3.1	9	5.0
A830513.B	47.00	-66.60	3.9	MN	3.6	28	5.0
A830516.A	47.69	-69.89	3.8	MN	3.4	22	11.0
A830527.A	45.54	-69.50	3.5	MN			10.0
A830529.A	44.48	-70.42	4.1	MN	3.7	29	2.0
A830812.A	44.99	-67.72	3.5	MN	3.0	3	10.0
A831007.A	43.94	-74.25	5.6	MN	5.0	113	4.0
A831007.B	43.95	-74.25	3.6	MN	3.2	35	13.0
A831011.A	45.20	-75.75	4.1	MN	3.6	39	14.0

A831117.A	47.00	-66.60	3.7	MN	3.3	15	5.0
A831228.A	47.07	-76.28	3.5	MN	2.9	13	9.9
A840119.A	44.90	-67.33	3.5	MN	3.3	19	12.0
A840224.A	47.00	-66.60	3.7	MN	3.3	51	5.0
A840411.A	49.30	-67.52	3.8	MN	3.3	20	9.9
A840923.A	46.00	-64.84	3.6	MN			9.9
A841130.A	47.00	-66.60	3.8	MN	3.5	8	5.0
A850303.A	47.39	-70.48	3.1	MN	2.8	5	14.1
A850410.A	47.52	-69.96	3.1	MN			12.7
A850412.A	45.37	-70.68	3.5	MN	2.8	26	9.0
A851005.A	47.00	-66.60	4.0	MN	3.4	12	5.0
A851019.A	41.11	-73.92	4.1	MN	3.6	39	9.9
A860111.A	47.71	-70.12	4.0	MN	3.3	27	5.0
A860131.A	41.65	-81.16	5.0	MB	4.8	149	10.0
A860712.A	40.54	-84.35	4.5	MB	4.5	154	9.9
A860806.A	46.37	-75.22	3.5	MN	3.1	6	9.9
A860818.A	47.53	-70.02	3.0	MN	2.6	3	5.6
A860919.A	47.30	-70.32	4.2	MN	3.5	48	22.0
A861025.A	43.42	-71.55	3.9	MB			9.0
A861109.A	49.23	-67.40	4.2	MN	3.6	38	9.9
A870318.A	47.72	-70.19	3.3	MN	2.8	5	4.2
A870405.A	51.86	-82.79	3.6	MN			9.9
A870530.A	46.54	-80.99	3.5	MN			9.9
A870713.A	41.93	-80.71	4.1	MN	3.6	48	5.0
A870806.A	47.43	-70.28	3.4	MN	2.9	12	10.0
A870926.A	44.48	-74.52	3.8	MN	3.3	19	5.0
A871023.A	45.76	-74.51	3.7	MN	3.1	33	14.0
A871111.A	45.76	-75.33	3.5	MN	3.0	23	17.0
A871111.B	45.78	-75.34	3.2	MN	3.0	23	21.1
A880102.A	47.42	-70.43	3.6	MN	3.1	10	11.0
A880124.A	47.44	-70.46	3.1	MN	2.7	5	10.1
A880128.A	47.00	-65.66	3.8	MN	3.5	6	9.9
A880310.A	46.34	-75.67	3.7	MN	3.1	55	12.0
A880310.B	46.34	-75.67	3.7	MN			12.0
A880313.A	47.45	-70.38	3.1	MN	2.8	9	6.8
A880424.A	46.02	-64.92	3.7	MN	3.2	14	5.0
A880509.A	47.00	-66.60	3.5	MN	3.1	6	5.0
A880515.A	45.16	-75.61	3.3	MN	2.9	6	8.5
A880809.A	45.01	-74.99	3.4	MN	2.8	11	9.5
A880826.A	47.00	-66.60	3.8	MN	3.5	6	5.0
A880826.B	47.00	-66.60	3.8	MN			5.0
A881020.A	44.56	-71.17	3.9	MN	3.4	15	5.0
A881114.A	44.52	-70.43	3.7	MN			9.9
A881123.A	48.13	-71.20	4.6	MN	4.1	190	29.0
A881125.A	48.12	-71.18	6.5	MN	5.8	517	29.0
A881126.A	48.14	-71.30	4.1	MN	3.4	166	26.0
A881228.A	44.70	-69.48	3.5	MN			9.9
A890119.A	48.06	-71.01	3.6	MN	3.1	63	25.0
A890131.A	47.44	-70.67	3.1	MN	2.7	29	19.7
A890210.A	50.07	-64.65	4.3	MN	3.7	144	9.9
A890309.A	47.72	-69.86	4.3	MN	3.7	77	10.0
A890316.A	60.04	-70.06	5.7	MN	5.0	126	5.0
A890524.A	58.57	-60.37	3.7	MN			9.9
A890810.A	46.66	-65.79	3.5	MN	3.2	6	5.0

A891013.A	47.39	-70.13	3.2	MN	3.0	30	22.7
A891104.A	46.22	-75.72	3.4	MN	2.8	26	7.9
A891116.A	46.59	-76.60	4.0	MN	3.6	65	9.9
A891122.A	47.46	-70.35	3.4	MN	3.0	12	8.1
A891225.W	60.06	-73.75	5.0	MN			5.0
A891225.Y	60.01	-73.56	6.1	MN	5.9	149	5.0
A900105.A	59.99	-73.80	4.4	MN			5.0
A900303.A	47.86	-69.98	3.6	MN	3.4	70	20.0
A900310.A	59.92	-74.08	3.5	MN			5.0
A900313.A	47.53	-70.14	3.2	MN	2.8	19	15.3
A900421.A	47.55	-70.07	3.1	MN	2.8	18	9.6
A900423.A	47.41	-70.18	3.0	MN	2.6	11	7.9
A901007.A	46.30	-75.10	3.9	MN	3.6	59	13.0
A901019.A	46.50	-75.60	5.1	MN	4.7	517	13.0
A901021.A	47.40	-70.36	3.3	MN	2.8	35	15.8
A901026.A	47.57	-69.99	3.1	MN			10.9
A901218.A	47.26	-70.34	3.3	MN	2.9	9	9.2

APPENDIX C

KEY COMPUTER PROGRAMS

PROGRAM: SPECLAG

PURPOSE: Compute Fourier spectra from ECTN velocity records, correcting for instrument response; also computes the noise spectrum, normalized to same window length.

INPUTS: Raw ECTN data files, a parameter file specifying options, a file giving station locations and instrument types, a file giving event locations and stations for which spectra are to be computed, a file giving windows for noise and signal.

OUTPUTS: Fourier spectra for both signal and noise windows.

```
c     program spec_lag
c
c     Calculates Fourier spectra of ECTN velocity records
c     (accn, vel or displ) for a specified list of events and
c     components.
c     Uses lag windows (50% overlap), averaging squared spectral
c     amplitudes, to reduce variance.
c     Program control is through options from an option file.
c     Options include phase, duration, components, gmotion parameter,
c     decimation, smoothing, deglitching, removal of instrument resp.
c     Can apply tapered cosine window, where %taper is applied
c     at both ends of the window.
c     Also has option to write a time series file for inset plotting
c     If record is not at least twice as long as the segment length,
c     then the segment length is reduced by a factor of two.
c
c     Maxm. no. points = 10000
c     Maxm. segment length = 512 points
c     Written for ECTN data files.
c     Output is in units of mm and s for input in counts.
c     G. Atkinson, Nov. 1990, modified Feb. 1991
c     Lag window modifications May 1991.
c     Noise spectrum output added June 11, 1991.
c     Minm, maxm. durn. specification, June 27, 1991.
c     Modified to write corrected PGV and freq, Aug. 20, 1991
c     Deglitch modified to repeat until no more glitches, Aug 22, 91
c
$LARGE
$STORAGE:4
      common stanam,stalat,stalon,nsta,itype
      integer bufx(10), nph(10)
      dimension stalat(100),stalon(100),x(15000),itype(100),xts(1000)
      dimension p(10,50),s1(10,50),s2(10,50),stop(10,50)
      dimension avg(512),ampns(512), inzero(2)
      character*9 fname, mag, fname2,evph(10)
      character*3 stanam(100), stadat, stapk(50),stnph(10,50)
      character*40 header
      character*1 comp, phase
      REAL PI, SR
      complex cx(512),xns(512),accresp,velresp,dspresp
C
      write(*,*)'filename for program options ?'
      read(*,10)fname
      open(5,file=fname)
      write(*,*)' filename for output spectra ?'
      read(*,10)fname
      open(7,file=fname, status='new')
      write(*,*)' filename for noise spectra ?'
      read(*,10)fname
      open(1,file=fname,status='new')
      read(5,10)header
      write(7,10)header
      write(1,10)header
      read(5,11)phase, fname2
```

```
 11    format(a1,2x,a9)
       read(5,*)icomp
       write(7,210)phase, icomp, fname2
       write(1,210)phase, icomp, fname2
 210   format(' phase = ',a1, '  icomp = ',i1,' from file ',a9)
       read(5,*)igmtn,npseg1,minseg,idec,nglit
       write(7,220)igmtn,npseg1,minseg,idec,nglit
       write(1,220)igmtn,npseg1,minseg,idec,nglit
 220   format(' igmtn = ',i1,'  npseg1 = ',i4,'  minseg = ',i2,
      *       '  idec = ',i2,'  nglit = ',i2)
       read(5,*)taper, dura1, durb1, dura2,durb2
       write(7,230)taper,dura1,durb1,dura2,durb2
       write(1,230)taper,dura1,durb1,dura2,durb2
       fname = '          '
 230   format(' taper = ',f5.2,' dura, durb (min, max) ',2(f6.0,f6.2))
       if (taper .gt. .50)write(*,*)' ERROR. Use taper<.5'
       read(5,*)iresp,its,idects
       if(its .eq. 1) then
         write(*,*)' filename for output time series ?'
         read(*,10)fname
         open(3,file=fname,status='new')
       endif
       write(7,231)iresp, its, fname
       write(1,231)iresp, its, fname
 231   format(' iresp = ',i2,' its = ',i2,2x,a10)
       write(7,*)'*******************************************'
       write(7,240)
       write(1,*)'*** NOISE SPECTRUM ONLY ********************'
       write(1,240)
 240   format(' LEGEND:',/,' phase: p=p s=sn 1=lg',/,
      * ' icomp: 0=vert, 1=horiz, 2=both',/,
      * ' igmtn: 0=disp, 1=vel., 2=accn',/,' npseg: #pts/FFT seg.',
      * /,' idec: decimation factor',/,' nglit: no. deglitch iterations',
      * /,' durn, tstart, from file (but durn between min, max)',/,
      *   ' iresp: 0=no instrument resp.')
       WRITE(*,*)' filename for event parameters >'
       READ(*,10)FNAME
       OPEN(4,FILE=FNAME)
 10    FORMAT(A)
       PI=3.141592654
 c
       open(2,file='pltsta.dat')
       read(4,10)
       read(2,10)
       nsta = 1
 20    read(2,30)stalat(nsta),stalon(nsta),stanam(nsta),itype(nsta)
 30    format(f6.2,1x,f7.2,2x,a3,2x,i1)
       if(itype(nsta) .gt. 6)write(*,31)stanam(nsta),itype(nsta)
 31    format(' WARNING. itype not defined ',a3,i5)
       if(stalat(nsta) .ne. 0.) then
         nsta = nsta + 1
         go to 20
       endif
       nsta = nsta-1
```

```
      write(*,*)' Have read station data'
      close(2)
c
      open(2,file=fname2)
      iph = 0
710   iph = iph + 1
      read(2,711,end=730) evph(iph), nph(iph)
711   format(a9,1x,i5)
      do 720 j = 1,nph(iph)
        read(2,712)stnph(iph,j),p(iph,j),s1(iph,j),s2(iph,j),stop(iph,j)
712     format(a3,2x,4f6.1)
        if (s2(iph,j) .eq. 0.)s2(iph,j) = s1(iph,j)
720   continue
      go to 710
730   continue
      iph = iph -1
      close(2)
c
c     LOOP ON EVENTS.
c
35    read(4,40,end=200)fname,elat,elon,mag,depth
40    format(a9,2x,f5.2,2x,f7.2,2x,a9,f3.0)
      open(6,file=fname)
      write(*,41) fname
41    format(' Reading event file ',a9)
      read(4,42)(stapk(j),j=1,50)
42    format(50(a3,1x))
c
c     LOOP ON COMPONENTS.
c
45    read(6,50,end=100)stadat,comp,sr,valmax,nsamp,nline
50    format(a3,3x,a1,/,f5.1,31x,f10.1,//,i6,10x,i5)
      if(nsamp .eq. 0) go to 45
c     If this component orientation is not wanted, skip it.
      if(icomp .eq. 0 .and. comp .ne. 'Z') go to 49
      if(icomp .eq. 1 .and. comp .eq. 'Z') go to 49
c     If this component is not listed in pltsta.dat, skip it.
      call table(stadat,xlon,xlat,it)
      if (xlon .eq. 0.)go to 49
c     If this component has not been asked for, skip it.
      iflag=0
      do 75 j=1,30
        if(stadat .eq. stapk(j)) iflag=1
75    continue
      if(iflag .eq. 0) go to 49
      go to 55
c
49    write(*,53)stadat
53    format(' Skipping  ',a3)
         do 51 kk = 1,nline
           read(6,60)
51       continue
         go to 45
c
```

```
 55     write(*,52) stadat
 52     format(' Working ',a3)
        npseg = npseg1
        call sdist(6367.,elon,elat,xlon,xlat,s,2)
        dist=sqrt(s*s + depth*depth)
        durmin = dura1 + durb1*dist
        durmax = dura2 + durb2*dist
c
c       PICK PHASE START AND STOP TIMES
C
        iev = 0
        ist = 0
        do 600 j = 1, iph
          if(fname .eq. evph(j)) iev = j
600     continue
        do 610 j = 1, nph(iev)
          if(stadat .eq. stnph(iev,j)) ist = j
610     continue
        if (iev .eq. 0 .or. ist .eq. 0) write(*,*)' NO PHASE PICK'
        valmax = 0.
        dt = (1./sr)*float(idec)
        dts = (1./sr)*float(idects)
        tseg = float(npseg*idec) * dt
        if (phase .eq. 's') tskip = s1(iev,ist)
        if (phase .eq. 'l') tskip = s2(iev,ist)
        if (phase .eq. 'p')then
          tskip = p(iev,ist)
          tplot = s1(iev,ist) - tskip - 0.05 * tseg
         else
          tplot = stop(iev,ist) - tskip
          if (tplot .lt. durmin) tplot = durmin
          if (tplot .gt. durmax) tplot = durmax
         endif
c
c       CHECK THAT DURN IS AT LEAST TWICE AS LONG AS TSEG
C
611     continue
        if (tplot .lt. (2.*tseg)) then
           npseg = npseg/2
           tseg = tseg/2.
           go to 611
        endif
        write(7,*)'*****************************************'
        write(1,*)'************ NOISE SPECTRUM ***************'
        if(its.eq.1)write(3,*)'*****************************************'
        if(its.eq.1)write(3,40)fname,elat,elon,mag,depth
        write(7,40)fname,elat,elon,mag,depth
        write(1,40)fname,elat,elon,mag,depth
        nseg = aint(2. * tplot/tseg) - 1
c**     CHECK THAT WE ARE NOT TOO CLOSE TO AN INTEGER MULTIPLE OF
C**     TSEG.  IF SO, INCREASE DURN BY 5% OF SEGMENT LENGTH.
C**     THIS ENSURES AVERAGING OF SIGNAL OVER SEGMENTS.
        time = tseg * float(nseg+1)/2.
        endfac = (tplot-time)/tseg
```

```
      if (endfac .lt. 0.05) tplot = tplot + 0.05*tseg
c**   USE 1-SEGMENT NOISE SAMPLE, STARTING 1.5 SEGMENTS BEFORE SIGNAL
c**   NORMALIZE ITS AMPLITUDE TO DURN OF ANALYZED SIGNAL.
      tskip1 = tskip - 1.5 * tseg
      nskip = ifix(sr*tskip1)
      nkeep = ifix(sr*tplot) + nskip + ifix(1.5*sr*tseg)
      ntaper = ifix(taper*sr*tplot)
      skip1 = aint(float(nskip)/10.)
      nrem = nskip-ifix(skip1)*10
      n2nois = nskip + npseg
      n1sig = nskip + ifix(1.5 * sr * tseg)
      nrems = n1sig-ifix(aint(float(n1sig)/10.))*10
      ntapns = ifix(taper * sr * tseg)
      inns = 1
      nread = 0
      index = 1
      iwts = 1
      jts = 0
      iwant = 1 + nrem
c
      do 80 j = 1,nline
        read(6,60)bufx
60      format(10i8)
        do 70 jj = 1,10
          ncheck = nread + jj
          if (ncheck .eq. (n2nois+1))iwant = nrems + 1
          if (ncheck .eq. iwts .and. its .eq. 1) then
            jts = jts + 1
            xts(jts) = float(bufx(jj))
            iwts = iwts + idects
          endif
          if(ncheck .le. nskip .or. ncheck .gt. nkeep) go to 70
          if(ncheck .gt. n2nois .and. ncheck .lt. n1sig) go to 70
          if(iwant .gt. 20 .or. iwant .lt. 1) iwant = jj
          if(jj .eq. iwant) then
            if(ncheck .lt. n1sig) then
c**           THIS IS IN THE NOISE WINDOW.
              call window(ncheck,nskip,n2nois,ntapns,wind)
              xre = wind * float(bufx(jj))
              xns(inns) = cmplx(xre,0.)
              inns = inns + 1
            else
c**           THIS IS IN THE SIGNAL WINDOW.
              call window(ncheck,n1sig,nkeep,ntaper,wind)
              xre = wind * float(bufx(jj))
              x(index)=xre
              if (abs(x(index)) .gt. valmax) valmax = abs(x(index))
              index = index + 1
            endif
            iwant = jj + idec
          endif
70      continue
        nread = nread + 10
        if(ncheck .gt. nskip .and. ncheck .le. n2nois)iwant=iwant-10
```

```
        if(ncheck .gt. nlsig .and. ncheck .le. nkeep)iwant=iwant-10
80     continue
       write(7,59)stadat,comp,dist,phase,tskip,tplot,dt,jts,nseg
       write(1,59)stadat,comp,dist,phase,tskip,tplot,dt,jts,nseg
59     format(2x,a3,2x,a1,' R = ',f6.1,/,2x,a1,4x,'tskip = ',
      *       f6.2, ' tplot = ',f6.2,' dt = ', f6.4,' jts = ',i5,
      *       ' nseg =',i5)
       if(its.eq.1)
      * write(3,59)stadat,comp,dist,phase,tskip,tplot,dts,jts,nseg
       if(its.eq.1)write(3,81)(xts(j),j=1,jts)
81     format(10e8.2)
       npts = index - 1
       if (nglit .ne. 0) call glitch(x,npts,valmax)
c
c      FIND PGV AND ASSOCIATED FREQUENCY (WITHIN SIGNAL WINDOW)
C
       pgv = 0.
       do 2000 ipgv = 1,npts
         if(abs(x(ipgv)) .gt. pgv) then
           pgv = abs(x(ipgv))
           inpgv = ipgv
         endif
2000   continue
        do 1000 ilook = 1,2
c            Look for zero-crossings in both directions from peak
             isign = (-1)**ilook
             is = 0
800          if(x(inpgv + isign*is) .gt. 0. .and.
     *          x(inpgv + isign*(is+1)) .le. 0.) go to 990
             if(x(inpgv + isign*is) .lt. 0. .and.
     *          x(inpgv + isign*(is+1)) .ge. 0.) go to 990
             is = is + 1
             go to 800
990          inzero(ilook) = inpgv + isign*(is+1)
1000     continue
           frpgv = 1./(2.*((inzero(2) - inzero(1))/sr))
         if (it.eq.1) call ectn1(frpgv,iresp,accresp,velresp,dspresp)
         if (it.eq.2) call ectn2(frpgv,iresp,accresp,velresp,dspresp)
         if (it.eq.3 .or. it.eq.4)
     *       call ectn3(frpgv,iresp,accresp,velresp,dspresp)
         if (it.eq.5) call ectn5(frpgv,iresp,accresp,velresp,dspresp)
         if (it.gt.6)write(*,*)' WARNING. itype not defined.'
         if (it .ne. 6) pgv = 1000. * pgv/cabs(velresp)
C
c      CHECK THAT THE SIGNAL IS LONG ENOUGH TO GIVE US THE
C      DESIRED MINM NUMBER OF SEGMENTS OVER WHICH TO AVERAGE.
       tsig = tplot
       if (nseg .lt. minseg) then
c        TOO FEW SEGMENTS.  FILL IN SIGNAL ARRAY WITH REPEATS
         tfill = tseg * float(minseg+1)/2. - tplot
         nfill = ifix(tfill/dt)
         i = 1
         do 120 ifill=1,nfill
           x(npts+ifill) = x(i)
```

```
          i = i + 1
          if (i .gt. npts) i = 1
120     continue
c**     RESET PARAMETERS TO NEW SIGNAL LENGTH.
        npts = npts + nfill
        nseg = minseg
        tplot = tsig + tfill
      endif
c
      ii=3
101   ncheck = 2**ii
      if (ncheck .ge. npseg) go to 110
      ii = ii+1
      go to 101
110   if(ncheck .ne. npseg) write(*,*)' ERROR. npseg must be power of 2'
      if(npts .gt. 15000 .or. jts .gt. 1000) then
        write(*,*)' Exceeds array dimensions.'
        stop
      endif
c
c     OBTAIN SPECTRUM FROM THE AVERAGE POWER OF THE SEGMENTS,
C     MULTIPLIED BY DURN.
C     FOR INCOMPLETE (UNANALYZED) SEGMENT AT END OF RECORD, ASSUME
C     POWER IS SAME AS PREVIOUS SEGMENT, AND ADJUST LAST SEGMENT
C     TO INCLUDE THIS POWER.
c     CORRECT FOR INSTRUMENT RESPONSE AMPLITUDE AFTER AVERAGING.
C
      ncall = npseg/2
      do 212 j = 1, ncall
        avg(j) = 0.
212   continue
      time = tseg * float(nseg+1)/2.
      endfac = 1. + (tplot-time)/tseg
      df = sr/(float(npseg * idec))
      istart = 0
c
      do 115 iseg = 1, nseg
        do 114 jj = 1, npseg
          cx(jj) = cmplx(x(jj+istart),0.)
114     continue
        call fork(npseg,cx,-1.)
c
      do 150 j=1, ncall
c      ACCUMULATE SQUARED AMPLITUDES.
       valsq = cabs(cx(j))**2
       if(iseg .eq. nseg)valsq = valsq * endfac
       avg(j) = valsq + avg(j)
150   continue
c
c     WE HAVE ADDED THIS SEGMENTS'S SQUARED SPECTRUM TO THE TOTAL POWER
C     ADJUST INDICES TO MOVE WINDOW ALONG.
      istart = istart + npseg/2
115   continue
C     FFT SQUARED AMPLITUDES HAVE BEEN SUMMED OVER ALL WINDOWS.
```

```
c     TAKE SPECTRUM OF NOISE WINDOW (NOT SQUARED)
c
      call fork(npseg,xns,-1.)
      scale = sqrt(float(npseg))/(sr*float(idec))
      do 130 k = 1, ncall
c      NORMALIZE TO AVG. POWER PER UNIT TIME, THEN GET TOTAL POWER FOR
c      DURN OF SIGNAL.  VELOCITY SPECTRUM IS ROOT OF THIS * SCALE FACTOR
c      .  FOR NOISE, NORMALIZE TO SIGNAL DURN.
       adnseg = float(nseg) + endfac - 1.
       avg(k) = ((avg(k)/adnseg)/tseg) * tsig
       avg(k) = scale * sqrt(avg(k))
       ampns(k) = scale * sqrt(tplot/tseg) * cabs(xns(k))
C     NOW CORRECT FOR INSTRUMENT RESPONSE (AMPLITUDE ONLY).
c
       f = float(k-1)*df
       if (f .eq. 0.) f = df/2.
c     Use it = 6 to skip all transfer functions (and mm conversion)
      if (it .eq. 6) go to 129
        if (it.eq.1) call ectn1(f,iresp,accresp,velresp,dspresp)
        if (it.eq.2) call ectn2(f,iresp,accresp,velresp,dspresp)
        if (it.eq.3 .or. it.eq.4)
     *      call ectn3(f,iresp,accresp,velresp,dspresp)
        if (it.eq.5) call ectn5(f,iresp,accresp,velresp,dspresp)
        avg(k) = avg(k)/cabs(velresp)
        ampns(k) = ampns(k)/cabs(velresp)
c
c       Convert to mm
        avg(k) = 1000. * avg(k)
        ampns(k) = 1000. * ampns(k)
C
c       CONVERT TO ACCN OR DISPLACEMENT IF DESIRED.
129     continue
        if (igmtn .eq.0) then
          avg(k) = avg(k)/(2.*pi*f)
          ampns(k) = ampns(k)/(2.*pi*f)
        endif
        if (igmtn .eq.2) then
          avg(k) = avg(k)*2.*pi*f
          ampns(k) = ampns(k) * 2.*pi*f
        endif
130   continue
c
      write(7,140)df,ncall,pgv, frpgv
      write(1,140)df,ncall,pgv, frpgv
140   format(' df = ',f10.4,2x,' npts = ',i4,
     *       ' PGV = ',1pe10.2, ' frpgv = ',0pf6.2)
      write(7,141)(avg(j),j=1,ncall)
      write(1,141)(ampns(j),j=1,ncall)
141   format(8(1pe10.2))
C     GO ON TO NEXT COMPONENT.
      go to 45
c
c     GO ON TO NEXT EVENT.
100   continue
```

```
      close(6)
      go to 35
c
200   stop
      end
c*****************************************************************
      subroutine table(stadat,xlon,xlat,it)
      common stanam,stalat,stalon,nsta,itype
      dimension stalat(100),stalon(100),itype(100)
      character*3 stanam(100),stadat
      do 100 j = 1, nsta
        if (stadat .eq. stanam(j)) then
          xlon = stalon(j)
          xlat = stalat(j)
          it = itype(j)
          return
        endif
100   continue
      xlon = 0.
      return
      end
c*****************************************************************
      SUBROUTINE SDIST(RAD,THET1,THI1,THET2,THI2,DIST,ID)
      REAL LAT1,LON1,LAT2,LON2,DIST
C
C     CALCULATES THE SURFACE DISTANCE BETWEEN TWO POINTS ON THE EARTH.
      IC=-ID
      CALL SPHER(X1,Y1,Z1,1.,THET1,THI1,IC)
      CALL SPHER(X2,Y2,Z2,1.,THET2,THI2,IC)
      DIST=(X1-X2)**2+(Y1-Y2)**2+(Z1-Z2)**2
      DIST=SQRT(DIST)
      RADIAN=2.*ASIN(DIST/2.)
      DIST=RAD*RADIAN
      RETURN
      END
C*****************************************************************
      SUBROUTINE SPHER(X,Y,Z,R,THETA,THI,IC)
C     CONVERTS RECTANGULAR TO SPHERICAL COORDINATES AND VICE-VERSA
C     IC+VE.......INPUT RECTANGULAR X,Y,Z
C     IC-VE.......INPUT WPHERICAL R,THETA,THI
C     IF(IABS(IC).EQ.2)ANGLES ARE IN DEGREES
      PI=3.14159
      DC=1.
       IF(IABS(IC).EQ.2)DC=PI/180.
      IF(IC.LT.0)GO TO 20
C     CHANGE RECTANGULAR TO SPHERICAL.
      R=SQRT(X*X+Y*Y+Z*Z)
      THETA=ATAN2(Y,X)/DC
      THI=ASIN(Z/R)/DC
      RETURN
C     CHANGE SPHERICAL TO RECTANGULAR.
20    X=R*COS(DC*THETA)*COS(DC*THI)
      Y=R*SIN(DC*THETA)*COS(DC*THI)
      Z=R*SIN(DC*THI)
```

```
      RETURN
      END
c*********************************************************************
      subroutine fork(lx,cx,signi)
c
c     fast fourier transform routine from Dave Boore.
c     result of sequence from time to freq to time requires no scaling.
c**   Scaling from time to freq = dt * sqrt(lx)
c**   Scaling from freq to time = sqrt(lx)/(lx*dt)
c**                        lx
c**   cx(k)=sqrt(1./lx)*sum(cx(j)*exp(2*pi*signi*iI(j-1)*(k-1)/lx))
c**                       j=1                  for k=1,2,...lx
c
c
$LARGE
      complex cx,carg,cexp,cw,ctemp
      dimension cx(lx)
      j=1
      sc=sqrt(1./lx)
      do 5 i=1,lx
          if(i .gt. j) go to 2
          ctemp = cx(j)*sc
          cx(j) = cx(i)*sc
          cx(i) = ctemp
2         m = lx/2
3         if(j .le. m) go to 5
            j = j - m
            m = m / 2
            if(m .ge. 1) go to 3
5     j = j + m
      l = 1
6     istep = 2 * l
      temp = 3.14159265 * signi/l
      do 8 m = 1, l
          carg=(0., 1.) * temp * (m-1)
          cw=cexp(carg)
          do 8 i = m, lx, istep
               ctemp = cw *cx(i+l)
               cx(i+l) = cx(i) - ctemp
8     cx(i) = cx(i) + ctemp
      l = istep
      if(l .lt. lx) go to 6
9     return
      end
c*********************************************************************
      subroutine glitch(x,npts,valmax)
c
c     Removes glitches from array x and makes corresponding
c     correction to valmax.
c     Anything >10* the (log) avg of a running 20-pt. amplitude
c     average is assumed to be a glitch.  Replaced with avg of
c     neighbour values.
c     Constant amplitude steps (more than 20 identical values
c     in a row) are assumed to be glitches.  Replaced with 0
```

```
c
c     G.M. Atkinson, Oct. 1990
c     Revised Aug. 1991
c
$LARGE
      dimension x(npts),ipick(10)
      valmax = 0.
c
c     First remove constant amplitude steps.
c     If next 20 values are exactly the same as this one,
c     we assume its an erroneous step.
c
      jstop = 0
      do 500 j=1,npts-20
        iflag = 1
        do 400 jj = 1,20
          if(x(j+jj) .ne. x(j)) iflag = 0
400     continue
      if (iflag .eq. 1) then
c     This is a step.
          jstop = j + 20
        write(*,*)' WARNING. LONG GLITCH REMOVED.'
        endif
        if (jstop .ge. j) x(j) = x(j+20)
500   continue
c
        ntotal = 0
49      continue
        runavg = 0.
        nspike = 0
        do 50 jj = 1,21
          if(x(jj) .eq. 0.) x(jj)=1.
          runavg = runavg + alog10(abs(x(jj)))
50      continue
        runavg=runavg/21.
      do 100 j=11,npts-11
           if(x(j-10) .eq. 0.) x(j-10)=1.
           if(x(j+11) .eq. 0.) x(j+11)=1.
         runavg =runavg - alog10(abs(x(j-10)))/21.
     *             + alog10(abs(x(j+11)))/21.
         spike = 10.* 10.**runavg
         if(abs(x(j)) .gt. spike) then
            nspike = nspike + 1
            x(j) = (x(j-1) + x(j+1))/2.
            if(abs(x(j)) .gt. spike)then
              x(j) = (x(j-2) + x(j+2))/2.
              if(abs(x(j)) .gt. spike) x(j) = 1.
            endif
          endif
        if(abs(x(j)) .gt. valmax) valmax = abs(x(j))
100   continue
      ntotal = ntotal + nspike
      if (nspike .gt. 1) go to 49
      if (ntotal .gt. 10) write(*,101) ntotal
```

```
101   format( ' WARNING.', i6, ' GLITCHES REMOVED FROM RECORD')
      return
      end
```

```
c*************************************************************************
      subroutine ectn1(freq, iresp,respa,velresp,dspresp)
$STORAGE:4
$LARGE
      complex s,z1,z2,z3,z4,z5,Z6,velresp,respa,dspresp
      velresp = 1.
      pi = 3.14159265
c
c     transfer function for ECTN Mark I stn
c     from Bill Shannon, Jan. 1989
c
      w = 2.*pi*freq
      s = cmplx(0.,w)
      if(iresp .eq. 0) go to 20
      z1=s/(s+0.6283)
      z2=s**2/(s**2+8.8844*s+(2.*pi)**2)
      z3=125.664/(s+125.664)
      z4=125.664**2/(s**2+203.324*s+125.664**2)
      z5=125.664**2/(S**2+77.66*S+125.664**2)
      velresp = z1*z2*z3*z4*z5
20    Z6=1.E08
      velresp=velresp*Z6
      respa=velresp*cmplx(0.,-1./w)
      dspresp=velresp*cmplx(0.,w)
      return
      end
```

PROGRAM: FIT

PURPOSE: Perform iterative regression analyses on ground motion data to determine source and site terms and attenuation coefficients. Options for linear, bilinear or trilinear forms. Program is run several times to refine site terms. Program is run iteratively to find transition distances.

INPUTS: Summary file of ground motion amplitudes to be regressed, including event names, station names and distances.

OUTPUTS: Files giving source terms, site terms and attenuation coefficients. Source terms are at a distance of 1 km. (Note: Geometric attenuation of r**-1 is assumed from 1 to 10km.)

```
      program fit
c
c     Program to find best fit (minimum squared-error) attenuation,
c     (geom. and Q), source and site terms for ECTN spectral data, read
c     from output files from SUMMARY or COMPILE programs.  Reads input
c     site terms from a station file, and writes a new site term file.
c     This version uses r**-c spreading for r>rfar km, and
c     fits applicable g.  Attenuation rnear<r<rfar km is also found.
c     This is similar to fitfi except b, c and t vary with freq.
c
c     G.M. Atkinson, Sept. 1991
c     Modified Oct. 1991
c     Modified to increment over transition slope, Feb. 1992
c     Constraint on average rock site term (=0), Apr. 92
c     Also print best freq-ind. values for b,t,c.  Note that
c     if we re-run program using these values we can generate
c     corresponding error arrays, residuals etc. (May 92)
c
$LARGE
$STORAGE:2
      common b. c, g, rnear, rfar, t
      common fa(1800,11), r(1800), reso(40,11), RES(40,11), istn(1800)
      character*3 stn(60), bufs
      character*9 bufe, eprev, event(200),fname
      character*60 header
      integer ievent(1800), nptev(150), ndiv(150,11)
      integer nres(40,11), nsum(11)
      dimension amag(150),fl(11), tval(10),cval(10),bval(10),qval(10)
      dimension savg(150,11), sd(10,10,10,10), bbest(11)
      dimension sigavg(150,11), resobs(1800,11), sdf(10,10,10)
      dimension sigres(40,11)
c
      nrdstn = 3
      nwrstn = 7
      nwr=6
      nrdopt = 4
      nrddat = 5
      nwrres = 2
      write(*,*)' Filename for program options ?'
      read(*,10) fname
10    format(a)
      open(nrdopt, file=fname)
      write(*,*)' Data filename ?'
      read(*,10)fname
      open(nrddat,file=fname)
      write(*,*)' Filename for input station terms ? '
      read(*,10)fname
      open(nrdstn, file=fname)
      write(*,*)' Output filename for fits ?'
      read(*,10)fname
      open(nwr,file=fname,status='new')
      write(*,*)' Filename for output station terms ?'
      read(*,10)fname
      open(nwrstn,file=fname,status='new')
```

```
      write(*,*)' Filename for output fit residuals ?'
      read(*,10)fname
      open(nwrres,file=fname,status='new')
c
      read(nrdopt,10) header
      write(nwr,10)header
      read(nrdopt,*) nfreq
      write(nwr,12) nfreq
      read(nrdopt,*)bo, binc, nb
      read(nrdopt,*)co, cinc, nc
      read(nrdopt,*)qo, qinc, nq
      write(nwr,16) bo, binc, nb
      write(nwr,16) co, cinc, nc
      write(nwr,16) qo, qinc, nq
      if(nq .gt. 10 .or. nb .gt. 10 .or. nc .gt. 10) write(*,*)
     *  '  ERROR.  TOO MANY ITERATIONS FOR DIMENSIONS.'
12    format(' Following are (initial value, delta, nval) for b, c, Q'
     *       ,/,' nfreq =',i5)
16    format(2f10.2,i5)
      read(nrdopt,*)iopd
      if(iopd .eq. 1)then
        read(nrdopt,*)rmin,rmax
        write(nwr,13)rmin,rmax
13      format(' fits for rmin to rmax: ',2f10.1)
      else
        rmin = 0.
        rmax = 10000.
      endif
      read(nrdopt,*)rnear, rfar
      write(nwr,14)rnear, rfar
14    format(/,' Attenuation between ', 2f10.1)
      read(nrdopt,*)to, tinc, nt
      write(nwr,17) to, tinc, nt
17    format(' Has slope (to, delta, nval) = ', 2f8.2,i5)
      read(nrdstn,10)header
      write(nwrstn,10)header
      read(nrdstn,10)header
      write(nwrstn,10)header
      i = 1
20    read(nrdstn,30,end=40)stn(i)
30    format(16x,a3)
      read(nrdstn,35)(reso(i,if),if=1,11)
35    format(3x,11f7.3)
      read(nrdstn,35)
      i = i + 1
      go to 20
40    nsta = i - 1
c
      do 34 jt = 1, nt
        do 32 ii = 1,nc
          do 31 iiii = 1,nb
            sdf(iiii,ii,jt)=0.
31        continue
32      continue
```

```
34    continue
      do 46 jf = 1, nfreq
        nsum(jf) = 0
        do 45 i = 1, 200
          ndiv(i,jf) = 0
45      continue
46    continue
c
      read(nrddat,50)f1,df
50    format(31x,2f10.2)
      write(nwrres,50)f1,df
      do 60 i = 1,18
        read(nrddat,10)header
60    continue
      iev = 0
      i = 1
      eprev = '          '
      do 65 ii = 1,200
        nptev(ii)=0
65    continue
70    read(nrddat,80,end=100)bufe,bufm,bufs,r(i),(fa(i,j),j=1,11)
      r(i) = 10.**r(i)
      if (r(i) .lt. rmin .or. r(i) .gt. rmax) then
c       WE WANT TO SKIP THIS POINT, SO SET FA TO 'UNDEFINED'
        do 71 j=1,11
          fa(i,j)=9.99
71      continue
      endif
c
      if(bufe .ne. eprev) iev = iev + 1
      event(iev) = bufe
      amag(iev) = bufm
      nptev(iev) = nptev(iev) + 1
      ievent(i) = iev
c
c     find corresponding station index
c
      do 75 ii = 1, nsta
        if(bufs .eq. stn(ii)) istn(i) = ii
75    continue
      do 76 jf = 1, nfreq
        if(fa(i,jf) .eq. 9.99) go to 76
        ndiv(iev,jf) = ndiv(iev,jf) + 1
        nsum(jf) = nsum(jf) + 1
76    continue
      i = i + 1
      eprev = bufe
      go to 70
80    format(a9,1x,f3.1,1x,a3,4x,f4.2,11f5.2)
100   nobs = i - 1
      nev = iev
      write(*,*)' Data read: nev, nobs, nsum(jf) are '
      write(*,*) nev, nobs, (nsum(jf),jf=1,nfreq)
c
```

```
c     Data have been read into arrays.  Do regression loops:
c     freq , b, c, g.
c
      sdfmin = 1000.
c     LOOP ON FREQUENCY
      do 2000 jf = 1, nfreq
        write(*,*)' FREQ LOOP'
        write(*,*)jf
        fl(jf) = fl + float(jf-1)*df
        freq = 10.**fl(jf)
c
      do 44 jt = 1, nt
        do 42 ii = 1,nc
         do 43 iii = 1,ng
          do 41 iiii = 1,nb
          sd(iiii,ii,iii,jt)=0.
41        continue
43       continue
42      continue
44    continue
c
        if(nsum(jf) .lt. 3) go to 2000
        do 110 j = 1, nev
          if(ndiv(j,jf) .lt. 3) nsum(jf)=nsum(jf)-ndiv(j,jf)
110     continue
        if (nsum(jf) .lt. 3) go to 2000
c       LOOP ON GEOMETRIC SPREADING VALUES.
        sdmin = 1000.
c       OUTER LOOP ON TRANSITION SLOPE.
C
        do 1900 jt = 1, nt
          t = float(jt-1)*tinc + to
          tval(jt) = t
c
c       loop over b values.
c
        do 1500 jb = 1, nb
          b = float(jb-1)*binc + bo
          bval(jb) = b
c
c       loop over c values.
c
        do 1000 jc = 1, nc
          c = float(jc-1)*cinc + co
          cval(jc) = c
c
c       loop over Q values
c
         do 900 jg = 1,nq
            q = float(jg-1)*qinc + qo
            g = 3.14159*freq*0.4342/(q*3.8)
            qval(jg) = q
            do 151 i = 1,nev
              savg(i,jf)=0.
```

```
151          continue
c
c           We have defined b, c, gamma, t. Find implied source levels.
c
            do 150 jobs = 1, nobs
              if(fa(jobs,jf) .eq. 9.99) go to 150
              savg(ievent(jobs),jf) =savg(ievent(jobs),jf) + src(jobs,jf)
150         continue
            do 155 iev = 1, nev
              if (ndiv(iev,jf) .ge. 3) then
               savg(iev,jf)=savg(iev,jf)/float(ndiv(iev,jf))
              else
               savg(iev,jf)=9.99
              endif
155         continue
c
c           COMPUTE ERRORS.
            do 160 jobs = 1, nobs
              if(fa(jobs,jf) .eq. 9.99) go to 160
              if(savg(ievent(jobs),jf) .eq. 9.99) go to 160
              err=abs(savg(ievent(jobs),jf) - src(jobs,jf))
              sd(jb,jc,jg,jt) = sd(jb,jc,jg,jt) + err
160         continue
c**         sd is the average absolute value of the error of
c            an observation.  Our best fit minimizes sd.
c
            if(nsum(jf) .ge. 3) then
              sd(jb,jc,jg,jt) = sd(jb,jc,jg,jt)/float(nsum(jf))
            else
              sd(jb,jc,jg,jt) = 9.99
            endif
c
            if (sd(jb,jc,jg,jt) .lt. sdmin) then
c             This is the best soln so far.
              sdmin = sd(jb,jc,jg,jt)
              iming = jg
              iminc = jc
              iminb = jb
              imint = jt
              gbest = g
              qbest = q
              cbest = c
              bbest(jf) = b
              tbest = t
            endif
900       continue
c
          sdf(jb,jc,jt)=sdf(jb,jc,jt) + sd(jb,jc,iming,jt)
           if (jf .eq. nfreq .and. sdf(jb,jc,jt) .lt. sdfmin) then
c            Best freq-independent solution
             sdfmin = sdf(jb,jc,jt)
             iminbf = jb
             imincf = jc
             imintf = jt
```

```
            bf = b
            cf = c
            tf = t
          endif
1000     continue
1500     continue
1900     continue
         WRITE(*,*)' ERROR SPACE MAPPED FOR F'
c
c        We have mapped the error space, sd(jb, jr, jg, jt).
c        Now we want to compute avg. residuals by station for this f.
c        But first we must recompute the soln SRC and SAVG arrays
c        We also compute standard errors of coefficients and SAVG
c
         do 184 i = 1, nev
           savg(i,jf)=0.
184      continue
         b = bbest(jf)
         c = cbest
         g = gbest
         t = tbest
         q = qbest
c
         do 185 jobs = 1, nobs
           if(fa(jobs,jf) .eq. 9.99) go to 185
           if(ndiv(ievent(jobs),jf) .lt. 3) go to 185
           savg(ievent(jobs),jf) = savg(ievent(jobs),jf) + src(jobs,jf)
185      continue
         kl = 0
         do 186 iev = 1, nev
           sigavg(iev,jf) = 0.
           if (ndiv(iev,jf) .ge. 3)then
            savg(iev,jf) = savg(iev,jf)/float(ndiv(iev,jf))
            do 187 ii = 1, nptev(iev)
             if (fa(kl+ii,jf) .eq. 9.99) go to 187
             sigavg(iev,jf) = sigavg(iev,jf) + (savg(iev,jf) -
     *                        src(kl+ii,jf))**2
187          continue
            sigavg(iev,jf) = sqrt(sigavg(iev,jf))/float(ndiv(iev,jf))
           else
            savg(iev,jf)=9.99
           endif
         kl = kl + nptev(iev)
186      continue
         do 190 i = 1, nsta
           res(i,jf) = 0.
           nres(i,jf) = 0
190      continue
         do 200 jobs = 1, nobs
           if(fa(jobs,jf) .eq. 9.99) go to 200
           if(savg(ievent(jobs),jf) .eq. 9.99) go to 200
           res(istn(jobs),jf) = res(istn(jobs),jf) + src((jobs),jf)
     *                          - savg(ievent(jobs),jf)
           nres(istn(jobs),jf) = nres(istn(jobs),jf) + 1
```

```
200     continue
c
        do 210 i = 1, nsta
          sigres(i,jf) = 0.
          if(nres(i,jf) .ge. 3) then
           res(i,jf) = res(i,jf)/float(nres(i,jf)) + reso(i,jf)
          else
           res(i,jf) = reso(i,jf)
          endif
210     continue
c
c       Now adjust station terms to get 0 average on rock.
c
        sum = 0.
        n = 0
        do 215 i = 1, nsta
          if (stn(i) .eq. 'WEO' .or. nres(i,jf) .lt. 3) go to 215
          sum = sum + res(i,jf)
          n = n + 1
215     continue
        sum = sum/float(n)
        do 218 i = 1, nsta
          if (nres(i,jf) .lt. 3) go to 218
            res(i,jf) = res(i,jf) - sum
218     continue
c
        do 220 jobs = 1, nobs
          resobs(jobs,jf) = 9.99
          if(fa(jobs,jf) .eq. 9.99) go to 220
          fact = src(jobs,jf) - savg(ievent(jobs),jf)
     *           - (res(istn(jobs),jf) - reso(istn(jobs),jf))
          if(ndiv(ievent(jobs),jf) .ge. 3) resobs(jobs,jf) = fact
          if(savg(ievent(jobs),jf) .eq. 9.99) go to 220
          if(nres(istn(jobs),jf) .lt. 3) go to 220
          sigres(istn(jobs),jf) = sigres(istn(jobs),jf) + fact*fact
220       continue
          do 230 i = 1,nsta
            if(nres(i,jf) .ge. 3) then
              sigres(i,jf)=sqrt(sigres(i,jf))/float(nres(i,jf))
            else
              sigres(i,jf) = 0.
            endif
230       continue
      WRITE(*,*)' STATION RESIDUALS DEFINED FOR F'
c
c     CALCULATE ERRORS IN COEFFICIENTS.
C
      sigb = 0.
      sigc = 0.
      sigt = 0.
      sigg = 0.
      nclos1 = 0
      nclos2 = 0
      nclos3 = 0
```

```
      rnl = alog10(rnear)
      rfl = alog10(rfar)
      do 600 jobs = 1, nobs
        if(fa(jobs,jf) .eq. 9.99) go to 600
        if(ndiv(ievent(jobs),jf) .lt. 3) go to 600
        rl = alog10(r(jobs))
        if(r(jobs) .le. rnear) then
c         The residual could only be due to an error in b.
          nclos1 = nclos1 + 1
          sigb = sigb + (resobs(jobs,jf)/rl)**2
        endif
        if (r(jobs) .gt. rnear .and. r(jobs) .lt. rfar) then
c         The residual could be due to an error in b or t.
          nclos2 = nclos2 + 1
          sigb = sigb + (resobs(jobs,jf)/rnl)**2
          sigt = sigt + (resobs(jobs,jf)/(rl-rnl))**2
        endif
        if (r(jobs) .ge. rfar) then
c         The residual could be due to an error in b, t, c or Q
          nclos3 = nclos3 + 1
          sigb = sigb + (resobs(jobs,jf)/rnl)**2
          sigt = sigt + (resobs(jobs,jf)/(rfl-rnl))**2
          sigc = sigc + (resobs(jobs,jf)/rl)**2
          sigg = sigg + (resobs(jobs,jf)/r(jobs))**2
        endif
600   continue
      sigb = sqrt(sigb/(float(nclos1+nclos2+nclos3)))
      sigt = sqrt(sigt/(float(nclos2+nclos3)))
      sigc = sqrt(sigc/float(nclos3))
      sigg = sqrt(sigg/float(nclos3))
c     Equivalent error in Q from that in g
      sigq = (sigg/g) * q
c
      write(nwr,221)freq
221   format(/,'freq = ', f7.3)
      write(nwr,232)b, t, c, g, Q
232   format(' Best values b, t, c, g, Q: ',3f10.2,f10.6,f10.1)
      write(nwr,234)sigb, sigt, sigc, sigg, sigq
234   format(' Errors in coefficients:    ',3f10.2,f10.6,f10.1)
      write(nwr,233)sdmin
233   format(' Average error in an observation = ',f10.4)
c
c     Now print out error arrays in contour-ready format.
c     First comparison of interest is trade-off between c and Q
c     (use the best b and t values).
c
      write(nwr,295)
295   format(/,' Average log errors as fn. of c and Q  ')
      write(nwr,300)(cval(i),i=1,nc)
300   format( '       c =',10f7.2)
      write(nwr,*)'  Q '
      do 310 jq = 1, nq
        write(nwr,320)qval(jq), (sd(iminb, ic, jq, imint), ic = 1,nc)
320     format(f8.1,2x,10f7.4)
```

```
310   continue
c
c     For best values of c and Q, show the trade-off between b and t
c
      write(nwr,330)
330   format(/,' Average log errors as fn. of b and t ')
      write(nwr,340)(bval(i),i=1,nb)
340   format('       b =',10f7.2)
      write(nwr,*)'  t '
      do 350 jt = 1, nt
        write(nwr,360)tval(jt), (sd(ib, iminc, iming, jt), ib = 1,nb)
360     format(f8.2,2x,10f7.4)
350   continue
c
2000  continue
      write(nwr,*)'  '
      write(nwr,*)' Best freq-independent coef:'
      write(nwr,700)bf, tf, cf
700   format(' b, t, c: ',3f10.2)
      errf = sdf(iminbf,imincf,imintf)/float(nfreq)
      write(nwr,710)errf
710   format(' Avg. error = ',f10.4)
c
      write(nwr,246)
246   format(//,' Source terms in log units(mm/s):'
     *  ,/)
      do 260 i = 1, nev
        iflag = 0
        do 261 ii = 1,nfreq
          if(savg(i,ii) .ne. 9.99) then
            iflag = 1
c           Correct source terms; R**-1 spreading from 1 to 10 km
            if (bbest(ii) .gt. 1.0) savg(i,ii) = savg(i,ii)
     *        - (bbest(ii) - 1.0)
          endif
261     continue
        if (iflag .eq. 0) go to 260
        write(nwr,250)event(i),(savg(i,jf),jf=1,nfreq)
        write(nwr,265)(sigavg(i,jf),jf=1,nfreq)
265     format(6x,'+/- ',11f6.2)
260   continue
250   format(a9,1x,11f6.2)
c
      do 280 i = 1,nsta
        write(nwrstn,30)stn(i)
        write(nwrstn,282)(res(i,jf),jf=1,nfreq)
282     format('Sj ',11f7.3)
        write(nwrstn,281)(sigres(i,jf),jf=1,nfreq)
281     format('+/-',11f7.3)
280   continue
c
c     Finally, print out the residuals for further analyses.
c
      write(nwrres,480)
```

```
480   format(,' Residuals of observations ',/,
     * '  Event     M  STN    log R    log FFT - log PRED : ')
      do 470 jobs = 1, nobs
        bufs = stn(istn(jobs))
        r(jobs) = alog10(r(jobs))
        write(nwrres,80)event(ievent(jobs)),amag(ievent(jobs)),bufs,
     *    r(jobs),(resobs(jobs,jf),jf=1,nfreq)
470   continue
      stop
      end
c*****************************************************************
      real function src(jobs,jf)
      common b, c, g, rnear, rfar, t
      common fa(1800,11), r(1800), reso(40,11), RES(40,11), istn(1800)
c
      x = fa(jobs, jf) - reso(istn(jobs), jf)
      if (r(jobs) .le. rnear) src = x + b*alog10(r(jobs)) + g * r(jobs)
      if (r(jobs) .gt. rnear .and. r(jobs) .lt. rfar) src = x
     *         + b*alog10(rnear) + g*r(jobs) + t*alog10(r(jobs)/rnear)
      if (r(jobs) .gt. rfar) src = x + b*alog10(rnear) + g*r(jobs)
     *         + c*alog10(r(jobs)/rfar) + t*alog10(rfar/rnear)
      return
      end
```

PROGRAM: MONTE

PURPOSE: Generate a simulated dataset for regression analysis, by Monte Carlo simulations based on modifications to ECTN dataset. (New dataset to have same distribution in distance.)

INPUTS: Summary ground motion data file, output files from regression analyses of the ground motion data, desired variance.

OUTPUTS: Simulated summary ground motion datafile.

```
      program MONTE
c
c     Reads a FA data file used for regression (FIT), and the output
c     files for source, site and residual terms.
c     Calculates underlying ideal FA values for the regression form,
c     subtracting off source, site and residuals (normalizing to
c     zero source and site, with no error).
c     Generates new data file for regression, for a specified value
c     of average standard error of observation (random error), using
c     Monte Carlo.
c     Regression of new data to same functional form should yield
c     zero source and site terms, and zero error.
c
c     G.M. Atkinson, April 23, 1992.
c*
$LARGE
$STORAGE:2
      dimension fft(12), evmag(200), source(200,11), sj(40,11), res(12)
      real*8 seed
      character*60 ti
      character*20 title
      character*9 bufe, eprev, evnam(20), evsrc(200), bufe2,fname
      character*3 bufs, bufc, site(40), bufs2, bufc2
      nrd=5
      nrdsrc =6
      nrdstn =3
      nrdres =2
      nwr = 4
      write(*,*)' Enter name of data file >'
      read(*,5) fname
5     format(a)
      open(nrd,file=fname)
      write(*,*)' Enter name of residual file >'
      read(*,5)fname
      open(2,file=fname)
      read(nrdres,*)
      read(nrdres,*)
      read(nrdres,*)
c
c     READ IN SOURCE AND SITE TERMS
C
c
      write(*,*)' Filename for site terms ?'
      read(*,5)fname
      open(nrdstn,file=fname)
      nstn = 1
      read(nrdstn,*)nfs,flch, dfch
300   read(nrdstn,310,end=390)site(nstn), (sj(nstn,j), j=1,nfs)
310   format(/,16x,a3,/,3x,12f7.3)
      nstn = nstn + 1
      go to 300
390   nstn = nstn - 1
c
      write(*,*)' Filename for source terms ?'
```

```
      read(*,5)fname
      open (nrdsrc,file=fname)
 16   read(nrdsrc,210)fname
      if (fname .ne. ' Source t')go to 16
      read(nrdsrc,5)
      nsrc = 1
 200  read(nrdsrc,210,end=290)evsrc(nsrc), (source(nsrc,j), j=1,nfs)
 210  format(a9,1x,12f6.2)
      nsrc = nsrc + 1
      read(nrdsrc,*)
      go to 200
 290  nsrc = nsrc - 1
c
      write(*,*)' Output filename ?'
      read(*,5)fname
      open(nwr,file=fname,status='new')
c
c     get random number generation working.
c
      write(*,*)' Enter seed, variance for data generation > '
      read(*,*) seed, var
      do 320 j = 1, 20
        call randerr(seed,var,error)
320   continue
c
      inev = 0
c**    Read data and correct point-by-point.
      eprev = '          '
8     format(31x,2f10.2)
      read(nrd,8)fl1,dfl
      write(nwr,8)fl1,dfl
        if(fl1 .ne. flch .or. dfl .ne. dfch)then
         write(*,*)' MISMATCH IN DATA VS. SOURCE TERM FREQUENCIES .'
        endif
        if (fl1 .eq. 0. .and. dfl .eq. 0.) ifpgv = 2
      do 10 i = 1,18
        read(nrd,5) ti
        write(nwr,5)ti
10    continue
c
c     LOOP OVER DATA POINTS.
C
149   read(nrd,150,end=500)bufe,valmag,bufs,bufc,bufr,fft
150   format(a9,1x,f3.1,1x,2a3,f5.2,12f5.2)
      read(nrdres,150)bufe2,valmag2,bufs2,bufc2,bufr2,res
c
      if (bufe .ne. eprev) then
c**    New event.
        eprev = bufe
        inev = inev + 1
        evnam(inev) = bufe
        evmag(inev) = valmag
c
c         FIND SOURCE TERM FOR THIS EVENT AND STN TERM 1ST OBS.
```

```
c
          iflag = 0
            do 400 ii = 1, nsrc
              if (evnam(inev) .eq. evsrc(ii)) then
                insrc=ii
                iflag = 1
              endif
400           continue
        if (iflag .eq. 0) write(*,401)evnam(inev)
401     format(' Cannot find source term for ',a9)
c
            do 410 ii = 1, nstn
              if(bufs .eq. site(ii)) insite=ii
410         continue
c
      else
c**     This is another component for the current event.
c
c       FIND STATION TERM FOR THIS OBSERVATION
C
            isfl = 0
            do 610 ii = 1, nstn
              if(bufs .eq. site(ii)) then
                insite=ii
                isfl = 1
              endif
610         continue
        if (isfl .eq. 0) write(*,611)bufs
611     format(' Cannot find site term for ',a3)
c
      endif
c
c     Have found index of source and site term for this observation.
c     Calculate underlying ideal observation.
c
      do 600 jf = 1, nfs
        if(fft(jf) .eq. 9.99) go to 600
        fft(jf) = fft(jf) - source(insrc,jf) - sj(insite,jf) - res(jf)
c       Add error to ideal observation.
        call randerr(seed, var, error)
        fft(jf) = fft(jf) + error
        if(source(insrc,jf) .eq. 9.99) fft(jf) = 9.99
600   continue
      write(nwr,150)evnam(inev),evmag(inev),bufs,bufc,bufr,
     *              (fft(j),j=1,nfs)
      go to 149
c
500   stop
      end
c*************************************************************
      subroutine randerr(seed, var, error)
c
c     Generates Gaussian noise by approx. method of Ross(1985)
c     G. Atkinson, May 92 (same as function ggnqf)
```

```
c
      real*8 seed, usum
      usum = 0.0000000000
      do 20 j=1,12
        usum = usum + randu(seed)
20    continue
      error = usum - 6.
c     error has 0 mean, variance of 1.  Convert to desired var
      error = error * sqrt(var)
      return
      end
c*************************************************************
c
      real*8 function randu(seed)
c
c     generates uniformly distributed random number
c     initial seed must be in [1,smod-1]
c
      real*8 seed, smult, smod, sdiv
      data smult/16807.d0/
      data smod/2147483647.d0/
      data sdiv/2147483648.d0/
      seed = dmod(smult * seed, smod)
      randu = seed/sdiv
      return
      end
```

PROGRAM: SEISM

PURPOSE: Simulate ground motion time histories by stochastic method of Boore (1983).

INPUTS: Parameter file specifying options for simulations, including magnitudes and distances to be simulated, number of trials per combination, sample rate, source and attenuation model, site terms, if desired, window shape and length.

OUTPUTS: Simulated time series; response spectra if desired.

```
      program seism
c
c     generates artificial acceleration time history using Boore(1983)
c     method as modified by Boore & Atkinson(1987).
c      Corrections to normalizing factor made June 1989.
c      Modified to allow multiple trials Sept. 1990.
c     Corrections to tapering made Jan. 91. Check for unit
c     spectral amplitude before shaping is built in.
c     Modified to allow Saragoni & Hart window, Jan. 92.
c     Optional specification of source & site FACCN, Apr. 92.
c     Units are cgs
c     If R=999., then program will query for desired value.
c     Can specify source OR site parameters now.
c     Modified to allow kappa filter instead of fmax, Sept 92
c                                        (change input format)
c     Modify Nov 92 to give option for Atkinson ENA model (isrc=2)
c     Also give option for multiple values of M, R to be read from a
c     file named mrset.par (icomp=1)
c     Also have new option to compute PSRV for all records,
c     using (ipsv=1), with output into file psrv.out.
c     If ipsv=1, then do not also select FACCN option (ifa=1)
c     Option to NOT write time series (iwr=0).
c
$LARGE
      common const,rho,beta,pi,amo,fo,fmax,r,qo,eta,h2v
      common isrc, nfr, fr, src, site, isite, ikap, amag
      dimension seism(4096),title(20),psa(100),rsavg(100)
      dimension fr(15), src(15), site(15),freq(100)
      complex s(4096)
      real*8 seed
      character*16 fname
      write(*,1)
1     format(' filename for program parameters ? '\)
      read(*,3)fname
3     format(a)
      open(5,file=fname)
      write(*,4)
4     format(' output filename? '\)
      read(*,3)fname
      open(6,file=fname,status='new')
      nrd=5
      nwr=6
      istart = 0
      read(nrd,15)title
      write(nwr,15)title
15    format(20a4)
      read(nrd,20)npts,dt
20    format(i5,f5.3)
      tmax=float(npts)*dt
c
c     check allowable values for npts
c
      icheck = 0
      do 35 ii = 1, 12
```

```
          ncheck = 2**ii
          if(npts .eq. ncheck) icheck = 1
35      continue
        if(icheck .ne. 1) go to 2020
c**      Read source parameters
        read(nrd,40)amag,stress,rho,beta,h2v
40      format(f5.1,f5.0,3f5.2,2i5)
        if (h2v .eq. 0.) h2v = 1.
        read(nrd,43)isrc,isite,icomp,ifa
43      format(5i5)
        if (ifa .eq. 1) open(4,file='seism.fa',status='new')
        if (isrc .eq. 1 .or. isite .eq. 1) then
          read(nrd,41)fo,f2,nfr
41        format(2f6.3,i6)
c         fr and src are read in log units.
          read(nrd,42)(fr(i),i=1,nfr)
42        format(15f6.3)
          if (isrc .eq. 1) read(nrd,42)(src(i),i=1,nfr)
        endif
        read(nrd,70)ikap,fmax,qo,eta,dura,durb,r
70      format(i5,2f5.2,f5.3,2f5.2,f5.0)
        if(r .eq. 999.) then
          write(*,*)' Enter desired R >'
          read(*,*)r
        endif
        if (icomp.eq.1) open(2,file='mrset.par')
c
c  set parameters
c
        prtitn = 1./sqrt(2.)
        rtp=0.55
        fs=2.
        pi = 4.* atan(1.)
c       Define constant, for r=1 km
        const=prtitn*rtp*fs*(1.e-20)/(4.*pi*rho*beta**3)
        read(nrd,90)seed,taper,ntrial, iopwin, wcon1, wcon2
90      format(f10.0,f5.2,2i5,2f5.2)
        read(nrd,43)ipsv,iwr
        if (ipsv .eq. 1)read(nrd,91)damp,freq1,freq2,Nfreq
91      format(3f5.2,i5)
c       damp is % of critical damping for psrv calcs.
        if (ipsv .eq. 1) open(4,file='psrv.out',status='new')
        seed = seed + 5.*r - 17.
        if (ntrial .lt. 1) ntrial = 1
        if (iopwin .ne. 1) iopwin = 0
c
c       loop over desired m, r combo's, if icomp=1
c
75      continue
        if(icomp .eq. 1)read(2,*,end=9999)amag,r
        amo = 10.**(1.5*amag + 16.05)
        if(isrc.eq.0) fo = (4.906e+06) * beta * (stress/amo)**0.333333
        if(isrc.eq.2)fo=10.**(2.41-0.533*amag)
        dur = 1./fo + dura + durb*r
```

```
      if(dur .gt. tmax) go to 2000
c** tapered boxcar
      ndur = dur/dt
c** ntaper is the number of taper pts added to each end of t.s.
      ntaper = ifix(taper * float(ndur))
      nstop =  ndur + ntaper + ntaper
      if(nstop .gt. npts) go to 2000
      write(nwr,30)nstop,dt,tmax, h2v
30    format(' npts = ',i5,' dt = ',f5.3,' tmax = ',f5.1,' h2v = ',f5.3)
      write(nwr,50)amag,stress,rho,beta
50    format(' Moment M = ',f5.1,' stress drop = ',f5.0,' rho(cm/cm**3)
     1= ',f5.2,' beta(km/s) = ',f5.2)
      write(nwr,60)amo,isrc,isite
60    format(' moment = ',1pe10.2,' isrc = ',i2,' isite = ',i2)
      if (ikap .eq. 0)write(nwr,80)fmax,qo,eta,dura,durb,r,dur
      if (ikap .eq. 1)write(nwr,81)fmax,qo,eta,dura,durb,r,dur
80    format(' fmax = ',f5.0,' Qo = ',f5.0,' eta = ',f5.3,'dura = ',
     1       f5.2,' durb = ',f5.2,/,' accn at dist(km) = ',f5.0,
     2       'duration(sec) = ',f5.1)
81    format(' kappa= ',f5.3,' Qo = ',f5.0,' eta = ',f5.3,'dura = ',
     1       f5.2,' durb = ',f5.2,/,' accn at dist(km) = ',f5.0,
     2       'duration(sec) = ',f5.1)
      write(nwr,100)seed,taper, ntrial, iopwin, wcon1, wcon2
100   format(' seed = ',f10.0,' taper = ',f5.2,' ntrial = ',i5,
     *       ' iopwin = ',i3,' with constants ',2f5.2)
      if(isite .eq. 1) read(nrd,42)(site(j),j=1,nfr)
c
      if (ipsv .eq. 1 .and. istart .eq. 0) then
c       Header block for file psrv.out
        write(4,15)title
        write(4,30)nstop,dt,tmax, h2v
        write(4,50)amag,stress,rho,beta
        write(4,60)amo,isrc,isite
        if (ikap .eq. 0)write(4,80)fmax,qo,eta,dura,durb,r,dur
        if (ikap .eq. 1)write(4,81)fmax,qo,eta,dura,durb,r,dur
        write(4,100)seed,taper, ntrial, iopwin, wcon1, wcon2
        write(4,*)
        istart = 1
      endif
c
      nnyq = npts/2 + 1
      df = 1./tmax
      do 105 i = 1, Nfreq
        rsavg(i) = 0.
105   continue
      avgpga = 0.
      write(*,*)amag,r
c
c** loop on trials
c
      do 999 itrial = 1, ntrial
c
      do 110 i = 1, npts
          seism(i)=0.
```

```
          s(i) = cmplx(0.,0.)
110     continue
c
c       generate Gaussian white noise with zero mean, unit variance.
c**     need to call ggnqf a few times to get it working.
c
        do 119 i = 1,10
          fix=ggnqf(seed)
119     continue
        do 120 i = 1,nstop
            if (iopwin .eq. 0) call window(i,1,nstop,ntaper,wind)
            if (iopwin .eq. 1)
     *          call wind2(i,1,nstop,ntaper,dur,wcon1,wcon2,wind)
            s(i) = wind * cmplx(ggnqf(seed),0.)
120     continue
c
c
c       transform to frequency domain.
c
        call fork(npts,s,-1.)
c
c       multiply spectrum by shape after normalizing to
c       unit spectral amplitude.
c
        call avg(nnyq,s,avamp)
        if (ifa .eq. 1 .and. itrial .eq. 1) write(4,15)title
        if (ifa .eq. 1 .and. itrial .eq. 1) write(4,129)nnyq
129     format(' npts',i5)
        do 130 i = 1,nnyq
            f = (i-1) * df
            if (f .eq. 0.) f= 0.01
            s(i) = shape(f) * s(i) / (avamp)
            s(npts+2-i)=conjg(s(i))
            fa = cabs(s(i))
          if(ifa .eq. 1 .and. itrial .eq. 1) write(4,131)f, fa
131       format(2g10.3)
130     continue
        s(nnyq) = cmplx(1.,0.) * s(nnyq)
c
c       transform back to time domain and print
c
        call fork(npts,s,+1.)
        afact = sqrt(float(npts))/ tmax
        amax = 0.
        do 140 i = 1, npts
            seism(i) = afact * real( s(i) )
            if(abs(seism(i)) .gt. amax) amax = abs(seism(i))
140     continue
        write(nwr,150) amax, itrial, dt
150     format(' Peak acceleration in cm/s**2 = ',f10.3,' Trial #',i5,/,
       1     ' Accelerogram (in cgs) follows by time steps of ',f5.3,
       2     ' sec, in 8e10.3 format.'/)
        if(iwr .ne. 0) write(nwr,170) (seism(j),j=1,nstop)
170     format(8e10.3)
```

```
      write(nwr,180) itrial
180   format(/,' END OF DATA FOR TRIAL #',i5,/)
      seed = seed + 55.
      if (ipsv .eq. 0)go to 999
c
c     Calculate response spectra, averaging logs over trials.
c
      call rscomp(seism,dt,dur,damp,freq1,freq2,Nfreq,freq,psa)
      do 185 i = 1, Nfreq
        rsavg(i) = rsavg(i) + alog10(psa(i))
185   continue
      avgpga = avgpga + alog10(amax)
c
999   continue
c
c     Have finished this M, R combo.
c
      if (ipsv .ne. 0) then
        pga = 10.**(avgpga/float(ntrial))
        write(4,1010)amag,r,pga
1010    format(' M = ',f5.2,' R = ',f6.1,' pga = ',f8.2)
        write(4,1015)damp,ntrial
1015    format(' freq  PSA(cm/s**2)','  %damp = ',f4.1,' ntrial =',i5)
        do 1030 i = 1, Nfreq
          psa(i) = 10.**(rsavg(i)/float(ntrial))
          write(4,1020)freq(i),psa(i)
1030    continue
1020    format(2g10.2)
      endif
c
      if (icomp.eq.1)go to 75
      go to 9999
c
c     skip over these error messages
c
2020  write(nwr,2030)
2030  format(' ERROR.  npts must be a power of 2. Max is 4096')
2000  write(nwr,2010) dur, tmax
2010  format(' dur=',f5.0,' tmax=',f5.0,' :npts too small')
c
9999  stop
      end
c*********************************************************************
      function ggnqf(seed)
c
c     generates Gaussian white noise by approx. method of Ross(1985)
c     Gail Atkinson, 29/5/86
c
      real*8 seed
      usum = 0.00000000
      do 20 j=1,12
          usum = usum + randu(seed)
20    continue
      ggnqf = usum - 6.00000000
```

```
      return
      end
c*************************************************************************
      subroutine avg(n,s,avamp)
$LARGE
      complex s
      dimension s(n)
      sum=0.
      do 10 j = 1, n
        sum=sum + cabs(s(j))
10    continue
      avamp = sum/float(n)
      return
      end
c*************************************************************************
      real*8 function randu(seed)
c
c     generates uniformly distributed random number
c     initial seed must be in [1,smod-1]
c
      real*8 seed, smult, smod, sdiv
      data smult/16807.d0/
      data smod/2147483647.d0/
      dat ' sdiv/2147483648.d0/
      seed = dmod(smult * seed, smod)
      randu = seed/sdiv
      return
      end
c*************************************************************************
      subroutine window(i, nstart, nstop, ntaper, wind)
c
c     apply cosine tapered window.
c     G. Atkinson, Jan. 1991
c
      pi = 3.141592654
      wind = 0.
      if(i .lt. nstart .or. i .gt. nstop) return
      wind = 1.
      if(i .ge. nstart+ntaper .and. i .le. nstop-ntaper) return
c
c     Value of wind goes from 0 to 1 from nstart to nstart+ntaper
c     Then from 1 to 0 from nstop-ntaper to nstop.
c
      ncheck = nstart+ntaper
      if(i .le. ncheck)then
        wind = abs(sin((float(i-nstart)/float(ntaper))*pi/2.))
        return
      else
        wind = abs(sin((float(nstop-i)/float(ntaper))*pi/2.))
        return
      end if
      end
c*************************************************************************
      subroutine wind2(i, nstart, nstop, ntaper, tw, eps, eta, wind)
```

```
c
c     apply Sargoni and Hart (1974) window, with parameters
c     tw (durn), eps (fraction of durn to reach peak), and
c     eta ( fraction of peak ampl. at tw)
c     The Sargoni and Hart window is applied between
c     nstart + ntaper, and nstop - ntaper.  Outside these
c     bounds we do a quick cosine taper down to 0.
c     G. Atkinson, Jan. 1992
c
      pi = 3.141592654
      wind = 0.
      if(i .lt. nstart .or. i .gt. nstop) return
      wind = 1.
c
c     Apply Sargoni and Hart window.
c
        b = -eps * alog(eta)/(1. + eps*(alog(eps)-1.))
        c = b/(eps*tw)
        a = (2.7182818/(eps*tw))**b
        if (i .ge. (nstart+ntaper) .and. i .le. (nstop - ntaper))then
          t =(tw/float(nstop-nstart-2*ntaper)) *
     *                (float(i-nstart-ntaper+1))
          wind = a*t**b * exp(-c*t)
          return
        else
c     Cos. taper goes from  0 to 1 from nstart to nstart+ntaper, from
c                           1 to 0 from nstop-ntaper to nstop.
c
        if (i .lt. (nstart+ntaper)) then
          t1 = tw/float(nstop-nstart-2*ntaper)
          wf = a*t1**b * exp(-c*t)
          wind = abs(sin((float(i-nstart)/float(ntaper))*pi/2.))*wf
        else
          wf = a*tw**b *exp(-c*tw)
          wind = abs(sin((float(nstop-i)/float(ntaper))*pi/2.))*wf
        endif
        return
      end if
      end
```

REFERENCES

Aki, K. (1982). Strong motion prediction using mathematical modeling techniques. Bull. Seism. Soc. Am., **72**, S29-S42.

Atkinson, G. (1984). Attenuation of strong ground motion in Canada from a random vibrations approach. Bull. Seism. Soc. Am., **74**, 2629-2653.

Atkinson, G. (1989). Attenuation of the Lg phase and site response for the Eastern Canada Telemetered Network. Seism. Res. Let., **60**, 2, 59-69.

Atkinson, G., and D. Boore (1990). Recent trends in ground motion and spectral response relations for North America. Earthquake Spectra, **6**, 15-36.

Atkinson, G. and P. Somerville (1992). Calibration of time history simulation methods. Ontario Hydro Report, Toronto.

Boatwright, J. (1982). A dynamic model for far-field accelerations. Bull. Seism. Soc. Am., **72**, 1049-1068.

Boatwright, J. (1984). Seismic estimates of stress release. J. Geophys. Res., **89**, B8, 6961-6968.

Boatwright, J. (1988). The seismic radiation from composite models of faulting. Bull. Seism. Soc. Am., **78**, 489-508.

Boatwright, J. and G. Choy (1992). Acceleration source spectra anticipated for large earthquakes in Northeastern North America. Bull. Seism. Soc. Am., **82**, 660-682.

Boatwright, J., J. Fletcher and T. Fumal (1991). A general inversion scheme for source, site, and propagation characteristics using multiply recorded sets of moderate-sized earthquakes. Bull. Seism. Soc. Am., 81, 1783-1812.

Boore, D. (1983). Stochastic simulation of high-frequency ground motions based on seismological models of the radiated spectra. Bull. Seism. Soc. Am., 73, 1865-1894.

Boore, D. (1986). The effect of finite bandwidth of seismic scaling relationships. Proc. 6th Ewing Symp., Amer. Geophys. Union, Geophysical Monograph, 37, 275-284.

Boore, D. and G. Atkinson (1987). Stochastic prediction of ground motion and spectral response parameters at hard-rock sites in eastern North America. Bull. Seism. Soc. Am., 77, 440-467.

Boore, D. and G. Atkinson (1989). Spectral scaling of the 1985-1988 Nahanni, Northwest Territories, earthquakes. Bull. Seism. Soc. Am., 79, 1736-1761.

Boore, D. and G. Atkinson (1992). Source spectra for the 1988 Saguenay, Quebec earthquakes. Bull. Seism. Soc. Am., 82, 683-719.

Boore, D., W. Joyner and L. Wennerberg (1992). Fitting the stochastic omega-squared source model to observed response spectra in western North America: trade-offs between stress drop and kappa. Bull. Seism. Soc. Am., 82, 1956-1963.

Bowman, J. and B. Kennett (1991). Propagation of Lg waves in the North Australian craton: Influence of crustal velocity gradients. Bull. Seism. Soc. Am., **81**, 592-610.

Brune, J. (1970). Tectonic stress and the spectra of seismic shear waves from earthquakes. J. Geophys. Res., **75**, 4997-5009.

Burger, R., P. Somerville, J. Barker, R. Herrmann, and D. Helmberger (1987). The effect of crustal structure on strong ground motion attenuation relations in eastern North America. Bull. Seism. Soc. Am., **77**, 420-439.

Campbell, K. (1981a). Near-source attenuation of peak horizontal acceleration. Bull. Seism. Soc. Am., **71**, 2039-2070.

Campbell, K. (1981b). A ground motion model for the central United States based on near-source acceleration data. Proc. Conf. Earthq. and Earthq. Eng. in the eastern U.S., Knoxville, Tn., **1**, 213-232.

Cartwright, D. and M. Longuet-Higgins (1956). The statistical distribution of the maxima of a random function. Proc. Roy. Soc. London, **Ser. A237**, 212-223.

Chael, E. (1987). Spectral scaling of earthquakes in the Miramichi region of New Brunswick. Bull. Seism. Soc. Am., **77**, 347-365.

Chopra, A. (1981). Dynamics of Structures: A Primer. Engineering Monographs, Earthquake Engineering Research Institute, El Cerrito, Calif.

Choy, G. and J. Boatwright (1988). Teleseismic and near-field analysis of the Nahanni earthquakes, Northwest Territories, Canada. Bull. Seism. Soc. Am., **78**, 1627-1652.

Chun, K., G. West, R. Kokoski and C. Samson (1987). A novel technique for measuring Lg Attenuation - Results from Eastern Canada between 1 to 10 Hz. Bull Seism. Soc. Am., **77**, 398-419.

Chun, K., R. Kokoski and G. West (1989). Source spectral characteristics of Miramichi earthquake: Results from 115 P-wave observations. Bull. Seism. Soc. Am., **79**, 15-30.

Cornell, C. (1968). Engineering seismic risk analysis. Bull Seism. Soc. Am., **58**, 1583-1606.

Dainty, A. (1981). A scattering model to explain seismic Q observations in the lithosphere between 1 and 20 Hz. Geophys. Res. L., **11**, 1126-1128.

EERI Committee on Seismic Risk (1989). The basics of seismic risk analysis. Earthquake Spectra, **5**, 675-702.

EPRI, (1988). Engineering model of earthquake ground motion for eastern North America. **EPRI NP-6074**, prepared by R. McGuire, G. Toro and W. Silva, Electric Power Research Institute, Palo Alto, Calif.

Fletcher, J. and J. Boatwright (1991). Source parameters of Loma Prieta aftershocks and wave propagation characteristics along the San Francisco Peninsula from a joint inversion of digital seismograms. Bull. Seism. Soc. Am., 81, 1783-1812.

Gupta, I. and K. McLaughlin (1987). Attenuation of ground motion in the eastern United States. Bull. Seism. Soc. Am., 77, 366-383.

Gusev, A. (1983). Descriptive statistical model of earthquake source radiation and its application to an estimate of short-period strong motion. Geophys. J. R. Astr. Soc., 74, 787-808.

Hanks, T. and A. Johnston (1992). Common features of the excitation and propagation of strong ground motion for North American earthquakes. Bull. Seism. Soc. Am., 82, 1-23.

Hanks, T. and H. Kanamori (1979). A moment magnitude scale. J. Geophys. Res., 84, 2348-2350.

Hanks, T. and R. McGuire (1981). The character of high-frequency strong ground motion. Bull. Seism. Soc. Am., 71, 2071-2095.

Hartzell, S. and J. Brune (1979). The Horse Canyon earthquake of August 2, 1975 - Two-stage stress-release process in a strike-slip earthquake. Bull. Seism. Soc. Am., 69, 1161-1173.

Hasegawa, H. (1985). Attenuation of Lg waves in the Canadian shield. Bull. Seism. Soc. Am., 75, 1569-1582.

Hasegawa, H., P. Basham and M. Berry (1981). Attenuation relations for strong seismic ground motion in Canada. Bull. Seism. Soc. Am., 71, 1943-1962.

Haskell, N. (1969). Elastic displacements in the near-field of a propagating fault. Bull. Seism. Soc. Am., 59, 865-908.

Herrmann, R. (1985). An extension of random vibration theory estimates of strong ground motion to large distances. Bull. Seism. Soc. Am., 75, 1447-1453.

Idriss, I. (1979). Characteristics of earthquake ground motions, in Earthquake Engineering and Soil Dynamics, Proc. Am. Soc. Civil Eng. Geotech. Eng. Div. Specialty Conf., June 19-21, 1978, Pasadena, Calif.,3, 1151-1265.

Joyner, W. (1984). A scaling law for the spectra of large earthquakes. Bull. Seism. Soc. Am., 74, 1167-1188.

Joyner, W. and D. Boore (1981). Peak horizontal acceleration and velocity from strong motion records including records from the 1979 Imperial Valley, California, earthquake. Bull. Seism. Soc. Am., 71, 2011-2038.

Joyner, W. and D. Boore (1982). Prediction of earthquake response spectra. Proc. 51st Annual Conv. Struct. Eng. Assoc. Calif.

Joyner, W. and D. Boore (1986). On simulating large earthquakes by Green's function addition of smaller earthquakes. In: Earthquake Source Mechanics. Maurice Ewing Volume 6. Geophys. Monogr. Am. Geophys. Union, 37, 269-274.

Joyner, W. and D. Boore (1988). Measurement, characterization, and prediction of strong ground motion. Proc. ASCE Conf. Soil Dynamics, Park City, Utah, June.

Kanamori, H. and D. Anderson (1975). Theoretical basis of some empirical relations in seismology. Bull. Seism. Soc. Am., 65, 1073-1095.

Kennett, B. (1986). Lg waves and structural boundaries. Bull. Seism. Soc. Am., 76, 1133-1141.

McGarr, A. (1981). Analysis of peak ground motion in terms of a model of inhomogeneous faulting. J. Geophys. Res., 86, 3901-3912.

McGuire, R. (1977). Seismic design spectra and mapping procedures using hazard analysis based directly on oscillator response. Intl. J. Earthq. Eng. Struct. Dyn., 5, 211-234.

McGuire, R., A. Becker and N. Donovan (1984). Spectral estimates of seismic shear waves. Bull. Seism. Soc. Am., 74, 1427-1440.

Mereu, R., D. Wang, O. Kuhn, D. Forsyth, A. Green, P. Morel, G. Buchbinder, D. Crossley, E. Schwarz, R. duBerger, C. Brooks and R. Clowes (1986). The 1982 COCRUST seismic experiments across the Ottawa-Bonnechere graben and Grenville Front in Ontario and Quebec. Geophys. J.R. Astr. Soc., **84**, 491-514.

Milne, W. and A. Davenport (1969). Distribution of earthquake risk in Canada. Bull. Seism. Soc. Am., **59**, 729-754.

Munro, P., W. Shannon, R. Halliday and D. Schieman (1986). Canadian seismograph operations - 1985. Seism. Series No. 94, Earth Physics Branch, Ottawa.

Nuttli, O. (1983). Average seismic source-parameter relations for mid-plate earthquakes. Bull. Seism. Soc. Am., **73**, 519-535.

Nuttli, O., D. Bowling, J. Lawson and R. Wheeler (1987). Some aspects of seismic scaling and the strong ground motion of the eastern Missouri earthquake of Jan. 12, 1984., Seism. Res. L., **58**, 53-58.

Nuttli, O. and R. Herrmann (1978). Credible earthquakes for the central United States. U.S. Army Eng. Waterways Experiment Station, Misc. Paper S-73-1, Rpt. 12, Vicksburg, Miss.

Ojo, S. and R. Mereu (1986). The effect of random velocity functions on the travel times and amplitudes of seismic waves. Geophys. J. R. Astr. Soc., **84**, 607-618.

Ou, G. and R. Herrmann (1990). A statistical model for peak ground motion from local to regional distances. Bull. Seism. Soc. Am., 80, 1397-1417.

Papageorgiou, A. and K. Aki (1983). A specific barrier model for the quantitative description of ingomogeneous faulting and the prediction of strong ground motion. Part I. Description of the model. Bull. Seism. Soc. Am., 73, 693-722.

Press, W., B. Flannery, S. Teukolsky, and W. Vetterling (1986). Numerical Recipes, Cambridge Univ. Press, Cambridge, U.K.

Sadigh, K., J. Egan and R. Youngs (1986). Specification of ground motion for seismic design of long period structures (abs.), Earthquake Notes, 57, 13.

Savage, J. (1972). Relation of corner frequency to fault dimensions. J. Geophys. Res., 77, 3788-3795.

Saragoni, G. and G. Hart (1974). Simulation of artificial earthquakes. Earthquake Eng. Structural Dyn., 2, 249-267.

Shin, T. and R. Herrmann (1987). Lg attenuation and source studies using 1982 Miramichi data. Bull Seism. Soc. Am., 77, 384-397.

Smith, K., J. Brune and K. Priestley (1991). The seismic spectrum, radiated energy, and the Savage and Wood inequality for complex earthquakes. Tectonophysics, 188, 303-320.

Somerville, P., J. McLaren, L. Lefevre, R. Burger and D. Helmberger (1987). Comparison of source scaling relations of eastern and western North American earthquakes. Bull. Seism. Soc. Am., 77, 322-346.

Somerville, P., J. McLaren, C. Saikia and D. Helmberger (1990). The Nov. 25, 1988 Saguenay, Quebec earthquake: source parameters and the attenuation of strong ground motion. Bull. Seism. Soc. Am., 80, 1118-1143.

Street, R., and F. Turcotte (1977). A study of northeastern North American spectral moments, magnitudes, and intensities. Bull. Seism. Soc. Am., 67, 599-614.

Toro, G. and R. McGuire (1987). An investigation into earthquake ground motion characteristics in eastern North America. Bull. Seism. Soc. Am., 77, 468-489.

Vanmarcke, E. and S. Lai (1980). Strong-motion duration and rms amplitude of earthquake records. Bull. Seism. Soc. Am., 70, 1293-1307.

Wetmiller, R., R. Horner, H. Hasegawa, R. North, M. Lamontagne, D. Weichert, and S. Evans (1988). An analysis of the 1985 Nahanni earthquakes. Bull. Seism. Soc. Am.,78, 590-616.

Woodgold, C. (1990). Estimation of Q in eastern Canada using coda waves. Bull. Seism. Soc. Am., 80, 411-429.